



**UCL**

**TOWARDS AN OPTIMAL PHOTONIC NETWORK:  
Optimising Performance, Cost and Flexibility**

**Gareth Lloyd Jones**

A thesis submitted to University College London for the degree of  
Doctor of Engineering (EngD)

Department of Electronic and Electrical Engineering

University College London

February 2013

I, Gareth Lloyd Jones confirm that the work presented in this thesis is my own. Where information has been derived from other sources, I confirm that this has been indicated in the thesis.

## ABSTRACT

This thesis investigates optical fibre transmission system technologies, and their impact on network architectures with the objective of lowering unit cost (\$/Gb/s/km) of data transmission in long-haul, and ultra long-haul dense wavelength division multiplexing (DWDM) photonic networks.

The importance of this work is driven by the exponential growth in Internet traffic of around 40% p.a., and economic pressures constraining network operators' ability to invest in their networks. Optical transport networks must therefore be designed to meet future bandwidth demands of end users, with optimum performance, cost and flexibility.

Dynamic gain equalisers (DGEs) are a key sub-system of ultra long-haul networks, enabling increased un-regenerated transmission reach and elimination of expensive optical-electrical-optical (OEO) regeneration. A theoretical framework was developed integrating models of wideband power variation, together with narrowband nonlinear propagation simulations using the split-step Fourier method. The optimum spacing of the also costly DGEs was determined for a 3,000km network field deployment. Optimum power pre-emphasis profiles were predicted and compared with simple linear calculations, showing <0.7dB performance penalty using the much faster, simplified method.

Optical dispersion management schemes were studied, with optical dispersion compensating fibre placed after every other span resulting in 6% cost reduction and little performance degradation compared to compensation after every span. A techno-economic comparison of optical and electronic dispersion compensation (EDC) strategies showed 25% cost reduction using EDC. Tolerance to fibre nonlinearities is reduced compared to optical compensation; splitting the EDC function equally between transmitter and receiver optimises performance.

Economic benefits of a single flexible, multi-reach DWDM system were investigated showing almost 20% cost savings compared to separate long-haul and ultra long-haul systems. Finally, the techno-economic benefits of optical bypass in meshed networks were analysed for increasing levels of optical transparency: from OEO regenerated to multi-degree reconfigurable optical add-drop multiplexers (MD-ROADMs), enabling up to 46% cost saving.

*I lovingly dedicate this thesis to Gracia, Megan, and my parents*

## **ACKNOWLEDGEMENTS**

I am grateful to Dr Wladek Forysiak for giving me the opportunity to pursue my EngD while working within his team at Ericsson, and for his constant support and guidance throughout many challenging years with the company.

I am grateful to Dr Robert Killey for giving me the opportunity to pursue my EngD at UCL, and for his constant support and guidance, in particular during the writing of this thesis. I would also like to thank the faculty, administrative staff and my fellow students in the Department of Electronic and Electrical Engineering who have helped me enjoy my experience at UCL.

I also acknowledge Professor Nick Doran, for making it possible for me to undertake the EngD, and also subsequent Ericsson management, for enabling me to continue with the programme.

Amongst others, I would particularly like to thank Dr Jeroen Nijhof for supervising my initial research with Marconi and for our close collaboration on a number of research projects in this thesis. I am also grateful for the continued support he has given me following my departure from Ericsson in July 2010.

I am grateful for the support of my former colleagues, who have contributed to the success and enjoyment of this work: Dr Roberto Magri, Dr Steven Alleston, Dr Paul Harper, Dr Patrick Bontemps, Dr Michal Dlubek, Dr Marc Stephens, Dr Liam Gleeson, Glyn Taylor, Giovanni Razzetta, Gianmarco Bruno, Dr Fabio Cavaliere, Dr Donald Govan, Dr Bimal Nayar and Dr Andrew Pratt. Acknowledgements of collaboration on specific works are given in the relevant sections of this thesis. I am also grateful for the support and encouragement of my mentor Richard Dorward.

I gratefully acknowledge support from the Engineering and Physical Sciences Research Council (EPSRC) and my former employer and industrial sponsor during the course of this research programme, Ericsson Limited (formerly Marconi Communications Limited). Ericsson copyrighted material is reproduced with their permission.

I would also like to thank my family and friends for supporting me through this challenging time. I am profoundly grateful to my mother for her constant love and support. I am also grateful to my step father, and my grandmother for their love and support. I would also like to give special mention to my late father, and my late

grandparents, who passed away around the time I started the EngD. I think they would all be proud to see me completing this thesis.

Finally but most importantly, I would like to thank my loving wife Gracia for her constant support, encouragement, patience, and love, which has made it possible for me to achieve this work. Last but not least a special mention to our wonderful daughter Megan whose arrival into our world has given me so much joy over the last eighteen months, and now that this thesis is complete I am looking forward to enjoying more time with Gracia and Megan.

# TABLE OF CONTENTS

<b>Abstract</b> .....	<b>3</b>
<b>Acknowledgements</b> .....	<b>5</b>
<b>Table of Contents</b> .....	<b>7</b>
<b>Acronyms and Abbreviations</b> .....	<b>9</b>
<b>List of Figures</b> .....	<b>14</b>
<b>List of Tables</b> .....	<b>22</b>
<b>1 Introduction</b> .....	<b>23</b>
1.1 Background to the Research .....	24
1.2 Research Aims and Objectives .....	25
1.3 Industry Context of the Research.....	26
1.4 Research Contributions.....	32
1.5 Publications Resulting from the Research .....	32
1.6 Impact on the Industrial Sponsor .....	33
1.7 Thesis Structure .....	34
<b>2 Transmission Modelling</b> .....	<b>36</b>
2.1 Introduction.....	36
2.2 Motivation.....	36
2.3 Research Contributions.....	38
2.4 Chapter Outline.....	39
2.5 DWDM System Architecture Overview .....	41
2.6 Transponder .....	44
2.7 Erbium-Doped Fibre Amplifier (EDFA) .....	52
2.8 Channel Equalisation .....	65
2.9 Light-Wave Propagation in Optical Fibre .....	70
2.10 Measuring Performance.....	91
2.11 Overview of Modelling Process and Tools.....	100
2.12 Wideband OSNR: Modelling and System Test .....	103
2.13 Predicting Optimum Pre-emphasis Profiles.....	111
2.14 ULH Field Deployment Modelling.....	120
2.15 Chapter Summary and Conclusions.....	126

<b>3</b>	<b>Dispersion Management Strategies</b> .....	<b>128</b>
3.1	Introduction and Motivation .....	128
3.2	Research Contributions.....	128
3.3	Chapter Outline.....	129
3.4	Dispersion of Common Fibre Types.....	130
3.5	Dispersion Compensating Fibre (DCF) .....	131
3.6	Other CD Compensation Technologies .....	132
3.7	Dispersion Management .....	133
3.8	Modelling Process.....	136
3.9	Optimising Dispersion Management .....	136
3.10	Comparison of Optical and Electronic Dispersion Compensation Strategies ...	141
3.11	Economics of Electronic Dispersion Compensation .....	150
3.12	Recommendations of Further Work .....	153
3.13	Future Trends.....	154
<b>4</b>	<b>Developing a Flexible WDM System</b> .....	<b>156</b>
4.1	Optical Transport System Evolution.....	158
4.2	Multi-Reach DWDM Systems.....	162
4.3	Multi-Reach Network Design Case Study.....	168
4.4	Chapter Summary and Conclusions.....	177
<b>5</b>	<b>Transparent Meshed Networks</b> .....	<b>178</b>
5.1	Optical Transport Network Evolution .....	178
5.2	OEO Node Architectures .....	180
5.3	MD-ROADM Node Architectures.....	182
5.4	Techno-Economics of Transparent Meshed Networks.....	192
5.5	Chapter Summary and Conclusions.....	209
5.6	Future Trends.....	210
<b>6</b>	<b>Summary and Conclusions</b> .....	<b>213</b>
6.1	Critical Evaluation of the Research and Recommendations For Further Research.....	214
	<b>Appendix 1: EDFA Black-Box Model</b> .....	<b>217</b>
	<b>References</b> .....	<b>224</b>

## **ACRONYMS AND ABBREVIATIONS**

3R	Re-amplification, Re-shaping and Re-timing
A/D	Analogue to Digital
ASE	Amplified Spontaneous Emission
ASIC	Application Specific Integrated Circuit
ASON	Automatic Switched Optical Network
AWG	Arrayed Waveguide Grating
BER	Bit Error Rate
BoM	Bill of Materials
CAGR	Compound Annual Growth Rate
CapEx	Capital Expenditure
CD	Chromatic Dispersion
CDC	Colourless Directionless Contention-less
CEU	Channel Equalising Unit
CFBG	Chirped Fibre Bragg Grating
CLE	Customer Located Equipment
CW	Continuous Wave
CWDM	Coarse Wavelength Division Multiplexing
D/A	Digital to Analogue
DCF	Dispersion Compensating Fibre
DCM	Dispersion Compensating Module
Demux	De-multiplexer
DFB	Distributed Feedback (laser)
DFE	Decision Feedback Equaliser
DGD	Differential Group Delay
DGE	Dynamic Gain Equalisation
DML	Directly Modulated Laser
DP-QPSK	Dual Polarization Quadrature Phase Shift Keying
DPSK	Differential Phase Shift Keying
DQPSK	Differential Quadrature Phase Shift Keying
DSA	Dual Stage Amplifier
DSF	Dispersion Shifted Fibre
DSL	Digital Subscriber Line

DSP	Digital Signal Processing
DWDM	Dense Wavelength Division Multiplexing
EDC	Electronic Dispersion Compensation
EDF	Erbium Doped Fibre
EDFA	Erbium Doped Fibre Amplifier
eFEC	Enhanced Forward Error Correction
ELH	Extended Long-Haul
EMS	Element Management System
EOADM	Extended Optical Add-Drop Multiplexer
FEC	Forward Error Correction
FFE	Feed Forward Equalisation
FFT	Fast Fourier Transform
FOADM	Fixed Optical Add-Drop Multiplexer
FOM	Figure of Merit
FTTH	Fibre to the Home
FWHM	Full Width Half Maximum
FWM	Four Wave Mixing
GbE	Gigabit Ethernet
GCG	Gross Coding Gain
GFF	Gain-Flattening Filter
GNLS	Generalised Nonlinear Schrödinger Equation
GV	Gain Variation
GVD	Group Velocity Dispersion
HPC	High Performance Computing
IETF	Internet Engineering Task Force
IFWM	Intra-channel Four Wave Mixing
IP	Internet Protocol
IPTV	Internet Protocol Television
ITU	International Telecommunications Union
IXPM	Intra-channel Cross Phase Modulation
LCOS	Liquid Crystal on Silicon
LDT	Link Design Tool
LEAF®	Large Effective Area Fibre
LH	Long-Haul

LST	Link Simulation Tool
LTE	Long Term Evolution
MD-ROADM	Multi-Degree Reconfigurable Optical Add-Drop Multiplexer
MEMS	Micro-Electro-Mechanical System
MLSE	Maximum Likelihood Sequence Estimation
MSA	Multi Source Agreement
Mux	Multiplexer
MZM	Mach-Zehnder Modulator
NCG	Net Coding Gain
NE	Network Element
NLS	Nonlinear Schrödinger Equation
NMS	Network Management System
NRZ	Non Return to Zero
NZ-DSF	Non-Zero Dispersion Shifted Fibre
OADM	Optical Add-Drop Multiplexer
ODB	Optical Duo Binary
OEO	Optical-Electrical-Optical (Regeneration)
OIF	Optical Internetworking Forum
OLA	Optical Line Amplifier
OLL	Optical Line Leveller
OLT	Optical Line Terminal
OOB	Out Of Band
OOK	On Off Keying
OpEx	Operational Expenditure
OSC	Optical Supervisory Channel
OSNR	Optical Signal-to-Noise Ratio
OSS	Operational Support System
OTN	Optical Transport Network
OTT	Over The Top (service provider)
OTU	Optical Channel Transport Unit
OXC	Optical Cross Connect
PDL	Polarisation Dependent Loss
PMD	Polarisation Mode Dispersion
PMU	Power Monitor Unit

PON	Passive Optical Network
POTP	Packet Optical Transport Platform
PRBS	Pseudo Random Bit Sequence
RAN	Radio Access Network
RFP	Request for Proposal
RFQ	Request for Quotation
ROADM	Reconfigurable Optical Add-Drop Multiplexer
RU	Rack Unit
Rx	Receiver
RZ	Return to Zero
SAN	Storage Area Network
SBS	Stimulated Brillouin Scattering
SD-FEC	Soft Decision Forward Error Correction
SDH	Synchronous Digital Hierarchy
SER-DES	Serialiser-De-Serialiser
SMF	Single Mode Fibre
SONET	Synchronous Optical Network
SPM	Self Phase Modulation
SRS	Stimulated Raman Scattering
SSA	Single Stage Amplifier
STM	Synchronous Transport Module
TCO	Total Cost of Ownership
TDM	Time Division Multiplexing
Tx	Transmitter
ULH	Ultra Long-Haul
VOA	Variable Optical Attenuator
VoD	Video on Demand
VPI	Virtual Photonics Inc.
WAN	Wide Area Network
WB	Wavelength Blocker
WDM	Wavelength Division Multiplexing
WRA	Wavelength Routing and Assignment
WSS	Wavelength Selective Switch
XFP	10 Gigabit Small Form-Factor Pluggable

XPM

Cross Phase Modulation

## LIST OF FIGURES

Figure 1 Optical networking value chain including examples of key players .....	27
Figure 2 Growth rates of Internet traffic and network bandwidth .....	28
Figure 3 High growth of Telco traffic and cost vs. low growth of revenue in multimedia era .....	28
Figure 4 DWDM technology roadmap 2000-2012 .....	30
Figure 5 Gain variation (GV) across a spectrum of DWDM channels .....	37
Figure 6 Architecture of a DWDM system .....	41
Figure 7 Schematic of DWDM system model .....	43
Figure 8 Equivalent OOK NRZ and RZ bit patterns .....	46
Figure 9 Basic architecture of an RZ transmitter consisting of a laser source, external modulator and RZ pulse carver (This figure was published in [37], page 55, Figure 2.16, Copyright © 2008, Elsevier. Permission to reproduce this figure has been granted by Elsevier). .....	46
Figure 10 Pulse spectra for (a) NRZ OOK and (b) RZ OOK (33% duty cycle RZ in black and 50% duty cycle RZ in grey) (This figure was published in [37], page 50, Figure 2.14, Copyright © 2008, Elsevier. Permission to reproduce this figure has been granted by Elsevier). .....	46
Figure 11 10G transponder architecture .....	49
Figure 12 Field constellation diagrams for OOK, DPSK and DQPSK .....	50
Figure 13 Pulse spectra for (a) DPSK and (b) DQPSK (NRZ versions in black and RZ versions in grey), (This figure was published in [37], page 50, Figure 2.14, Copyright © 2008 Elsevier. Permission to reproduce this figure has been granted by Elsevier). .....	51
Figure 14 Energy levels of $\text{Er}^{3+}$ ions in silica glass .....	53
Figure 15 Architecture of a basic EDFA comprising two stages of EDF .....	54
Figure 16 SSA high-level architecture .....	56
Figure 17 DSA high-level architecture .....	57
Figure 18 DSA21 output spectra under normal operation for (a) pre-amplifier (b) booster .....	58
Figure 19 Variation of EDFA NF with VOA loss .....	59
Figure 20 Example EDFA gain spectrum for DSA booster amplifier stage (after [25]) .....	61

Figure 21 OSNR along a link of regular 17dB spans for varying signal power .....	63
Figure 22 OSNR along a link of regular 17dB and 21dB spans at 0dBm/ch signal power .....	63
Figure 23 Principle of pre-emphasis. Left: Input channel powers. Centre: Channel powers with SRS tilt. Right: Output channel powers with combined SRS and EDFA tilt. (a) no pre-emphasis resulting in tilted spectrum after EDFA (b) pre-emphasis results in flattened output (after [19]).....	66
Figure 24 Levelling sub-system architecture .....	67
Figure 25 Input power spectra at start of 3,173km link with: (a) no pre-emphasis (b) ideal OSNR equalisation pre-emphasis (c) linear OSNR equalisation pre-emphasis.....	69
Figure 26 OSNR spectrum at end of 3,173km link with: (a) no pre-emphasis (b) ideal OSNR equalisation pre-emphasis and (c) linear OSNR equalisation pre-emphasis.....	69
Figure 27 Received power spectrum at end of 3,173km link with: (a) no pre-emphasis (b) ideal OSNR equalisation pre-emphasis and (c) linear OSNR equalisation pre-emphasis.....	70
Figure 28 Silica fibre attenuation spectrum .....	71
Figure 29 Attenuation profile of SMF fibre over C-band (after [25]) .....	72
Figure 30 Attenuation profile of SMF-DCF over C-band (after [25]).....	73
Figure 31 Principle and effect of Inter Symbol Interference (ISI).....	73
Figure 32 Material and waveguide dispersion contributions to total dispersion in G.652 fibre .....	74
Figure 33 Fibre nonlinear effects classification .....	77
Figure 34 Linear and nonlinear transmission regimes .....	78
Figure 35 Schematic of SRS showing energy transfer between shorter and longer wavelengths (after [25]).....	83
Figure 36 Raman gain for a 100km span of SMF and NZ-DSF with 20dBm total input power (after [25]).....	85
Figure 37 BER as a function of Q-factor (pre-FEC).....	92
Figure 38 Eye diagram for NRZ-OOK signal with parameters used in Q-factor definition.....	93
Figure 39 Q-factor (dB) as a function of OSNR (dB).....	95

Figure 40 BER performance vs. received signal power and OSNR for 10Gb/s RZ transponder.....	96
Figure 41 Post-FEC (Output) BER vs. pre-FEC (Input) BER for G.975.1 FEC code (after [65], Copyright © ITU. Permission to reproduce this figure has been granted by the ITU).....	98
Figure 42 Overview of modelling tool suite and main data flows between each tool. ....	100
Figure 43 OSNR vs. no. of EDFA for 3,091km link (solid lines are simulation with no pre-emphasis and dots are measurements with optimum pre-emphasis). 104	
Figure 44 OSNR vs. no. of EDFA for 3,091km link optimum linear pre-emphasis applied to simulation (solid lines) and measurements (dots).....	105
Figure 45 Modelled OSNR spectrum for 3,091km link with and without pre-emphasis and experimental OSNR measurements with pre-emphasis.....	105
Figure 46 OSNR ripple across C-band for measured data and model with and without pre-emphasis. ....	106
Figure 47 Measured and modelled power flatness vs. no. of EDFA for 3,091km link. ....	107
Figure 48 Modelled launch power spectrum for both no pre-emphasis and optimum linear pre-emphasis profile for OSNR equalisation in 3,091km link .....	107
Figure 49 Power spectrum at end of 3,091km link with no pre-emphasis and with optimum pre-emphasis.....	108
Figure 50 Measured power spectrum at end of 3,091km link.....	108
Figure 51 Grey area highlights region of operation where OSNR and power spread are both optimised within acceptable limits .....	109
Figure 52 Optimum pre-emphasis across C-band vs. channel count. ....	110
Figure 53 “Short Dispersion Map” of 2,940km link (per span dispersion compensation).....	112
Figure 54 Q-factor at end of 2,940km link for 10Gb/s RZ channels with varying pre-emphasis profile and average power per channel as a result of: (a) full nonlinear simulations (b) linear simulations (after [19]) .....	114
Figure 55 Optimum pre-emphasis setting determined by both nonlinear and linear simulations .....	115

Figure 56 Worst channel Q-factor at end of 2,940km link (10Gb/s RZ) computed by full nonlinear simulations with 3 different pre-emphasis schemes (after [19]) .....	116
Figure 57 Q-penalty between nonlinear simulation results applying optimised pre-emphasis predicted by nonlinear simulations vs. optimum pre-emphasis determined by linear simulations, and no pre-emphasis.....	116
Figure 58 Q-factor spectrum at end of 2,940km link obtained from full nonlinear simulations at 0dBm per channel with different pre-emphasis schemes (after [19]) .....	118
Figure 59 Q-factor spectrum vs. pre-emphasis setting for the 2,940km link at 0dBm/channel .....	118
Figure 60 2,872km Perth to Adelaide link of pan-Australia national network (after [20]) .....	122
Figure 61 Relative cost of zero channel network infrastructure vs. number of OLL in a 3,360km link .....	123
Figure 62 Simulated Q-factor performance spectrum vs. number of OLLs in a 3,360km link.....	124
Figure 63 Simulated and measured BER for 5,745km looped back link (after [20]) .....	125
Figure 64 Dispersion coefficient profile of common fibre types over C-band .....	130
Figure 65 Relative cost of DCM vs. compensated SMF span length .....	132
Figure 66 Example dispersion map for dispersion management .....	134
Figure 67 DWDM system with short dispersion map (upper) and long dispersion map (lower).....	135
Figure 68 Long DCF and Short DCF dispersion maps for 1,360km link .....	137
Figure 69 Single channel Q-factor performance at 1,360km.....	138
Figure 70 DWDM Q-factor performance at 1,360km .....	139
Figure 71 Total system cost reduction achievable vs. DCF length for a zero channel system .....	140
Figure 72 Electronic dispersion compensation techniques for various DWDM applications .....	142
Figure 73 600km DWDM system with inline DCF (long dispersion map) and DSA / SSA .....	143

Figure 74 600km DWDM system with EDC at transmitter and receiver with DSA / SSA .....	143
Figure 75 600km DWDM system with EDC at transmitter and receiver with all SSA .....	143
Figure 76 Q-factor contour plot for varying channel launch power and % pre-compensation for 600km 10Gb/s NRZ transmission.....	144
Figure 77 IXPM pulse interactions (after [22]).....	145
Figure 78 IFWM pulse interactions (after [22]).....	145
Figure 79 Q-factor for varying channel launch power and CD compensation scheme for 600km 10Gb/s NRZ transmission (after [22]) .....	146
Figure 80 Q-factor for varying channel launch power and CD compensation scheme for 600km 10Gb/s RZ transmission.....	147
Figure 81 Q-factor for varying channel launch power and CD compensation scheme for 1,200km 10Gb/s RZ transmission (after [22]) .....	147
Figure 82 Q-factor for varying channel launch power and CD compensation scheme for 1,200km 10Gb/s RZ DQPSK transmission (after [22]).....	148
Figure 83 Q-factor for varying channel launch power and CD compensation scheme for 600km 40Gb/s RZ DQPSK transmission (after [22]).....	149
Figure 84 Network cost savings in a 600km link vs. channel count and EDC transponder cost premiums .....	152
Figure 85 Network cost savings in a 1,200km link vs. channel count and EDC transponder cost premiums .....	152
Figure 86 Schematic of conventional LH DWDM line system .....	160
Figure 87 Schematic of ULH DWDM line system .....	160
Figure 88 Simplified cost comparison of LH and ULH DWDM line systems.....	161
Figure 89 Ericsson's <i>Marconi MHL 3000</i> DWDM system .....	163
Figure 90 Ericsson <i>Marconi MHL 3000</i> WDM system shelves for metro and core applications .....	163
Figure 91 High level schematic of FOADM.....	166
Figure 92 High level schematic of ROADM .....	166
Figure 93 Modular EDFA, transponder and OADM system options for multi-reach DWDM applications.....	167
Figure 94 Outline WDM network design process.....	168
Figure 95 Reference network topology.....	169

Figure 96 Length in km of connections between each network node.....	170
Figure 97 Traffic demand matrix in period 1.....	170
Figure 98 Traffic demand matrix in period 2.....	170
Figure 99 Un-regenerated feasible connections using 10G NRZ transponders with LH amplifiers.....	171
Figure 100 Un-regenerated feasible connections using 10G NRZ and 10G RZ transponders with ULH amplifiers .....	171
Figure 101 LH network design .....	172
Figure 102 ULH network design.....	172
Figure 103 Low initial cost multi-reach network design MR1 .....	174
Figure 104 Low per wavelength cost multi-reach network design MR2.....	174
Figure 105 Total network cost for each network design in period 1 .....	175
Figure 106 Total cumulative network cost for each network design in period 2.....	176
Figure 107 OEO architecture at degree-3 node with manual reconfiguration.....	180
Figure 108 OEO architecture at degree-3 node with automated reconfiguration ....	181
Figure 109 Degree-2 ROADM node architecture.....	182
Figure 110 Degree-3 node using a degree-2 ROADM and a terminal .....	185
Figure 111 Degree-4 node using a degree-2 ROADM and 2 terminals.....	186
Figure 112 Degree-5 node using a degree-2 ROADM and 3 terminals.....	186
Figure 113 Degree-4 node using 2 degree-2 ROADMs.....	187
Figure 114 Degree-3 “broadcast and select” WB MD-ROADM node architecture	187
Figure 115 Degree-4 “broadcast and select” WB MD-ROADM node architecture	188
Figure 116 Degree-5 “broadcast and select” WB MD-ROADM node architecture	189
Figure 117 Degree-4 “broadcast and select” MD-ROADM upgraded to degree-5 node architecture with an additional terminal.....	189
Figure 118 Degree-4 MD-OADM node architecture with WSS .....	191
Figure 119 Network topology and parameters (after [24]) .....	193
Figure 120 Traffic distribution and growth forecast .....	194
Figure 121 Period 1 traffic matrix.....	195
Figure 122 Period 2 cumulative traffic matrix .....	195
Figure 123 Period 3 cumulative traffic matrix .....	195
Figure 124 Distribution of all possible working and protection connection lengths (after [24]).....	196

Figure 125 Connection length distribution separating working and protection paths .....	197
Figure 126 Connection length distribution with approximate reach performance of 10G NRZ and 10G RZ transponders .....	197
Figure 127 Connection lengths and approximate transponder reach in US and German networks. US network connection lengths from <i>OPNET SP Guru Transport Planner</i> .....	198
Figure 128 Connection lengths in km coded by amplifier and transponder types required to support adequate span budget performance for error free transmission .....	199
Figure 129 Opaque OEO LH network design.....	201
Figure 130 Semi-transparent network design with degree-2 ROADM .....	202
Figure 131 Semi-transparent network design with WB MD-ROADM .....	203
Figure 132 Fully transparent network design with WSS based MD-ROADM .....	204
Figure 133 Network routes upgraded from 40 to 80 channels in period 3 .....	205
Figure 134 Total network CapEx cost for different solutions at each planning period (% cost savings of the WSS MD-ROADM solution versus each of the other solutions are highlighted in red text) (after [24]).....	206
Figure 135 Period 1 total network cost split between DWDM infrastructure and transponders.....	207
Figure 136 Period 2 total network cost split between DWDM infrastructure and transponders.....	208
Figure 137 Period 3 total network cost split between DWDM infrastructure and transponders.....	208
Figure 138 Schematic of a multi-section EDFA, showing optical isolators ( $\rightarrow$ ), couplers (C) a gain equalising filter (F), and taps (T) for power monitoring (after [44]).....	217
Figure 139 Gain vs. signal power $P_{in}$ measurements for $\lambda_{ref}$ (1546nm), the slope is equal to $a_T$ (after [25]) .....	218
Figure 140 Measured and modelled spectral gain variation across C-band for DSA booster stage amplifier vs. signal power. Each curve shows the model fit at $P_{in}$ of 0,1,2,3,4 and 5dBm (after [25]).....	220

Figure 141 Measured and modelled spectrally dependent spontaneous emission factor of DSA booster amplifier stage vs. signal power. Each curve shows the fit to the data at $P_{in}$ values of 0, 1, 2, 3, 4, and 5dBm (after [25]) .....	222
Figure 142 Comparison of measurements and black-box model for DSA booster stage amplifier gain spectrum .....	223
Figure 143 Comparison of measurements and black-box model for DSA booster stage amplifier noise figure.....	223

## LIST OF TABLES

Table 1 10Gb/s transponder approximate transmission reach .....	48
Table 2 EDFA specification summary for ULH DWDM system .....	55
Table 3 Measured Raman tilts for 100km spans and tilt over C-band with a total signal power of 22.5dBm, calculated $\beta$ values (after [25]) .....	84
Table 4 System penalties for effects included and not include in 10Gb/s numerical simulations .....	97
Table 5 Q-factor targets from nonlinear simulations for various interfaces .....	99
Table 6 Key parameters of SMF fibre (G.652) and SMF DCF .....	113
Table 7 Performance summary from combined nonlinear simulations with wideband power variation model for 2,940km link with 0dBm/channel average launch power and varying pre-emphasis .....	119
Table 8 Key fibre parameters for SMF fibre (G.652) and SMF DCF.....	131
Table 9 Summary of LH, ULH and multi-reach DWDM system architectures .....	164
Table 10 Total network % cost savings for each solution and period (after [24])...	206
Table 11 Total numbers and type of transponders required for each network solution and period with % saving in transponder numbers with respect to previous generation solution.....	209

# 1 INTRODUCTION

Since its birth in the late 19<sup>th</sup> century the telecommunications industry has seen massive growth and has transformed the world's economy such that today out of a population of 6.8 billion people there are<sup>1</sup>:

- 5.6 billion mobile subscriptions
- 2.08 billion Internet users
- 1.2 billion fixed telephone lines
- 940 million mobile broadband subscriptions
- 550 million fixed line broadband subscriptions
- 28 Exabytes ( $28 \times 10^{18}$  bytes) Internet Protocol (IP) traffic per month
- \$3.85 trillion annual revenue of the telecommunications industry

While many technologies and applications have been developed to support this growth, one of the less visible but key enablers of the low cost and mass-market availability of global communications today are optical fibre communication systems. Through whatever device a subscriber accesses the network, be it a PC via a digital subscriber line (DSL) broadband connection, a long term evolution (LTE) wireless smartphone, or a fixed line telephone, the transmitted data or voice will traverse an optical fibre communication link at some point within the network between source and destination.

Optical fibre communication systems are coming increasingly close to subscribers through the deployment of fibre to the home (FTTH) passive optical networking (PON) technology in access networks. However the subject of this thesis is the dense wavelength division multiplexing (DWDM) networking technology (often called photonic network) which forms the transmission infrastructure of core backbone and metro networks i.e. the Internet. Specifically this thesis aims to make progress towards optimising the performance, cost and flexibility of photonic networks to economically meet future bandwidth requirements.

---

<sup>1</sup> Sources: Gartner Inc, ITU, Cisco, IETF

## 1.1 BACKGROUND TO THE RESEARCH

Since optical fibre was first proposed as a potential new form of communication medium by Kao and Hockham in 1966 [1] massive progress has been made in increasing the capacity of optical communications systems towards the theoretical nonlinear bandwidth limit on single mode fibres of around 100Tb/s [2], [3] and [4]. Most DWDM systems installed within telecommunications networks today operate at line rates of 10Gb/s with a small but increasing proportion operating at 40Gb/s. Assuming 80 channel systems the total capacity per fibre pair is 0.8Tb/s and 3.2Tb/s respectively. Emerging state of the art DWDM systems are capable of transporting up to 96 channels each carrying 100Gb/s with an aggregate capacity of 9.6Tb/s per fibre pair and R&D work has already commenced on the next generation line rates of 400Gb/s and 1Tb/s [5] and [6].

### **Computer Simulation and Modelling of DWDM Systems and Networks**

Computer simulation and modelling is a cost-effective and vital tool in the development of DWDM systems and networks with several commercial software packages available on the market since around 2000.

New modulation techniques, system architecture concepts and application of new photonic device technologies can be investigated by modelling before committing to full-scale developments. Producing prototype hardware and embedded software and carrying out laboratory tests of the many possible trade-offs between parameters and network scenarios is unfeasible in terms of the significant resources required. A much wider range of network configurations and architectures and parameter trade-offs can be explored by simulations than could ever be performed in a laboratory.

Modelling results can be used to set engineering rules for the configuration of a DWDM transmission system for varying network requirements. Automated link engineering and network design tools capture the engineering rules and can be relied upon to produce robust and cost-effective designs for customer networks.

Today's telecommunications industry is a highly competitive and fast changing business environment with rapidly shifting expectations and demands on equipment vendors. Requests for proposals (RFP) and quotations (RFQ) are issued by network operators with tight deadlines placing large demands on network architects to quickly produce robust network designs at the lowest possible cost requiring analysis of

multiple design options. Efficient and accurate simulation tools, link design tools, and network planning tools enable rapid assessment of link feasibility and network cost and provide equipment vendors with a competitive advantage when responding to customer requests. These tools also provide network operators with the means to plan the future evolution of their networks.

## **1.2 RESEARCH AIMS AND OBJECTIVES**

The primary objective of the research presented in this thesis is to optimise the performance, cost and flexibility of DWDM systems and networks. A key metric to measure the cost-effectiveness of a DWDM system is the cost per unit capacity per unit distance i.e. \$/Gb/s/km and this parameter can be optimised in a number of ways:

1. Improve the performance i.e. increase distance
2. Increase capacity
3. Use lower cost components or more efficient architectures

However each of these interventions can interact with and influence one another, for example:

1. Increasing reach performance requires increased cost components
2. Increasing capacity requires increased cost components and can limit the distance
3. Using lower cost components can decrease the distance and limit capacity.

The first aim of this research is to optimise channel power equalisation to maximise reach while limiting the additional infrastructure cost. A combined model of wideband power variation and nonlinear simulation is required to investigate techniques for power equalisation including methods for optimising signal power pre-emphasis profiles.

The second aim of this thesis is to investigate the cost and performance trade-off of different optical dispersion compensation schemes, and to compare the performance and cost of optical and electronic dispersion compensation strategies.

Another key characteristic of a DWDM system is its flexibility i.e. its ability to be applied in widely differing network scenarios. By combining the features of

traditionally separate DWDM system domains of metro, long-haul (LH), extended long-haul (ELH) and ultra long-haul (ULH) onto a common modular multi-reach platform, a more flexible approach to network design can be implemented with resulting cost reduction. This thesis aims to evaluate the cost reduction which can be achieved through the convergence towards a common multi-reach DWDM system.

Finally increased transmission reach has led to the requirement for and feasibility of all-optical networks, replacing optical-electrical-optical (OEO) regeneration with transparent optical bypass nodes such as multi-degree reconfigurable optical add-drop multiplexers (MD-ROADM). This thesis aims to assess the economic benefit of increasing levels of optical transparency in core networks.

### **1.3 INDUSTRY CONTEXT OF THE RESEARCH**

Ericsson (formerly Marconi)<sup>2</sup> was the industrial sponsor of this EngD research programme; Ericsson is a telecommunications systems vendor and a market leader in mobile and fixed network infrastructure and services. The research was conducted within the optical networks product development unit, which is an organisation responsible for the development of Ericsson's portfolio of optical transport products. These products include core DWDM and metro C/DWDM<sup>3</sup> systems, SDH<sup>4</sup>/OTN<sup>5</sup>/Ethernet switches and packet optical transport platforms (POTP).

More specifically the work was conducted within the photonics modelling team which is part of the systems and technology group focused on the design of core and metro C/DWDM systems. Sadly the UK division of the optical networks product development unit was disbanded in 2010 due to the requirement to reduce the business's cost base and focus product development at fewer global locations.

#### **Optical Networking Value Chain**

Figure 1 shows the optical networking value chain and examples of its key players. With a few exceptions system vendors purchase optical components and modules from component vendors. System vendors integrate the optical components and modules within line cards controlled by silicon electronics and embedded software. Line cards are integrated into a complete system housed within shelves as network

---

<sup>2</sup> Marconi was acquired by Ericsson in 2006; only Ericsson will be referred to in the rest of this thesis

<sup>3</sup> CWDM = Coarse Wavelength Division Multiplexing (CWDM is not considered in this thesis)

<sup>4</sup> SDH = Synchronous Digital Hierarchy

<sup>5</sup> OTN = Optical Transport Network

elements (NE). NEs are controlled by an element management system (EMS) and the complete network by a network management system (NMS).

Network operators purchase complete systems deploying within their networks with each network element or node connected by owned or leased fibre; the NMS is also integrated within their operational support system (OSS). These optical transport networks form the infrastructure upon which all services are offered either directly to end users or on a wholesale basis to 3<sup>rd</sup> party service providers.

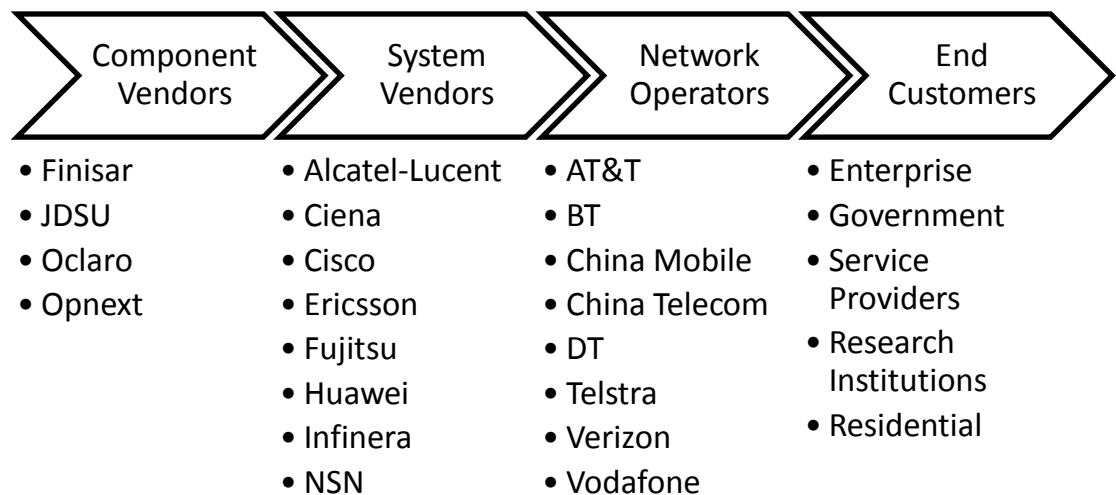


**Figure 1 Optical networking value chain including examples of key players**

### 1.3.1 TELECOMS NETWORK OPERATORS' CHALLENGES

Challenges faced by network operators today are well documented and include the need to invest in network capacity to meet the exponential growth in traffic of approximately 40% p.a. (equivalent to doubling every 24 months) e.g. as forecasted by Cisco in their annual forecast of global IP traffic growth [7].

Compounding the operator's problems is the fact that traffic growth is driven primarily by consumer video applications from so called over-the-top (OTT) service providers such as Netflix, YouTube/Google, Facebook and Skype who are also capturing most of the revenue growth and value from the bandwidth explosion.

Traditional Telco's are facing the realities of becoming commoditised bandwidth providers while a widening gap between cost and revenue growth is negatively impacting their profitability and ability to invest in new network capacity as highlighted in Figure 2 and Figure 3. These facts relentlessly drive network operators

towards lowering the \$/Gb/s/km of data transport capital expenditure (CapEx) and operational expenditure (OpEx).

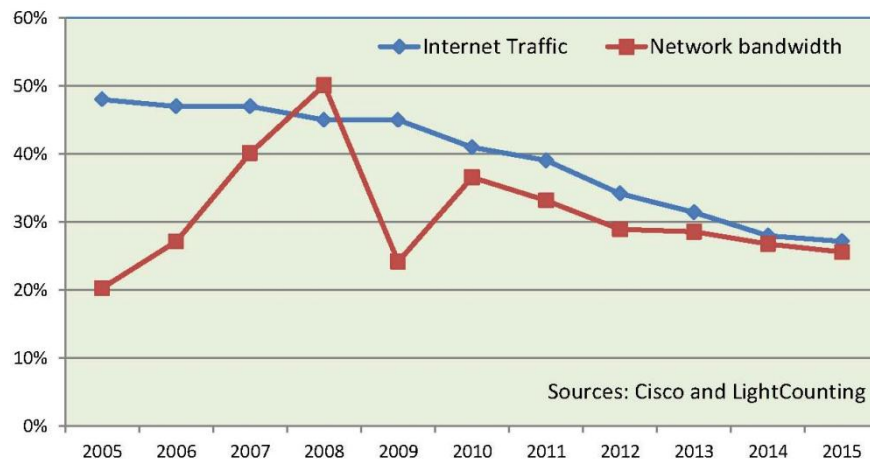


Figure 2 Growth rates of Internet traffic and network bandwidth<sup>6</sup>

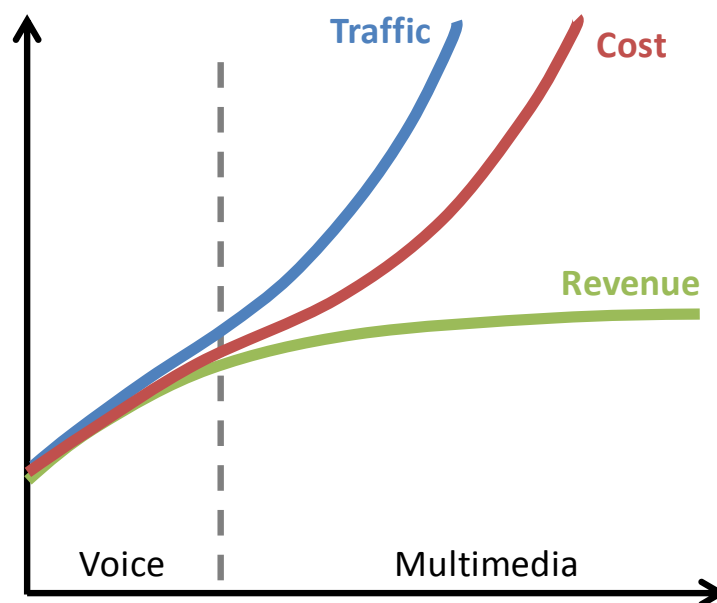


Figure 3 High growth of Telco traffic and cost vs. low growth of revenue in multimedia era

CapEx can be reduced by developing and deploying advanced DWDM systems with more efficient and cost effective system and network architectures. Cost depends heavily on system vendors' choice of appropriate component technology and specification for a given application and how these are combined at a system and network level (i.e. architecture).

<sup>6</sup> Source: Gazettabyte © Roy Rubenstein. Plotting transceiver shipments versus traffic growth. <http://www.gazettabyte.com/home/2011/8/1/plotting-transceiver-shipments-versus-traffic-growth.html>  
This work is licensed under a Creative Commons Licence for Attribution, No Derivatives. <http://creativecommons.org/licenses/by-nd/3.0/>

OpEx is an increasingly large proportion of network operators' cost base and includes the cost of installing, commissioning and operating a network. In order to reduce OpEx system vendors must develop systems which are simple to install and operate thereby accelerating the time to provision new revenue generating services. Automation of processes and minimising manual and on-site human intervention is a key objective towards reducing OpEx.

Power consumption is a significant contributor to OpEx especially as traffic is increasing significantly. Power consumption cost can be reduced by performing switching all-optically at the DWDM layer rather than electronic switching at the OTN/SDH layer, Layer 2 (Ethernet) or routing at Layer 3 (IP) [8].

### **1.3.2 TELECOMS EQUIPMENT VENDORS' CHALLENGES**

The investment bubble of the late 1990's saw billions of dollars invested in telecommunications equipment start-ups and established players brought products to market to meet the growing demand for bandwidth. De-regulation and increased competition in the telecommunications service market led established and new entrant carriers to build out global communications networks in particular across North America and Europe, building up large debts in the process. The Internet bubble burst in early 2000 resulting in several bankruptcies among carriers. Carrier spending dried up hitting equipment vendors hard leading to major business restructuring and the loss of hundreds of thousands of jobs across the industry during 2001-2004.

During this time the market for DWDM transmission systems posed many challenges for system vendors. To meet the reduced capital expenditure of network operators, the focus in optical transport system design shifted from extending distance and capacity (for minimising \$/Gb/s/km of fully loaded systems) towards minimising the initial cost for low channel counts and maintaining low incremental upgrade cost and OpEx requirements.

It was important for system vendors to continue investing in R&D to develop competitive products and be well positioned for the market upturn as bandwidth requirements continued to grow. Internal efficiency savings were also sought by rationalising product portfolios cutting out duplication and focusing R&D on fewer platforms.

### 1.3.3 TECHNOLOGY ROADMAP

Figure 4 shows the roadmap of three key technologies within DWDM systems between 2000 and 2012, which are most relevant to this thesis.

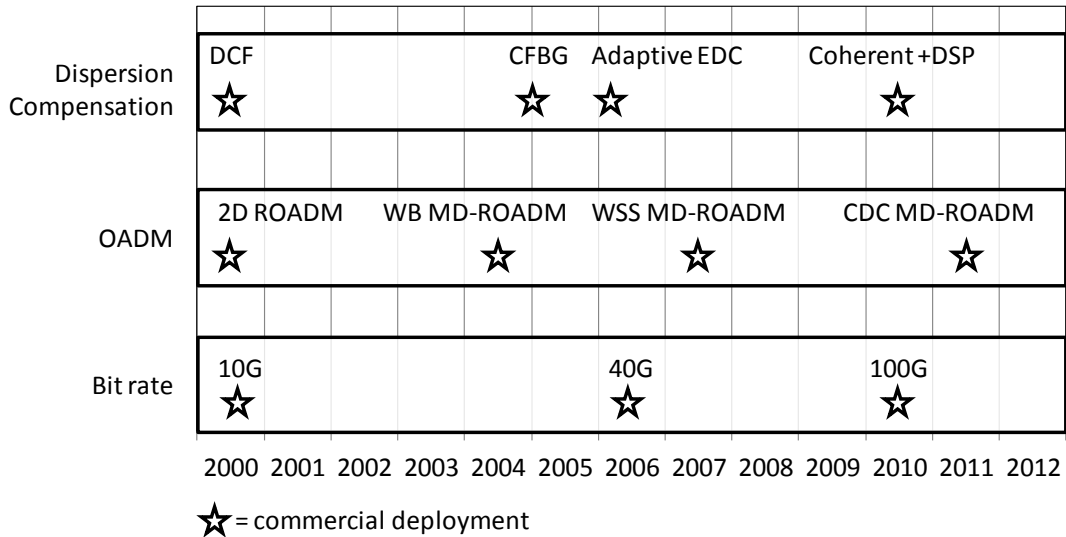


**Figure 4 DWDM technology roadmap 2000-2012**

#### Bit Rate

In 2002 10Gb/s was becoming the widespread deployed line rate of DWDM systems in most core networks as the price of 10Gb/s had reached 2.5× that of the earlier generation 2.5Gb/s i.e. a 4× increase in capacity for 2.5× the cost. Development of the next generation 40Gb/s had started as early as 1999 but the glut of capacity and carrier spending squeeze of 2001-2004 led to a slowdown in 40Gb/s development with commercial deployments delayed until 2006. 40Gb/s still hasn't reached cost parity of 4×10Gb/s at a transponder level due to the complexity of components for advanced phase modulation formats [9], [10] and lack of economy of scale due to the development of many alternative modulation formats. At a network level 40Gb/s can be economical when faced with fibre capacity exhaustion, and the choice of either deploying 40Gb/s transponders on an existing DWDM system, or deploying a parallel 10Gb/s DWDM system on an unlit fibre in order to meet traffic demand.

100Gb/s systems have been in development since 2006 with commercial deployment starting in 2010 following the conclusion of standardisation [11] and initial product releases.

Most of the research presented here is focused on 10Gb/s systems with some work on 40Gb/s systems reported in Chapter 3.

### **Optical Add-Drop Multiplexer (OADM)**

As transmission reach of DWDM systems increased beyond the 600km of first generation LH systems, to 3,000km with ULH systems (which is much greater than the distances between major population centres in most geographies) it has become important to add and drop a subset of traffic at intermediate sites along optical links without the added cost of terminating all traffic. OADMs have enabled the evolution from OEO regenerated point to point links to transparent all-optical meshed networks with optical bypass. First generation reconfigurable OADM (ROADM) based on wavelength blocker (WB) technology was pioneered by Marconi in 2000 and capable of all-optical bypass in 2 fibre directions (2D). Multi-degree ROADM (MD-ROADM) based on WB was first deployed in 2004 and capable of optical bypass in up to 4 directions. Wavelength selective switch (WSS) MD-ROADM were deployed in 2007 and enabled optical bypass in up to 6 directions and was more scalable in cost than its WB MD-ROADM predecessor. Colourless directionless and contentionless (CDC) MD-ROADM emerged in 2011 enabling true remote re-configurability of network bandwidth on demand.

### **Dispersion Compensation**

Dispersion compensating fibre (DCF) became an essential component of DWDM systems with the transition from 2.5Gb/s to 10Gb/s, since the chromatic dispersion (CD) limit on single-mode fibre (SMF) is around 40km at 10Gb/s vs. 640km at 2.5Gb/s. Lower cost alternatives such as chirped fibre Bragg gratings (CFBG) have been deployed from around 2005 [12] and electronic dispersion compensation (EDC) by transmitter pre-distortion pioneered by researchers at Nortel Networks [13], [14] and UCL [15], [16], [17] entered deployment in 2006. Coherent detection and digital signal processing (DSP) has by now become the standard approach to compensate not only CD but polarisation mode dispersion (PMD) and nonlinear effects in emerging 100Gb/s networks [18].

## 1.4 RESEARCH CONTRIBUTIONS

The original research contributions made during the work presented in this thesis are:

1. Developed a combined model of wideband power variation and narrowband nonlinear simulation<sup>7</sup> to accurately model performance in DWDM links.
2. Developed a simplified method for predicting the optimal pre-emphasis profile in nonlinear limited ULH DWDM links [19].
3. Determined the optimum spacing of channel equalising network elements in ULH links and applied the engineering rule to a network field deployment of the world's longest un-regenerated terrestrial DWDM system [20].
4. Investigated the optimal performance and cost of alternative dispersion maps for ELH DWDM links [21].
5. Compared the performance of optical and electronic dispersion compensation strategies, determining the impact of fibre nonlinearities and their interactions with fibre dispersion for 10Gb/s and 40Gb/s transmission with various modulation formats [22].
6. Analysed the cost benefit of EDC vs. DCF in LH and ELH networks [22].
7. Analysed the cost and flexibility advantage to network operators of deploying a single multi-reach DWDM system for core network applications [23].
8. Analysed the economic benefits of increasing levels of optical transparency from OEO regenerated LH DWDM systems to degree-2 ROADM to WB based MD-ROADM to WSS based MD-ROADM [24].

## 1.5 PUBLICATIONS RESULTING FROM THE RESEARCH

The research presented in this thesis resulted in the following publications:

**G. L. Jones**, J. H. B. Nijhof, and W. Forysiak, "Optimisation of 80× 10Gbit/s Ultra long-haul DWDM systems," Proceedings of the London Communications Symposium, 2002.

A. Pratt, P. Harper, S. Alleston, P. Bontemps, B. Charbonnier, W. Forysiak, L. Gleeson, D. Govan, **G. L. Jones**, D. Nettet, J. Nijhof, I. Phillips, M. Stephens, A. Walsh, T. Widdowson, and N. Doran, "5,745 km DWDM transcontinental field trial using 10 Gbit/s dispersion managed solitons and dynamic gain equalization,"

---

<sup>7</sup> Software implementation by Dr Jeroen Nijhof

Optical Fiber Communications Conference, 2003. OFC 2003, 2003, Post-deadline paper PD26.

**G. L. Jones**, “Dispersion maps for extended long-haul DWDM”, UCL Postgraduate Poster Session, London, 2003.

**G. L. Jones**, J. H. B. Nijhof, and W. Forysiak, “Cost and flexibility advantage of a multi haul DWDM platform” Proceedings of the London Communications Symposium, 2003.

**G. L. Jones**, J. H. B. Nijhof, and W. Forysiak, “Economic benefits of all-optical cross connects and multi-haul DWDM systems for European national networks” Optical Fiber Communications Conference, 2004. OFC 2004, 2004, paper WH2.

**G. L. Jones**, “Optimal Transport Layer for Next Generation Networks”, UCL Postgraduate Poster Session, London, 2004.

**G. L. Jones**, J. H. B. Nijhof, and W. Forysiak, “Computational modelling for long-haul transmission system design”, IOP Nonlinear Optics in Communications Meeting, London, 2004.

**G. L. Jones**, J. H. B. Nijhof, R. I. Killey and W. Forysiak, “Comparison of Optical and Electronic Dispersion Compensation Strategies”, IEE (IET) Seminar on Optical Communications and Electronic Signal Processing, London, 2005.

S. K. Nazeer, **G. L. Jones**, P. A. Callan, J. H. B. Nijhof, “Dynamic, impairment-aware GMPLS based, multi bit-rate optical network with two level path protection”, Fotonica Conference, Pisa, 2009.

## 1.6 IMPACT ON THE INDUSTRIAL SPONSOR

The research reported in this thesis has contributed to the development of Ericsson’s market leading Multi-Reach WDM Optical Transport platform *Marconi MHL 3000*, making it a cost-effective solution for a wide range of network applications. This platform was first released in 2003, with ongoing development continuing over subsequent years up to the present time. The majority of the work presented in this thesis was conducted between 2002 and 2006. System and network design improvements have been identified and developed with resulting improvements in transmission performance, system flexibility and cost.

System and network simulation models and algorithms have been developed and integrated in link design and simulation tools, enabling rapid virtual prototyping of new systems and accurate link feasibility assessment for customer network designs.

## **1.7 THESIS STRUCTURE**

This thesis consists of 2 main parts:

1. Chapters 2 and 3 are focused on optimising DWDM system performance and cost through physical layer modelling.
2. Chapters 4 and 5 are focused on optimising DWDM network cost and flexibility through techno-economic analysis of different system and network architectures.

The literature review is integrated within each of chapters 1-5, since each chapter covers quite different subject matter.

### **Chapter 2: Transmission Modelling**

Chapter 2 covers the theoretical background necessary to understand the majority of the rest of the thesis. A comprehensive overview of a commercial DWDM system and its most important sub-systems and components is given. Particular focus is placed on the sources of wideband power variations including the spectral dependence of amplifier gain and noise, stimulated Raman scattering (SRS) tilt and fibre attenuation profile. Techniques for channel power equalisation are introduced including signal power pre-emphasis and dynamic channel equalisation.

The theoretical aspects of light-wave propagation in optical fibre are detailed including key transmission impairments and computer simulation techniques.

A new link simulation approach, combining models of wideband spectral power variations with narrowband nonlinear simulation is detailed, including an overview of the modelling tool framework. This work builds upon the model of wideband spectral power variations previously developed [25].

A simplified method of predicting the optimum pre-emphasis profile to equalise the performance across the C-band in ULH links is proposed and its performance impact analysed.

### **Chapter 3: Dispersion Management Strategies**

Further theoretical background on dispersion compensation is given including DCF and other compensation technologies.

Two alternative dispersion maps are investigated: per span dispersion compensation with DCF after each fibre span, and alternate span dispersion compensation where DCF is consolidated in longer units typically every other span. The resilience of these dispersion maps to interaction with fibre nonlinearities is investigated. An analysis of the potential cost savings by consolidating DCF and eliminating dual stage amplifiers (DSA) is presented.

Strategies for electronic and optical dispersion compensation are investigated including a comparison of nonlinear performance between lumping dispersion compensation at either or both ends of a transmission link and standard in line dispersion compensation. An economic analysis of the cost benefits of introducing EDC in LH DWDM systems with the resulting redundancy of DSAs and DCF is presented.

#### **Chapter 4: Developing a Flexible WDM System**

The concept of a multi-reach WDM platform is introduced as a system capable of addressing previously separate network domains of metro, LH, ELH and ULH using a common platform of modular system elements.

A techno-economic analysis is presented which demonstrates the low initial and incremental upgrade cost achievable with a multi-reach platform in a typical national ring network.

#### **Chapter 5: Transparent Meshed Networks**

The evolution of WDM networks from point to point OEO regenerated LH systems towards meshed all-optical networks with optical bypass enabled by MD-ROADMs is described. Node architectures are presented for multi-degree nodes ranging from degree-2 to degree-5 with technology evolution from WB to WSS.

An analysis of the economic benefits of optical transparency in a European national network is presented.

#### **Chapter 6: Summary and Conclusions**

The main conclusions of this thesis are summarised including their significance and contribution to existing theory and practice, and impact on the industrial sponsor and wider industry. Finally the limitations of the research are discussed together with recommendations for further research and development work.

## 2 TRANSMISSION MODELLING

This chapter is mainly focused on optimising the PERFORMANCE of WDM systems. Performance optimisation is traded off against COST by optimising channel power equalisation in ULH DWDM links. The research resulted in publication [19] and contributed towards an OFC post-deadline paper [20].

### 2.1 INTRODUCTION

Commercial terrestrial ULH DWDM systems were first developed around 2000 with the aim of significantly reducing the unit cost (\$/Gb/s/km) of data transport [26]. These systems had capacities of 80 or more DWDM channels in a single fibre pair with un-regenerated transmission over distances up to 3,000km. By increasing the un-regenerated transmission distance from the 600km of standard LH DWDM systems, significant cost savings could be achieved due to the reduction in OEO regeneration equipment required for each DWDM channel.

The research presented in this chapter, carried out over the period 2002-2003, played a key role in the design of Ericsson's (then Marconi) ULH DWDM system named *UPLx160* and its first field deployment in 2003 over a 3,000km link between Perth and Adelaide, Australia [20].

ULH DWDM systems initially operated at line rates of 10Gb/s and were based upon a number of enabling technologies outlined in [27] including: return-to-zero (RZ) modulation, dispersion management, forward error correction (FEC) [28], dynamic gain equalisation (DGE), gain flattened erbium doped fibre amplifiers (EDFA) and / or distributed Raman amplification (EDFA only is assumed in this thesis).

In dispersion management group velocity dispersion (GVD) is managed to carefully balance the nonlinear effect of self-phase modulation (SPM) in optical fibre.

Advanced modulation formats have since enabled LH and ULH transmission at higher line rates of 40Gb/s and 100Gb/s by encoding information within the polarisation and / or phase of the signal [10].

### 2.2 MOTIVATION

The main motivation for the research presented in this chapter is to optimise and equalise the performance across many (80+) DWDM wavelengths, densely spaced

(50GHz) over a large bandwidth in the C-band on the ITU<sup>8</sup> frequency grid, enabling ULH transmission reach of up to 3,000km between OEO regeneration. Equalising performance can mitigate the effect of transmission impairments leading to improved transmission reach and performance margin. The increased reach can be used to remove unnecessary and costly OEO regeneration or the increased margin can be traded-off with cost by selecting lower specification and cheaper component options.

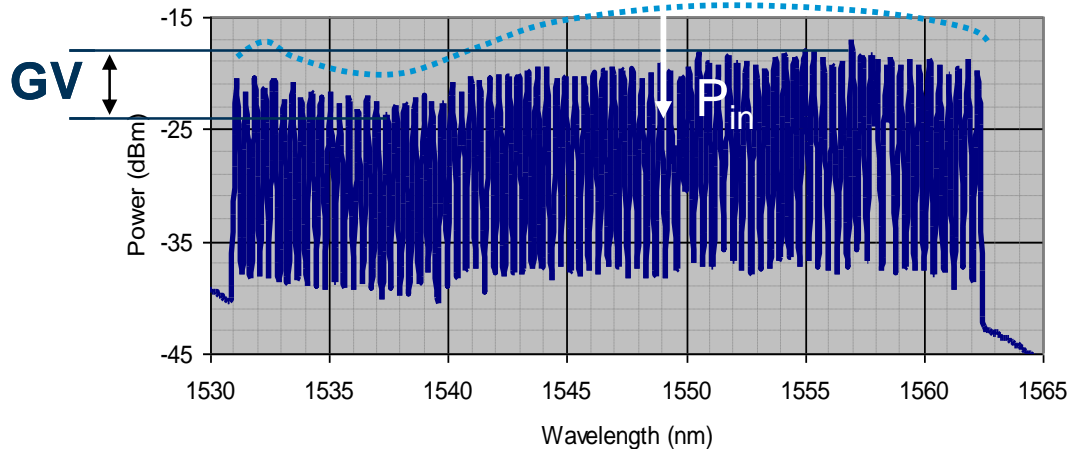


**Figure 5 Gain variation (GV) across a spectrum of DWDM channels<sup>9</sup>**

Optimum performance of a ULH DWDM system requires equalisation of OSNR and power variations across a wide spectrum of DWDM channels to minimise transmission penalties due to nonlinear effects and gain variation (GV) caused by SRS tilt, EDFA gain tilt and ripple and fibre attenuation profile as illustrated in Figure 5. Pre-emphasis at the transmitter end of an optical communications link has long been proposed [29], and demonstrated experimentally [30] to overcome the effects of GV. More recently the technique has been implemented as a solution for performance optimisation of long chains of optical amplifiers in commercial ULH DWDM optical transport systems [20] and [31] where the procedure is enhanced by periodic per channel power equalisation (re-emphasis) at intermediate locations.

Pre-emphasis can be configured to equalise either the power spectrum or OSNR spectrum at the end of a link, an analysis of power and OSNR equalisation is given in [32] and [33]. OSNR equalisation pre-emphasis requires OSNR monitoring [34] and does not guarantee a flat power spectrum and therefore power dependent nonlinear penalties are likely to differ resulting in signal quality (Q-factor) and bit error rate

<sup>8</sup> ITU = International Telecommunications Union

<sup>9</sup> Source: Ericsson

(BER) variations across the spectrum of DWDM channels. Q-factor equalisation pre-emphasis can be achieved but requires lengthy nonlinear simulations to determine the optimum pre-emphasis profile offline at the time of commissioning the link. Subsequent research has recently led to successful implementation of automated BER equalisation schemes [35], [36].

Optimum pre-emphasis profiles can be determined by faster linear OSNR calculations which are more suitable from an operational perspective for commercial networks. It is therefore necessary to investigate the nonlinear penalty induced when OSNR equalisation pre-emphasis is applied to a ULH system which is operating in a nonlinear regime.

Predicting the optimum pre-emphasis profile by modelling techniques enables networks to be deployed using design rules quickly and accurately determined in advance. A simplified commissioning procedure is preferable to reduce operational cost with automated adjustment of pre-emphasis profiles by the network management system as channels are added or removed from a system with resulting changes in channel power variations.

## 2.3 RESEARCH CONTRIBUTIONS

### **Combined Model of Wideband Power Variations and Nonlinear Simulation**

A new system modelling approach was developed<sup>10</sup>, combining nonlinear simulations with a wideband spectrally dependent model of power variation and noise accumulation in amplified DWDM systems. Nonlinear simulations are usually performed over a narrow bandwidth since the dominant effects are intra-channel and inter-channel interactions with nearest neighbours. Computation time increases significantly with the number of channels and errors are within acceptable limits when simulating around 6 neighbouring channels, therefore it is reasonable to simulate narrowband.

Because of power variations due to gain and loss tilts, some channels will suffer nonlinear effects to a greater extent than other channels, resulting in different nonlinear penalties across the C-band [35]. It is therefore important to take into

---

<sup>10</sup> The wideband power variation and OSNR model was initially developed by the author and published in [25]. The combined wideband power variation and nonlinear simulation tool was implemented by Dr Jeroen Nijhof.

account the power variations between channels across the band when carrying out full nonlinear simulations. By combining the wideband power variation model and nonlinear simulation techniques this issue is investigated effectively to provide insight to system design and definition of engineering rules.

### **Simplified Pre-emphasis Prediction**

Using the modelling framework developed above, the transmission performance of a ULH system with the optimum pre-emphasis profile predicted by the combined nonlinear simulation and wideband power variation model is compared with the performance using the pre-emphasis profile predicted by the linear wideband model alone. Results show little performance penalty using the pre-emphasis predicted by the linear wideband model. In conclusion simple and fast linear calculations can be relied upon to determine an optimum pre-emphasis with little performance penalty with respect to full nonlinear simulations; this work resulted in publication [19].

### **Optimising Dynamic Gain Equalisation**

The optimum location of dynamic gain equalising network elements along an ULH DWDM transmission link was investigated with the objective of minimising the network infrastructure cost while optimising transmission performance across all channels. Recommendations were adopted in the design of a commercial ULH DWDM system setting link engineering rules which resulted in significant cost reduction at the network level. The rules were implemented in the first field deployment of the ULH system which at the time in 2002 was the world's longest un-regenerated terrestrial optical transmission link<sup>11</sup> and contributed to publication [20]. Actual system performance characteristics were found to be in good agreement with modelling predictions.

## **2.4 CHAPTER OUTLINE**

An overview of a DWDM system and its most important sub-systems and components is given in section 2.5 together with an overview of DWDM system modelling approaches and transmission impairments. Section 2.6 provides details on the transponder, including transmitter, receiver, modulation and FEC. Section 2.7 provides details on the EDFA principle of operation and design, including models for

---

<sup>11</sup> Source: [http://www.lightreading.com/document.asp?doc\\_id=13172](http://www.lightreading.com/document.asp?doc_id=13172)

the spectral dependence of gain and noise figure tilt and ripple. Section 2.8 discusses channel power and OSNR equalisation, the levelling sub-system and pre-emphasis techniques.

The relevant theoretical aspects of light-wave propagation in optical fibre are detailed in section 2.9, including key transmission impairments, and computer simulation methods. Section 2.10 provides details on the measurement of Q-factor and BER performance from nonlinear simulations, and estimation of Q-factor and BER from OSNR calculations.

The simulation approach combining models of wideband spectral power variations with narrowband nonlinear simulations is outlined in section 2.11 including an overview of the modelling toolset.

Remaining sections detail results and analysis of various studies optimising the performance and cost of DWDM systems:

- Spectral OSNR modelling and comparison with system test results in section 2.12.
- Prediction of the optimum pre-emphasis profile in section 2.13.
- Modelling a ULH network for field deployment in section 2.14

Finally section 2.15 summarises the main conclusions of the research presented in this chapter.

## 2.5 DWDM SYSTEM ARCHITECTURE OVERVIEW

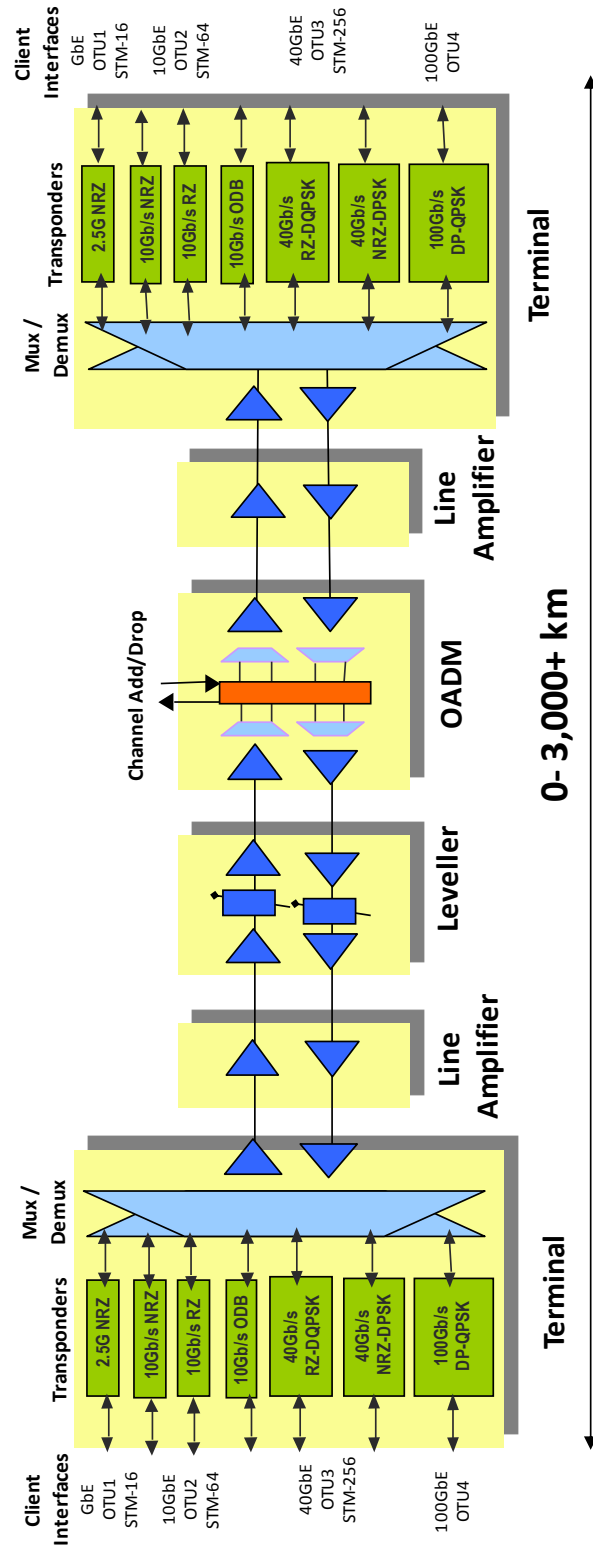


Figure 6 Architecture of a DWDM system<sup>12</sup>

<sup>12</sup> Source: Ericsson (adapted from an Ericsson diagram)

Figure 6 shows the high-level architecture of a typical DWDM line system comprising of 4 different types of network elements: terminals, line amplifiers, levelling amplifiers and OADMs.

Terminals, also called optical line terminals (OLT) form the end points of a point-to-point DWDM line system. Terminals accommodate transponder cards which are a bi-directional transmit and receive unit described in detail in section 2.6. A multiplexer (mux) combines individual wavelength signals from each transponder into a common fibre pair for DWDM transmission, a de-multiplexer (demux) performs the reverse operation; typically they are based on arrayed waveguide grating (AWG) or thin film filters.

Line amplifiers, also called optical line amplifiers (OLA) are placed after each fibre span (where no traffic is to be added and dropped) simply to amplify signals following the loss of a fibre span. The EDFA is the most common type of optical amplifier and its usage is assumed throughout this thesis; section 2.7 provides detailed background on the EDFA.

Levelling amplifiers, also called optical line levellers (OLL) are placed approximately after every 8<sup>th</sup> fibre span to perform DGE to compensate for channel to channel power variations and tilt; section 2.8 provides detailed background on channel equalisation and the OLL sub-system.

OADMs are deployed at locations where traffic is to be added and dropped from the DWDM multiplex. OADMs are explored in detail in chapters 4 and 5 in the context of wavelength routed optical network design.

Optical fibre forms the link between each node in the network; the physical impairments of the optical fibre channel are described in detail in section 2.9. Dispersion compensation is required periodically along the link; chapter 3 covers dispersion compensation in detail.

### **2.5.1 SYSTEM MODEL OVERVIEW**

Figure 7 shows schematically a model of a DWDM system. Starting with a transmitter (Tx) with optional (but commonly deployed) FEC, the signal is modulated; either 10Gb/s intensity modulated NRZ or RZ, or 40Gb/s phase modulated RZ differential Quadrature phase shift keying (RZ-DQPSK). A transmit

EDFA boosts the signal power launching into the transmission fibre which in the process adds amplified spontaneous emission (ASE) noise to the signal.

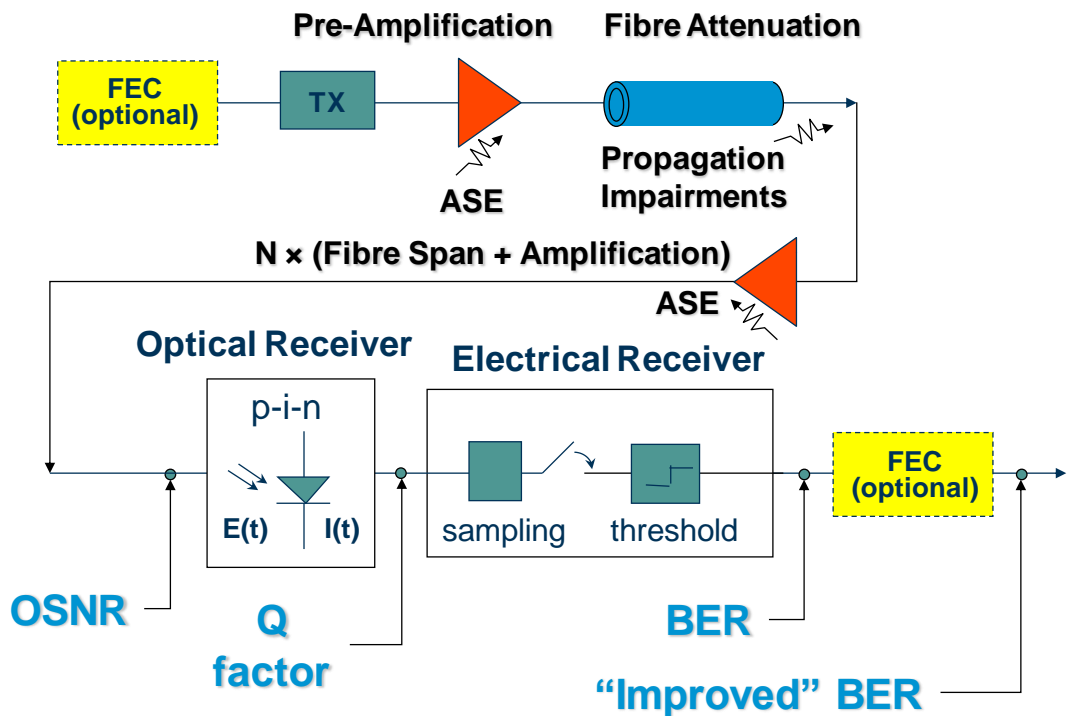


Figure 7 Schematic of DWDM system model<sup>13</sup>

As the signal propagates through the  $N$  spans of transmission fibre it is subject to attenuation of the optical power and various linear and nonlinear propagation impairments including GVD, Kerr nonlinear effects, scattering nonlinear effects and polarisation effects.

Lumped optical amplification at the end of each span with EDFA restores the optical signal power but adds ASE noise to the signal thus degrading the OSNR. Dispersion compensation is also performed periodically at intermediate nodes in addition to at the transmitting and receiving terminals.

At the receiver typically direct detection is used, whereby the optical signal is demultiplexed and optically filtered before detection by a pin photodiode where the optical field is converted to a current through square law detection thus losing the phase information. Receiver performance is characterised by an OSNR which is required to obtain a certain Q-factor or BER. An electric receiver samples the signal measuring it against a threshold to determine if the received bit is a 0 or a 1. At this point the BER is the ratio of the number of bits received in error i.e. a 1 when it

<sup>13</sup> Source: Ericsson

should have been a 0 or vice versa) and the total number of bits received. FEC is used to correct the received BER resulting in a significantly improved BER. The BER is compared to a required BER to determine the system margin and ultimately the maximum transmission reach before OEO regeneration is required.

Numerical simulations are the most accurate method of optical link performance evaluation. There are many different system parameters which must be considered including: power per channel, channel spacing, number of channels, signal modulation format, transmission distance (individual span lengths, and number of spans), amplification scheme, fibre chromatic dispersion, dispersion compensation scheme, fibre PMD, and fibre nonlinear coefficient. The lengthy computation time of numerical simulations combined with the vast parameter space has led to the development of analytical models of many transmission impairments. Faster analytical models are preferred for link design where many design options need to be analysed and trade-off of performance and cost under tight timescales; an example approach is given in section 2.10.2. However for the transmission studies carried out in chapters 2 and 3, numerical simulations are preferred due to their accuracy.

## **2.6 TRANSPONDER**

This section gives an overview of the main functions of a DWDM transponder, including: transmitters, modulators, forward error correction (FEC), receivers and modulation formats. There are many possible modulation formats which can be used in DWDM transmission systems [10] however this thesis will focus on those formats which are most widely deployed in commercial systems: RZ and NRZ on-off keying (OOK) at 10Gb/s and RZ-DQPSK at 40Gb/s (all defined later).

### **2.6.1 TRANSMITTERS**

DWDM transmitters are typically based on distributed feedback (DFB) lasers which offer narrow linewidth and wideband tunability; these are desirable characteristics for improved performance and deployment flexibility respectively.

### **2.6.2 MODULATORS**

The simplest form of modulation is intensity based modulation known as OOK whereby the data bit pattern is encoded onto the laser signal; this can be accomplished either by direct modulation or external modulation.

In direct modulation lasers (DML) the bit pattern is encoded onto the signal by directly modulating the laser drive current i.e. switching the transmitter laser on and off. Direct modulation is the simplest and cheapest form of modulation and is typically used in 2.5Gb/s and short reach, low cost 10Gb/s small form factor pluggable (XFP) transponder modules. Direct modulation has a number of performance disadvantages including frequency chirp which broadens the signal, and low extinction ratio (the ratio of power in a 1 bit to the power in a 0 bit).

External modulation is preferred for long-haul and high speed applications due to their improved performance with little or no frequency chirp and higher extinction ratio. A continuous wave (CW) laser output is switched on and off by altering the drive current of the external modulator. The most widely deployed external modulator is the Mach-Zehnder modulator (MZM). A MZM consist of two waveguide arms joined by 3dB couplers onto a common waveguide at each end. The incoming CW signal is split into two waveguide paths by a 3dB coupler; the waveguides are typically constructed from lithium niobate ( $\text{LiNbO}_3$ ) or indium phosphide (InP). A voltage is applied to electrodes on each waveguide arm which alters the refractive index and thus the relative velocity of light through each path, resulting in either constructive or destructive interference at the 3dB coupler at the modulator output. MZM have the advantages of wavelength independent modulation characteristics, high extinction ratio and low insertion loss [10].

### 2.6.3 OOK MODULATION FORMATS: RZ AND NRZ

At 10Gb/s the most common signal modulation formats are OOK NRZ and RZ; bit streams encoded with these formats are illustrated schematically in Figure 8. For RZ generation a pulse carver is required in addition to the data modulator as illustrated in Figure 9, this added complexity increases the cost of RZ compared to NRZ.

With NRZ modulation a pulse representing a 1 bit occupies the entire bit slot whereas the absence of a pulse represents a 0 bit. With RZ modulation a pulse representing a 1 occupies a fraction of the bit slot called the duty cycle, as with NRZ a 0 bit is represented by the absence of a pulse across the whole bit slot.

Each channel is intensity modulated with bit rate  $R = 1/T$ , where  $T$  is the bit period. The 1's are transmitted using pulses with duration  $\rho T$  where  $\rho$  is the duty cycle; with NRZ modulation  $\rho = 1$ , and with RZ modulation  $0 < \rho < 1$ .

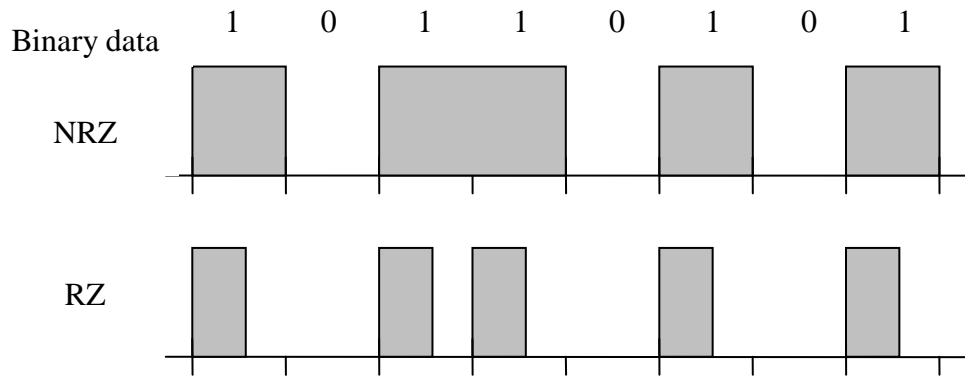


Figure 8 Equivalent OOK NRZ and RZ bit patterns

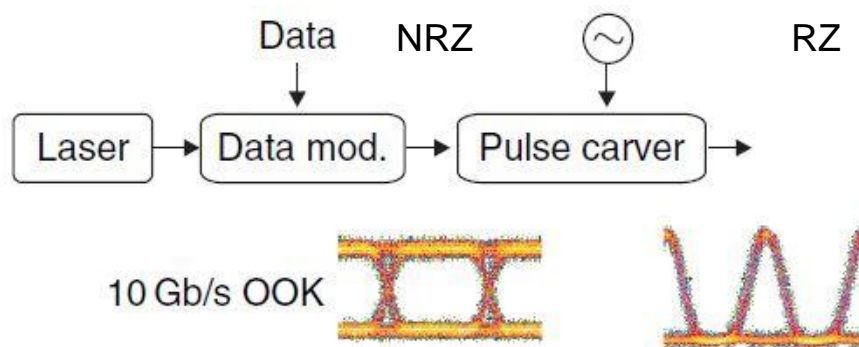


Figure 9 Basic architecture of an RZ transmitter consisting of a laser source, external modulator and RZ pulse carver (This figure was published in [37], page 55, Figure 2.16, Copyright © 2008, Elsevier. Permission to reproduce this figure has been granted by Elsevier).

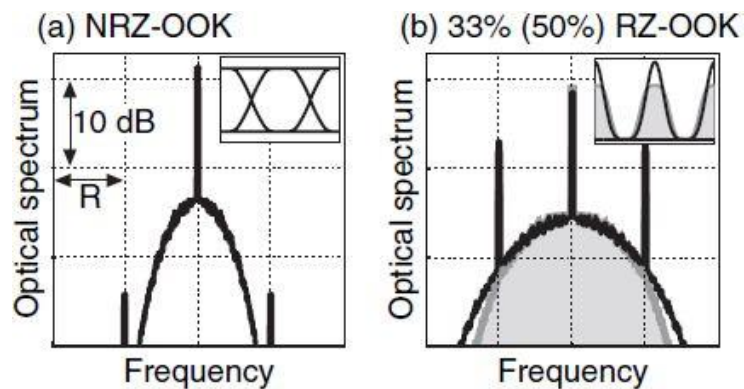


Figure 10 Pulse spectra for (a) NRZ OOK and (b) RZ OOK (33% duty cycle RZ in black and 50% duty cycle RZ in grey) (This figure was published in [37], page 50, Figure 2.14, Copyright © 2008, Elsevier. Permission to reproduce this figure has been granted by Elsevier).

Figure 10 shows the corresponding pulse spectra for OOK NRZ and RZ modulation formats; modulation sidebands occur at 10GHz and spectral components at multiples of 10GHz. RZ with longer duty cycles (50%) are preferred since a narrower optical spectrum is produced than at shorter duty cycles (33%), (see Figure 10 (b)) however peak power is reduced with increased duty cycle.

Advantages of RZ include improved tolerance to fibre nonlinear effects and PMD; however the wider spectrum incurs higher filtering penalties versus NRZ making it less suitable for spectral efficiency beyond 10Gb/s. RZ also has improved OSNR performance over NRZ: with narrower RZ pulse widths the detector integrates over the whole of the pulse whereas part of the signal is lost with NRZ due to the finite rise and fall time; with the same integration time the same amount of noise is captured in both cases resulting in reduced OSNR for NRZ.

The main advantage of NRZ is that the signal occupies a much smaller bandwidth than RZ (typically half as much) as shown in Figure 10 and therefore has lower walk-off effects improving dispersion tolerance.

The main disadvantage of NRZ is its lower nonlinear tolerance which places an upper limit on the optimum signal power thus limiting transmission distance. Another disadvantage of NRZ is that there are no transitions in long strings of 1's or 0's making it more difficult for the receiver to perform clock recovery. RZ reduces this problem since long strings of 1's produce transitions (however long strings of 0's do not).

### **Cost**

RZ modulation is more complex and costly to implement than NRZ as an external modulator and additional pulse carver is required in initial designs as shown in Figure 9. Alternatively a more recently developed electrical RZ transponder is implemented with a single MZM driven by an RZ electrical signal; this has significantly simplified and reduced the cost of RZ transponders. Due to this and other developments the cost difference between RZ and NRZ has narrowed significantly: in 2004 the relative cost multiple of a 10Gb/s RZ and NRZ transponder was 1.6 to 1, by 2008 the cost multiple had reduced to 1.1 to 1.

Over the last decade 10Gb/s technology has matured with significantly increased manufacturing volumes accompanied by year on year cost erosion equivalent to a

compound annual growth rate (CAGR) of approximately -20%. Over this period there has been a significant shift from vertically integrated network equipment vendors producing their own transponders based on discrete optical components to outsourced development by optical component vendors producing standardised multi source agreement (MSA) transponder modules.

### Transmission Reach

Transmission reach depends strongly on the modulation format and specification of the transmitters and receivers as shown in Table 1. These figures are approximate best case reaches; actual reach depends on details of individual fibre spans (length, loss, fibre type, CD, PMD), number of spans and signal power. Different amplification technology also plays an important part in determining reach: e.g. hybrid EDFA + Raman offers improved reach compared to EDFA only, due to their lower effective noise figure. The network cost impact of varying reach for different modulation formats and amplifier types is investigated in chapters 4 and 5.

<b>Transponder</b>	<b>Approximate Reach</b>
10Gb/s XFP (NRZ)	up to 1,000km
10Gb/s NRZ	up to 1,500km
10Gb/s RZ	up to 3,000km

**Table 1 10Gb/s transponder approximate transmission reach**

## 2.6.4 TRANSPONDER FUNCTION AND ARCHITECTURE

### Transponder Function

A DWDM transponder is a bi-directional interface unit, with independent traffic paths for transmit (client to WDM) and receive traffic (WDM to client). The architecture described here is based on a 10Gb/s transponder however the principles are much the same at higher bit rates.

The transponder maps the client signal (SDH, OTN, Ethernet or IP) to the payload of an optical channel, adding the optical channel overhead and FEC overhead. For 10Gb/s the resultant data stream is then converted to an NRZ or RZ encoded optical

signal, depending on the transponder variant, with a user selectable wavelength, 80 channels tuneable in the C-Band.

### Transponder Modules

The transponder can house factory pluggable 300pin MSA modules with either NRZ or RZ modulation or a hot-pluggable XFP module (NRZ), either tuneable or fixed wavelength. Tuneable interface modules are more expensive, but benefits include simplifying network operations by reducing the required inventory and enabling rapid maintenance and deployment of new links; a single module variant can be tuned to the frequency required for the network configuration.

Transponder modules have evolved from 300pin MSA modules of approximately 115×89×12mm to tuneable XFP modules of approximately 78×19×9mm: a reduction in volume of almost a factor of 10. Tuneable 10Gb/s SFP+ are expected to emerge in 2012, reducing the module footprint to 56.5×13.4×8.5mm; a further factor of 2 reduction in volume.

### Transponder Architecture

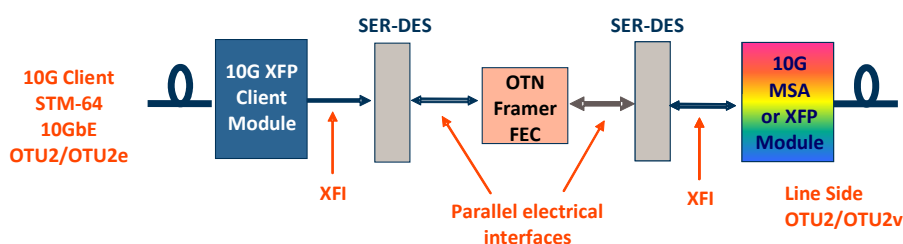


Figure 11 10G transponder architecture<sup>14</sup>

Figure 11 illustrates the architecture of a 10G transponder card. In ingress direction (west to east) the optical client signal is converted into electrical format by an XFP hot pluggable transceiver (so called grey interface i.e. non DWDM). Via the XFI interfaces (a standard 10G chip-to-chip electrical interface) the client signal is sent to a Serialiser / De-Serialiser (SER-DES) where the serial data stream is converted into multiple parallel electrical signals suitable to be put in ingress to the OTN framer. The OTN framer adds the digital wrapper to the client signals and sends the data streams to the line side module via the SER-DES. In the egress (east to west) direction the opposite operations are performed.

<sup>14</sup> Source: Ericsson

The overhead information transported within the optical channel supports the monitoring and control of optical channels within the context of OTN. The DWDM line side supports enhanced FEC (eFEC) for improved reach or standard G.709 FEC (G.FEC). OEO regeneration can be performed via a pair of transponders linked in a back to back configuration.

### 2.6.5 PHASE MODULATION FORMATS: RZ-DQPSK & NRZ-DPSK

Various modulation formats have been adopted at 40Gb/s since its initial commercial introduction in 2006, resulting in a notoriously fragmented market [38]. By today RZ-DQPSK is the most widely deployed modulation format in commercial systems [39] and NRZ differential phase shift keying (DPSK) is the next most widely deployed format. Initial 40Gb/s deployments adopted the optical duo-binary (ODB) modulation format due to its simplicity, low cost and commercial availability, however the more robust modulation formats mentioned above are now readily available and ODB is not favoured and therefore will not be analysed in this thesis.

In chapter 3 investigations into optical and electronic dispersion compensation strategies, 10Gb/s and 40Gb/s RZ-DQPSK transmission is analysed.

DQPSK is a multi-level modulation format which transmits four different phase shifts  $\{0, +\pi/2, -\pi/2, +\pi\}$  at a symbol rate of half the aggregate bit rate [10]. The field constellation diagram in Figure 12 shows these phase states compared to those for OOK and DPSK modulation.

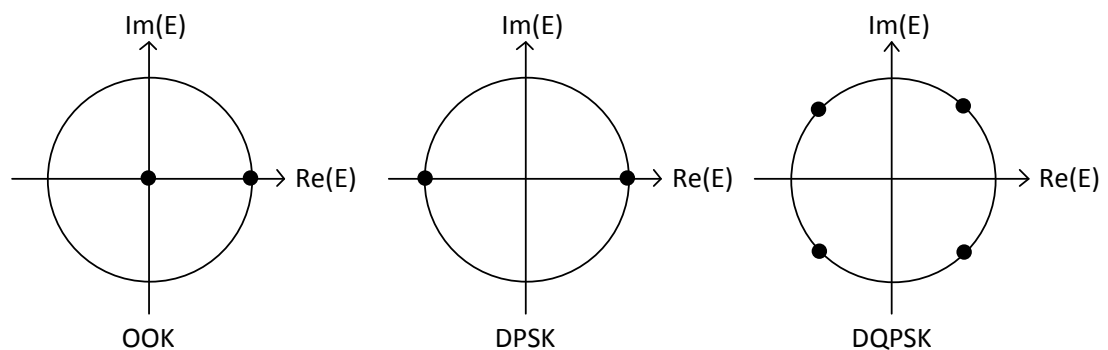


Figure 12 Field constellation diagrams for OOK, DPSK and DQPSK

RZ-DQPSK has not been widely adopted at 10Gb/s since RZ OOK provides adequate reach however the lower baud rate of RZ-DQPSK does improve dispersion tolerance.

DPSK does have an approximately 3dB OSNR sensitivity advantage compared to OOK [40] and approximately 1-2dB advantage over RZ-DQPSK [10]. The greatest disadvantage of DPSK is a significantly broader spectrum than RZ-DQPSK as shown in Figure 13, which becomes problematic at 40Gb/s since the spectrum is wide relative to 50GHz spaced ROADMs, incurring significant penalties for each ROADM the signal passes through. The requirement for compatibility with 50GHz ROADMs the signal passes through is important since it means existing 10Gb/s optimised links can be easily upgraded with 40Gb/s transponders. RZ-DQPSK has a much narrower spectrum thus is more compatible with 50GHz network infrastructure; this thesis will therefore focus on RZ-DQPSK for 40Gb/s transmission.

Due to its reduced symbol rate RZ-DQPSK is also more robust to PMD which is a significant performance limiting transmission impairment on poor quality fibre. RZ-DQPSK is more complex due to the number of optical components required for implementation (2 nested MZM as phase modulators and a pulse carver for the transmitter, and 2 delay interferometers and 4 photodiodes for the receiver [10]). Component costs continue to fall due to increased manufacturing volume, photonic integration and design improvements making RZ-DQPSK economically viable for today's LH 40Gb/s networks. 40Gb/s RZ-DQPSK has a transmission reach performance of as much as 1,500km under optimal link conditions.

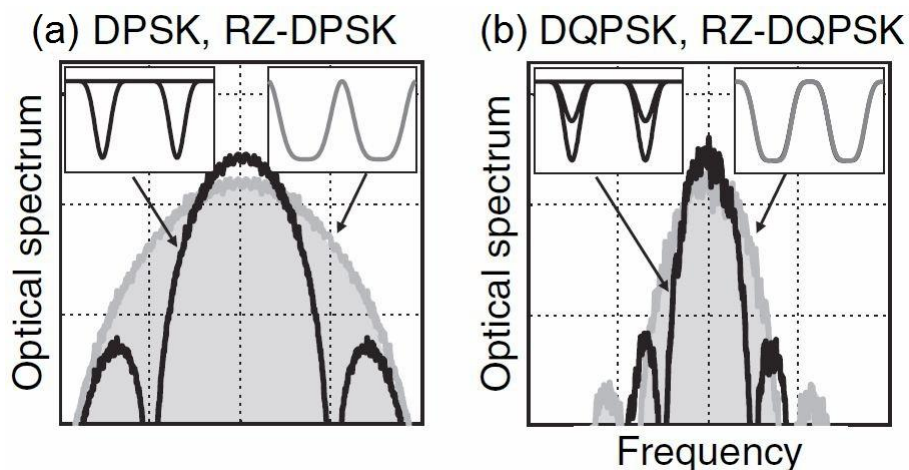


Figure 13 Pulse spectra for (a) DPSK and (b) DQPSK (NRZ versions in black and RZ versions in grey), (This figure was published in [37], page 50, Figure 2.14, Copyright © 2008 Elsevier. Permission to reproduce this figure has been granted by Elsevier).

### 2.6.6 FORWARD ERROR CORRECTION (FEC)

FEC is used in LH and ULH systems to correct errors due to transmission impairments and to reduce the required BER so that transmission reach can be

increased. A FEC encoder introduces coding on the transmitted bit sequence, usually by adding additional bits to produce encoded data at a higher line rate (out-of-band FEC). Standard FEC overhead is 7% which increases the transmitted bit rate of 10Gb/s to 10.7Gb/s or from 40Gb/s to 42.8Gb/s. At the receiver a FEC decoder uses the redundancy to correct the received data payload to that of the input sequence. Further details on the error correcting capabilities of FEC are given in section 2.10.4.

## 2.7 ERBIUM-DOPED FIBRE AMPLIFIER (EDFA)

The EDFA is a key technology enabling modern WDM systems [41]; reference [42] provides a detailed overview of the EDFA and reference [26] provides sufficient background information on the EDFA for the purpose of understanding this thesis. EDFAs are capable of simultaneously amplifying all channels in a WDM system over bandwidths of around 30nm, most commonly over the C-band between 1530 and 1560nm. EDFAs can compensate fibre attenuation losses for spans of around 80km (20dB at 0.25dB/km) and higher. EDFAs are bit-rate and modulation format independent in contrast to the alternative of OEO regeneration.

### Principle of EDFA Operation

The energy levels of  $\text{Er}^{3+}$  ions of the rare earth element erbium in silica glass are shown in Figure 14, and are labelled  $E_1$ ,  $E_2$  and  $E_3$  in order of increasing energy.

Pumping by an external laser creates a population inversion thus a signal can be amplified by stimulated emission. Pumping at 980nm results in carrier absorption from the ground level  $E_1$  to the third level  $E_3$ ; ions in  $E_3$  will quickly transit to level  $E_2$  due to phonon relaxation with a relatively short lifetime of  $1\mu\text{s}$ . Pumping at 1480nm results in carrier absorption from the ground level  $E_1$  to the second level  $E_2$ .

A photon from the input signal incident on an erbium ion stimulates it to fall back to the lower energy level while also emitting a photon of the same frequency and state of polarisation, thus providing signal gain.

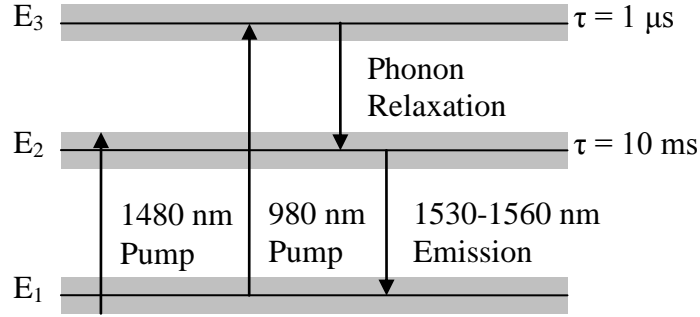


**Figure 14** Energy levels of  $\text{Er}^{3+}$  ions in silica glass

Due to the non-crystalline nature of silica the energy levels are not discrete levels but in fact spread into bands by the Stark splitting effect thus enabling amplification over a large signal bandwidth rather than at a single wavelength.

Spontaneous emission also occurs in EDFAs whereby an ion in energy level  $E_2$  spontaneously falls back to the ground level  $E_1$  emitting a photon with an arbitrary frequency and state of polarisation which is amplified causing amplified spontaneous emission (ASE). ASE noise is added to the amplified signal thus reducing the OSNR.

The noise performance of an optical amplifier is characterised by a noise figure  $F$  given by

$$F = \frac{OSNR_{input}}{OSNR_{output}}$$

**Equation 1**

where  $OSNR_{input}$  and  $OSNR_{output}$  are the OSNR at the input and output of the amplifier respectively.

The noise figure is related to the spontaneous emission factor  $n_{sp} = N_2 / (N_2 - N_1)$  by [43]

$$F = 2n_{sp} \left( \frac{G - 1}{G} \right) \cong 2n_{sp} \geq 2$$

**Equation 2**

where  $N_1$  and  $N_2$  are the population density of  $\text{Er}^{3+}$  ions in the energy states  $E_1$  and  $E_2$  respectively. The minimum noise figure is 3dB since  $n_{sp} \geq 1.0$  however practical EDFA noise figures are generally between 4 and 6dB.

### 2.7.1 EDFA ARCHITECTURE

The architecture of a basic EDFA is shown in Figure 15. It consists of two lengths of silica fibre doped with  $\text{Er}^{3+}$  ions of the rare earth element Erbium; Erbium-Doped Fibre (EDF). The EDF is pumped using pump lasers with wavelengths of 1480nm or 980nm. A wavelength selective coupler (WDM) combines the pump with the input signal which is to be amplified.

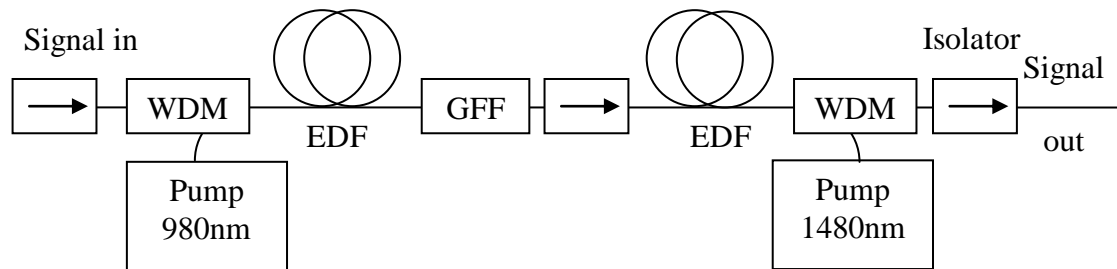


**Figure 15 Architecture of a basic EDFA comprising two stages of EDF**

A gain-flattening filter (GFF) commonly based on dielectric thin-film filter technology is included between the EDF coils in order to achieve the specified gain flatness across the amplifier's gain bandwidth.

The main input and output ports of the EDFA contain optical isolators to limit the backward travelling ASE and to prevent lasing action. An additional isolator is embedded in the amplifier for improved noise figure performance.

Important amplifier characteristics from a ULH system design perspective include: low noise figure, high gain, large output power, gain flatness and a large gain bandwidth.

#### **980nm Pumping Improves Noise Figure**

980nm pumping is more efficient i.e. uses less pump power for a particular gain than 1480nm pumping since the emission cross section is zero at 980nm. A higher population inversion is achieved by 980nm pumping which leads to a lower noise figure.

#### **1480nm Pumping Improves Power Output**

Higher power efficiency can be achieved with 1480nm pumping since excitation to the energy level  $E_3$  with subsequent energy loss through phonon relaxation to energy level  $E_2$  does not occur as is the case for 980nm pumping. However, longer EDF coils are required due to the reduced gain efficiency of 1480nm pumping.

## 2.7.2 EDFA DESIGN AND SPECIFICATIONS

The ULH DWDM system *UPLx160* can be configured using four different varieties of EDFA in the C-band, chosen to cover a wide range of span losses.

Improved noise performance for high loss spans can be achieved in conjunction with 10dB Raman gain. Systems based on Raman amplification are not studied in this thesis since hybrid EDFA/Raman amplifiers are expensive and despite improving transmission reach, the \$/Gb/s/km increases compared to EDFA only<sup>15</sup>.

### C-band EDFA

The four C-band EDFA variants whose specifications are shown in Table 2 consist of two single stage amplifiers (SSA), and two dual stage amplifiers (DSA), where the suffix '17dB' or '21dB' indicate the span loss for which the amplifier is optimised.

Amplifier	Operating Gain (dB)	Span Loss (dB)	Noise Figure (dB)	Mid Stage Access (dB)	Output power (dB)**	Gain tilt (dB)
1. SSA-17dB	20.2	10 - 17	5 - 9	-	21.6	-1.6
2. SSA-21dB	24.2	17 - 21	4.5 - 7	-	21.6	-1.6
3. DSA-17dB	20.2	10 - 17	6.8-9.8	12.4	21.6	-2.2
4. DSA-21dB	24.2	17 - 21	5.8-7.5	12.4	21.6	-2.2

\*\*Total output power, 80 channels end-of-life.

**Table 2 EDFA specification summary for ULH DWDM system<sup>16</sup>**

The SSA variants are used as line amplifiers where no DCF is required; in addition the SSA-17 variant is also used on the drop path of OADM nodes and at levelling nodes to compensate for filtering losses.

The two DSA variants consist of separate pre-amplifier gain blocks and a booster amplifier gain block common to both variants. Mid stage access is 12.4dB to accommodate DCF.

The DSA are used at terminals and line amplifiers where DCF is required; in addition the DSA-21 amplifier is used on the through path of OADM nodes to compensate for the mux/demux and filter losses.

### L-band EDFA

A complementary set of amplifiers exists in the L-band with similar specifications enabling transmission of a total 160 DWDM channels. However L-band systems are

<sup>15</sup> Source: Ericsson internal study

<sup>16</sup> Source: Ericsson

rarely deployed due to the increased cost of components which do not benefit from the same degree of economy of scale as the C-band. L-band performance is also degraded due to inefficiencies in L-band amplifiers.

L-band WDM systems are preferred for deployment on G.653 fibre since the zero dispersion in the C-band with such fibres results in undesirable four wave mixing (FWM) nonlinear effects whereas dispersion is non-zero in the L-band with G.653 fibre. This thesis focuses on G.652 fibre therefore L-band amplifiers will not be considered.

### Single Stage Amplifier (SSA)

An SSA contains up to four pump lasers and is operated in constant output power mode. Also provided at the input and output of the EDFA are tap couplers and photodiodes to monitor the input and output powers respectively.

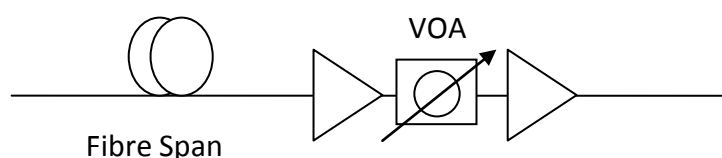


Figure 16 SSA high-level architecture<sup>17</sup>

Each SSA gain block contains a variable optical attenuator (VOA) embedded between the erbium coils as shown in Figure 16. This VOA is used to compensate for span losses shorter than the optimised span losses of 17dB for SSA17 and 21dB for SSA21. In essence this VOA is used to build out the span loss so that the amplifier operates at the specified operating gain. This ensures that the flat gain condition can be satisfied over a range of different input powers. For example, an SSA17 amplifier immediately following a 15dB span would have the line build out VOA turned up by an extra 2dB.

Under normal operating conditions the line build out VOA is set close to its minimum insertion loss. A direct consequence of increasing the line-build-out VOA is to increase the amplifier noise figure as shown in Figure 19. For an SSA-17, the noise figure degradation for 7dB line build out is <5dB.

<sup>17</sup> Source: Ericsson

### Dual Stage Amplifier (DSA)

A DSA comprises a pre-amplifier stage, paired with a booster stage configured as shown in Figure 17, with a dispersion compensation module (DCM) containing DCF included in the mid-stage of the amplifier. The DCM includes an integrated VOA, which is used to pad out the mid-stage-loss to 12.4dB.

The DSA pre-amp configuration is consistent with that shown for an SSA in Figure 16 with an embedded line build out VOA.

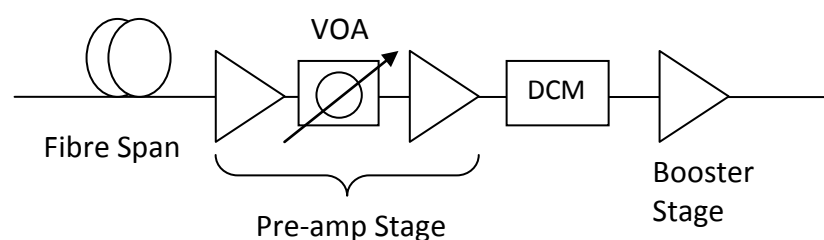


Figure 17 DSA high-level architecture<sup>18</sup>

The pre-amplifiers are operated in constant output power mode. To reduce non-linear effects in the DCF, while at the same time maintaining a reasonable DSA noise figure, the maximum output power out of the pre-amplifier is kept to 4dBm below the output power of the booster stage. Trimming fibre and the mid-stage-padding VOA immediately preceding the DCF ensure that no significant non-linear DCF penalties are incurred for typical span losses.

The booster amplifier stage contains up to three pump lasers and is operated in constant output power mode.

### Gain Flatness

The SSA and DSA are specified with a negative gain tilt of -1.6dB and -2.2dB respectively (see Table 2), which is included to help compensate for fibre SRS tilt of ~1dB/100km (see Table 3 in section 2.9.13 for details of SRS tilt for various fibre types) and fibre attenuation tilt of ~0.7dB/100km (see Figure 29 for fibre attenuation profile) and DCF attenuation tilt of ~0.4dB/DCM-100 (see Figure 30 for DCF attenuation profile). Figure 18 (b) shows the negative gain tilt of the DSA booster stage amplifier; the DSA-21 pre-amplifier stage has a flat tilt shown in Figure 18 (a).

<sup>18</sup> Source: Ericsson

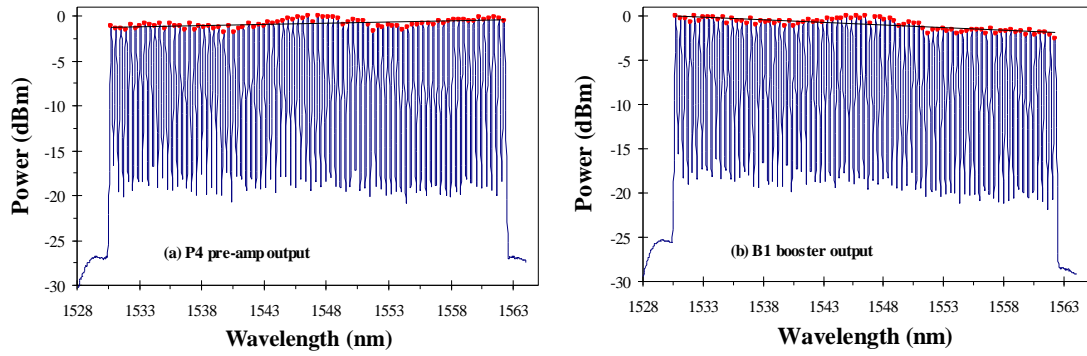


Figure 18 DSA21 output spectra under normal operation for (a) pre-amplifier (b) booster<sup>19</sup>

### Noise Figure

The line-build-out VOA embedded in the DSA pre-amp stage is used to compensate for span losses shorter than the optimal span loss, as described for the SSA. As mentioned previously, increasing the line-build-out VOA increases the amplifier noise figure. For the DSA the embedded VOA is biased towards the front of the amplifier and thus has a bigger impact on the combined noise figure of the amplifier. Alternatively a significant problem with positioning the VOA in the booster stage is still being able to achieve the required output power from the booster when the VOA is set at its maximum value.

For varying span losses, it is necessary to consider the noise figure degradation with setting of the line build out VOA. The noise figure in linear units as a function of the VOA loss  $VOA(lin)$  is modelled as

$$F(lin) = F_a + F_b \cdot VOA(lin) + F_c \cdot VOA(lin)^2$$

Equation 3

where  $F_a$ ,  $F_b$  and  $F_c$  are constants specific to each gain block. Figure 19 shows the noise figure as a function of VOA loss for each of the EDFA gain blocks.

<sup>19</sup> Source: Ericsson

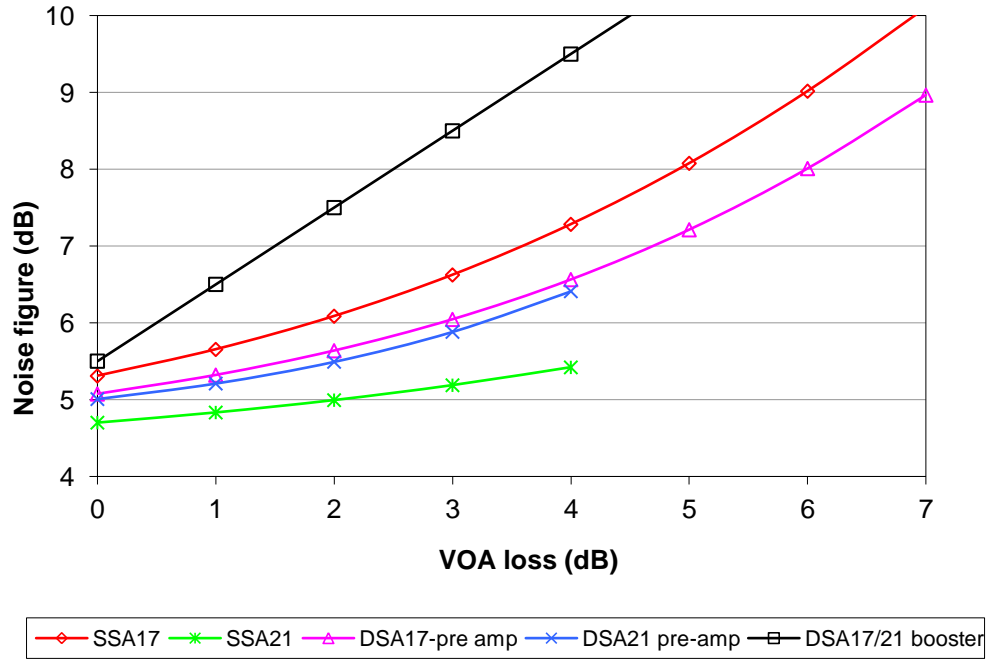


Figure 19 Variation of EDFA NF with VOA loss<sup>20</sup>

### 2.7.3 EDFA SPECTRAL GAIN AND NOISE FIGURE

From a system design perspective the spectral dependence of gain and noise figure in an EDFA is most suitably described by a black-box model [44]. An advantage of this type of approach is that a detailed knowledge of the active gain medium and amplifier components is not required: only input-output test measurements of amplifier gain block modules.

The model is based on the physics of an effective two-level laser system, meaning that it is valid for most commercially available EDFAs according to the simplified energy level diagram in Figure 14. From [44] the gain of an EDFA as a function of wavelength  $\lambda$  and input power  $P_{in}$  can be derived<sup>21</sup> (see Appendix 1 for derivation) as in [25] after [44]

$$G^{dB}(\lambda, P_{in}) = G_{ref}^{dB}(\lambda) + T_{\lambda_{ref}}(\lambda) \cdot a_T \cdot P_{in}^{dB},$$

Equation 4

where  $G_{ref}(\lambda)$  is the gain at a reference point  $P_{in_{ref}} = 0dBm$  and  $a_T$  is a constant.  $T_{\lambda_{ref}}(\lambda)$  is a characteristic tilt function given by

<sup>20</sup> Source: Ericsson

<sup>21</sup> Derivation by Dr Jeroen Nijhof

$$T_{\lambda_{ref}}(\lambda) = \frac{G_1^{dB}(\lambda) - G_2^{dB}(\lambda)}{G_1^{dB}(\lambda_{ref}) - G_2^{dB}(\lambda_{ref})},$$

**Equation 5**

where  $G_1$  and  $G_2$  are the gains measured at different amplifier saturation conditions (input powers), and  $\lambda_{ref} = 1546nm$ .  $G_{ref}(\lambda)$  and  $T_{\lambda_{ref}}(\lambda)$  can be modelled as third order polynomials by fitting to experimental measurements of gain against wavelength at various saturation conditions.

A similar expression for the spectral noise figure  $F(\lambda, P_{in})$  is also derived<sup>22</sup> (see Appendix 1 for derivation) [25] from [44] as the spontaneous emission factor  $n_{sp}$ , with  $F = 2n_{sp}$  (linear units)

$$n_{sp}(\lambda, P_{in}) = n_{sp0} + f(\lambda) \cdot g(P_{in}^{dB}),$$

**Equation 6**

where  $n_{sp0}$  is a constant and  $f(\lambda)$  and  $g(P_{in})$  can be modelled as third and second order polynomials fits to experimental measurements.

Characterisation of EDFA gain and noise figure profile was done by fitting the black-box model to experimental data<sup>23</sup> as shown by the example for the DSA booster stage EDFA in Figure 20. The models show good agreement with experimental measurements to  $\pm 0.2dB$  for the gain and  $\pm 0.3dB$  for the noise figure.

<sup>22</sup> Derivation by Dr Jeroen Nijhof

<sup>23</sup> Source: Ericsson, EDFA characterisation measurements by Dr Marc Stephens

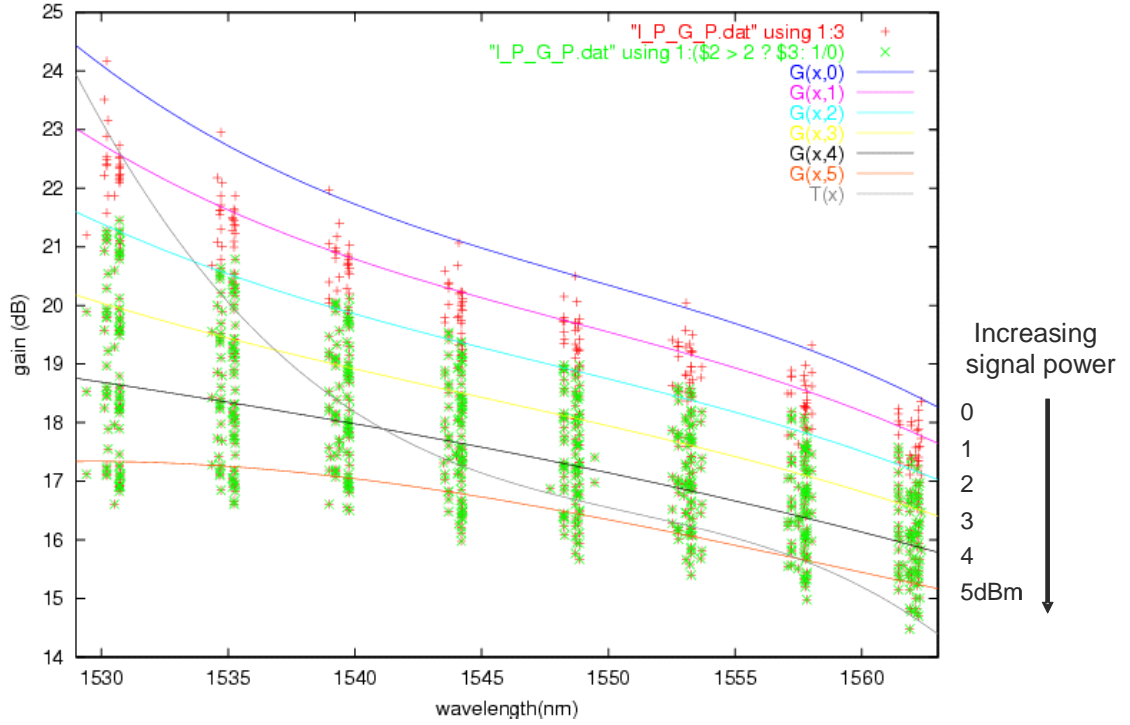


Figure 20 Example EDFA gain spectrum for DSA booster amplifier stage (after [25])

## 2.7.4 OSNR AND LINK NOISE ACCUMULATION

ASE noise generated by optical amplifiers is the dominant source of noise in LH links, other noise sources such as receiver shot noise and thermal noise can be neglected.

The ASE noise generated by an EDFA is assumed to be additive white Gaussian noise. Inline amplifiers typically operate with a moderately large optical input signal therefore the signal to noise at the output of the amplifier is dominated by signal-spontaneous beat noise. The OSNR after a number of spans  $N$  is defined as the ratio of the signal power to the total ASE power, assuming that each amplifier adds a noise power  $P_{ASE}$  and that each span has an equal loss, the OSNR is given by

$$OSNR = \frac{P_{out}}{P_{ASE}N}$$

Equation 7

where  $P_{out}$  is the signal power out of the final amplifier in the link. It is also assumed that the signal power at the input of the link is equal to the signal power at the end of the link; this is a relatively accurate assumption when the ASE is small compared to the signal power.

The ASE noise power spectral density per polarisation around a reference frequency  $\nu$  is given by [43]

$$S_{sp} = n_{sp} h \nu (G - 1) N$$

**Equation 8**

where  $G$  is the amplifier gain,  $h$  is Plank's constant and  $n_{sp}$  is the spontaneous emission factor and assuming the span loss  $L$  is equal to the amplifier gain.

Taking account of both polarisations in SMF and measuring the signal in a bandwidth  $B_0$  Equation 7 can be re-written as

$$OSNR = \frac{P_{out}}{2S_{sp}B_0}$$

**Equation 9**

Combining Equation 8, and Equation 9 and where  $P_{out} = GP_{in}$  with  $P_{in}$  being the power of the signal at the amplifier input, we obtain

$$OSNR = \frac{P_{out}}{2n_{sp}h\nu(G-1)NB_0} = \frac{GP_{in}}{2n_{sp}h\nu(G-1)NB_0}$$

**Equation 10**

When the gain of the amplifier is sufficiently high the OSNR given by Equation 10 becomes independent of the gain and dependent only on the input power and the population inversion parameter.

Substituting Equation 2 into Equation 10 we obtain an expression for the OSNR as a function of amplifier noise figure and number of spans

$$OSNR = \frac{P_{in}}{Fh\nu NB_0}$$

**Equation 11**

The typical degradation of the OSNR along a link of regular 17dB amplified spans is shown in Figure 21 for varying signal power per channel and in Figure 22 for varying span losses at 0dBm/channel signal power.

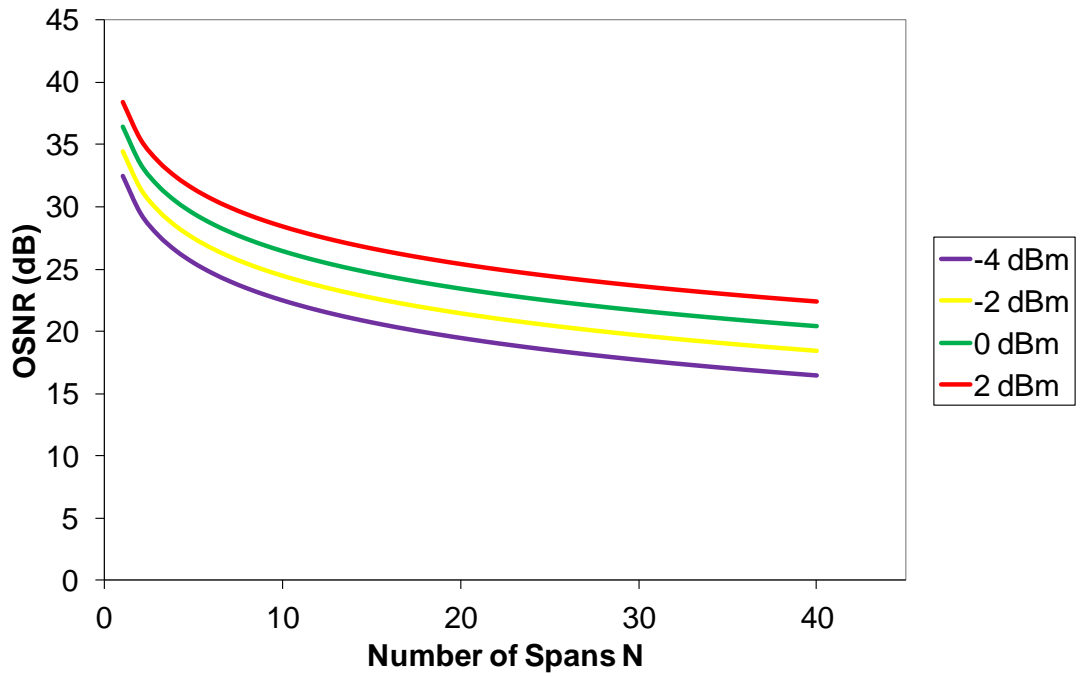


Figure 21 OSNR along a link of regular 17dB spans for varying signal power

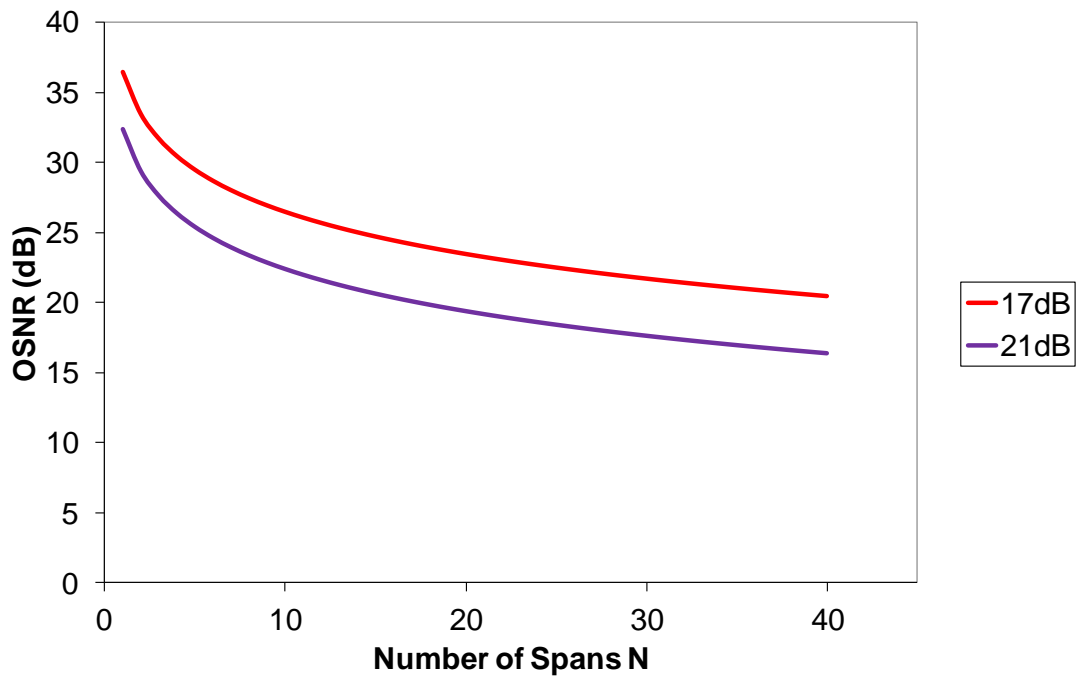


Figure 22 OSNR along a link of regular 17dB and 21dB spans at 0dBm/ch signal power

Expressing Equation 11 in [dB] gives a useful engineering rule for the OSNR after  $N$  spans [37]

$$OSNR[dB] = 10 \log_{10} \left( \frac{1000}{h \nu B_0} \right) + P_{in}[dBm] - F[dB] - 10 \log_{10} N$$

**Equation 12**

Using a reference bandwidth  $B_0$  of 12.5GHz (0.1nm) around a reference frequency of 193.4THz (1550nm) the first term in Equation 12 becomes 58dBm, and by substituting  $P_{out} = GP_{in}$  with  $G = L$  we obtain

$$OSNR[dB] = 58[dBm] + P_{out}[dBm] - L[dB] - F[dB] - 10 \log_{10} N$$

**Equation 13**

Equation 13 shows that in order to increase the OSNR, we can increase the signal power (non-linear effects will constrain the maximum signal power), decrease the noise figure (this has a 3dB quantum limit), or decrease the span loss.

The most effective way to increase OSNR is to decrease the span loss [45]. However  $N$  increases because  $N \cdot L$  is a constant set by the total link length. OSNR decreases linearly with  $L$  and only logarithmically with  $N$ , amplified systems should therefore logically be designed with many short spans with small losses  $L$  [45]. This strategy commonly deployed in submarine systems would maximise the OSNR performance but would conflict with economic and operational issues for terrestrial systems [45] such as cost and availability of real-estate to house the network equipment, which tends to favour minimising the number of amplified spans in a link.

### **Real World Terrestrial Links with Irregular Span Losses**

The OSNR at the end of a link of  $N$  amplified spans of irregular span loss and amplifier gain is given by

$$OSNR = \frac{P_{out}}{F_m h \nu B_0}$$

**Equation 14**

where  $F_m$  is the effective noise figure of the link given by [25]

$$F_m = F_1 L_1 + F_2 L_2 \frac{L_1}{G_1} + \dots + F_N L_N \prod_{i=1}^{N-1} \frac{L_i}{G_i}$$

**Equation 15**

where  $L_i$  and  $G_i$  refer to the span loss prior to and the gain of the amplifier  $i$  in a link respectively; with equal span lengths  $F_m \equiv N \cdot L \cdot F$ .

### **Spectral Dependence of Amplifier Gain and Noise Parameters**

The OSNR of each channel in a DWDM system can be calculated separately with wavelength specific gain and noise figure given by Equation 4 and Equation 6. Linear wideband OSNR calculations form an important part of the foundations of this work and are published in the author's MSc thesis [25].

## **2.8 CHANNEL EQUALISATION**

Channel equalisation is necessary in a ULH DWDM system due to the accumulation of spectral power tilts and ripples across a large number of network nodes leading to variations in performance across many DWDM channels. Channel equalisation is also useful in ROADM based networks where different channels may have travelled on different paths and hence will accumulate different power variations [37].

The primary sources of tilt are: SRS tilt, transmission fibre and DCF attenuation tilt. Fibre and DCF induced tilt is static, but strongly length and fibre type dependent, whilst the SRS contribution is dynamic being dependent on the total signal power (and hence the number of channels) in addition to the fibre type. SRS amplifies longer wavelength channels at the expense of shorter wavelength channels and increases log-linearly with total signal power (and hence channel count). Amplifiers are designed to have a static gain tilt, chosen to minimise the net tilt across a number of channels by opposing the SRS tilt, and fibre / DCF attenuation tilt.

Amplifier gain and noise figure variations are the primary sources of power ripple. The exact shape of the ripple is dependent on the number and types of amplifier in the transmission line.

### **Pre-Emphasis**

Dynamic channel equalisation and signal power pre-emphasis (changing the channel power profile at the input of the link) helps equalise the net gain and hence the power spectrum at the end of the transmission link as shown in Figure 23.

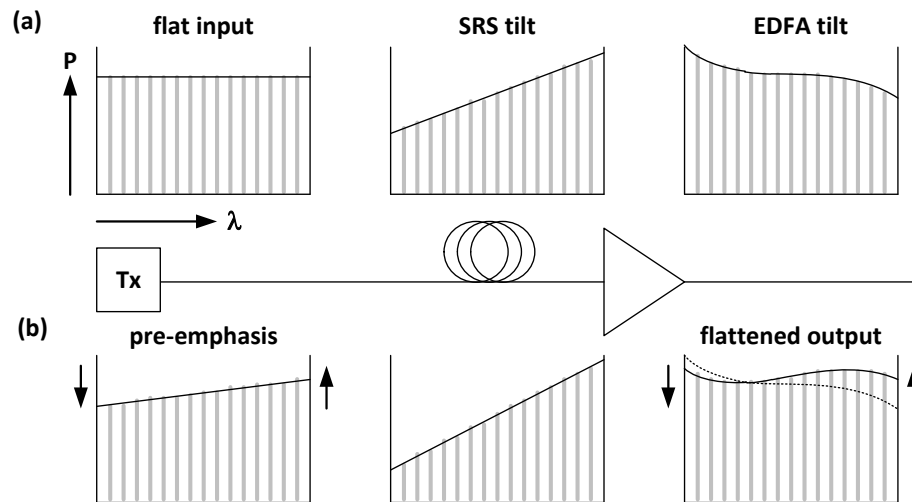


**Figure 23 Principle of pre-emphasis. Left: Input channel powers. Centre: Channel powers with SRS tilt. Right: Output channel powers with combined SRS and EDFA tilt. (a) no pre-emphasis resulting in tilted spectrum after EDFA (b) pre-emphasis results in flattened output (after [19])**

At the terminals pre-emphasis involves altering the launch powers of each individual channel according to a spectral profile which either minimises the variation in power across all channels or minimises the variation of a channel performance measure such as OSNR, Q-factor or BER.

### Re-Emphasis

Re-emphasis involves repeating the pre-emphasis process periodically along a link to ensure channel power and performance remains within suitable limits. Re-emphasis is performed at dedicated levelling nodes and can also be performed at ROADM nodes since the ROADM can act as a channel specific VOA.

### Levelling Sub-System

Figure 24 shows the sub-system architecture of a levelling node. A power monitor unit (PMU) accurately measures the signal power of each channel at the output of the node providing electronic feedback to the channel equalising unit (CEU) which adjusts the power of each channel to achieve the desired spectral profile. The CEU is based on a liquid crystal spatial light modulator capable of independently attenuating individual channels spaced on a 50GHz grid [46]. An SSA-17 EDFA compensates for the loss and channel attenuation due to the CEU. It is assumed that the CEU can correct for channel-to-channel variations to achieve any desired linear tilted channel profile.

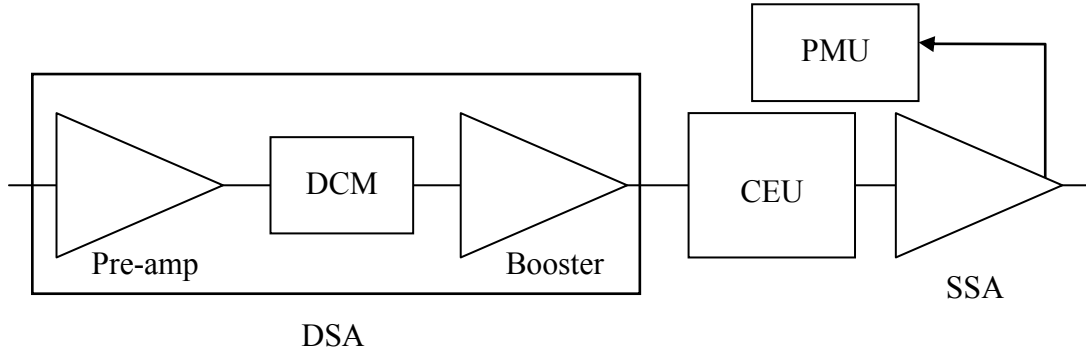


Figure 24 Levelling sub-system architecture<sup>24</sup>

Levelling nodes are significantly more expensive than standard amplifier nodes due to the high cost of the CEU, PMU and additional amplification; the cost ratio of a leveller to an average line amplifier node is about 2 to 1. Levelling nodes also impact the OSNR due to the extra EDFA required. It is therefore desirable when designing ULH networks to place as few levelling nodes as possible along the link. Work initially carried out in [25] determined the optimum spacing between levellers to be 6 spans. Following further development of the combined wideband and nonlinear simulation model presented in this thesis, publication [20], and section 2.14 of this thesis show that the trade-off between performance and cost extends the optimum spacing of levelling nodes to 8 spans apart.

### 2.8.1 OSNR EQUALISATION PRE-EMPHASIS

Pre-emphasis is usually performed to equalise either power or OSNR across the spectrum at the end of a link [32] and [33].

To perform OSNR equalisation pre-emphasis, the power in each channel is scaled by a factor inversely proportional to the initial end of line OSNR of that channel. The power of the  $i$ th channel  $P_i^{new}$  should be set according to [29]

$$P_i^{new} = P_{TOT} \left[ \frac{P_i / OSNR_i}{\sum_{i=1}^N P_i / OSNR_i} \right],$$

Equation 16

where  $OSNR_i$  is the OSNR of the  $i$ th channel and  $P_i$  is the input power of the  $i$ th channel with no pre-emphasis and  $P_{TOT}$  is the total signal power; the denominator ensures a constant total system input power. Multiple iterations of the algorithm are

<sup>24</sup> Source: Ericsson

normally required, as changing the signal powers will change the saturation conditions of the amplifiers. This pre-emphasis will be re-applied at levelling nodes (re-emphasis) to maintain the required power spectrum for end-to-end OSNR equalisation.

### **Linear Pre-emphasis Tilt Approximation**

Applying the algorithm given by Equation 16 will result in an ideal input power spectrum which can perfectly equalise the OSNR spectrum. An example input power spectrum and the resulting flat OSNR spectrum is shown by the pink lines in Figure 25 and Figure 26 respectively.

In practice, it is impractical to control up to 80 channels in a field-deployed DWDM system with the precision required to achieve this complex pre-emphasis profile due to dynamic control issues such as amplifier transients, forcing system designers to simplify algorithms. The pre-emphasis is therefore approximated with a linear fit to the ideal profile as shown by the green line in Figure 25. The resulting OSNR spectrum shown in green in Figure 26 has an OSNR spread of 1.1dB compared to the 0.0dB with ideal pre-emphasis (pink line) and 1.9dB with no pre-emphasis (blue line). The performance of the worst channel is improved from 15.7dB with no pre-emphasis to 16.3dB with linear pre emphasis and 17.1dB with an ideal pre-emphasis profile.

Equalising the OSNR spectrum does not necessarily result in equal channel powers across the C-band due to the complex balance of the various sources of channel power variation. Figure 27 however does show a small improvement in the spread of output powers from 5.5dB with no pre-emphasis to 3.9dB with the ideal OSNR pre-emphasis and 4.6dB with the linear tilt approximation.

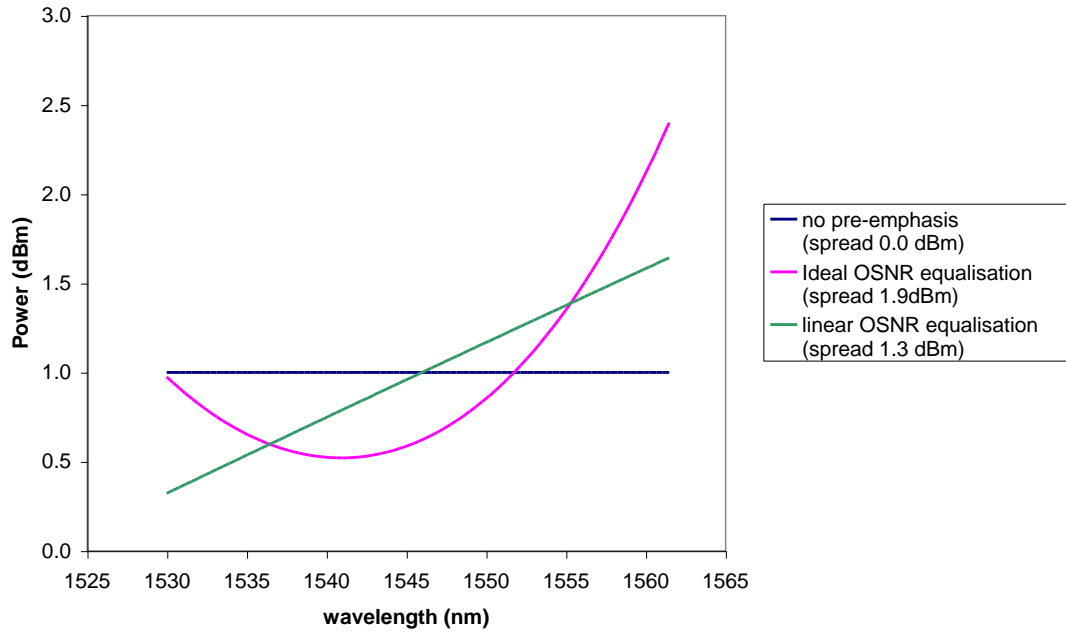


Figure 25 Input power spectra at start of 3,173km link with: (a) no pre-emphasis (b) ideal OSNR equalisation pre-emphasis (c) linear OSNR equalisation pre-emphasis.

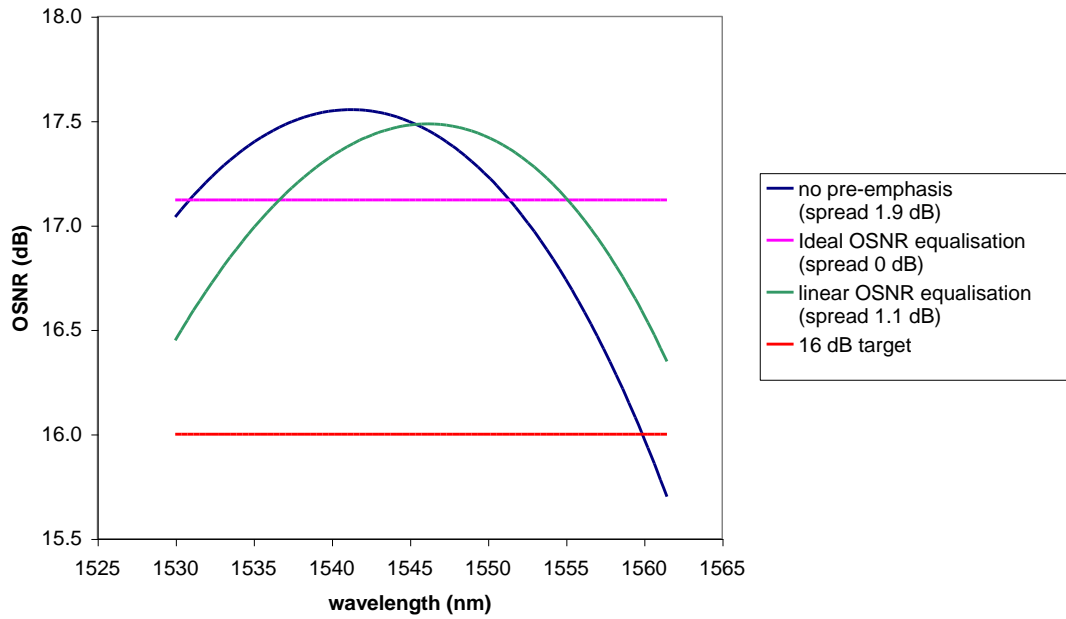


Figure 26 OSNR spectrum at end of 3,173km link with: (a) no pre-emphasis (b) ideal OSNR equalisation pre-emphasis and (c) linear OSNR equalisation pre-emphasis

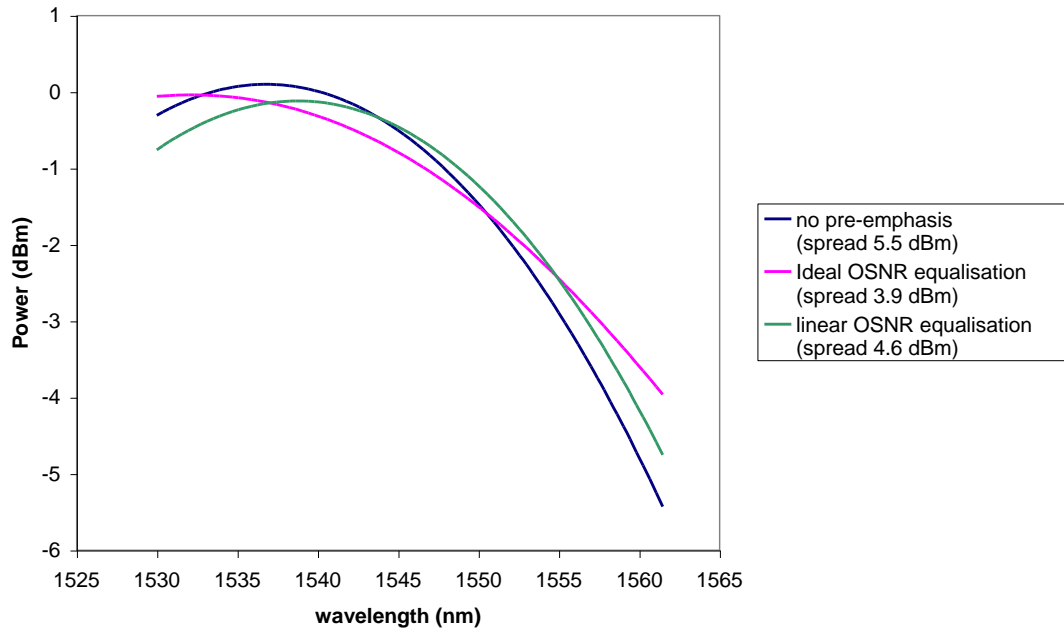


Figure 27 Received power spectrum at end of 3,173km link with: (a) no pre-emphasis (b) ideal OSNR equalisation pre-emphasis and (c) linear OSNR equalisation pre-emphasis

## 2.9 LIGHT-WAVE PROPAGATION IN OPTICAL FIBRE

### 2.9.1 INTRODUCTION

The theory of light-wave propagation in optical fibre is described comprehensively in [47]; the key theories are presented here for each of the considered physical impairment effects.

### 2.9.2 FIBRE ATTENUATION

The optical signal power decreases exponentially when propagating in optical fibres. Rayleigh scattering and infrared absorption are the main physical sources of attenuation in the 1550nm window commonly used in WDM systems (see Figure 28). Other physical sources of attenuation include ultraviolet absorption and attenuation due to fibre impurities.

If  $P_{in}$  is the power launched into a fibre of length  $L$ , the output power  $P_{out}$  is given by

$$P_{out} = P_{in} e^{-\alpha L},$$

Equation 17

where  $\alpha$  is the fibre attenuation coefficient, which is commonly expressed in units of dB/km according to

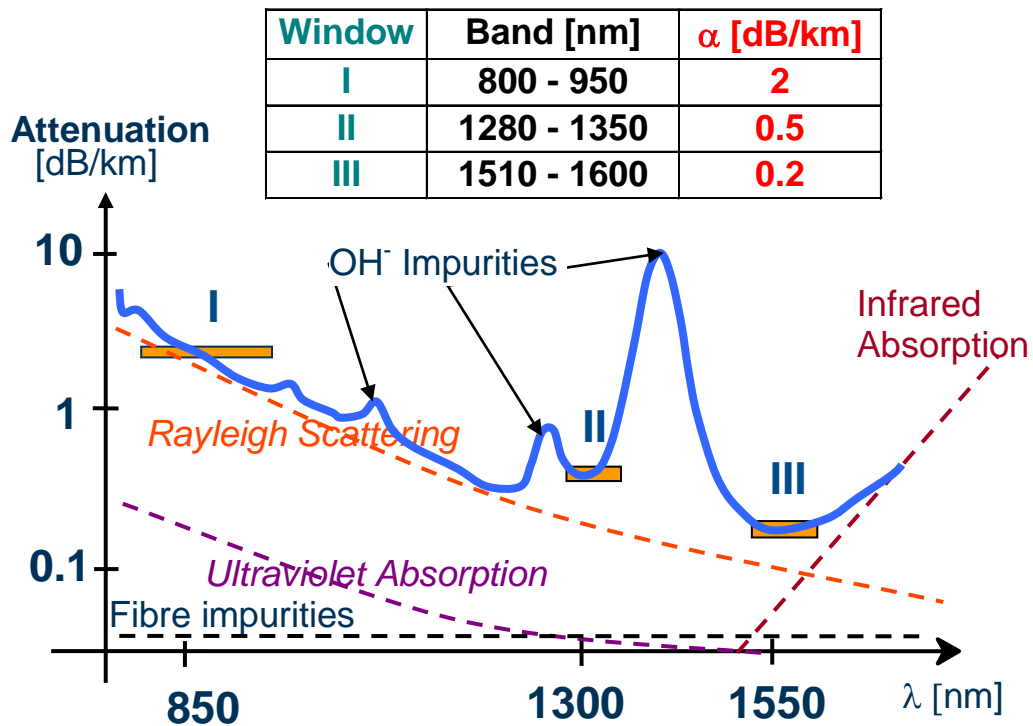
$$\alpha_{dB/km} = -\frac{10}{L} \log \left( \frac{P_{out}}{P_{in}} \right) = (10 \log_{10} e) \alpha \approx 4.343 \alpha$$

Equation 18

Sometimes it is useful to work with attenuation values in linear units by inverting Equation 18

$$\alpha = \frac{\log_e 10}{10} \alpha_{dB/km} \approx \frac{\alpha_{dB/km}}{4.343}$$

Equation 19

Figure 28 Silica fibre attenuation spectrum<sup>25</sup>

Fibre attenuation is at its lowest within transmission window III from 1510-1600nm where attenuation of around 0.2dB/km and lower can be achieved. This window is split into three transmission bands: S-band, C-band and L-band which are based on optical amplifier availability in the lowest loss region around 1550nm. The C-band (1530-1570nm) is the most commonly used in commercial DWDM systems due to it

<sup>25</sup> Source: Ericsson

having the lowest fibre attenuation and the availability of cost-effective, efficient, conventional EDFA optical amplifiers. The EDFA has extended the reach of optical communications systems and allowed an evolution from regenerated optical transmission to that of transparent optically amplified transmission with WDM.

Some DWDM systems provide extended transmission capacity in the L-band (1570-1612nm) with gain shifted EDFAs. The S-band (1492-1529nm) is the least commonly used where fibre Raman amplifiers provide amplification since commercially viable EDFAs are not widely available in this transmission window due to ASE in the C-band and L-band suppressing S-band amplification [48].

All transmission simulations, modelling and experimental results presented in this thesis were carried out in the C-band where channels are centred on the ITU defined grid with either 50GHz or 100GHz spacing, depending on whether 80 or 40 DWDM channels are provisioned. The range of channel frequencies and wavelengths are: 191.90-195.85THz (1562.24-1530.74nm).

### Fibre Attenuation Tilt

There is a small spectral variation of fibre attenuation within the C-band. The spectral variation of SMF and SMF DCF attenuation were modelled as quadratic and linear fits to measurements<sup>26</sup> shown in Figure 29 and Figure 30.

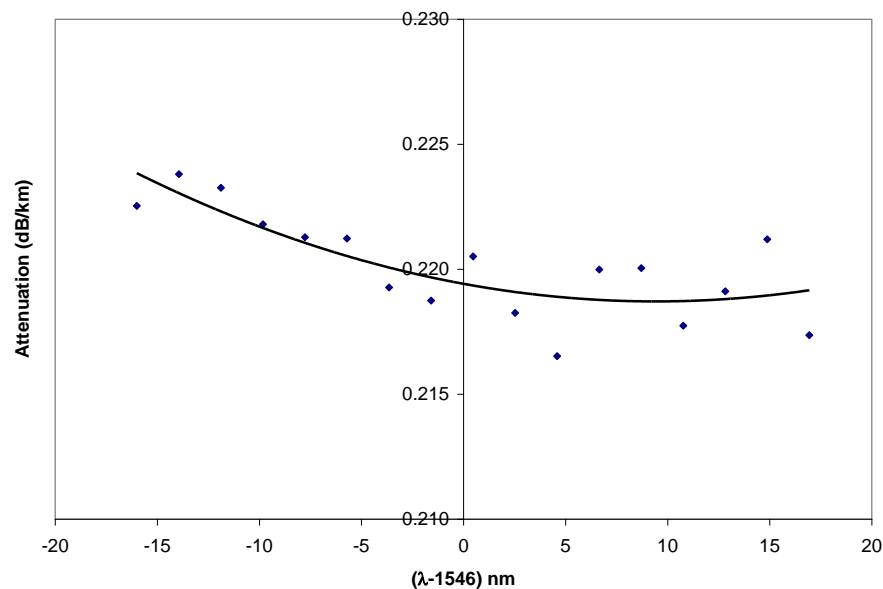


Figure 29 Attenuation profile of SMF fibre over C-band (after [25])

<sup>26</sup> Source: Ericsson, measurements by Dr Liam Gleeson

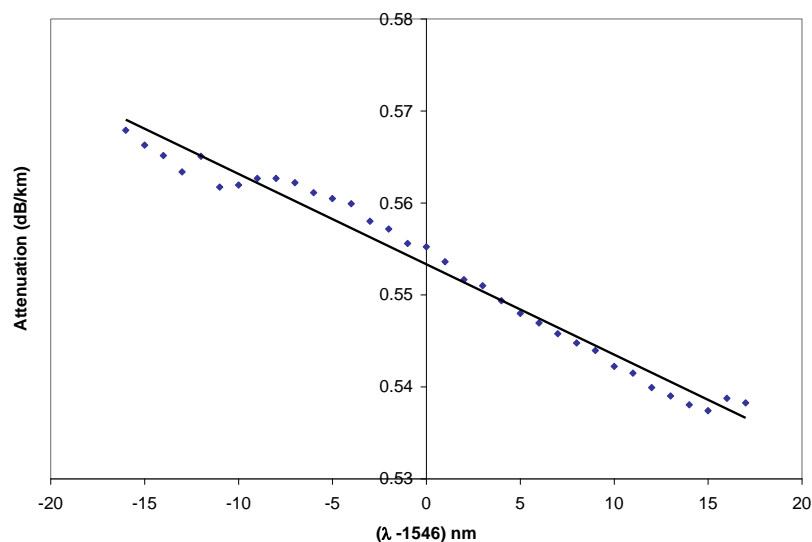


Figure 30 Attenuation profile of SMF-DCF over C-band (after [25])

### 2.9.3 CHROMATIC DISPERSION (CD)

CD or GVD is a phenomenon whereby different spectral components of a pulse travel at different velocities within a fibre causing temporal broadening of pulses. Shorter wavelength components travel faster than longer wavelength components. Temporal broadening of a narrow light pulse causes it to spread itself over a time interval larger than a single bit slot leading to inter symbol interference (ISI) and impaired performance as illustrated in Figure 31. The speed at which different spectral components associated with the pulse travel at is the phase velocity given by  $c/n(\omega)$ , where  $c$  is the speed of light in a vacuum and  $n$  is the frequency dependent refractive index of the guiding material.

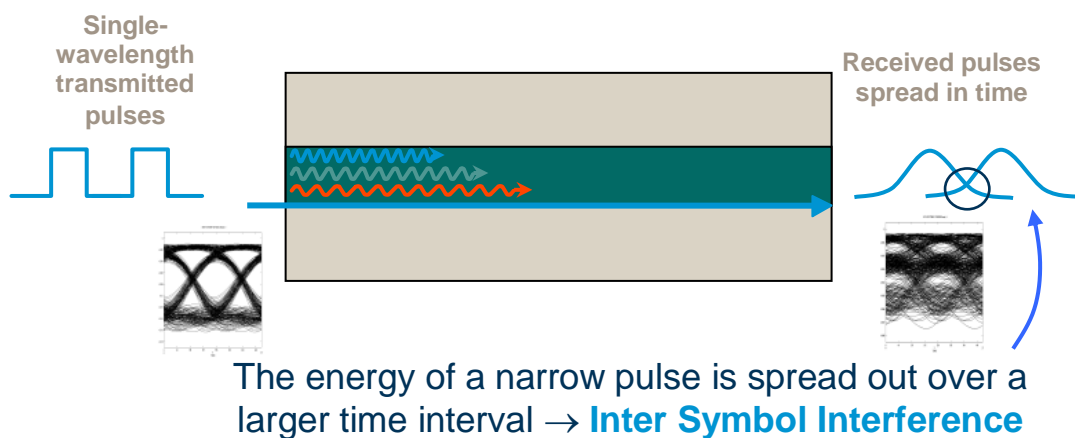
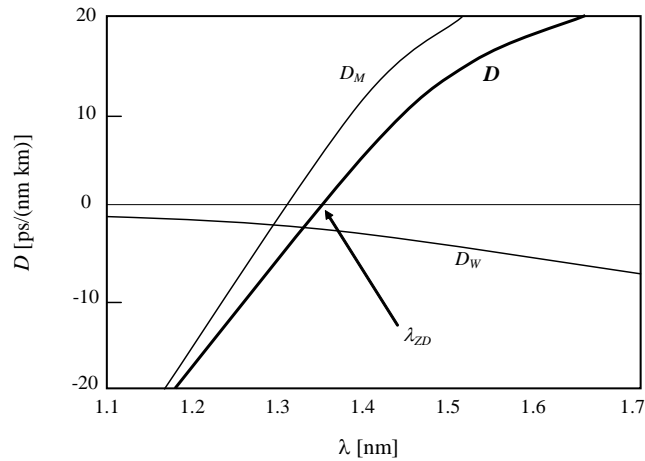


Figure 31 Principle and effect of Inter Symbol Interference (ISI)<sup>27</sup>

<sup>27</sup> Source: Ericsson

CD has two contributions, material dispersion  $D_M$  and waveguide dispersion  $D_W$  as shown in Figure 32 for G.652 fibre. Material dispersion arises because the refractive index of silica is frequency dependent, and waveguide dispersion arises because the guiding properties of the fibre are frequency dependent. Waveguide dispersion can be altered by careful design of the fibre refractive index profile which is traded-off against the material dispersion in order to manufacture fibres with different dispersion profiles e.g. DCF with negative dispersion coefficient or dispersion shifted fibre (DSF) (G.653) with zero dispersion  $\lambda_{ZD}$  at 1550nm.



**Figure 32 Material and waveguide dispersion contributions to total dispersion in G.652 fibre<sup>28</sup>**

It is well known that in the absence of nonlinearity, pulse propagation and distortion can be estimated from the derivatives of the mode propagation constant  $\beta(\omega)$  with respect to  $\omega$  [27], [47].  $\beta(\omega)$  can be expanded in a Taylor series about the central reference frequency of the pulse  $\omega_0$  as

$$\beta(\omega) = n(\omega) \frac{\omega}{c} = \beta_0 + \beta_1(\omega - \omega_0) + \frac{1}{2} \beta_2(\omega - \omega_0)^2 + \frac{1}{6} \beta_3(\omega - \omega_0)^3 + \dots,$$

**Equation 20**

where

$$\beta_m = \left( \frac{d^m \beta}{d\omega^m} \right)_{\omega=\omega_0} \quad (m = 0, 1, 2, 3, \dots).$$

**Equation 21**

<sup>28</sup> Source: Ericsson

The term  $\beta_0$  represents a frequency independent phase shift while the envelope of an optical pulse moves at the group velocity,  $v_g$  given by  $1/\beta_1$ .  $\beta_2$  represents the frequency dependence of the group velocity i.e. GVD and is responsible for pulse broadening;  $\beta_2$  is known as the GVD parameter [47].

The dispersion parameter  $D$  defined as  $d\beta_1/d\lambda$  is also used in practice as a measure of dispersion in a fibre with respect to wavelength rather than frequency; it is related to  $\beta_2$  and  $n$  as

$$D = \frac{d\beta_1}{d\lambda} = -\frac{2\pi c}{\lambda^2} \beta_2 = -\frac{\lambda}{c} \frac{d^2 n}{d\lambda^2}.$$

**Equation 22**

$D$  is expressed in units of ps/(nm·km) and is the broadening in picoseconds that would occur in a pulse with bandwidth of 1nm propagating through 1km of fibre; chromatic dispersion accumulates linearly with transmission distance.

The slope of the dispersion  $S$  gives rise to what is known as third-order dispersion where the dispersion is frequency dependent [43]

$$S = \frac{dD}{d\lambda} = \frac{2\pi c}{\lambda^3} \left[ 2\beta_2 + \frac{2\pi c}{\lambda} \beta_3 \right]$$

**Equation 23**

This wavelength dependence is problematic in LH WDM systems at high bit rates and in particular on fibres where the dispersion slope cannot be well compensated e.g. G.653 or G.655. Details of the dispersion characteristics of common fibre types are given in chapter 3 section 3.4

Much of the fibre deployed around the world is standard SMF conforming to the G.652 specification where the zero chromatic dispersion wavelength,  $\lambda_0$  is near 1300nm. Commercial optical amplifiers operate in the 1530-1560nm band of the spectrum, where significant fibre dispersion is present in G.652. Dispersion compensation is therefore required in amplified WDM systems in order to overcome limitations on the received optical signal quality and hence the maximum transmission distance between OEO regeneration. DCF is the most common approach to CD compensation and is explored in depth in Chapter 3.

With the advent of optical transparency, optical channels will have multiple different paths through the network, each with different dispersion characteristics which need to be compensated. Complex dispersion maps can be defined so that channels added and dropped at intermediate OADM nodes have the right amount of dispersion compensation. Coherent detection and DSP now enables adaptive EDC giving the ultimate in dispersion compensation flexibility without the need for complex analogue link design.

#### **2.9.4 POLARISATION MODE DISPERSION (PMD)**

PMD occurs as a result of the two orthogonal polarisations of light travelling at different group velocities causing a time delay called the differential group delay (DGD). This birefringence arises due to the non cylindrical profile of the fibre core as a result of either manufacturing defects or physical stress and strain on field deployed fibre. PMD scales with the square of the bit rate and is therefore mainly a problem at 40Gb/s and higher bit rates over older fibre plant. PMD is not considered a problem at 10Gb/s and at 40Gb/s over good quality fibre, especially since advanced phase modulation formats such as RZ-DQPSK can help improve PMD (and CD) tolerance due to the halved symbol rate. Electronic PMD compensation using DSP and coherent detection is becoming widespread in 40Gb/s and 100Gb/s dual-polarisation quadrature phase shift keying (DP-QPSK) systems enabling enhanced reach and deployment on older installed fibre [18].

PMD will not be modelled within the numerical simulations included in this thesis; instead a PMD penalty of 1dB is subtracted from simulated Q-factor when determining the system margin. Since PMD is a statistical process varying over time it is common to specify a mean DGD such that a 1dB penalty has a low probability of occurrence. Resulting mean DGD tolerance is 12ps for 10Gb/s RZ, 8ps for 40Gb/s RZ-DQPSK and 4ps for 40Gb/s NRZ-DPSK. The PMD coefficient of typical fibres is assumed to be  $0.15\text{ps/km}^{1/2}$ , thus DGD accumulates with the square root of transmission distance.

#### **2.9.5 POLARISATION DEPENDENT LOSS (PDL)**

Various optical components in a DWDM line system have a polarisation dependent loss (PDL) i.e. the insertion loss of the component depends on the signal's state of polarisation. PDL can accumulate over many components leading to OSNR

degradation [27]. PDL is minimised by selecting optical components with as stringent PDL specification as possible. According to [49] approximately 3dB of average PDL will result in a penalty of 1dB. Therefore a penalty of 1dB is subtracted from simulated Q-factor when determining system margin.

### 2.9.6 INTRODUCTION TO FIBRE NONLINEAR EFFECTS

Fibre nonlinear effects can be divided into two main categories: Kerr nonlinearities arising from the intensity dependence of the refractive index and stimulated scattering effects arising from interactions between photons and silica molecules. The most important effects within each category are summarised in Figure 33. A comprehensive review of nonlinear effects from a systems perspective is given by [27] and [50], a deeper mathematical treatment can be found in [47] and [51].

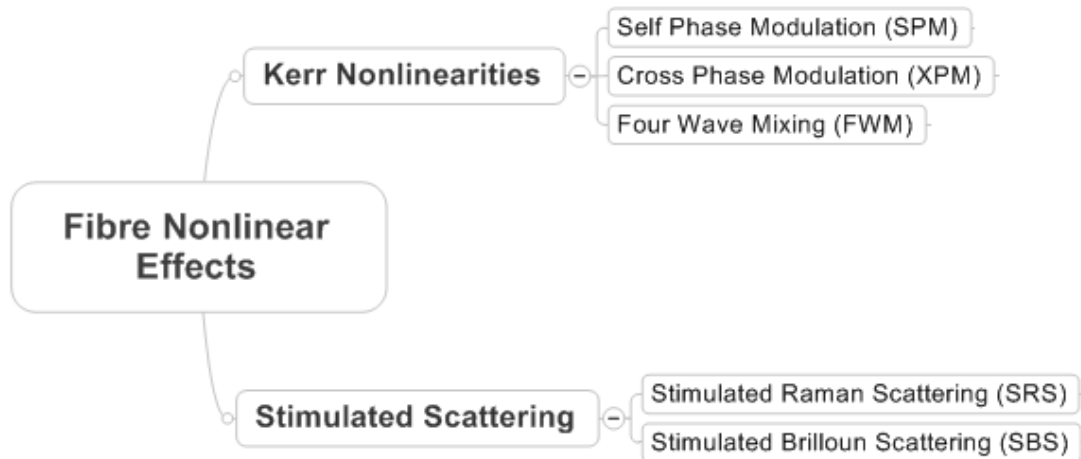


Figure 33 Fibre nonlinear effects classification

High transversal confinement of optical signals in fibre cores results in very high field intensities typically measured in  $\text{MW}/\text{cm}^2$  resulting in changes to the fibre core's refractive index through the Kerr effect which leads to phase rotations. The Kerr effect leads to pulse broadening in the frequency domain through self phase modulation (SPM) induced chirp. GVD introduces an opposing chirp which when the link dispersion map is carefully designed, can balance and mitigate the SPM induced chirp. SPM and other Kerr nonlinear effects of four-wave mixing (FWM) and cross-phase modulation (XPM) set a higher limit on the optical signal power. Stimulated Raman scattering (SRS) is the most important scattering effect and leads to intensity dependent transfer of energy from high to low frequency channels.

### Balancing Noise and Fibre Nonlinearity

A lower limit on the signal power is set by ASE noise accumulation due to the optical amplification and resultant OSNR degradation induced by a long chain of EDFAs. The trade-off between maximising signal power for improved OSNR performance and minimising signal power to mitigate nonlinear effects, results in an optimum signal power for a given optical link as shown schematically in Figure 34.

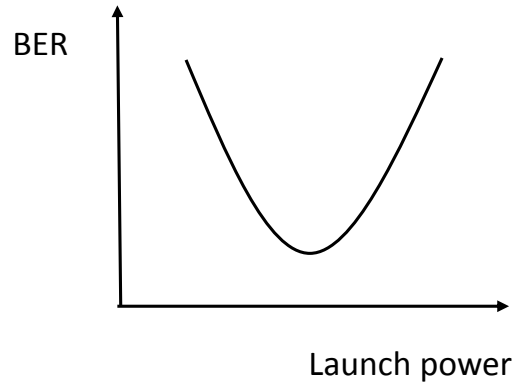


Figure 34 Linear and nonlinear transmission regimes

### Interactions between Nonlinearities and Wideband Power Variations

In massive DWDM systems spectral power variations across the wide band of channels can lead to spectral variations in Kerr nonlinearities. It is therefore important to model the spectral dependence of various sources of wideband power variations including amplifier gain, noise figure, SRS and fibre attenuation tilt when performing nonlinear system simulations.

#### 2.9.7 KERR EFFECT

Due to the Kerr effect the refractive index of the silica fibre is slightly dependent on the electrical field intensity of the optical signal in the fibre as [50]

$$n = n_0 + n_2 I = n_0 + n_2 \frac{P}{A_e}$$

Equation 24

where  $n_0$  is the linear refractive index of silica at low intensities ( $\sim 1.5$ ),  $n_2$  is the nonlinear refractive index coefficient =  $2.6 \times 10^{-20}$  m<sup>2</sup>/W for silica fibres,  $I$  the intensity of the pulse measured in W/m<sup>2</sup>,  $P$  the optical power and  $A_e$  is the effective area of the optical mode in the fibre core.  $A_e$  is the equivalent cross sectional area over which the light intensity can be assumed uniform. For standard SMF,  $A_e$  is typically 80  $\mu\text{m}^2$ , for dispersion-shifted fibre types (G.653 and G.655)  $A_e$  is typically between 55 and 72  $\mu\text{m}^2$  and for SMF-DCF  $A_e$  is typically 19  $\mu\text{m}^2$ .

### 2.9.8 NONLINEAR PHASE SHIFT

During light-wave propagation in optical fibre the nonlinear contribution to the refractive index induces an intensity dependent phase shift  $\Phi_{NL}$  given by [50]

$$\Phi_{NL} = \gamma P L_e$$

Equation 25

where  $P$  is the optical power of the signal (assuming lossless fibre),  $L_e$  is the nonlinear effective length (defined below) and  $\gamma$  the nonlinear coefficient (in units of W<sup>-1</sup>km<sup>-1</sup>) which is a measure of the size of the nonlinearity defined by [50]

$$\gamma = \frac{n_2 \omega_0}{c A_e}$$

Equation 26

where  $\omega_0$  is the optical carrier frequency of the pulse.

#### Nonlinear Effective Length

Because nonlinear effects are dependent on the light intensity, the effects become less significant as the intensity of the wave decreases thus the nonlinear effects tend to diminish as the wave propagates further down the fibre span. It is therefore useful to define the nonlinear effective length  $L_e$  of an amplified fibre span, as the length of fibre over which the same nonlinear phase shift would accumulate at constant signal power i.e. over a loss-less fibre [27]

$$L_e = \frac{1 - e^{-\alpha L}}{\alpha}$$

Equation 27

where  $L$  is the length of the fibre span in km and  $\alpha$  is the linear loss of the fibre. In the case where  $\alpha L \gg 1$ , we have  $L_e \approx 1/\alpha$  which for typical fibres is about 20 km in the 1550nm window.

### 2.9.9 SELF PHASE MODULATION (SPM)

Self induced phase change of ultra short pulses results in a variation of the instantaneous frequency across the pulse or chirp, which is maximised where the rate of change of intensity is greatest i.e. at the middle of the rising and falling edges of the pulse. The leading edge of the pulse is shifted down in frequency (red shift) and the trailing edge of the pulse is shifted up in frequency (blue shift). Spectral broadening of pulses in the frequency domain is given by the time derivative of Equation 25 [50]

$$\Delta\omega = \frac{d\phi_{NL}}{dt} = \gamma L_e \frac{dP}{dt}$$

Equation 28

Pulses at higher bit rates will have a higher rate of change of optical power with time resulting in larger optical frequency broadening due to SPM. However a combination of high bit rate and high chromatic dispersion causes a rapid pulse broadening thus reducing the SPM induced frequency broadening [50].

In a direct detection system where only intensity is measured, the phase information is lost due to square law detection principle so the SPM induced chirp has no effect on the BER [50]. System performance is however impacted by the conversion of phase modulation to amplitude jitter by the interaction between GVD and SPM. In normal dispersion regimes ( $D < 0$ ps/nm/km) the SPM blue-shifted leading pulse edge accelerates while the red-shifted trailing edge slows with increased pulse broadening leading to increased ISI and BER degradation [50]. SPM followed by anomalous dispersion regimes ( $D > 0$ ps/nm/km) results in pulse compression which balances the pulse broadening to a certain degree. Careful dispersion management as discussed in section 3.7 and 3.9 can mitigate SPM and enable extended transmission reach. SPM causes the optimum accumulated dispersion for a given link to be a slight under-compensation.

In amplified systems SPM accumulates over multiple spans and to reduce the impact of SPM the phase change is limited by placing an upper limit on the signal power

which is dependent on the number of spans [43]. This is investigated by numerical simulations in section 2.13.

### 2.9.10 CROSS PHASE MODULATION (XPM)

XPM results from phase changes in one channel caused by the nonlinear refractive index changes due to the power of neighbouring channels present in WDM systems. The frequency shift caused by intensity variations in a neighbouring channel is given by [27]

$$\Delta\omega = 2\gamma L_e \frac{dP}{dt}$$

Equation 29

where  $dP/dt$  is the time derivative of the power in the interfering pulse. Comparing Equation 29 with Equation 28 would suggest that XPM is a more severe performance limiting effect than SPM.

#### Walk-Off Effect

Optical pulses at different wavelengths propagate at different speeds in fibre because of a mismatch in their group velocities due to GVD. This group velocity mismatch leads to pulses not completely overlapping in time and a walk-off effect leading to a reduction in the XPM effect [47]. The walk-off length over which two adjacent channels interact is given by [27]

$$L_w = \frac{1}{RD\Delta\lambda}$$

Equation 30

where  $R$  is the signal bit rate,  $D$  is the fibre dispersion coefficient and  $\Delta\lambda$  is the wavelength spacing between channels. For a 10Gb/s signal over G.652 fibre where  $D = 17$  ps/nm.km and channel spacing of 50GHz ( $\Delta\lambda = 0.4$ nm) the walk-off length is 14.7km and at 40Gb/s the walk-off length is 3.7km resulting in significantly reduced XPM at higher bit rates.

XPM is also reduced when the WDM channel spacing is increased since group velocity mismatch is greater thereby reducing the interaction length. XPM is negligible in standard SMF fibre operating in the 1550nm band with 100GHz channel spacing [26]. With 50GHz spaced channels XPM is a significant penalty and

can be minimised by careful dispersion management and optimisation of signal power.

### 2.9.11 FOUR WAVE MIXING (FWM)

FWM also occurs in optical fibre affecting multi-channel WDM transmission. Pulses of different frequencies interact to cause phase modulation of channels which results in the generation of new optical signals. For example if three signals co-propagate at frequencies  $\omega_i$ ,  $\omega_j$ , and  $\omega_k$  a new signal is generated with a frequency  $\omega_{ijk}$  [50] where

$$\omega_{ijk} = \omega_i + \omega_j - \omega_k$$

Equation 31

FWM causes a depletion of the signal channel powers and cross talk due to the FWM products coinciding with the frequency of existing channels. FWM is largest when phase matching is strong which can occur with close channel spacing and / or around a zero dispersion region such as the 1550nm window in DSF (G.653).

FWM is not really an issue in SMF due to the walk-off created by the large anomalous dispersion; FWM is best avoided by using fibres with high local dispersion. On legacy DSF unequal channel spacing can minimise its effect since new signals generated do not overlap with existing channels [52], however such a channel plan reduces the total number of wavelengths that can be supported on a fibre pair significantly lowering spectral efficiency.

The numerical simulation studies carried out in this thesis are focused on SMF since it is the most widely deployed fibre and therefore FWM is not the most severely limiting nonlinear effect.

### 2.9.12 INTRA-CHANNEL XPM AND FWM

At bit rates of 40Gb/s and above high pulse walk-off is such that pulses in neighbouring channels do not interact over long distances and therefore inter-channel WDM nonlinear effects such as XPM and FWM are less limiting than in 10Gb/s systems. However nonlinear interactions between pulses within a channel are increased due to the rapid pulse broadening in time.

Two forms of intra-channel interactions have been identified: intra-channel XPM (IXPM) and intra-channel FWM (IFWM) [53]. The effect of IXPM and IFWM on

40Gb/s transmission is investigated in Chapter 3 section 3.10.3. IXPM produces timing jitter and IFWM leads to amplitude jitter and ghost pulses located in the centre of zero bit slots [53].

Optimising pre-compensation in dispersion management helps minimise IXPM and IFWM by minimising pulse overlap during transmission [50].

### 2.9.13 STIMULATED RAMAN SCATTERING (SRS)

The effect of SRS on a DWDM system leads to pumping of longer wavelength channels with a transfer of energy from shorter to longer wavelength channels as shown schematically in Figure 35. SRS cross talk results in a tilted power spectrum with OSNR degradation of the shorter wavelength channels.

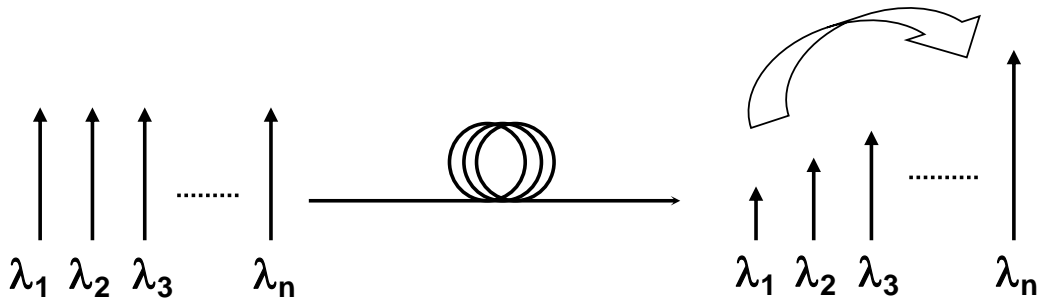


**Figure 35 Schematic of SRS showing energy transfer between shorter and longer wavelengths (after [25])**

SRS tilt is log linear and proportional to the product of total channel power and bandwidth [54]. The SRS tilt per fibre span measured in dB/nm can be approximated by [25] after [54]

$$R_{tilt} = 4.34\beta L_{eff} P_{total}$$

**Equation 32**

where  $\beta$  is the Raman gain slope (dB/nm/km/mW),  $L_{eff}$  the effective length of the fibre span (km) as defined earlier,  $P_{total}$  is the total power in the fibre (mW). The absolute Raman gain / loss for each channel will depend on the input power distribution into each fibre span. Generally the distortion of the input spectrum  $R(\lambda)$  in dB is a linear function of wavelength [55], [25]

$$R(\lambda) = R_{tilt} \cdot (\lambda - \lambda_{min}) - R_0$$

**Equation 33**

where  $\lambda_{min}$  is the shortest wavelength channel and  $R_0$  is calculated from the input spectrum to ensure conservation of the total optical power.

Measurements<sup>29</sup> of  $R_{tilt}$  for a 100km span of various fibre types and a DCM100 were carried out to determine the value of  $\beta$  for use in the system modelling as shown in Table 3.

Fibre Type	$R_{tilt}$ (dB/nm)	Tilt over C-band (dB)	$\beta$ (dB/nm/km/mW)
SMF (G.652)	0.049	~1.5	$1.6 \times 10^{-5}$
LEAF (G.655)	0.070	~2.2	$2.3 \times 10^{-5}$
TW (G.655)	0.075	~2.4	$2.4 \times 10^{-5}$
SMF-DCM100	0.105	~3.3	$7.3 \times 10^{-5}$

**Table 3 Measured Raman tilts for 100km spans and tilt over C-band with a total signal power of 22.5dBm, calculated  $\beta$  values (after [25])**

Figure 36 shows the SRS gain and loss over the C-band after a 100km span of various fibre types, all with flat input spectra of 20dBm total signal power. SRS is strongest over fibres with low dispersion such as NZ-DSF (G.655) due to the higher Raman tilt slope,  $\beta$  for such fibres. However signal launch powers tend to be lower on such fibres in order to avoid higher Kerr nonlinear penalties caused by longer walk-off lengths therefore SRS will be reduced. DCF has even larger Raman tilt slope, and its small effective area of the optical mode of the fibre core contributes to a strong SRS tilt, however signal powers into DCF are significantly lower thus compensating the SRS effect to a degree [56].

### Compensating the Effects of SRS: Pre-Emphasis and Re-Emphasis

The power spectrum tilt effect of SRS can be compensated by input power pre-emphasis, and periodic re-emphasis along a link, using either dedicated DGE levelling nodes or ROADMs nodes which incorporate DGE functionality as described in section 2.8.

<sup>29</sup> Source: Ericsson, measurements by Dr Paul Harper

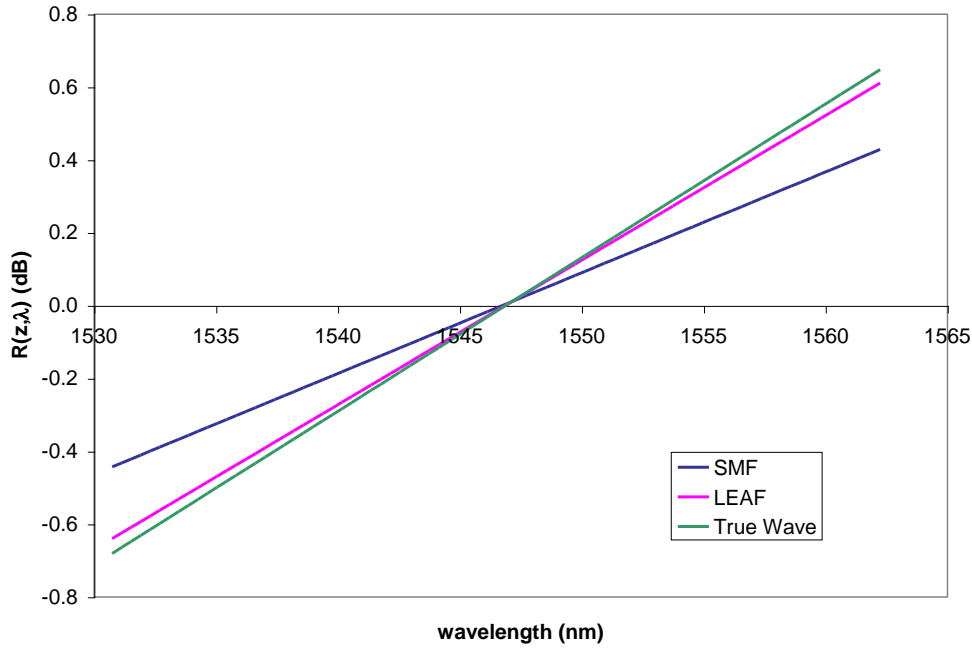


Figure 36 Raman gain for a 100km span of SMF and NZ-DSF with 20dBm total input power (after [25])

### 2.9.14 STIMULATED BRILLOUIN SCATTERING (SBS)

SBS occurs as a result of the optical signal interacting with acoustic waves or phonons. Acoustic vibrations cause refractive index changes to form a Bragg grating which results in the incident optical signal reflecting backwards towards the source. Brillouin scattering becomes stimulated as signal powers are increased producing gain in the counter-propagating direction thus depleting the transmitted signal.

The SBS threshold power is of the order of 1mW which is comparable with the channel powers used in commercial DWDM systems. However SBS has a narrow gain bandwidth of about 20MHz therefore much of the signal power lies outside this bandwidth significantly increasing the SBS threshold power [26]. Further techniques for mitigating SBS penalties include applying a frequency dither to increase the source linewidth or phase modulation which reduces the power in the optical carrier [26]. SBS is therefore not a problem in commercial DWDM systems and won't be considered further in this thesis.

### 2.9.15 NONLINEAR SCHRÖDINGER EQUATION (NLS)

Dispersion, loss and nonlinear phase shifts occur simultaneously as signals propagate through fibre. The nonlinear Schrödinger equation (NLS) is derived from Maxwell's equations by simultaneously describing the effects of attenuation, dispersion and

nonlinearity in optical fibre; details of the derivation are given in [47], this is the resulting equation in its simplified form

$$\frac{\partial A}{\partial z} + \frac{\alpha}{2}A + \frac{i\beta_2}{2}\frac{\partial^2 A}{\partial T^2} = i\gamma|A|^2A$$

**Equation 34**

Equation 34 describes propagation of a linearly polarised electrical field of amplitude  $A(z, t)$  in optical fibre, normalised such that optical power =  $|A|^2$ . In Equation 34, the terms in  $\alpha$  and  $\beta_2$  are coefficients describing attenuation and GVD respectively, the term in  $\gamma$  represents the nonlinearity, where the Kerr effect is typically the main source of nonlinearity. A frame of reference moving at the group velocity  $v_g$  (the so-called retarded frame) is used by making the transformation [47]

$$T = t - z/v_g \equiv t - \beta_1 z$$

**Equation 35**

The NLS is solved using an input field of the form [51]

$$A(0, T) = \sum_{m=1}^M A_m(0, T) e^{[i(\omega_m - \omega_0)T]}$$

**Equation 36**

where  $A_m(0, T)$  is the input signal of the  $m$ th channel.

In order to simplify the presentation of the theory, excluded from this form of the NLS in Equation 34 are higher order terms, including third order dispersion (i.e. dispersion slope), SRS, SBS and PMD.

### **Generalised Nonlinear Schrödinger Equation (GNLS)**

Third order dispersion is included in the simulations by using the generalised NLS equation (GNLS). From [47] and ignoring the shock term due to its negligible contribution [51] and the Raman term which is also negligible for pulse widths greater than 1ps [51] the simplified form of the GNLS becomes

$$\frac{\partial A}{\partial z} + \frac{\alpha}{2}A + \frac{i\beta_2}{2}\frac{\partial^2 A}{\partial T^2} - \frac{\beta_3}{6}\frac{\partial^3 A}{\partial T^3} = i\gamma|A|^2A$$

**Equation 37**

where  $\beta_3$  includes the effects of third order dispersion (dispersion slope); higher order dispersion curvature is negligible in the C-band for G.652 fibre therefore it is not considered.

Equation 37 is solved with the following input [51]

$$A(0, T) = \sum_{m=1}^M \sqrt{P_m} \left[ \sum_{k=1}^K b_k U_m(T - kT_B) \right] e^{[i(\omega_m - \omega_0)T]}$$

Equation 38

where  $P_m$  is the power and  $U_m$  is the pulse shape for the  $m$ th channel,  $T_B = 1/B$  is the bit slot at the bit rate  $B$ ,  $K$  represents the number of bits included in the numerical model, and  $b_k = 0$  or  $1$  depending on whether the  $k$ th time slot contains a 0 or 1 bit. A pseudo random bit sequence (PRBS) of length  $2^7-1$  is used in most of the numerical simulations presented in this thesis.

Equation 37 can be solved numerically using the split step Fourier method described in section 2.9.16. The fibre parameters:  $\alpha$ ,  $\beta_2$ ,  $\beta_3$  and  $\gamma$  become  $z$  dependent since they vary for different fibre types and can be included numerically as a piecewise constant function of  $z$ .

### Pulse Shape

The pulse shape  $U_m$  depends on the signal modulation format. For RZ modulation the pulse carver is modelled as a sinusoidally driven MZM, usually driven at a bias voltage  $V_{bias} = 0.29V_\pi$  and amplitude voltage  $V_{amp} = 0.21V_\pi$ , for which combination the full width at half maximum (FWHM) of the pulse is  $0.454T_B$  i.e. 45.4% duty cycle; a perfect ER is assumed for RZ. This is the resulting transfer function of the data modulator and RZ pulse carver

$$U(t) = \sqrt{P_0} \cos \left( \pi \frac{V_{bias}}{V_\pi} + \pi \frac{V_{amp}}{V_\pi} \cdot \cos \left( 2\pi \frac{t}{T} \right) \right)$$

Equation 39

With NRZ modulation format the pulse occupies the entire bit slot and is modelled as a Mach Zehnder modulator driven by a raised cosine electrical signal. So the electrical signal is  $V(t) = C \left[ \frac{1}{2} + \frac{1}{2} \cos \left( \frac{t}{T} \right) \right]$  in the transition regions, with a rise and fall time of  $0.1T_B$ . Perfect extinction ratio is assumed, therefore 0 in “0” bits and  $C$  in “1” bits outside the transition regions; which then drives a Mach Zehnder modulator

$$U(t) = \sqrt{P_0} \cos\left(\frac{\pi}{2} - \frac{\pi}{2}V(t)\right)$$

Equation 40

### Amplification and Noise

Signal amplification and noise can be included through the following equation in the frequency domain such that each spectral component of the field is modified at each amplifier location as [51]

$$\tilde{A}_{out}(\nu) = \sqrt{G}\tilde{A}_{in}(\nu) + \tilde{a}_n(\nu)$$

Equation 41

where  $G = \exp(\alpha L_A)$  is the amplifier gain,  $L_A$  is the amplifier spacing, and  $\tilde{a}_n$  is a complex Gaussian random variable whose real and imaginary parts have the same variance [51]

$$\sigma^2 = \frac{1}{2}n_{sp}h\nu_0(G-1)\delta\nu$$

Equation 42

where  $\delta\nu$  is the bandwidth occupied by each spectral component which is inversely related to the width of the temporal window used for numerical simulations. The noise figure of the amplifier is related to  $n_{sp}$  as  $F = 2n_{sp}$  given by Equation 2.

The spectral dependency of EDFA gain and noise figure described in section 2.7.3 can be calculated explicitly in the nonlinear simulation since Equation 41 is in the frequency domain. The noise is included as Gaussian noise in the frequency domain in every bin multiplied by the bandwidth of the bin.

### Fibre Attenuation

Fibre attenuation is also treated in the frequency domain so spectral dependence of transmission fibre and DCF attenuation described in section 2.9.2 can be calculated explicitly in the nonlinear simulation.

### SRS in Combined Wideband / Narrowband Simulations

Raman tilt gain and loss is modelled in the local linear step of the split-step Fourier method (defined in section 2.9.16) as a distributed Raman gain. In the narrowband nonlinear simulations the NLS is calculated according to [43]

$$\frac{\partial A}{\partial z} + \frac{i\beta_2}{2} \frac{\partial^2 A}{\partial T^2} = i\gamma|A|^2A + \frac{1}{2}[g_0(z) - \alpha]A$$

**Equation 43**

where  $g_0(z)$  is the Raman tilt at the centre frequency of the narrowband simulations, but governed by the wideband power distribution according to Equation 32 and Equation 33 (divided by  $L_{eff}$ ). The Raman gain is calculated as

$$P_{total}(z) = P_{total}(0) \cdot \exp(-\alpha(z))$$

**Equation 44**

and

$$g(z, \lambda_0) = P_{total}(z) \cdot (\beta(\lambda_0 - \lambda_{min}) - A_0)$$

**Equation 45**

with  $A_0$  such that the total gain is zero. Therefore  $A_0$  depends on the power distribution and depending on which side of the band  $g(z)$  will be positive (Raman gain) or negative (Raman loss); see Figure 36 for illustration of gains and losses.

### 2.9.16 SPLIT-STEP FOURIER METHOD

The GNLS cannot be solved analytically for the case of arbitrarily shaped pulses. Numerical procedures are required to solve it, the most commonly adopted and computationally efficient being the split-step Fourier method [57]. It is based on the principle that over short enough distances, the linear and nonlinear propagation effects can be considered separately to each other.

To understand the split-step Fourier method it is useful to re-write the GNLS of Equation 37 as [47]

$$\frac{\partial A}{\partial z} = (\widehat{D} + \widehat{N})A$$

**Equation 46**

where  $\widehat{D}$  is the differential operator that accounts for linear effects of chromatic dispersion and fibre loss and  $\widehat{N}$  is the differential operator that accounts for nonlinear effects on pulse propagation (Kerr nonlinearities). From Equation 37 these operators are given by

$$\hat{D} = -\frac{i\beta_2}{2} \frac{\partial^2}{\partial T^2} + \frac{\beta_3}{6} \frac{\partial^3}{\partial T^3} - \frac{\alpha}{2}$$

**Equation 47**

$$\hat{N} = i\gamma|A|^2$$

**Equation 48**

Generally, dispersion and nonlinearity act together along the length of fibre. An approximate solution is obtained with the split-step Fourier method by treating the nonlinear and dispersive effects independently as the optical field propagates over a small distance  $h$  [47]. In propagating from a distance  $z$  to  $z + h$  two steps are taken with nonlinearity and dispersion acting alone and with  $\hat{D} = 0$  and  $\hat{N} = 0$  in the first and second step respectively. This is written mathematically as [47]

$$A(z + h, T) \approx \exp(h\hat{D})\exp(h\hat{N})A(z, T)$$

**Equation 49**

where the linear operator  $\exp(h\hat{D})$  is solved in the frequency domain and the nonlinear operator  $\exp(h\hat{N})$  is solved in the time domain. The fast Fourier transform (FFT) algorithm [58] is used to switch from one domain to another. The choice of integration step size is critical in determining the accuracy of the solution and there exists a trade-off between accuracy and computational efficiency of the split-step method [47].

### Adaptive Step Size

Commonly an adaptive step size is used in order to keep calculation error within acceptable limits while keeping the computation time as low as possible. Typically the step size is limited by a maximum allowable nonlinear phase shift as well as a maximum phase shift due to chromatic dispersion between the furthest separated signal components [27]. As an example, in [27] the step size is calculated to keep the phase shift due to nonlinearities  $\Phi < 3\text{mrad}$  in a single step, with the maximum step size limited to 100m. In this thesis a proprietary adaptive step size method was used to maximise computational efficiency.

Higher order split step methods can be used to improve the computational efficiency and accuracy [47]. A higher order scheme is implemented in the simulator used throughout this thesis as described in [59] and [60]. Four steps forward of length  $\delta z$  are taken, followed by one backwards step of length  $2\delta z$ , then four more forward

steps of length  $\delta z$ . The leading order term in the accumulated error is proportional to  $4\delta z^3 + (-2\delta z)^3 + 4\delta z^3$  which cancels out at this order, leaving the leading term in the error per step proportional to  $\delta z^5$  i.e. fourth order accurate [59]. The fourth order method has an overhead due to performing more Fourier transforms but the reduction in step size makes it generally more computationally efficient.

### 2.9.17 SIMULATION PROCESS

The nonlinear simulation process is computationally intensive especially when simulating DWDM systems where the simulation time increases with approximately  $N^2$  where  $N$  is the number of channels [61]. Simulating up to 6 neighbouring co-polarised channels at a time, centred around 3 points across the C-band (1530, 1545 and 1560nm) with the remaining channels as CW radiation has been shown to be a valid approximation for simulating DWDM systems with greatly reduced computational time [61]. Even with an optimised adaptive step size and the simulation of a reduced number of channels, nonlinear simulations typically have a computation time in the order of hours or a day.

The spectral width of an FFT window is given by number of points per bit  $\times$  bit rate. To avoid numerical error from aliasing and FWM the FFT window must be wide enough, at least  $2 \times$  channel count  $\times$  channel spacing. For 100GHz channel spacing the spectral width must be greater than 1200GHz, therefore at 10Gb/s more than 120 points per bit are required; we use 128 points per bit and for 50GHz simulations we use 64 points per bit.

Linear simulations can be carried out by setting the nonlinear coefficient to zero and by making a slight adjustment to the dispersion map to fully compensate GVD with net zero dispersion at the end of the link in the absence of any opposing SPM. Without the need to use the split step algorithm and FFT for fibre transmission the simulation process takes seconds rather than hours.

## 2.10 MEASURING PERFORMANCE

This section gives details of different performance measurement parameters and techniques, including bit-error rate (BER), Q-factor calculation, estimating Q-factor from OSNR as well as details of physical impairment effect penalties not accounted for in simulations, and the performance enhancement capabilities of FEC.

### 2.10.1 BER AND Q-FACTOR

At the receiver the ultimate measure of performance is the bit-error rate (BER). If the total noise is assumed to follow Gaussian statistics and the effect of timing jitter is ignored then the BER is given by [51]

$$BER = \frac{1}{2} \operatorname{erfc}\left(\frac{Q}{\sqrt{2}}\right) \approx \frac{\exp(-Q^2/2)}{Q\sqrt{2\pi}}$$

Equation 50

where the  $Q$  factor parameter is defined as

$$Q = \frac{I_1 - I_0}{\sigma_1 + \sigma_0}$$

Equation 51

where  $I_1$  and  $\sigma_1$  represent the average and standard deviation values of the signal for 1 bits;  $I_0$  and  $\sigma_0$  are the corresponding values for 0 bits as indicated in Figure 38.

The relationship between Q-factor and BER of Equation 50 is plotted in Figure 37.

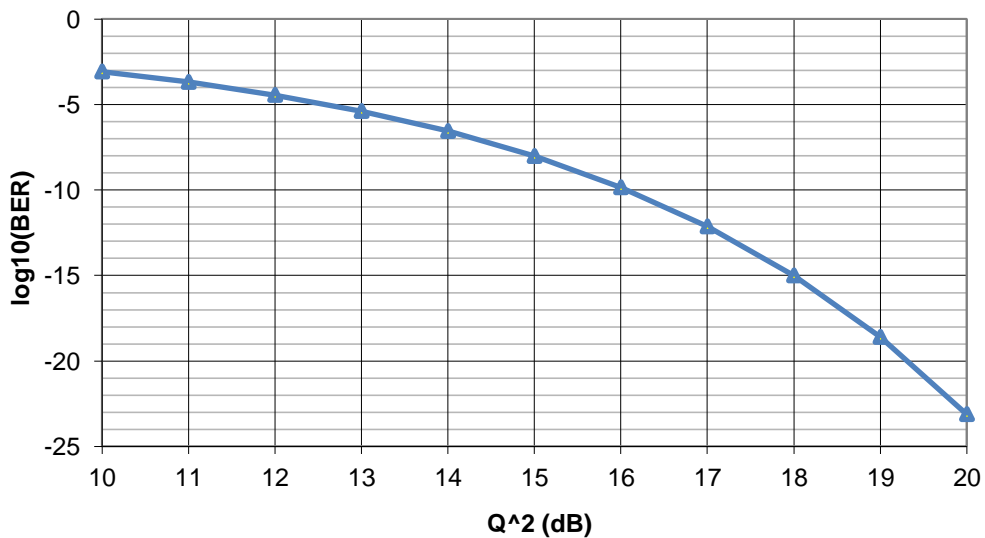


Figure 37 BER as a function of Q-factor (pre-FEC)

Thus to achieve the target BER of  $10^{-15}$  requires a  $Q=18$ dB without FEC.

We cannot usually observe the BER directly in system simulations since the computational power available limits the practical PRBS lengths to  $2^7-1$  and for pulse streams of that length we will not observe any errors at typical system BER. The Q-factor is therefore a more meaningful measurement of performance in system

simulations and is used throughout this thesis to characterise the performance of optical transmission systems.

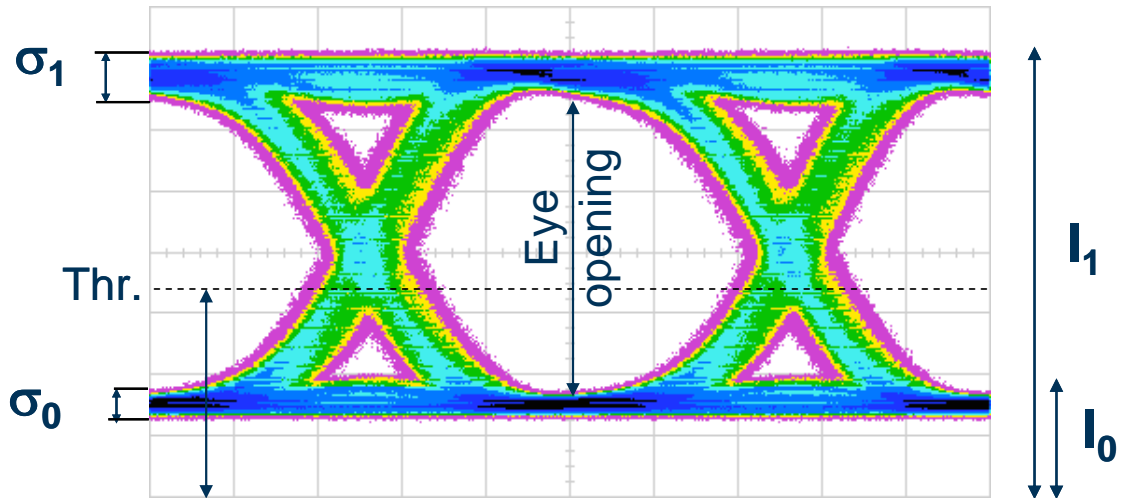


Figure 38 Eye diagram for NRZ-OOK signal with parameters used in Q-factor definition<sup>30</sup>

### Obtaining Q-factor from Nonlinear Simulations

Calculating the Q-factor in numerical simulations is described in [51] as follows: first the field at the end of a link of length  $L$ ,  $A(L, t)$  is optically filtered with a filter of bandwidth  $B_o$  to select a fixed channel, converting the bit stream to the electrical domain with a current  $I(T) = R_d |A(L, t)|^2$  where  $R_d$  is the photodetector responsivity. The electrical signal is then filtered with a filter whose bandwidth  $B_e$  is smaller than the bit rate  $B$  and is typically in the range 0.6 to 0.8 $B$ ;  $B_e = 7\text{GHz}$  is assumed, and  $B_o$  is of the order 38 to 60GHz depending on the exact mux / demux configuration used in the system.

Q-values are usually obtained as the worst of 6 channels, averaging five different simulation runs with different noise seeds, using the same  $2^7-1$  PRBS sequence for each channel, with a random timing offset between each channel in order to decorrelate between each channel and simulation run.

<sup>30</sup> Source: Ericsson

### Alternative Approach: Eye Closure Penalty

The eye closure penalty is a measure of the change in the opening of the eye, quantified through the minimum value of  $I_1$  and the maximum value of  $I_0$  at the bit centre of a noisy bit stream [51] as illustrated in Figure 38.

### Optimum Threshold

The optimum decision threshold, minimising the BER, is given by

$$Thr. = \frac{I_1\sigma_0 + I_0\sigma_1}{\sigma_1 + \sigma_0}$$

Equation 52

### Limitations of the Q-factor

The relationship between Q and BER depends on the statistical model of the channel and is only valid in the case of noise with Gaussian distribution: an approximation that is not generally the case but nonetheless the result is reasonably accurate [62], [63].

## 2.10.2 ESTIMATING Q-FACTOR FROM OSNR

Since the OSNR at the receiver is converted to an electrical SNR which eventually defines the Q-factor and BER it is possible to infer the BER performance from the received OSNR. Having calculated the OSNR at the receiver neglecting receiver thermal noise and shot noise (a valid approximation with high gain), the Q-factor is related to the OSNR by [26]

$$Q[dB] = 20 \log \left[ \frac{2OSNR}{1 + (4OSNR + 1)^{1/2}} \left( \frac{B_o}{B_e} \right)^{1/2} \right]$$

Equation 53

where  $B_o$  and  $B_e$  are the optical and electrical bandwidths. The electrical bandwidth is given by  $B_e = 0.7 \times \text{baud rate} = 7\text{GHz}$  for a 10Gb/s OOK signal.

The OSNR within Equation 53 is measured in the optical bandwidth of the demux filter and not the 12.5GHz reference bandwidth, therefore any OSNR calculated from Equation 14 which defines the link OSNR must be rescaled as  $OSNR \times \frac{12.5\text{GHz}}{B_o}$  before substituting in Equation 53. For 40 channel systems  $B_o$  is a 60GHz second

order Gaussian filter and for 80 channel systems  $B_0$  is a 38GHz second order Gaussian filter.

The relationships between Q-factor and OSNR for these two bandwidths are plotted in Figure 39 (red line for 40 channel filter, green line for 80 channel filter). Thus to achieve the target Q-factor of 18dB, the required OSNR is approximately 17dB with it being slightly lower for the narrower filter. The target Q-factor of 18dB is driven by the required BER (defined earlier).

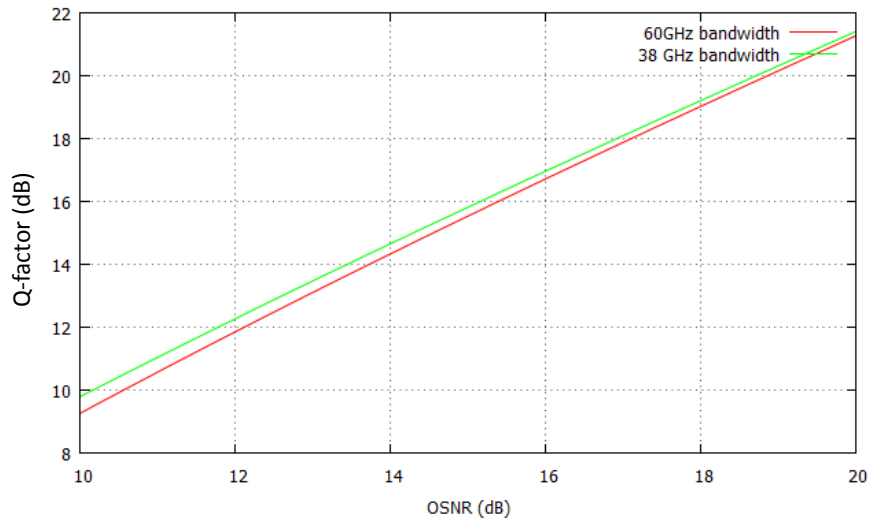
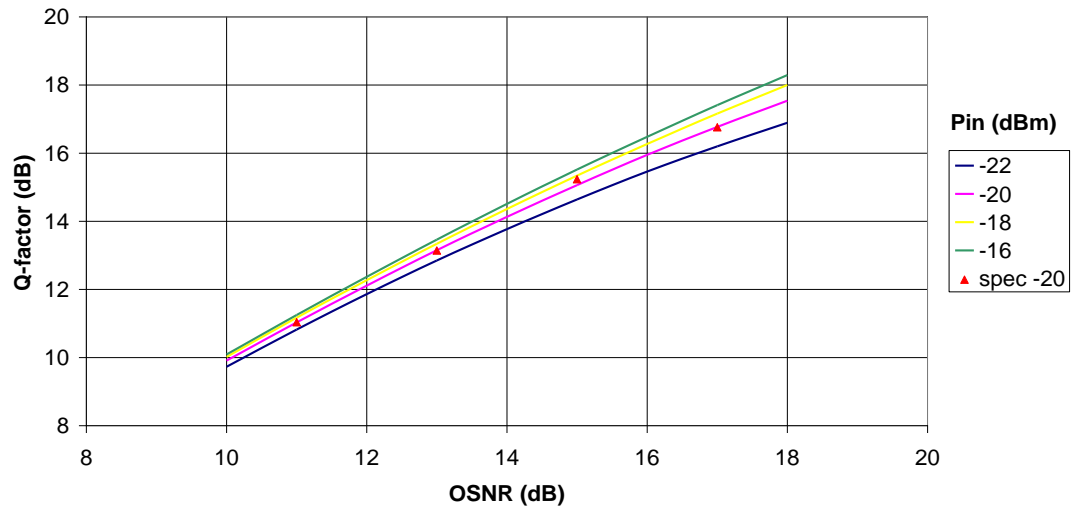


Figure 39 Q-factor (dB) as a function of OSNR (dB)

### Realistic Receiver Model

Equation 53 and Figure 39 represent an ideal receiver model. Actual receiver performance differs and is dependent on a number of parameters including the received signal power and detailed receiver characteristics. A more complex model is required to characterise the BER performance of a receiver for a given OSNR. Figure 40 shows the actual BER performance vs. received signal power and OSNR for a 10Gb/s RZ transponder<sup>31</sup>. Details of the model are not presented however Figure 40 shows that a slightly higher OSNR is required to achieve a specific BER than predicted by the ideal receiver model. A higher received signal power  $P_{in}$  results in improved BER performance for a given OSNR.

<sup>31</sup> Receiver model developed by Dr Fabio Cavaliere and Gianmarco Bruno



**Figure 40 BER performance vs. received signal power and OSNR for 10Gb/s RZ transponder<sup>32</sup>**

The simple relationship of Equation 53 and the realistic receiver model in Figure 40 don't include fibre transmission impairments such as those due to dispersion and nonlinearities. Q-factor penalties must be calculated for transmission impairments and subtracted from the raw Q-factor in order to determine the actual Q-factor. An example of this approach to system margin calculation can be found in [64].

### **Simplified Analytical Modelling for Link Engineering**

Various analytical models have been developed to characterise linear and nonlinear transmission impairment penalties for DWDM systems. An analytical approach can enable rapid estimation of BER as an alternative to computationally intensive but more accurate numerical simulations. Analytical models can be incorporated in link engineering tools to quickly evaluate link feasibility in customer networks. Simplified models can also be used as a photonic path computation engine within network planning tools for impairment aware wavelength routing and assignment (WRA).

While simplified analytical models are useful for link design, numerical simulations are preferred for transmission studies where accuracy is essential for testing new concepts and establishing engineering rules. This is especially true for transmission over ULH distances where fibre nonlinearities are a major performance limiting impairment. Analytical modelling is not considered in this thesis.

<sup>32</sup> Source Ericsson

### 2.10.3 IMPAIRMENT PENALTIES FOR NON-SIMULATED IMPAIRMENTS

Certain transmission impairment effects are not accounted for in the numerical simulations. These include: transmitter and receiver wavelength drift, mux / demux filter drift, GV, PDL, PMD, OADM filtering and part of the dispersion penalty. Q-factor penalties have been calculated for each of these impairments by Photonics Modelling Team colleagues; the penalties are summarised in Table 4, details of the models are not presented here. A total 7.2dB Q-factor penalty should be accounted for in addition to the simulated fibre nonlinear effects and receiver model optical and electrical filtering. Out of 7.2dB, 1.2dB are included in the simulations (see Table 4) therefore a net total of 6dB Q-factor penalties are excluded from the simulations.

Impairment Effect	Q-factor Penalty (dB)	Included in Simulations (dB)	Excluded from Simulations (dB)
Tx/Rx Drift	1.0	0.0	1.0
Mux/Demux Filter Drift	1.5	0.5	1.0
GV	1.0	0.0	1.0
PDL	1.0	0.0	1.0
PMD	1.0	0.0	1.0
OADM Filtering	0.5	0.5	0.0
Dispersion	1.2	0.2	1.0
<b>Total</b>	<b>7.2</b>	<b>1.2</b>	<b>6.0</b>

Table 4 System penalties for effects included and not include in 10Gb/s numerical simulations

### 2.10.4 FEC CODING GAIN

A BER performance of  $10^{-15}$  or better is usually required to provide sufficient margin for a commercial DWDM system over its expected lifetime. In order to achieve a BER of  $10^{-15}$  with no FEC, a Q-factor of 18dB would be required. Various FEC implementations are available and some are capable of correcting pre-FEC BER as bad as  $10^{-3}$  to a post-FEC BER of  $10^{-15}$ . Enhanced FEC (eFEC) is assumed in this thesis as detailed in ITU-T Recommendation G.975.1 (Appendix I.7) [65].

In order to define a coding gain parameter from a systems perspective, the BER reduction by the FEC is transformed into dB based on a theoretical reference system;

the coding gain  $CG$  is defined as the reduction in required SNR or Q-factor at a reference BER [65]

$$CG = 20 \log_{10} \left[ \frac{\text{erfc}^{-1}(2BER_{FEC})}{\text{erfc}^{-1}(2BER_{RAW})} \right] \text{ (dB)}$$

Equation 54

where  $\text{erfc}^{-1}$  is the inverse of the complementary error function,  $\text{erfc}(x) = 1 - \text{erf}(x)$ .

Net coding gain is characterised by the code rate,  $R$  where ( $R < 1$ , is the ratio of the bit rate without FEC to the bit rate with FEC) [65] as

$$NCG = CG + 10 \log_{10}(R) \text{ (dB)}$$

Equation 55

Figure 41 summarises the error correcting capability of eFEC with overheads of 7%, 11% and 25%; a 7% overhead is assumed in this thesis. Interpolating from Figure 41 or more accurately from a table of error correcting capability in [65]: eFEC with 7% overhead can correct an input BER as high as  $1.3 \times 10^{-3}$  to an output BER of  $10^{-15}$ , with  $CG = 8.41 \text{ dB}$  and  $NCG = 8.09 \text{ dB}$ .

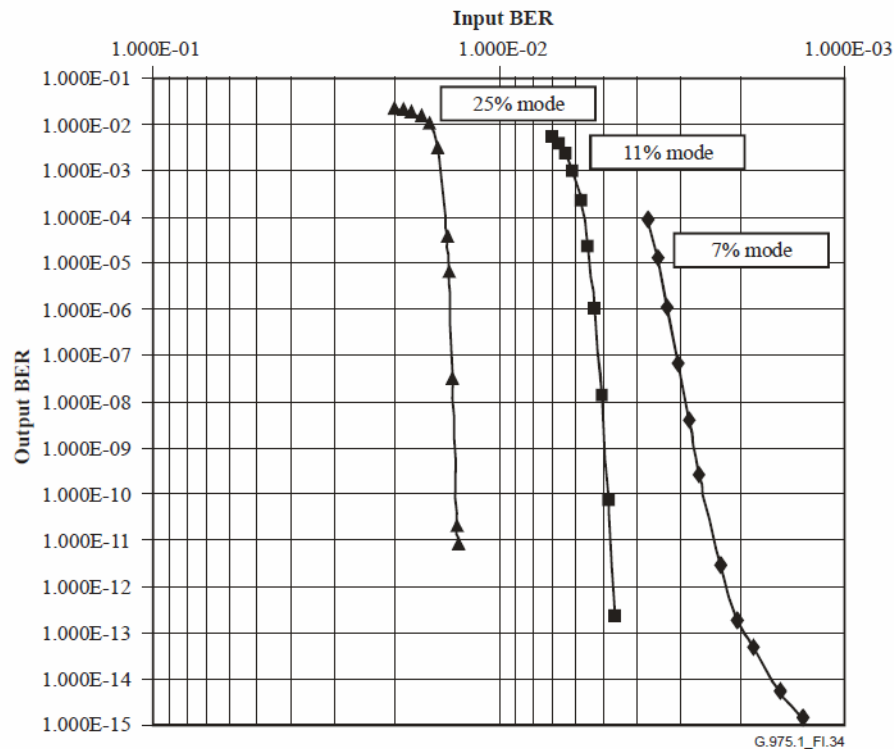


Figure 41 Post-FEC (Output) BER vs. pre-FEC (Input) BER for G.975.1 FEC code (after [65], Copyright © ITU. Permission to reproduce this figure has been granted by the ITU).

State of the art soft decision FEC (SD-FEC) is been introduced in many next generation 100Gb/s DWDM systems [66], which can further increase the coding gain by about 2dB, correcting BER as high as  $1.9 \times 10^{-2}$ .

### 2.10.5 REQUIRED Q-FACTOR FROM SIMULATIONS

For link simulations, the Q target is the minimum required Q-factor of the input signal for the receiver decision circuit to achieve a reference BER, it is defined as

$$Q_{target} [dB] = 18[dB] - CG[dB] + Q_{penalties}[dB]$$

Equation 56

where  $Q_{penalties}[dB]$  are power penalties for physical impairment effects which are not accounted for in propagation simulations (see section 2.10.3). The Q-target for the most common interfaces considered in this thesis are shown in Table 5.

	10Gb/s RZ	10Gb/s NRZ	40Gb/s RZ-DQPSK
Q-factor target for $10^{-15}$ BER (dB)	18	18	18
Q penalties (dB)	6.0	6.0	6.0
eFEC GCG (dB)	8.4	8.4	8.8
<b>Q-factor target pre-FEC (dB)</b>	<b>15.6</b>	<b>15.6</b>	<b>15.2</b>

Table 5 Q-factor targets from nonlinear simulations for various interfaces

It must be emphasised that these Q-targets are budgetary and only serve as an indication of the likely Q-margin, due to the simple allocation of a fixed penalty regardless of individual link details. More complex link dependent penalty models have been developed but since this thesis generally benchmarks one system architecture approach against another, the absolute Q-margin is of less importance than the relative differences between compared Q-factors.

## 2.11 OVERVIEW OF MODELLING PROCESS AND TOOLS

Ericsson's in-house modelling tool suite for optical system simulation and link engineering<sup>33</sup> is used throughout the research presented in this thesis. This research programme contributed to the development of these tools, in particular the combined wideband power variation model and narrowband nonlinear simulations. The author specified the functionality and carried out the testing of these components of the modelling tool suite. *Link Design Tool (LDT)* performs link engineering, OSNR calculations and Q margin estimation using simplified analytical models. *Link Simulation Tool (LST)*, performs full nonlinear system simulations, wideband OSNR calculations and combined nonlinear simulations with wideband power variations. A commercially available network planning tool *OPNET SP Guru Transport Planner* is used for higher-level network planning research presented in Chapter 5. Figure 42 shows the three main modelling tools including the main data flows between each tool. The following sections give further details on the *LST* and *LDT*; the Network Planning Tool is described in section 5.4.3.

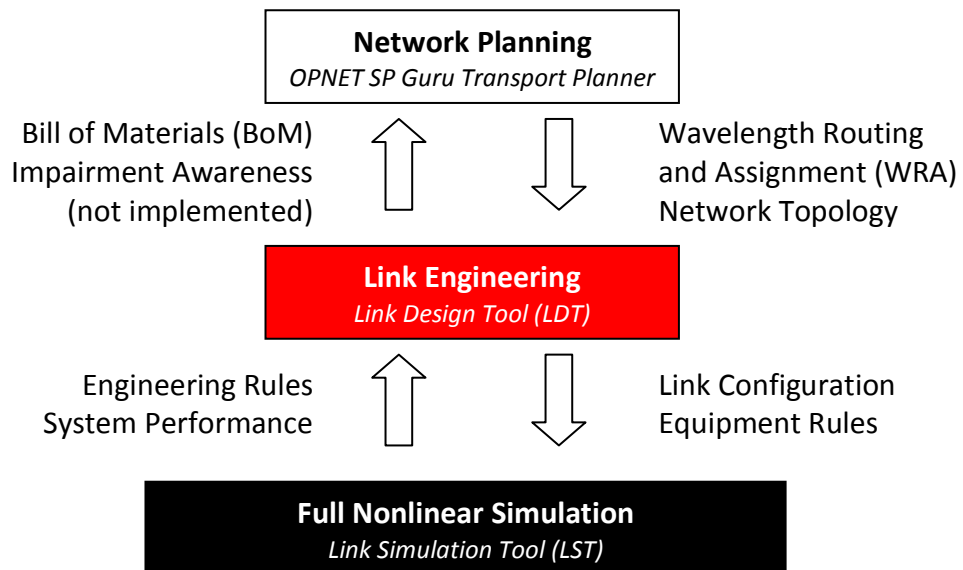


Figure 42 Overview of modelling tool suite and main data flows between each tool.

### 2.11.1 LINK ENGINEERING

*LDT* is developed primarily for use by systems engineers in designing networks for customer deployment, and for potential customers when responding to RFPs and

<sup>33</sup> The algorithms within the tools were jointly developed by Ericsson's Photonics Modelling Team of which the author was a member. Software implementation is the work of Dr Jeroen Nijhof and Gianmarco Bruno.

RFQs. It is also used by expert system designers and network architects where extra features are available to carry out more detailed design and analysis, particularly for non-standard network applications. It also allows modification of the underlying component specifications and models which is useful when developing new system features (e.g. 100Gb/s) and analysing performance trade-offs due to component specification changes.

*LDT* allocates transponders, amplifiers and DCF to individual network elements within a user-defined network topology, based on user-defined per span fibre characteristics and traffic matrix.

*LDT* also calculates performance metrics including OSNR, various transmission impairment penalties (CD, PDL, PMD, nonlinearity, and filtering penalties) using analytical / semi-analytical models. Following subtraction of penalties and conversion of OSNR to Q via a suitable optical interface model and addition of FEC gain, a Q margin is calculated from which the BER can be estimated. This approach is computationally more efficient than full numerical simulation and more appropriate for multi-reach applications where nonlinear effects are not always a limiting factor as is the case for ULH applications.

For the research presented in this chapter *LDT* is only used to allocate network elements, amplifiers and DCF based on the fibre span data producing a configuration file. Optical performance along a link defined by *LDT* in a configuration file is accurately evaluated by running full nonlinear simulations using *LST*.

### **2.11.2 LINK NONLINEAR SIMULATION**

*LST* is a C++ based library for numerically solving the NLSE using the Split-Step Fourier method as described in section 2.9.15 to 2.9.17. The library includes models of selected system elements: transmitters, amplifiers, fibres, filters, multiplexers and receivers. Narrowband nonlinear simulations can be carried out either in isolation or combined with wideband OSNR calculations. It is also possible to carry out wideband OSNR calculations in isolation.

*VPI Transmission Maker*,<sup>34</sup> a commercial physical layer modelling tool [67], was used to test and validate results during the development of the in-house modelling tools.

A high performance computing cluster (HPC) was used to run lengthy nonlinear simulation jobs in parallel. The cluster consists of a number of blades, some with dual processor, dual core and some with dual processor, quad core (*AMD Opteron 2.4GHz*) with a grand total of 132 cores. Simulation jobs are launched and processed for analysis by executing *Perl* scripts.

*LST* reads a link configuration file produced by *LDT* and simulates propagation of the optical field through the defined link, writing out *Q* versus distance for all the channels, and the evolution of power and spectral width.

A limitation of nonlinear simulations is that they are usually carried out narrowband, in that at most 6 channels can be simulated due to computation time constraints and fairly limited errors. Spectral variations in signal gains and losses are not normally accounted for. To investigate performance across the C-band, simulations are done in 3 sets of 6 channels at a time at 1530, 1545 and 1560nm wavelengths.

### **Dispersion Map Optimisation**

Dispersion map optimisation is carried out by reading the raw output, i.e. the field which is stored after the nonlinear compensation, and then calculating *Q* after applying various amounts of linear post-compensation to that field and selecting the best value which gives optimum performance for the 18 channels simulated across the C-band (i.e. the 3 groups of 6 channels near to 1530, 1545, 1560nm).

### **Combined Nonlinear Simulation and Model of Wideband Power Variations**

As part of this research programme *LST* was extended<sup>35</sup> with models to account for wideband power variations due to EDFA gain and noise figure spectrum, fibre attenuation spectrum and SRS induced gain tilt. Nonlinear simulations are carried out with amplifier gain and noise figure calculations driven by the wideband EDFA black-box model of spectral gain and noise. Wideband power variations are mitigated by input signal power pre-emphasis and periodic signal re-emphasis or levelling.

---

<sup>34</sup> [www.vpiphotonics.com](http://www.vpiphotonics.com)

<sup>35</sup> Software implementation by Dr Jeroen Nijhof

## 2.12 WIDEBAND OSNR: MODELLING AND SYSTEM TEST

In this section the wideband OSNR model is tested for a 3,091km ULH link and compared with system test lab measurements<sup>36</sup>. This study was carried out as preparation for the final deployment of the equipment in the 3,000km link between Perth and Adelaide in Australia, in order to test the spectral OSNR model before integration with the nonlinear simulation method.

### 2.12.1 LINK CONFIGURATION

The 3,091km system test-bed link comprises 39 spans of approximately 80km each. A total of 6 levelling nodes were distributed along the link approximately 6 spans between each leveller; a slightly more conservative distribution of levelling nodes than required. *LDT* was used to configure the link according to the EDFA, DCM and levelling node combinations available for use in the test-bed. *LST* was then used to perform wideband OSNR calculations at the output of each EDFA along the link.

Measurements were also carried out at the output of each EDFA for a total of 80×10Gb/s RZ channels with an average signal launch power of -1dBm/channel. *LST* was used to calculate the optimum linear pre-emphasis profile at that average launch power of -0.3dB/THz or +1.2dB over the entire C-band on a nm scale; this pre-emphasis profile was applied in the system test-bed.

### 2.12.2 RESULTS AND ANALYSIS

#### OSNR Evolution

Figure 43 shows the OSNR as a function of the number of EDFA along the link: solid lines are simulation results with no pre-emphasis and dots are measurements with optimum pre-emphasis applied (unfortunately there are no measured results available without pre-emphasis for comparison).

The simulated performance at 1561nm shows the OSNR is significantly lower than other parts of the C-band with an OSNR of 13.4dB at the end of the link, compared with the best OSNR of 15.4dB at the centre of the C-band. Measured OSNR are generally higher than simulated OSNR (14.9dB and 16.3dB for the worst and best measured OSNR respectively). One possible factor behind this difference is that

<sup>36</sup> Source: Ericsson, measurement results are the work of Dr Liam Gleeson and Dr Paul Harper

optimum pre-emphasis is applied to all measured results whereas no pre-emphasis is applied to the simulations in this case.

Figure 44 shows the equivalent results where the optimum linear pre-emphasis profile is applied to both simulation and measurements. Simulated OSNR of the worst channel increases to 14.0dB while the best OSNR remains at 15.4dB around the centre of the C-band. These figures are still almost 1dB lower than the measured results, which is not perfect but it shows a reasonable agreement between simulations and measurements. Other possible factors which could cause the difference between simulations and measurements: statistical variations in the amplifier data used to derive the black box model or errors in the Raman gain tilt.

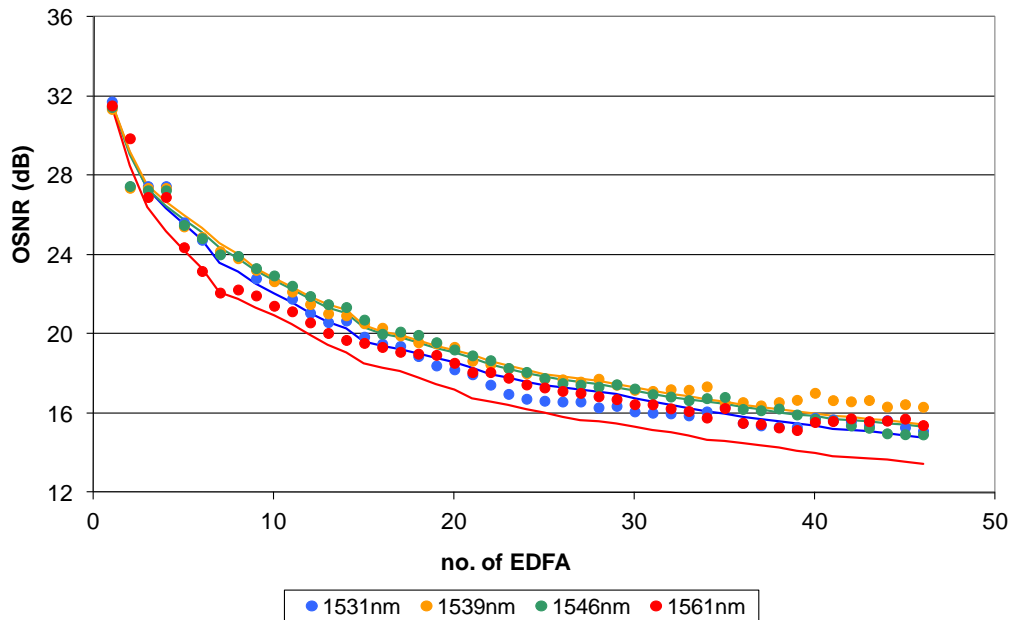


Figure 43 OSNR vs. no. of EDFA for 3,091km link (solid lines are simulation with no pre-emphasis and dots are measurements with optimum pre-emphasis).

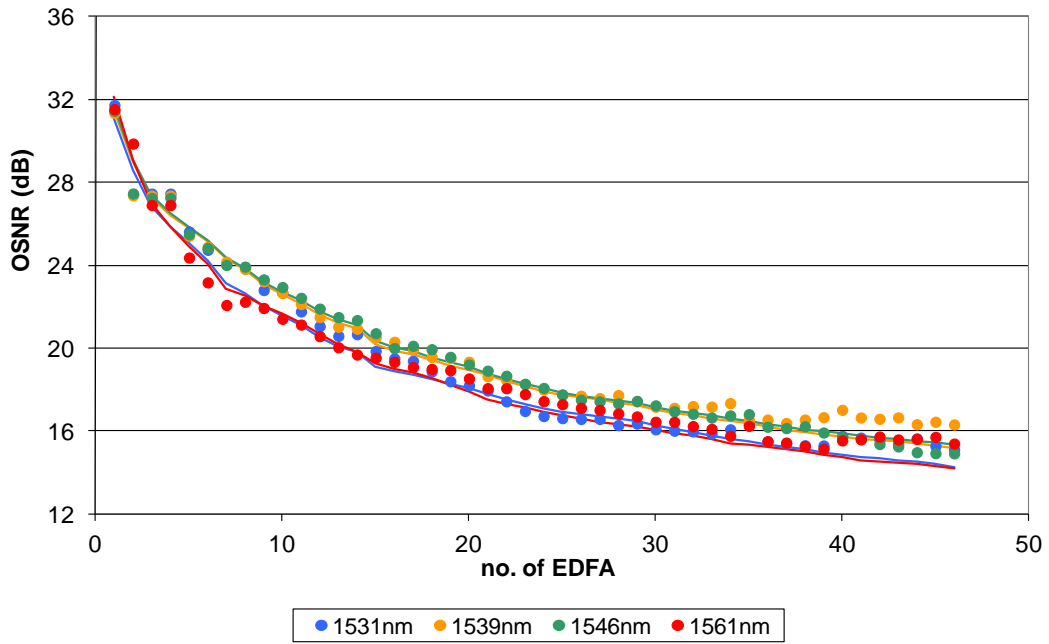


Figure 44 OSNR vs. no. of EDFA for 3,091km link optimum linear pre-emphasis applied to simulation (solid lines) and measurements (dots).

### OSNR Spectrum

Figure 45 shows the measured and modelled OSNR spectrum at the end of the transmission link. The linear pre-emphasis can be seen to decrease the spread in OSNR spectrum by increasing the performance at the 1560nm end of the C-band above the required OSNR threshold with a corresponding decrease in the performance at the 1530nm end of the band.

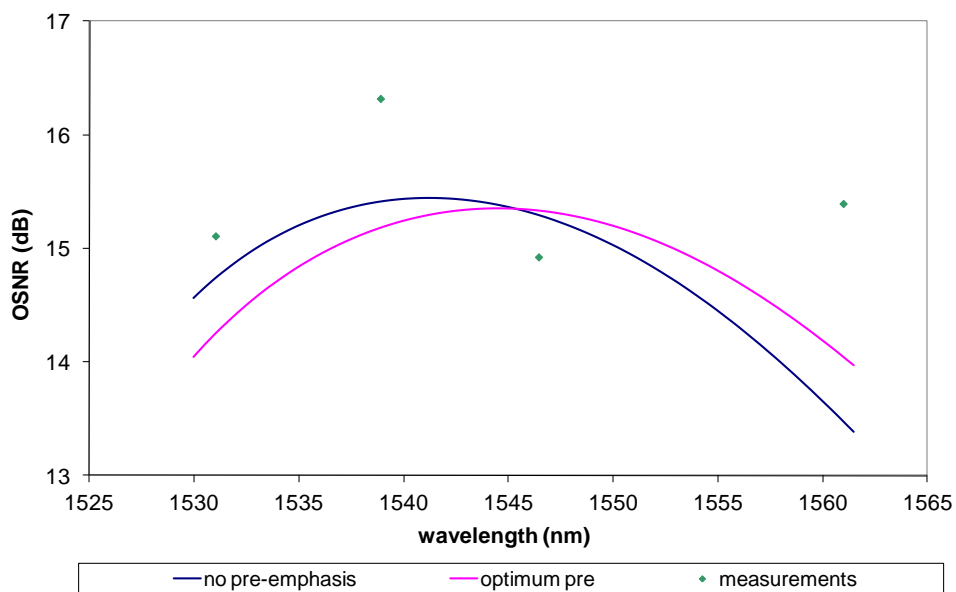
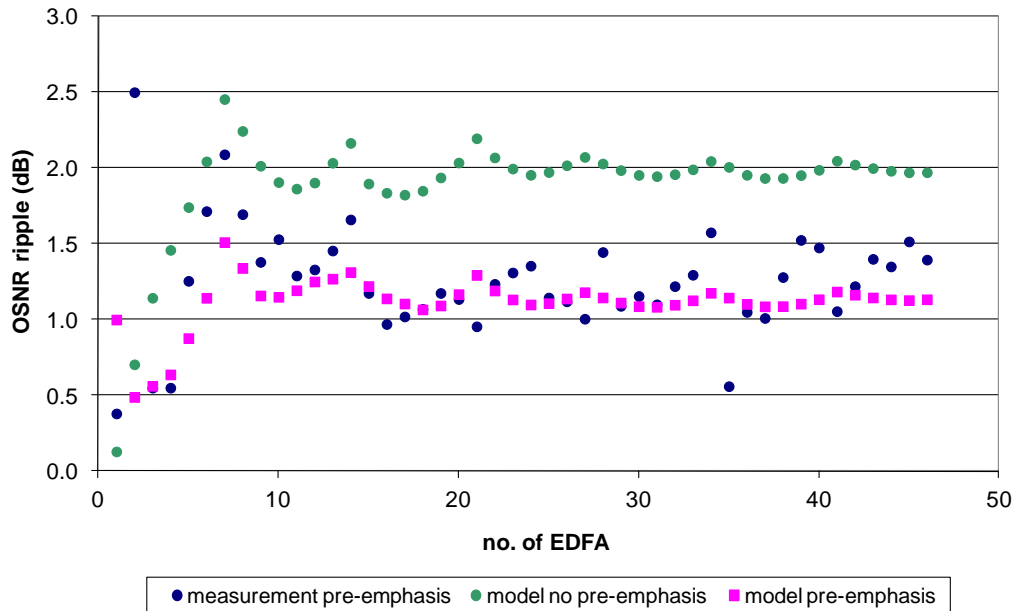


Figure 45 Modelled OSNR spectrum for 3,091km link with and without pre-emphasis and experimental OSNR measurements with pre-emphasis

### OSNR Ripple

Evaluating the OSNR ripple at the end of the link i.e. ( $OSNR_{max} - OSNR_{min}$ ) across the C-band as shown in Figure 46 indicates an improvement in the simulated OSNR ripple from around 2dB with no pre-emphasis down to around 1dB with optimum linear pre-emphasis. The measured OSNR ripple where optimum linear pre-emphasis was also applied shows good agreement to within  $\pm 0.5$ dB of the simulated figures.



**Figure 46 OSNR ripple across C-band for measured data and model with and without pre-emphasis.**

### Power Flatness

Measured and modelled power flatness along the link is shown in Figure 47; the minima in power flatness indicate the location of the levelling nodes which minimise the power variations across the C-band. Measured data and model are in good agreement until the location of the 4<sup>th</sup> levelling node (EDFA no. 28) from where the measured flatness increases significantly more than the model predicts. The model assumes ideal levelling i.e. that the channel profile can be completely levelled with single channel resolution to the desired profile. The levelling device used in the measurements was an early prototype with lower resolution and could not correct for large channel to channel power variations.

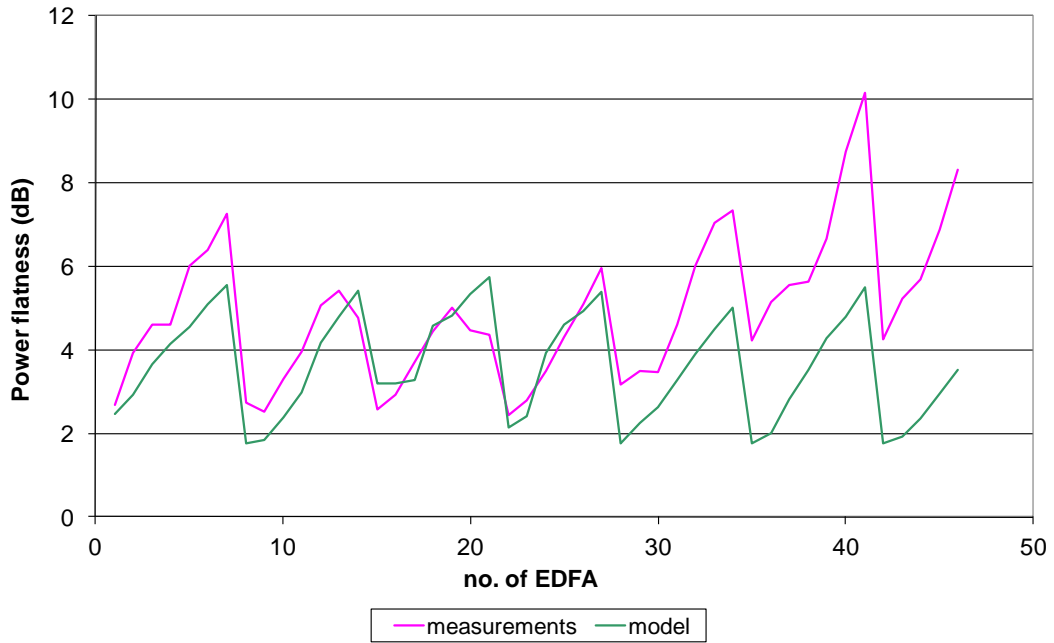


Figure 47 Measured and modelled power flatness vs. no. of EDFA for 3,091km link.

### Power Spectrum

Figure 48 shows the launch power profile with no pre-emphasis and with optimum linear pre-emphasis tilt of  $-0.3\text{dB/THz}$  ( $+1.2\text{dB}$  over the C-band on nm scale). Figure 49 shows the spread in the power spectrum at the end of the link also improves with the pre-emphasis which is applied to optimise OSNR.

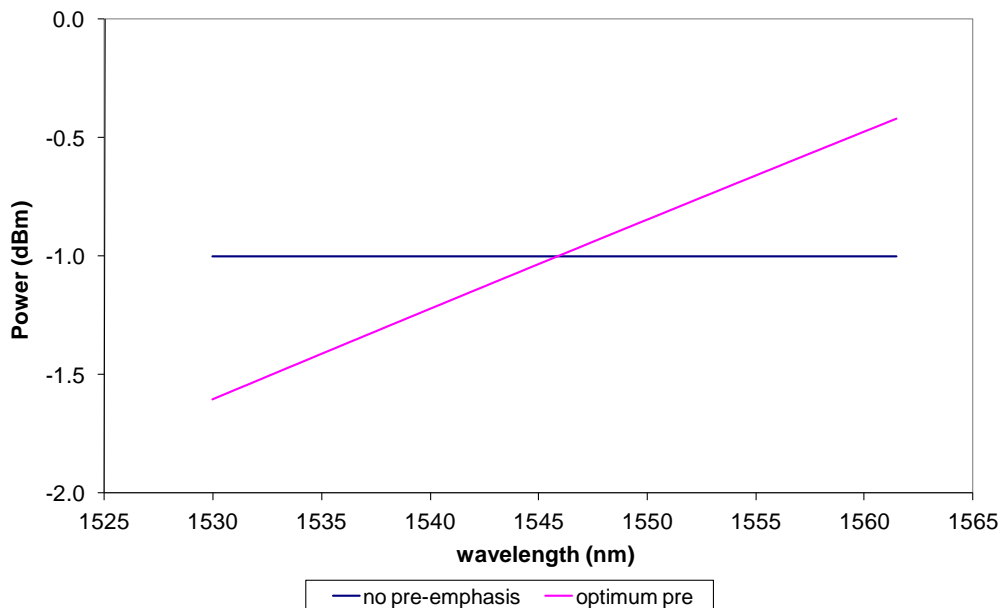
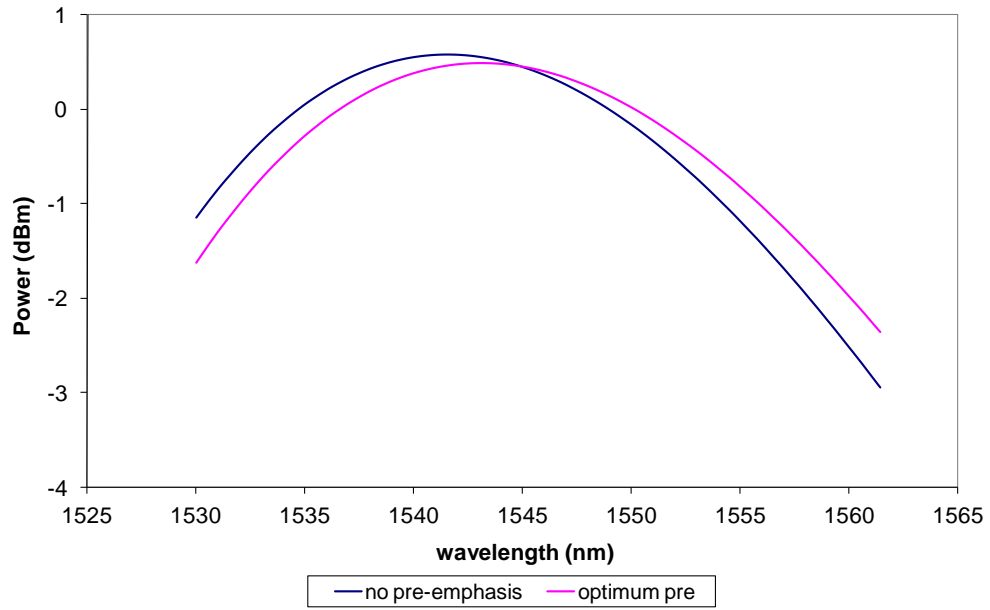
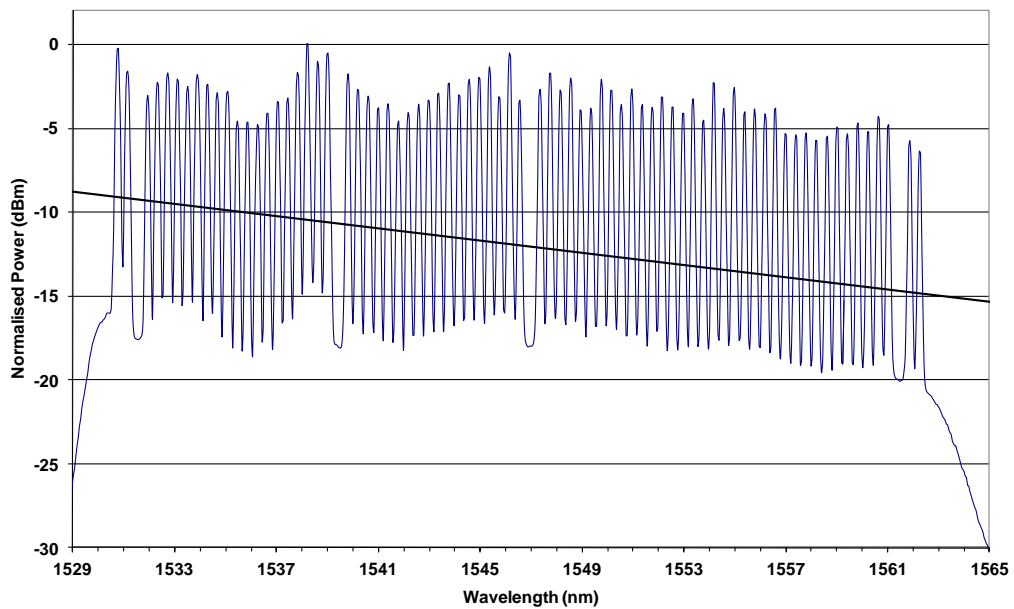


Figure 48 Modelled launch power spectrum for both no pre-emphasis and optimum linear pre-emphasis profile for OSNR equalisation in 3,091km link



**Figure 49** Power spectrum at end of 3,091km link with no pre-emphasis and with optimum pre-emphasis

The equivalent measured spectrum is shown in Figure 50 with the power tilt indicated by the straight line. It is clear that the measured spectrum contains more ripple than the simulations predict, however the tilt is comparable.



**Figure 50** Measured power spectrum at end of 3,091km link<sup>37</sup>

<sup>37</sup> Source: Ericsson

### System Tolerance to Pre-Emphasis Variation

Figure 51 summarises the OSNR of the best performing channel (pink line), the worst performing channel (green line) and power spread (blue line) at the end of the link for varying pre-emphasis.

Depending upon the exact required OSNR for a particular system, the worst channel OSNR (green line) may only be above the threshold for a limited range of pre-emphasis values. As an example, if the required OSNR was 13.6dB, the worst performing channel will have an OSNR which is above the threshold only within the region highlighted by the grey box i.e. for a pre-emphasis between 0.4 and 2.2dB across the C-band.

The permitted power spread at the receiver should also be within the limits of the system. This limit is set by the receiver dynamic range, less the uncertainty in demux filter losses. Assuming a 14dB receiver dynamic range and 7.5dB uncertainty in demux filter losses, the maximum received power spread should be less than 6.5dB. The simulated received power spread (blue line in Figure 51) remains below the permitted limit of 6.5dB across the full operating range of the system.

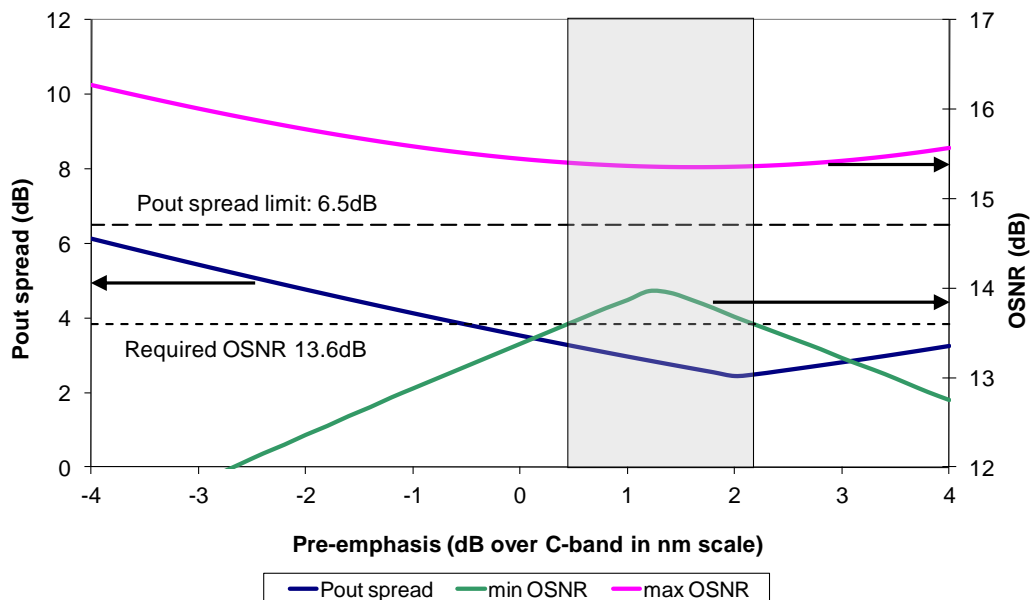


**Figure 51** Grey area highlights region of operation where OSNR and power spread are both optimised within acceptable limits

### Optimum Pre-Emphasis vs. Number of Channels

Due to the influence of SRS which increases log linearly with total signal power amplifying long wavelength channels at the expense of shorter wavelength channels, the optimum pre-emphasis changes with the number of channels present in a DWDM system as shown in Figure 52. The optimum pre-emphasis measured in dB across the C-band (nm scale) decreases linearly with channel count.

The modelling tool developed as part of this research programme is used when configuring links to define the relationship between the number of channels and the optimum pre-emphasis; a relationship which is unique to each individual link but similar to the example in Figure 52. As channels are added to the system, the EMS and NMS automatically adjusts the pre-emphasis profile according to the relationship defined by the modelling tool.

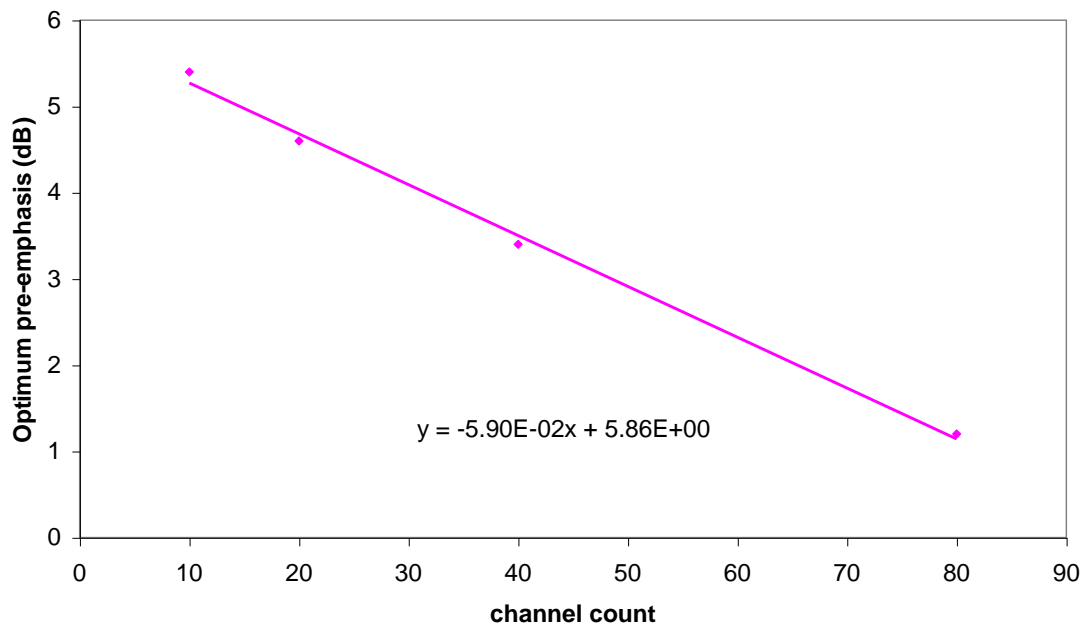


Figure 52 Optimum pre-emphasis across C-band vs. channel count.

### 2.12.3 CONCLUSIONS OF WIDEBAND OSNR MODELLING AND TEST

Analysis using the framework developed for modelling the spectral dependence of wideband OSNR variations showed good agreement with system measurements. Pre-emphasis profiles which maximise OSNR performance across the C-band were determined by fast linear calculations integrated within a link simulation tool. System tolerance to inaccuracies in the pre-emphasis setting were determined as part of OSNR margin calculations. The optimum pre-emphasis tilt required for different

channel counts is a log linear function of channel count enabling simple automated adjustment of pre-emphasis as channels are added to, or dropped from a DWDM system.

Now that the wideband OSNR model has been tested, in section 2.13 the combined wideband power variation model and nonlinear simulation tool outlined in section 2.11.2 is used to predict the optimum power pre-emphasis profile taking into account interactions between wideband power variations and Kerr nonlinear effects.

### **2.13 PREDICTING OPTIMUM PRE-EMPHASIS PROFILES**

Predicting the optimum pre-emphasis profile for ULH DWDM systems requires modelling tools and processes which not only account for the spectral variations in channel power due to ASE, SRS and fibre attenuation profile but which integrate these models into a full nonlinear simulation. This requirement is due to the fact that large channel power differences due to EDFA gain and ASE tilt and ripple, SRS tilt and fibre attenuation profile will lead to variations in Kerr nonlinear penalties across the transmission band. Reference [46] (published after the research presented here was published in [19]) elegantly explains the problem: spectral power variations across the transmission band lead to OSNR reduction for the channels with minimum power and Kerr nonlinear penalties for the channels with maximum power. In [46] an experimental implementation of signal levelling is reported which ensures minimum variations in path averaged power among WDM channels between dynamic gain equalising nodes, resulting in uniform nonlinear and spontaneous emission penalties across the WDM spectrum in a ULH system.

Using the modelling framework developed in this chapter and outlined in section 2.11 the performance of  $80 \times 10$  Gb/s RZ channels transmitted over approximately 3,000 km is analysed with both linear and full nonlinear simulations. The optimum pre-emphasis which results in the best performance across the band for both linear and nonlinear simulations is investigated. The performance penalty when operating the system with the sub-optimal pre-emphasis determined by linear simulations vs. the optimum pre-emphasis determined by nonlinear simulations is determined. A small but acceptable penalty is incurred, which confirms the dominance of linear impairments and allows quick and simple calculations to be integrated in link engineering tools for automated pre-emphasis optimisation.

### 2.13.1 SYSTEM SETUP AND MODELLING PROCEDURE

Using *LDT* a 2,940km point to point ULH link consisting of 35 fibre spans each of 84km of SMF was configured with  $\alpha = 0.25\text{dB/km} + 1\text{dB}$  overhead per span (total span loss 22dB).

The transmission fibre was standard SMF with dispersion and dispersion slope compensation achieved using broadband DCF at the end of each span. This type of dispersion map is referred to throughout this thesis as “**Short dispersion map**”; further details of this and alternative dispersion maps are provided in Chapter 3 section 3.7. Pre and post compensation at the launch and receive terminals were optimised with a small positive residual GVD at the end of the link to balance the opposing effects of SPM; the average dispersion of the complete transmission line varied by only 0.04ps/nm.km across the C-band. Figure 53 shows the “short dispersion map” for the 2,940km link and Table 6 summarises the transmission fibre and DCF parameters used in this study.

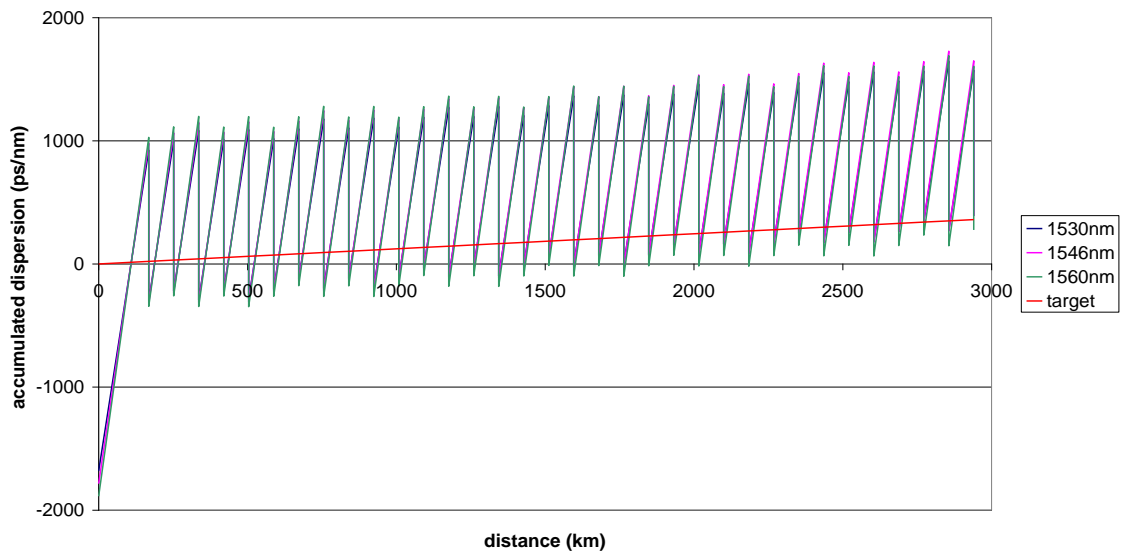


Figure 53 “Short Dispersion Map” of 2,940km link (per span dispersion compensation)

Parameter	SMF (G.652) Fibre	SMF DCF	Unit
Attenuation	0.25	0.54	dB/km
Dispersion	16.45	-93.4	ps/nm/km
Dispersion Slope	0.0575	-0.336	ps/nm <sup>2</sup> /km
Dispersion Curvature	$-4 \times 10^{-5}$	0	ps/nm <sup>3</sup> /km
Effective Area	80	19	$\mu\text{m}^2$
Nonlinear Index	$2.6 \times 10^{-20}$	$2.6 \times 10^{-20}$	$\text{m}^2/\text{W}$

**Table 6 Key parameters of SMF fibre (G.652) and SMF DCF**

Four dynamic gain equalising network elements (levelling nodes as described in section 2.8) were distributed along the link each spaced 7 spans apart. Levelling nodes perform re-emphasis to correct for power tilt and ripple variations and are capable of equalising the power spectrum to any desired linear tilt profile.

A full system of  $80 \times 10\text{Gb/s}$  RZ modulated wavelengths spaced 50GHz apart in the C-band was assumed.

Simulations were carried out using a straight line linear pre-emphasis profile with a tilt ranging from -1 to +1dB/THz in steps of 0.25dB/THz and for average signal power per channel ranging from -1 to +3dBm/channel in steps of 0.5dB.

Note: tilt of +1dB/THz is equivalent to a tilt of +4dB over the C-band (4THz bandwidth) or -4dB over the wavelength scale.

Full nonlinear simulations were carried out using the framework outlined in section 2.11 for 6 neighbouring DWDM channels at a time, repeating the simulations across the C-band at 1530, 1545 and 1560nm. Q-values were obtained as the worst of 6 channels, averaging five different simulation runs with different noise seeds, using the same  $2^7-1$  PRBS sequence for each channel, with a random timing offset between each channel in order to de-correlate between each channel and simulation run.

Linear simulations were carried out by setting the nonlinear coefficient to zero and a slight adjustment of the dispersion map to fully compensate GVD with net zero dispersion at the end of the link in the absence of any opposing SPM.

### 2.13.2 RESULTS AND ANALYSIS

Contour plots of the Q-factor of the worst performing channel across the C-band are plotted against pre-emphasis tilt and average power per channel for full nonlinear simulations in Figure 54 (a) and linear simulations in Figure 54 (b). As expected

linear simulation results show steadily increasing Q-factor performance with increasing signal power due to the inexorably increasing OSNR performance given by Equation 13. Nonlinear simulations show a similar trend of linear behaviour at low signal powers (up to 1dBm/channel) however a peak in Q-factor performance is seen at around 2dBm/channel with performance decreasing beyond this power level because of penalties due to Kerr nonlinear effects.

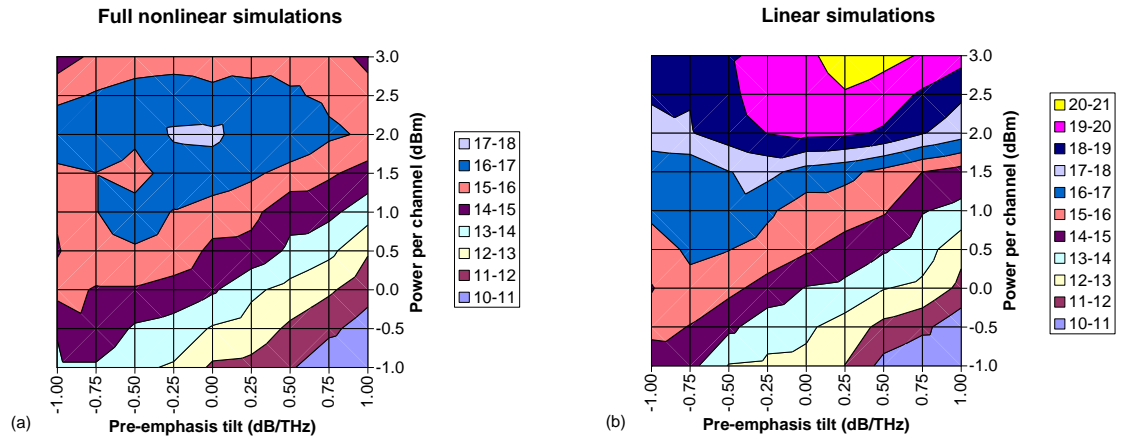


**Figure 54** Q-factor at end of 2,940km link for 10Gb/s RZ channels with varying pre-emphasis profile and average power per channel as a result of: (a) full nonlinear simulations (b) linear simulations (after [19])

### Optimum Pre-Emphasis

The pre-emphasis setting which provides the optimum Q-factor performance at each signal power for both full nonlinear and linear simulation results is presented in Figure 55.

As average signal powers increase the optimum pre-emphasis which results in the best Q-factor performance shifts from low to high pre-emphasis tilt (measured in dB/THz). This is predominantly due to the increasing SRS effect which amplifies shorter frequency channels at the expense of longer frequency channels as the total signal power in the fibre is increased.

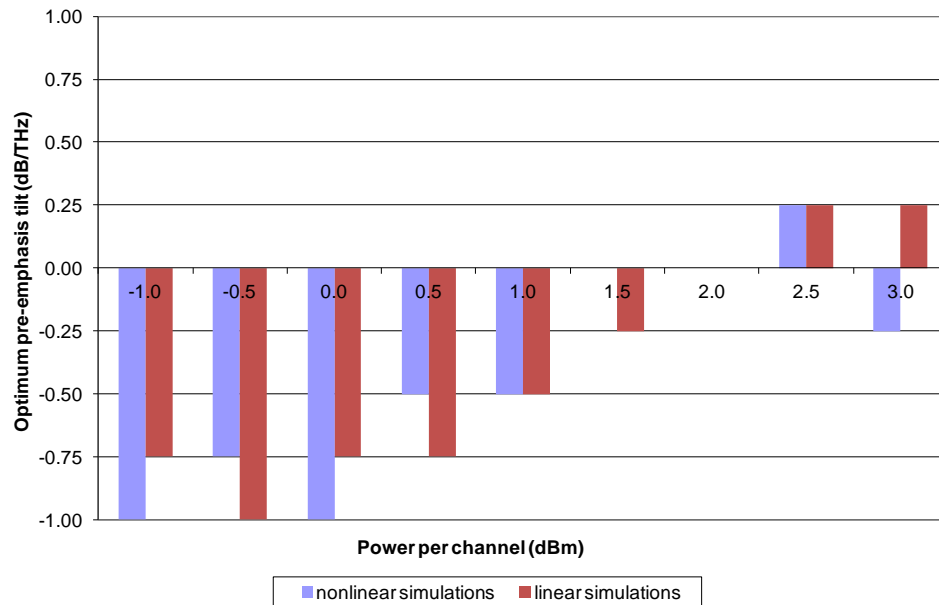


**Figure 55 Optimum pre-emphasis setting determined by both nonlinear and linear simulations**

After applying the optimum pre-emphasis setting determined by linear simulations to the full nonlinear data set a comparison of the Q-factor performance was carried out for three pre-emphasis settings:

1. Optimum pre-emphasis determined by **nonlinear** simulations
2. Optimum pre-emphasis determined by **linear** simulations
3. No pre-emphasis

Q-factor performance of the full nonlinear simulations with each of the above operating conditions is shown in Figure 56 and the Q-factor penalty between the fully optimised pre-emphasis setting 1 and settings 2 & 3 are shown in Figure 57.

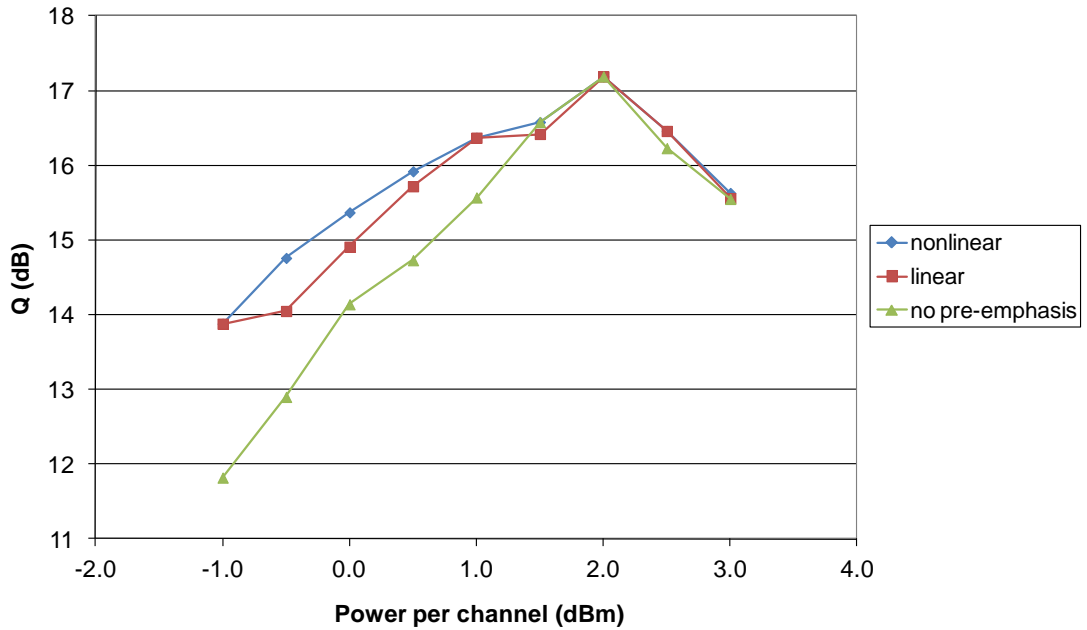


Figure 56 Worst channel Q-factor at end of 2,940km link (10Gb/s RZ) computed by full nonlinear simulations with 3 different pre-emphasis schemes (after [19])

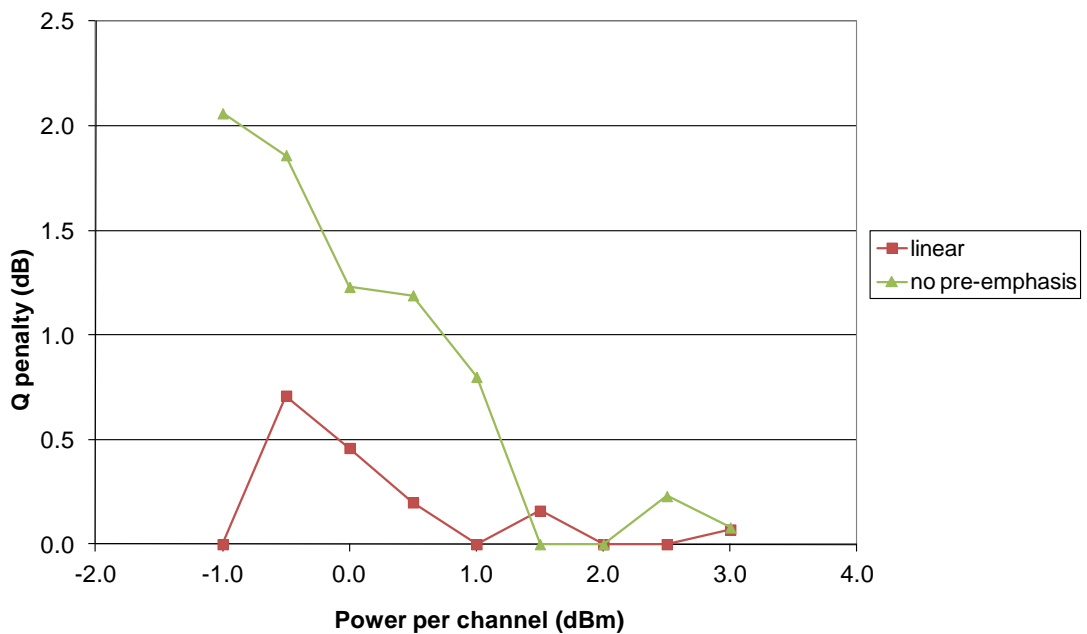


Figure 57 Q-penalty between nonlinear simulation results applying optimised pre-emphasis predicted by nonlinear simulations vs. optimum pre-emphasis determined by linear simulations, and no pre-emphasis

At low signal powers (up to +1dBm/channel) applying no pre-emphasis incurs a significant performance penalty of between 0.8 and 2.1dB. This penalty reduces to zero when operating in the optimum performance region of +1.5 to +2dBm/channel. This is a result of careful system design by specifying amplifier gain tilts which

balance the SRS tilt so that zero pre-emphasis is the optimum operating condition at full channel capacity.

Operating the system with the optimum pre-emphasis determined by linear simulations incurs a penalty of at worst 0.7dB and in most cases <0.2dB; at the optimum signal power of +2dBm/channel the penalty is 0dB.

By including models of channel to channel wideband power variations in nonlinear simulations of DWDM transmission systems, it has been shown that a small penalty is incurred when applying an optimum launch power pre-emphasis determined by simple and quick linear simulations. Since the optimum pre-emphasis is not strongly influenced by the inclusion of Kerr nonlinearities at typical signal powers, these results show that wideband channel power variations do not significantly alter the penalties due to Kerr nonlinear effects in DWDM channels. In conclusion, linear simulations are reliable at predicting an optimum pre-emphasis profile.

Linear simulations are simpler and significantly faster than nonlinear simulations and can be easily integrated into link engineering tools. Commissioning data such as the optimum pre-emphasis can be automatically downloaded to the network elements from a link engineering tool such as *LDT* via the NMS. Such a process results in reduced OpEx by minimising human intervention and subsequent errors, reducing commissioning time and simplifying training; it's preferable not to require a PhD or EngD in nonlinear fibre optics in order to install and commission a DWDM system!

When a network operator wishes to increase capacity with additional wavelengths, transponders are simply plugged into an available slot at the end terminals and/or intermediate OADM sites, with the pre-emphasis settings automatically adjusted to compensate for changes in wideband power variations.

CapEx is also reduced since pre-emphasis and dynamic channel equalisation can extend transmission reach and increase system margins. Improved system margins can be exploited to reduce the frequency of costly OEO regeneration or enable deployment of lower performance and cheaper component options; these aspects are investigated in Chapters 4 and 5.

### **System Dynamics**

Looking closer at the Q-factor spectrum at the end of the link provides further insight into the dynamics of the system. Figure 58 shows the performance across the C-band

for the three pre-emphasis settings with 0dBm/channel signal power and Figure 59 shows the equivalent performance over the full range of pre-emphasis settings (-1 to +1dB/THz).

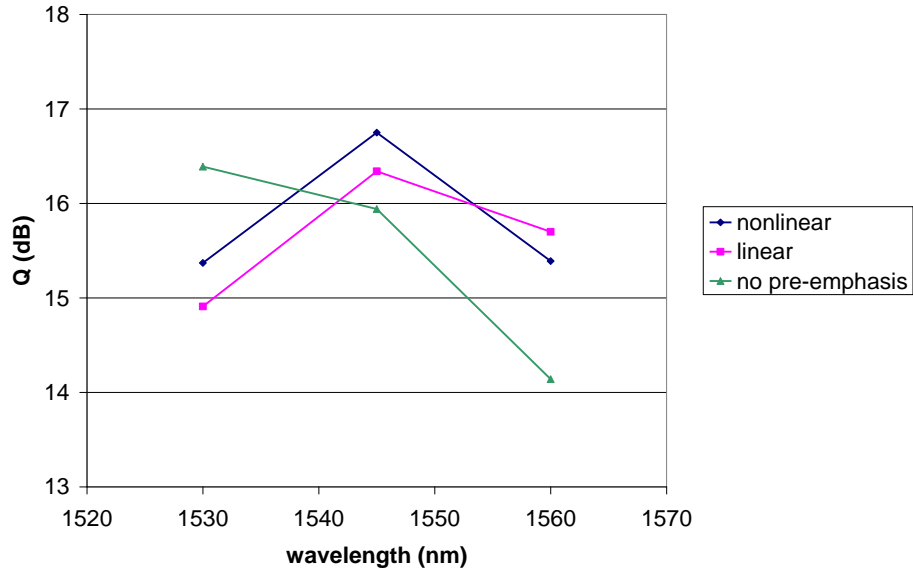


Figure 58 Q-factor spectrum at end of 2,940km link obtained from full nonlinear simulations at 0dBm per channel with different pre-emphasis schemes (after [19])

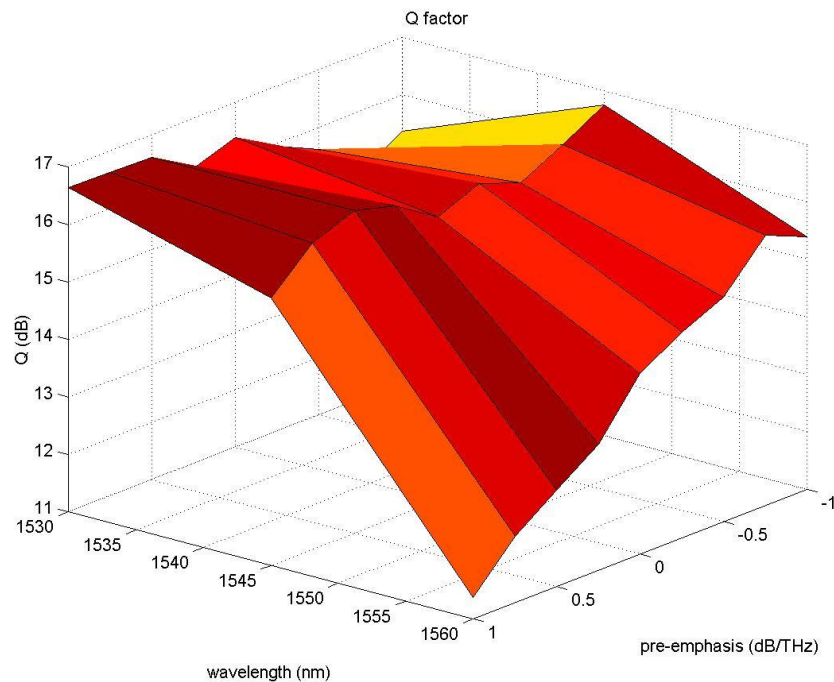


Figure 59 Q-factor spectrum vs. pre-emphasis setting for the 2,940km link at 0dBm/channel

At 0dBm/channel the optimum performance i.e. best case for the worst performing channel occurs with a pre-emphasis of -1dB/THz. As the pre-emphasis is increased

from -1 through to +1dB/THz the worst performing channel switches over from the 1530nm end of the C-band to the 1560nm end as shown in Figure 59. Table 7 summarises the Q-value of the worst performing channel and the Q-factor ripple ( $Q_{max} - Q_{min}$ ) for 4 main pre-emphasis settings.

Configuration	Pre-emphasis	Worst Q	Q ripple
Optimum nonlinear	-1.00dB/THz	15.4dB @1530nm	1.4dB
Optimum linear	-0.75dB/THz	14.9dB @1530nm	1.4dB
No pre-emphasis	0.00dB/THz	14.1dB @1560nm	2.3dB
Worst case	+1.00dB/THz	11.4dB @1560nm	5.3dB

**Table 7 Performance summary from combined nonlinear simulations with wideband power variation model for 2,940km link with 0dBm/channel average launch power and varying pre-emphasis**

With no pre-emphasis, performance at 1560nm is significantly worse than other parts of the C-band with worst Q=14.1dB and Q-ripple=2.3dB. Performance at 1560nm suffers because of low SRS tilt at 0dBm/channel which is overcompensated by the opposing EDFA gain tilt.

Applying the optimum nonlinear pre-emphasis (-1dB/THz) increases the signal powers at the 1560nm end of the C-band resulting in flatter performance with worst Q=15.4dB at 1530nm and Q-ripple=1.4dB. At the optimum pre-emphasis determined by linear simulations (-0.75dB/THz) performance at 1530nm is slightly impacted with a small Q penalty of <0.5dB; Q ripple is the same 1.4dB for both nonlinear and linear pre-emphasis settings.

### 2.13.3 CONCLUSIONS OF OPTIMUM PRE-EMPHASIS PREDICTION

A new implementation of the split-step Fourier method of modelling light-wave propagation in optical fibre was developed, which takes into account the wideband variation of channel power in amplified DWDM systems due to the spectral dependence of fibre attenuation, SRS tilt, and EDFA gain and noise figure tilt / ripple, as well as dispersion and Kerr nonlinear effects. This combination of modelling techniques enables the investigation of performance degradation in

DWDM channels due to increased Kerr nonlinear effects when path averaged signal power levels vary significantly across the C-band.

Performance of an 80 channel, 10Gb/s OOK RZ modulated DWDM system over a 2,940km ULH link was analysed with varying pre-emphasis profiles. It was shown that simple linear calculations, which only account for tilt and ripple of amplifier ASE / gain, SRS tilt, and fibre attenuation profile can predict a pre-emphasis which is close to the optimum determined by the new, combined nonlinear simulations with wideband power variation model. At the optimum power per channel, where noise and nonlinear effects are typically well balanced, the Q-factor performance penalty is 0dB with the simplified pre-emphasis prediction method; a penalty of no more than 0.7dB was seen over a wide signal power operating range.

This result is significant in that simple linear simulations can be trusted to calculate an optimum pre-emphasis profile without recourse to complex and computationally intensive nonlinear simulations. Linear simulations can be more easily integrated within link engineering and network planning tools, thereby simplifying and automating the commissioning of DWDM systems, with an optimum pre-emphasis profile. This development has resulted in more competitive network designs with reduced OpEx and CapEx for network operators.

## **2.14 ULH FIELD DEPLOYMENT MODELLING**

Modelling and simulation is a vitally important tool in optical communications, not only for designing a DWDM system but tailoring the system to a real world network application, either for the purpose of tendering for new business opportunities, or before actual network deployment with existing network operator customers. The following section details the first field deployment of the Ericsson *UPLx160* ULH DWDM system in a 2,872km link with performance modelled and measured over a total looped back distance of 5,745km. Particular focus is placed on the author's contribution to this engineering achievement: analysis of the optimum spacing of DGE nodes (also known as OLL or levelling nodes) to minimise cost while ensuring adequate performance.

### **2.14.1 OPTIMUM LEVELLING NODE SPACING**

By accurately simulating link performance, part of any Q-factor margin can be traded-off against reduced cost by optimising link parameters and choice of system and network architecture. For long ULH links an important design parameter is the optimum location of DGE nodes. Cost can be reduced by spacing the levelling nodes as far apart as possible within the constraints of: maintaining adequate Q-factor / BER and OSNR performance across the C-band and keeping received channel powers within the limits of the receiver dynamic range.

Additional OLL nodes can reduce variation in Q-factor, BER, OSNR and channel power across the C-band, thereby increasing the worst channel BER above the FEC limit, while also reducing power variations or GV. More frequent OLL spacing however, negatively impacts the overall OSNR due to the added noise of the additional EDFA compared with a standard OLA node. The combined wideband power variation model and nonlinear simulation tool developed in this thesis, enables accurate assessment of link performance with varying system architecture, optimising levelling spacing well in advance of network deployment.

Figure 60 shows a 2,872km ULH link between Perth and Adelaide within Telstra's pan-Australian national network, which was deployed by Ericsson in 2002; at the time it was the world's longest terrestrial un-regenerated DWDM link. The deployment is detailed in an OFC post-deadline paper [20] (published by OSA); the author's contribution to this publication was the development of the wideband power variation model and nonlinear simulation method detailed in this chapter, together with its application in setting engineering rules optimising the performance and cost of network designs.



Figure 60 2,872km Perth to Adelaide link of pan-Australia national network (after [20])<sup>38</sup>

The link consists of 31 spans of standard SMF and average span loss of 18.5dB. The final link design contains 26 OLAs (red dots in Figure 60), 4 OLLs (blue dots), with 8 spans between each OLL and 3 / 4 spans between the final OLLs and terminals (black dots) at Perth and Adelaide respectively. The final OLLs are placed closer to the terminals in order to minimise received GV and BER performance across the C-band. Dispersion compensation is arranged in the Long Dispersion Map, as detailed in section 3.7.

The chosen link design spaced the OLLs as far apart as possible to minimise cost while maintaining adequate BER performance and received power variation across the C-band. Earlier studies carried out by the author in [25] set the limit at 6 spans between OLL, however the improved model presented in this thesis resulted in better performance prediction, thereby relaxing the engineering rules with resulting cost reduction.

Unfortunately, data on this particular installation was not available to the author at the time of publishing this thesis, however a study of a similar link of 3,360km (42×80km spans) in Figure 61 shows a cost reduction in network infrastructure of 6% when reducing the number of OLL in the link from 7 to 4: which is equivalent to

<sup>38</sup> Source: Ericsson, diagram by Dr Andrew Pratt

changing the spacing between OLL from the original engineering rule of 6 spans to 9 spans<sup>39</sup>.

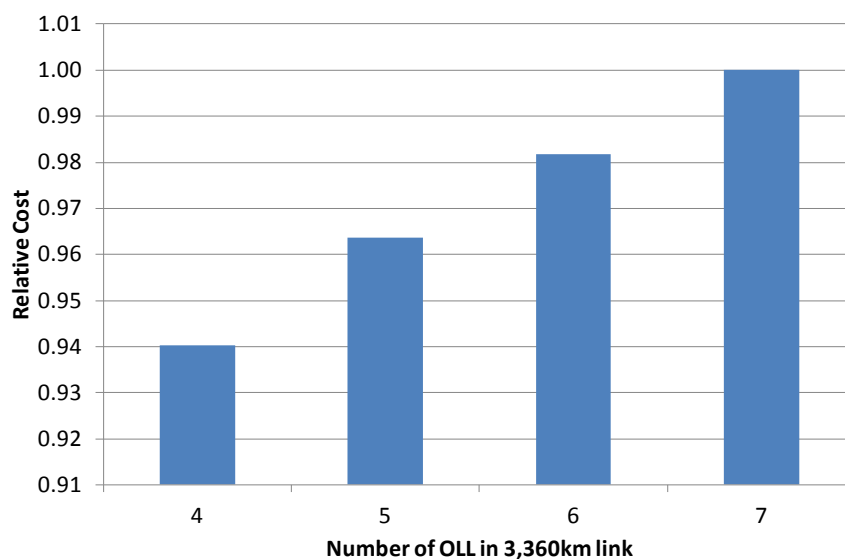


**Figure 61 Relative cost of zero channel network infrastructure vs. number of OLL in a 3,360km link**

Figure 62 shows optimum Q-factor performance is achieved with 7 OLLs (5 span spacing) with almost 1dB improvement in the worst channel Q-factor compared with 4 or 6 OLLs. Since performance with 4 OLLs (9 span spacing) is not significantly worse than with 6 OLLs (7 span spacing), it is a reasonable trade-off with the improved cost saving (6% vs. less than 2%) to set the engineering rule at 4 OLLs (9 span spacing). Worst channel performance with 5 OLLs is however almost 0.5dB worse than with either 4 or 6 OLLs at the 1530nm end of the C-band. An increase in link OSNR due to additional amplification could be the reason for the degradation.

<sup>39</sup> Due to reasons of commercial sensitivity, the underlying cost assumptions for each network element cannot be disclosed in this thesis.

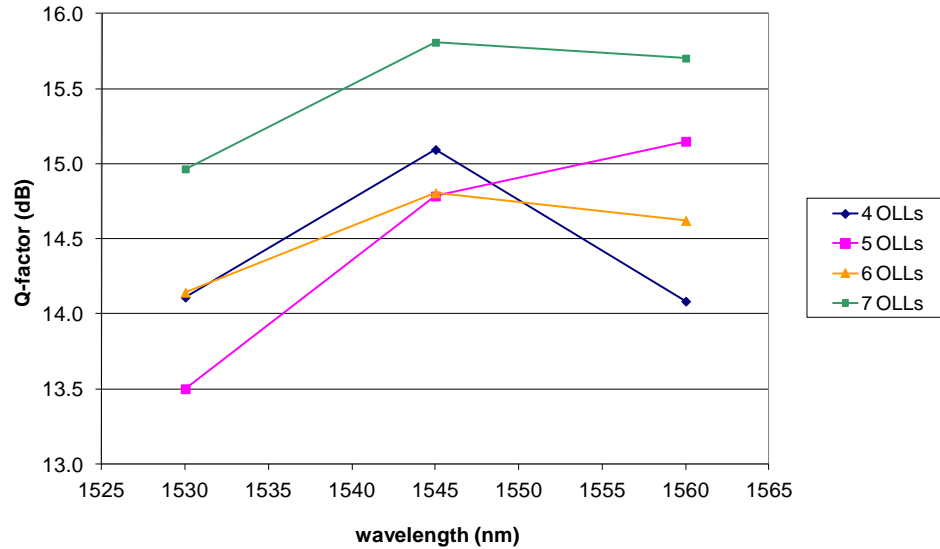


Figure 62 Simulated Q-factor performance spectrum vs. number of OLLs in a 3,360km link

### 2.14.2 5,745KM LOOPED BACK TRANSMISSION PERFORMANCE

Figure 63 shows both the measured and modelled BER performance, along the 2,872km link looped back over a total transmission distance of 5,745km. The modelled BER was calculated from simulated Q-factors using Equation 50; good agreement was achieved between modelling predictions and field measurements, with satisfactory post-FEC BER at a transmission distance beyond 5,000km. The troughs in BER along the link correspond to the improved BER performance following the power re-emphasis at each OLL.

This result shows the relatively good accuracy of system modelling and its usefulness in predicting performance in real network applications.

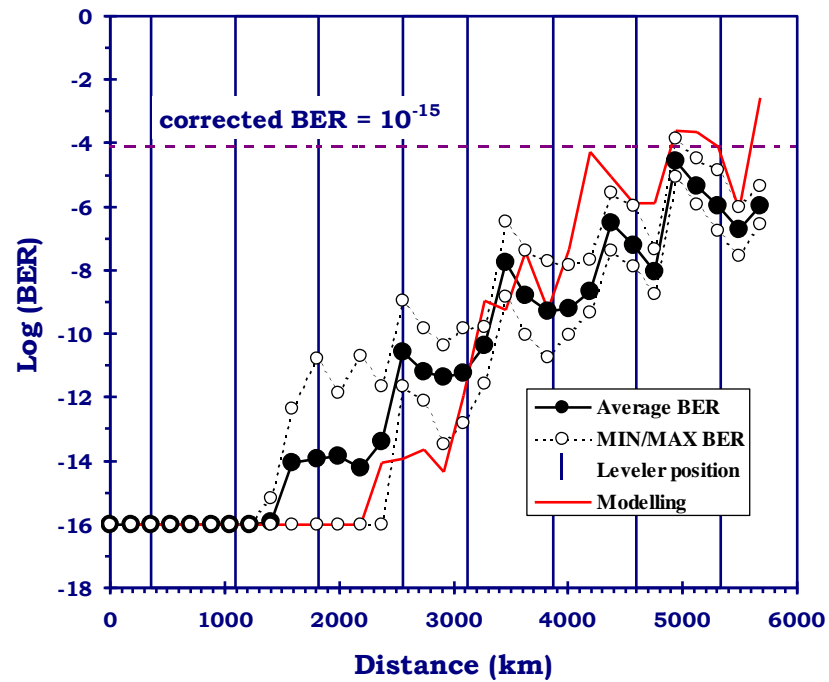


Figure 63 Simulated and measured BER for 5,745km looped back link (after [20])<sup>40</sup>

### 2.14.3 CONCLUSIONS OF ULH FIELD DEPLOYMENT MODELLING

In conclusion, the combined wideband power variation model and nonlinear simulation tool enabled the testing of and relaxation of engineering rules for the ideal spacing of OLL nodes in ULH links with up to 6% infrastructure cost reduction and acceptable performance penalty.

<sup>40</sup> Source: Ericsson, measurements by Dr Andrew Pratt and Dr Paul Harper, modelling by Dr Jeroen Nijhof

## **2.15 CHAPTER SUMMARY AND CONCLUSIONS**

In conclusion this chapter has detailed the system architecture of a commercial DWDM system, including the most important components and sub-systems relevant to this thesis. Following this introduction, a comprehensive numerical model of a DWDM system was developed. Firstly a model of wideband power variation including EDFA gain and noise figure tilt and ripple, SRS tilt and fibre attenuation profile was developed. This model was tested against OSNR and power evolution measurements with good alignment. The wideband power variation models were then integrated into a nonlinear link simulation tool based on the split-step Fourier method. The main purpose of the link simulation tool is to test the impact of wideband power variations on performance penalties due to Kerr nonlinear effects.

Using the link simulation tool, engineering rules were developed for optimising the spacing of OLL nodes by analysing the impact on performance and cost. Increasing the number of spans between OLL nodes from an earlier defined rule of 5 spans, to approximately 8 or 9 spans between each OLL resulted in 6% infrastructure cost saving for a typical ULH link of over 3,000km with acceptable performance. The engineering rule developed here, was adopted in what was the longest un-regenerated terrestrial DWDM link on the planet, resulting in a post-deadline paper at OFC 2003 [20].

A simplified pre-emphasis prediction method was proposed and tested, resulting in simple, fast, linear calculations being reliable in predicting an optimum pre-emphasis setting, with 0dB Q-factor penalty at optimum signal power levels vs. the optimum pre-emphasis predicted by more computationally intensive nonlinear simulations.

### **Future Outlook**

Since the research carried out in this chapter was published, DWDM systems and networks have evolved significantly from point-to-point links to transparent meshed optical network architectures with ROADMs. Intermediate ROADMs include a DGE function at no extra cost; therefore there is no longer a significant requirement for dedicated OLL nodes, except where inter-ROADM spacing is greater than approximately 10 spans.

BER and OSNR monitoring has become a common feature of modern DWDM systems enabling improved feedback and control for the optimisation of pre-emphasis profiles.

### **Recommendations for Further Work**

Quadratic pre-emphasis, emphasising both edges of the C-band could offer improved performance vs. the straight line fit, since most often the performance degradation is seen at the edges of the band; due to reduced gain, higher noise figure in the blue band and also higher gain variation. Quadratic pre-emphasis is however complex to implement and raises a number of issues: how much exactly should the pre-emphasis curvature be altered, and if the channel allocation changes, the system may be over-emphasised resulting in worse performance. Random gain ripple of EDFAs and dynamic effects such as spectral hole burning [56] also make it virtually impossible to compensate all of the gain variation with a pre-determined pre-emphasis profile.

### **Next Chapter**

Chapter 3 will investigate dispersion compensation strategies: both optical and electronic dispersion compensation, including their relative performance and cost saving potential.

### 3 DISPERSION MANAGEMENT STRATEGIES

Optimising PERFORMANCE and COST are the primary objective of the research presented in this chapter by investigating the optimisation of different optical and electronic dispersion compensation strategies. Electronic dispersion compensation introduces greater FLEXIBILITY by adaptively adjusting to the dispersion accumulated for each individual channel which will have transmitted over different connection paths in an optical bypass enabled network.

#### 3.1 INTRODUCTION AND MOTIVATION

Moving from 2.5Gb/s to 10Gb/s line rates chromatic dispersion becomes a reach limiting physical impairment effect due to the increased pulse broadening induced by fibre dispersion at higher bit rates (see section 2.9.3 for details on the effects of CD). Without dispersion compensation, reach of 10Gb/s is limited to ~50km on SMF whereas 2.5Gb/s is limited to around 800km. Dispersion compensation is therefore a vitally important feature of metro, LH, ELH and ULH DWDM systems. The most common dispersion compensation technology is DCF although other options exist including electronic dispersion compensation [68]. DCF is a relatively expensive technology and much engineering effort has been devoted to lowering the overall cost impact on the network equipment. Here the trade-off between performance and cost is investigated for different DCF dispersion maps and also for electronic dispersion compensation schemes.

#### 3.2 RESEARCH CONTRIBUTIONS

##### Optimising Dispersion Management

Investigated the trade-off between performance and cost for two types of dispersion map over a typical ELH link:

1. DCF at the end of each span (**short dispersion map**)
2. Lumped DCF approximately every other span (**long dispersion map**)

Demonstrated little appreciable penalty with the long dispersion map vs. short dispersion map for DWDM simulations. Single channel simulations showed better nonlinear tolerance with the short dispersion map.

Showed a cost saving of 6% in the DWDM infrastructure required on day one for a zero channel system using the long dispersion map with DCM-150. Cost saving is achieved as a result of consolidating DCM into fewer longer units and substitution of DSA with cheaper SSA. An increased saving of 13% is possible by deploying high figure of merit (FOM) DCM-250 (see [69] for discussion of FOM). However poorer performance is achieved due to the large residual dispersion slope. This research was presented in [21].

### **Investigation of Optical and Electronic Dispersion Compensation Strategies**

Investigated lumped optical and electronic dispersion compensation strategies compared with in line optical dispersion compensation with DCF: this work resulted in a peer-reviewed publication [22].

Demonstrated that from a nonlinear transmission perspective the optimum strategy is to equally share the electronic dispersion compensation between the transmitter and receiver ends. A small Q-penalty is seen compared to inline optical dispersion compensation with DCF. Investigated a range of modulation formats including OOK (NRZ & RZ) and RZ-DQPSK at 10Gb/s and RZ-DQPSK at 40Gb/s. RZ-DQPSK results in improved tolerance to dispersion and nonlinearity vs. OOK formats.

Conducted an economic analysis of optical and electronic dispersion compensation strategies showing a cost benefit of 25% is achieved on day one for a zero channel system with EDC. A cost benefit is maintained over the lifecycle of the network provided the EDC cost premium on each transponder is below 5%.

## **3.3 CHAPTER OUTLINE**

Sections 3.4 to 3.7 provide background on the dispersion characteristics of common transmission and dispersion compensating fibre, alternative dispersion compensation technologies and the principle of dispersion management. Section 3.8 describes the modelling process.

The dispersion management optimisation study is detailed in section 3.9. A technical performance comparison between optical and electronic dispersion compensating strategies is detailed in section 3.10, and an economic comparison is detailed in Section 3.11. Section 3.12 gives recommendations for further work and section 3.13 details future trends in dispersion compensation within high bit rate DWDM systems.

### 3.4 DISPERSION OF COMMON FIBRE TYPES

Chromatic dispersion grows linearly with distance, and is evaluated by means of the fibre dispersion coefficient,  $D$  expressed in ps/(nm·km). There are 3 main single mode fibre types that are deployed in metro, LH and ULH networks:

- **Standard Single Mode Fibre (SMF)**  
Designed with zero dispersion at 1310nm (ITU-T Recommendation G.652).
- **Dispersion Shifted Fibre (DSF)**  
Designed with zero dispersion at 1550nm (ITU-T Recommendation G.653).
- **Non-zero Dispersion Shifted Fibre (NZ-DSF)**  
Designed with a small dispersion at 1550nm (ITU-T Recommendation G.655)

Figure 64 shows the dispersion profile over the C-band of each of these fibre types.

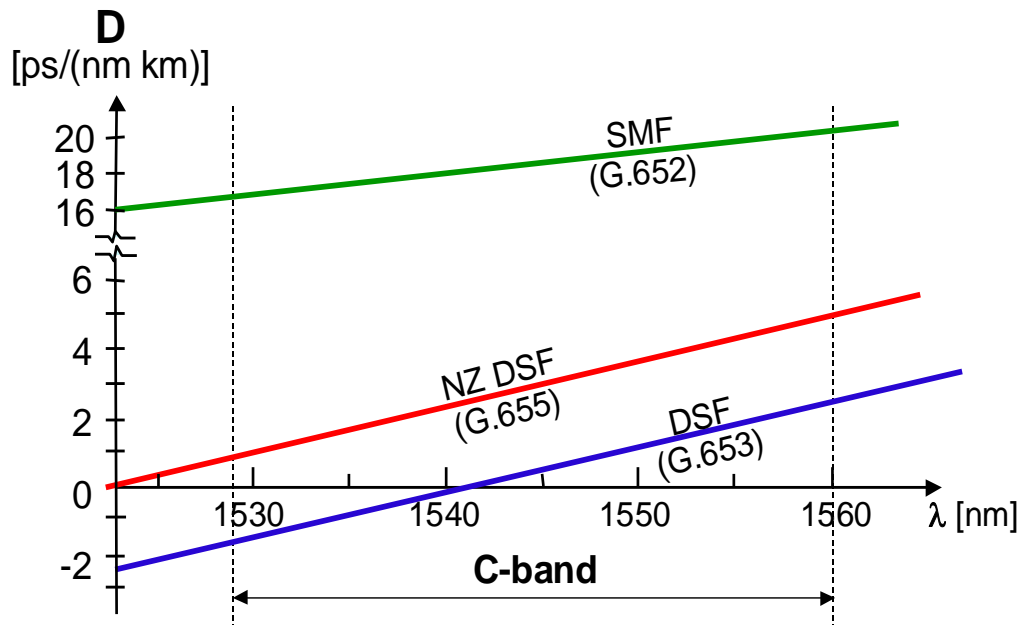


Figure 64 Dispersion coefficient profile of common fibre types over C-band<sup>41</sup>

Standard SMF (G.652) fibre is the most commonly deployed fibre worldwide therefore the research work presented in this thesis is entirely focused on links over G.652 fibre. Table 8 gives the key parameters of SMF (G.652) fibre and SMF DCF. Unless stated otherwise in the text, these parameters are assumed in this thesis.

<sup>41</sup> Source: Ericsson

Parameter	SMF (G.652) Fibre	SMF DCF	Unit
Attenuation	0.25	0.47	dB/km
Dispersion	16.46	-113.7	ps/nm/km
Dispersion Slope	0.06	-0.41	ps/nm <sup>2</sup> /km
Dispersion Curvature	$-4 \times 10^{-5}$	0	ps/nm <sup>3</sup> /km
Effective Area	80	19	$\mu\text{m}^2$
Nonlinear Index	$2.6 \times 10^{-20}$	$2.6 \times 10^{-20}$	$\text{m}^2/\text{W}$

Table 8 Key fibre parameters for SMF fibre (G.652) and SMF DCF

### 3.5 DISPERSION COMPENSATING FIBRE (DCF)

Due to its linear dependency on distance, chromatic dispersion can easily be compensated by a length of fibre with opposite sign dispersion coefficient; such fibre is called Dispersion Compensating Fibre (DCF). In commercial DWDM systems DCF is packaged within a dispersion compensating module (DCM) which is normally placed in the mid-stage of a DSA. DCMs are expressed in equivalent length of SMF transmission fibre, e.g. a DCM-150 module can compensate the dispersion due to 150km of SMF.

Referring to fibre parameters in Table 8:  $D = -113.7\text{ps}/(\text{nm km})$  for SMF DCF and  $D = 16.46\text{ps}/(\text{nm km})$  for SMF a 150km span of SMF has a dispersion of 2469ps/nm, an equivalent DCF would be  $2469/113.7 = 21.7\text{km}$  long with a loss of  $0.47 \times 21.7 = 10.2\text{dB}$ .

**Advantages of DCF:** A simple passive component which is field proven, tested and readily available.

**Disadvantages of DCF:** Large footprint, relatively expensive, high insertion loss requiring additional amplification, finite DCM granularity and often imprecise knowledge of actual field deployed fibre dispersion leads to residual dispersion error and sub-optimal dispersion compensation. For G.655 fibres, dispersion slope compensation is not perfect resulting in residual dispersion error which can be problematic at ULH distances and high bit rates (40Gb/s and above).

**DCM Cost:** Cost of DCM = fixed cost element + variable cost element (compensation length dependent) as shown in Figure 65.

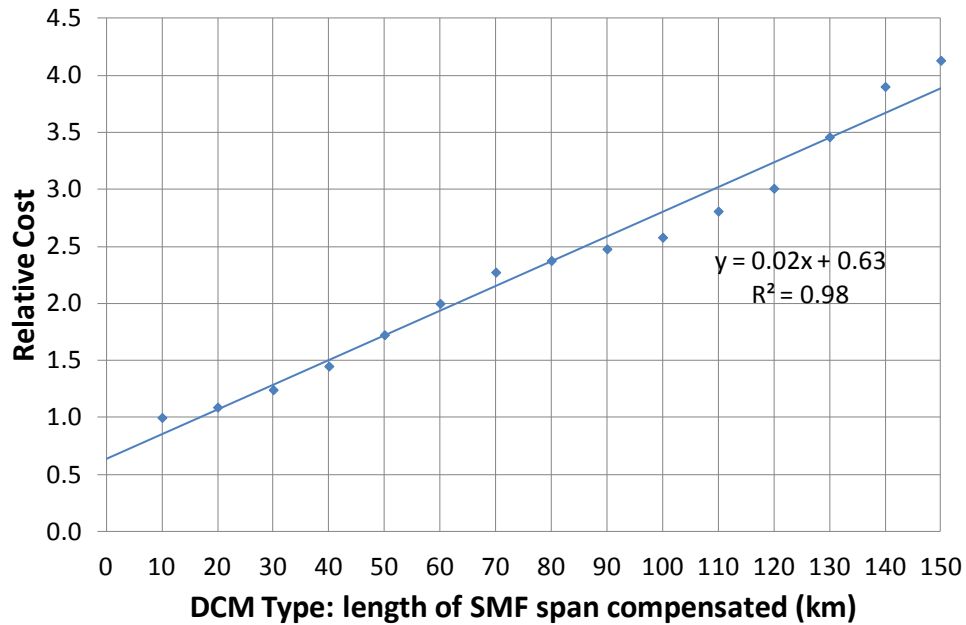


Figure 65 Relative cost of DCM vs. compensated SMF span length

Consolidating multiple short DCM into fewer long DCM has a cost saving benefit not only due to replacement of DSA with SSA but also removal of a fixed cost element per DCM eliminated i.e. the combined cost of a DCM-70 and DCM-80 is slightly higher than the cost of a single DCM-150.

**Transmission Performance:** Consolidating DCM into fewer, longer units, results in a small improvement in OSNR due to the lower noise figure of SSA compared with DSA (approximately 1dB lower NF). The performance impact on nonlinear transmission is investigated in section 3.9.

## 3.6 OTHER CD COMPENSATION TECHNOLOGIES

Various other options exist for chromatic dispersion compensation in metro and long-haul networks, the most common examples are detailed here; electronic dispersion compensation is discussed in section 3.10.1.

### 3.6.1 CHIRPED FIBRE-BRAGG GRATINGS (CFBG)

CFBG have recently been adopted in commercial DWDM systems as an alternative optical component technology for dispersion compensation over metro and LH distances [12].

Benefits of CFBG compared with DCF include low insertion loss, small size and low latency. Most importantly their low insertion loss enables the use of lower cost SSA leading to lower DWDM infrastructure cost.

Disadvantages of CFBG include; phase ripple impairments which limit the number of CFBG that can be cascaded; they require a circulator which is relatively expensive; they are channelized which leads to filtering effects at higher bit rates and in common with DCF they do not enable adaptive compensation of link dispersion error and variations.

### **3.6.2 TUNEABLE OPTICAL DISPERSION COMPENSATION**

High speed optical transmission i.e. 40Gb/s and above is more susceptible to chromatic dispersion and thus have a narrower window of operation where dispersion penalty is acceptable. Per-channel tuneable optical dispersion compensation can be useful in 40Gb/s and above line rate transponders, in addition to DCF to correct for channel to channel dispersion variations due to dispersion slope and curvature, and non-optimal dispersion maps when upgrading existing 10Gb/s links to 40Gb/s.

### **3.6.3 DISPERSION TOLERANT MODULATION FORMAT**

Optical Duobinary (ODB) is a correlative coding partial response signalling format, which benefits from a narrower spectrum than conventional OOK formats (RZ and NRZ), which results in improved resilience to CD [9]. Dispersion tolerance of 3,400ps/nm can be achieved which can support an uncompensated transmission reach of 200km over SSMF at 10Gb/s [70]. This modulation scheme can therefore enable a seamless capacity upgrade of existing uncompensated 2.5Gb/s links in metro applications.

Disadvantages of ODB include; poor OSNR performance; and poor nonlinear tolerance compared to NRZ or RZ.

## **3.7 DISPERSION MANAGEMENT**

The process of allocating DCF to various positions in the transmission line is known as dispersion management or dispersion mapping; a simple example is given in Figure 66. DCF is introduced within the mid-stage of DSA at terminals and intermediate nodes including: line amplifiers, ROADMs and levelling amplifiers. Pre-

compensation shown in green at the terminal starting the link is followed by fibre spans shown in grey and in line compensation using DCF shown in red at the end of each span. Finally post-compensation shown in green at the receiving terminal at the end of the link targets an optimum accumulated dispersion to counterbalance SPM. It is an accepted rule of thumb that total dispersion should be slightly under-compensated to include the SPM effect [71].

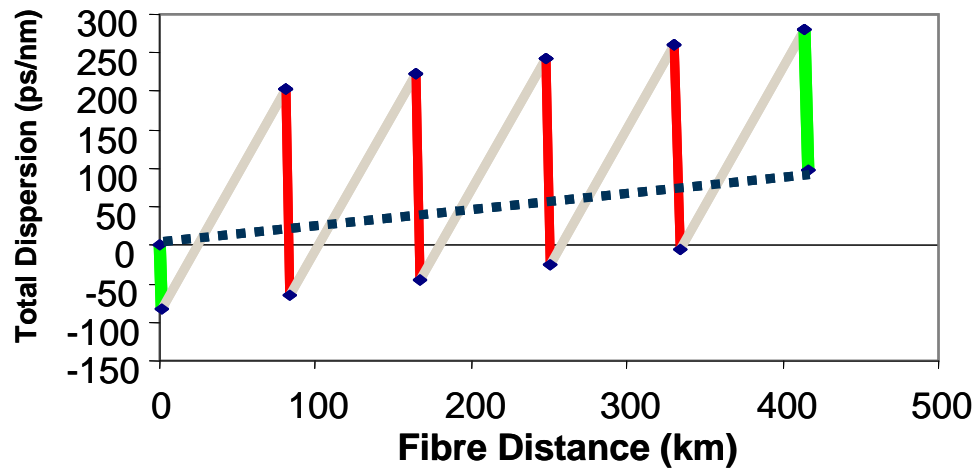


Figure 66 Example dispersion map for dispersion management<sup>42</sup>

The balancing of CD and nonlinearity (in particular SPM) is an important trade-off in LH and ULH link design. Compensating dispersion at the end of each amplified span limits the accumulated dispersion along the link. However DSAs are required at every node within the network which is costly and also degrades OSNR. Therefore two types of dispersion maps will be investigated to determine the trade-off between performance and cost. Figure 67 shows the system architecture of each dispersion map with DSA in blue and SSA in green. The residual dispersion for each map can be seen in Figure 68.

<sup>42</sup> Source: Ericsson

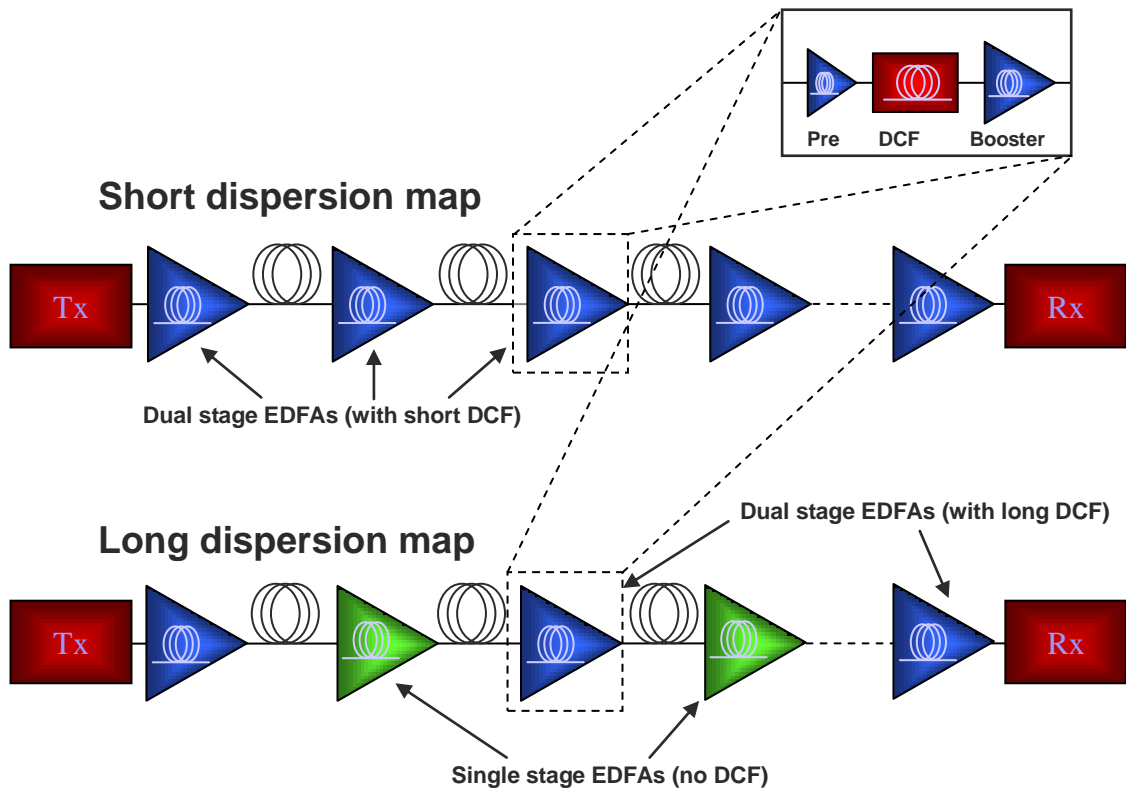


Figure 67 DWDM system with short dispersion map (upper) and long dispersion map (lower)<sup>43</sup>

**Short Dispersion Map:** This is the basic dispersion map commonly adopted in the industry with pre-compensation at the start of a link, dispersion compensation at the end of each span and targeting a small residual accumulated dispersion at the end of a link with post compensation. DSAs are required at each node to accommodate the DCM.

**Long Dispersion Map:** This novel dispersion map aims to reduce the deployment of expensive DSAs thereby reducing cost and improving OSNR performance. Pre-compensation at the start of a link is followed by in line dispersion compensation maximising the deployment of the longest DCM available (DCM-150) and post compensation targeting a small residual accumulated dispersion. With fibre spans averaging about 80km length this scheme results in DCM-150 compensating approximately every other span accommodated in the mid-stage of DSAs. Maximum DCF length is limited by the allowed mid-stage loss and limit on power inputted into the DCF due to non-linearity; the limit of 12.4dB loss corresponds to a standard DCM-150, for high-FOM DCF the limit is a DCM-250.

<sup>43</sup> Source: Ericsson

### 3.8 MODELLING PROCESS

*LST* introduced in section 2.11.2 was used to perform full nonlinear simulations. *LDT* introduced in section 2.11.1 was used to design each link allocating appropriate EDFA types and DCF lengths according to the input fibre parameters of the link and the chosen dispersion map.

Performance across the C-band was optimised following initial simulation of the defined links. Post compensation was added sweeping through a range of values and continuing the simulations from the output files produced from the main simulation runs until Q performance was optimised across the C-band with a single value of post compensation as described in section 2.11.2.

### 3.9 OPTIMISING DISPERSION MANAGEMENT

In this section the trade-off between performance and cost optimisation of alternative optical dispersion management schemes is investigated.

#### 3.9.1 SYSTEM SETUP AND MODELLING PROCEDURE

A 1,360km point to point ELH link consisting of 16 fibre spans each of 85km SMF with the following parameters:  $\alpha = 0.22\text{dB/km} + 1\text{dB}$  overhead per span (total span loss 19.7dB) was configured using *LDT*.

Two configurations were created each with the different dispersion maps as introduced in section 3.7:

- **Short dispersion map** compensating dispersion after each fibre span.
- **Long dispersion map** compensating approximately every other span.

The accumulated dispersion of each map is shown in Figure 68.

The long dispersion map results in a reduction in the number of DSA from 16 to 10.

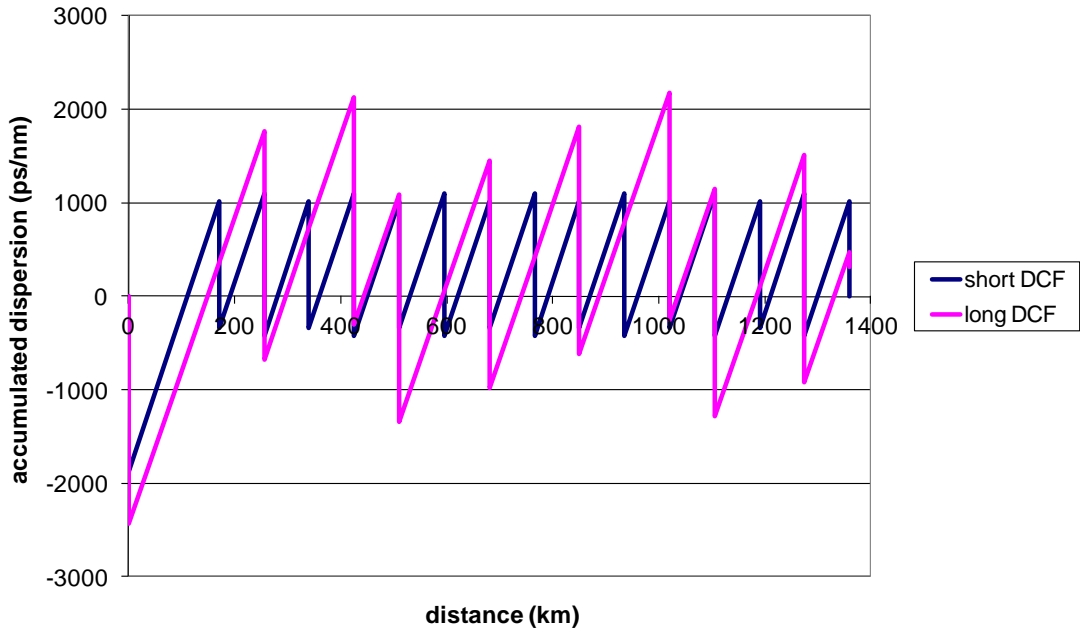


**Figure 68 Long DCF and Short DCF dispersion maps for 1,360km link**

Nonlinear simulations were carried out by *LST* using the split-step Fourier method with propagation of 6 adjacent 10Gb/s NRZ channels centred at 1530nm, 1546nm and 1560nm spaced 50GHz apart. Q-values were obtained as the worst of 6 channels, averaging five different simulation runs with different noise seeds, using the same  $2^7-1$  PRBS sequence for each channel, with a random timing offset between each channel in order to de-correlate between each channel and simulation run.

Single channel simulations were also carried out to determine the difference between WDM and single channel nonlinear effects.

Power was varied from -1 to +5.5dBm/channel in increments of 0.5dB and the tolerance to inaccuracies in dispersion was investigated by changing the dispersion coefficient  $D$  from 16.0 to 18.6ps/nm/km in increments of 0.2ps/nm/km. The base configuration was created using the default 16.46ps/nm/km and  $D$  was varied while keeping the link design configuration the same with a constant OSNR by padding span and DCM losses.

### 3.9.2 SIMULATION RESULTS AND ANALYSIS

Single channel simulation results in Figure 69 show an improved nonlinear tolerance for the short dispersion map (optimum power per channel 4.5dBm vs. 2.5dBm). The short dispersion map uses shorter DCF lengths (DCM-80) which have a significantly lower loss than the DCM-150 used in the long dispersion map. Consequently the

VOA preceding the DCM-80 is used to pad the mid-stage loss up to the nominal value resulting in lower power into the DCF. Due to its low effective area  $A_{eff}$ , DCF is highly nonlinear therefore increased nonlinear penalties are incurred with higher powers into the DCF.

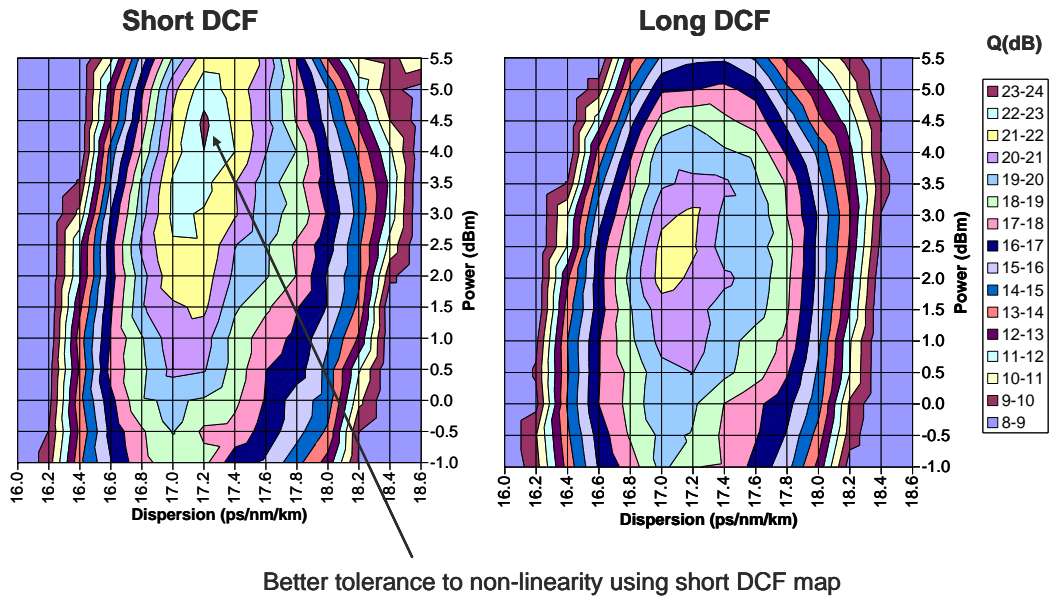


Figure 69 Single channel Q-factor performance at 1,360km

In single channel systems SPM is the dominant Kerr nonlinear effect resulting from inter pulse interactions. With long DCF there is greater pulse overlap due to the higher accumulated dispersion resulting in the increased SPM penalty.

Multi-channel DWDM simulation results in Figure 70 show comparable performance for both short and long dispersion map with slightly increased nonlinear tolerance with short DCF with an optimum power per channel of 1.5dBm vs. 1.0dBm with the long DCF.

Increased tolerance to dispersion error is another advantage of the short DCF.

OSNR performance is slightly improved with the long dispersion map 19.0dB vs. 18.6dB due to the replacement of some DSA with lower noise SSA.

A further explanation of the significantly reduced performance of short DCF in multi-channel DWDM with respect to single channel simulations, is due to an increase in XPM induced phase distortions from the walk-off effect which is exacerbated by the frequent realignment of channels, leading to increased nonlinear penalty with regular per span dispersion compensation. An experimental

investigation confirms similar results when comparing dispersion maps with varying levels of per span compensation [72].

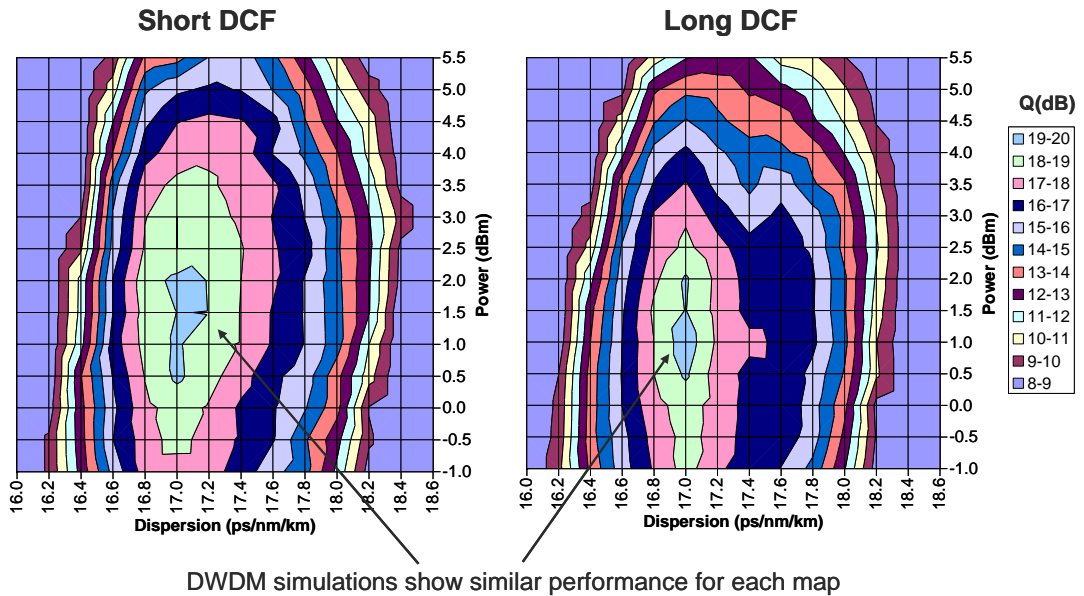


**Figure 70 DWDM Q-factor performance at 1,360km**

In conclusion the trade-off of OSNR improvement, increased SPM nonlinear penalty and decreased inter-channel XPM nonlinear penalty with long dispersion map results in comparable Q-factor performance to short dispersion map for a typical ELH link.

### 3.9.3 NETWORK COST IMPACT OF OPTIMISING DISPERSION MAPS

Lowering first installed cost of DWDM infrastructure (i.e. the cost of the equipment required before any DWDM transponders are added) is a very important objective for system vendors to meet the business needs of network operators seeking to deploy their networks on a “pay as you grow” basis.

This was very much the focus of equipment vendors and network operators during the time of this research while the telecoms industry downturn was in full effect and CapEx budgets were constrained. Network traffic was relatively low in today’s terms but growing due to the recent introduction of DSL consumer broadband services. It was difficult to sell a value proposition based on long term reduced Total Cost of Ownership (TCO) over the multi-year lifetime of the network.

Optimising dispersion maps played an important role in lowering the cost of DWDM infrastructure. By consolidating DCMs at longer intervals compensating for more than one fibre span at a time significant cost savings can be realised. For each DCM removed a DSA could be replaced by a significantly cheaper SSA and the fixed cost

element of a DCM highlighted in Figure 65 could also be eliminated. A further advantage of replacing DSA with SSA is improved reliability due to the reduction in number of pump lasers deployed.

Cost reductions in the DWDM infrastructure for zero channels in a 1,360km link (16×85km spans) are shown in Figure 71 and amount to 6% where the longest DCM compensates the dispersion due to 150km (DCM-150). If a DCM-250 was available the cost saving would be as much as 13%<sup>44</sup>.

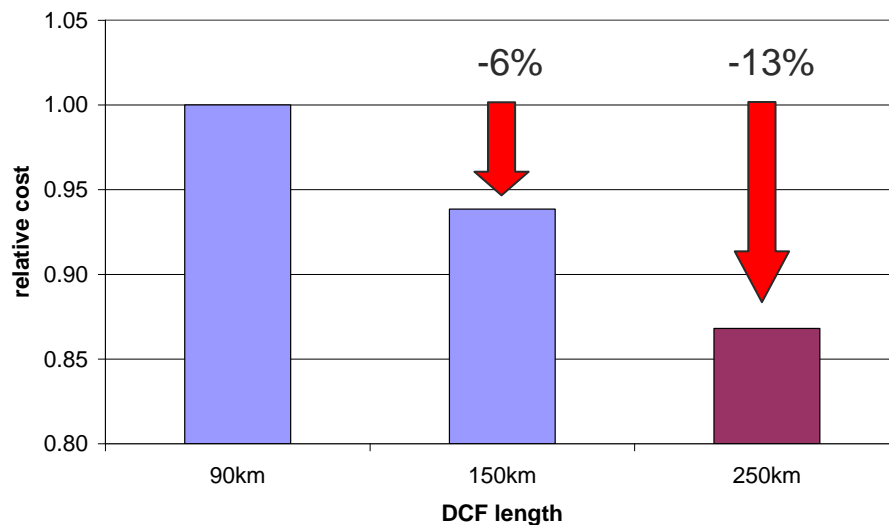


Figure 71 Total system cost reduction achievable vs. DCF length for a zero channel system

### 3.9.4 CONCLUSIONS OF OPTIMISING DISPERSION MANAGEMENT

The long dispersion map significantly reduces the cost of DWDM infrastructure while maintaining adequate performance over an ELH transmission distance, offering flexibility in the network design approach. Conversely if a link is borderline feasible and increased margin is required to avoid costly OEO regeneration, then the short dispersion map could be a suitable alternative due to its slightly improved tolerance to WDM nonlinear effects. The 6% cost saving due to reduced EDFA and DCM would be significantly outweighed by the saving in back-to-back transponders, especially in heavily loaded networks.

<sup>44</sup> Due to reasons of commercial sensitivity, the underlying cost assumptions for each network element cannot be disclosed in this thesis.

### **3.10 COMPARISON OF OPTICAL AND ELECTRONIC DISPERSION COMPENSATION STRATEGIES**

Advances in electronic dispersion compensation (EDC) techniques in recent years have provided an alternative to optical dispersion compensation using DCF in core and metro WDM networks [68]. Here it is shown that an equal balance of transmitter pre-distortion and receiver electronic equalisation results in the optimum robustness to nonlinear effects. A small Q-penalty is seen comparing with inline optical dispersion compensation using DCF. This research work resulted in a peer-reviewed publication [22] (published by IET, formerly IEE).

#### **3.10.1 ELECTRONIC DISPERSION COMPENSATION**

Advantages of EDC compared with DCF include: potentially lower cost, reduced footprint, reduced optical losses, fewer amplifiers required, improved OSNR performance and adaptive operation with flexibility to dynamically compensate for changes in connection paths.

Advances in DSP initially made EDC possible at 10Gb/s, followed by 40Gb/s and is emerging as a universal feature of all 100Gb/s LH DWDM systems following the Optical Internetworking Forum's (OIF) implementation agreement to adopt the modulation format DP-QPSK with coherent detection [11].

EDC can be implemented at either transmitter or receiver of a DWDM system. Receiver based techniques include maximum likelihood sequence estimation (MLSE) [73], feed-forward equaliser (FFE) and decision feedback equalisers (DFE) [74]. A fundamental limit on the performance of receiver based EDC results from the loss of phase information following detection. Coherent detection although complex and costly can be used to recover the optical phase information into the electrical domain where linear equalisation can be applied to correct for chromatic dispersion and other physical impairment effects [75].

The most common transmitter based technique is signal pre-distortion [13], [15], which was first demonstrated for 10Gbit/s transmission over 5,120km of standard single mode fibre without any optical dispersion compensation [14]. Figure 72 shows the DWDM network application areas appropriate for different EDC techniques.

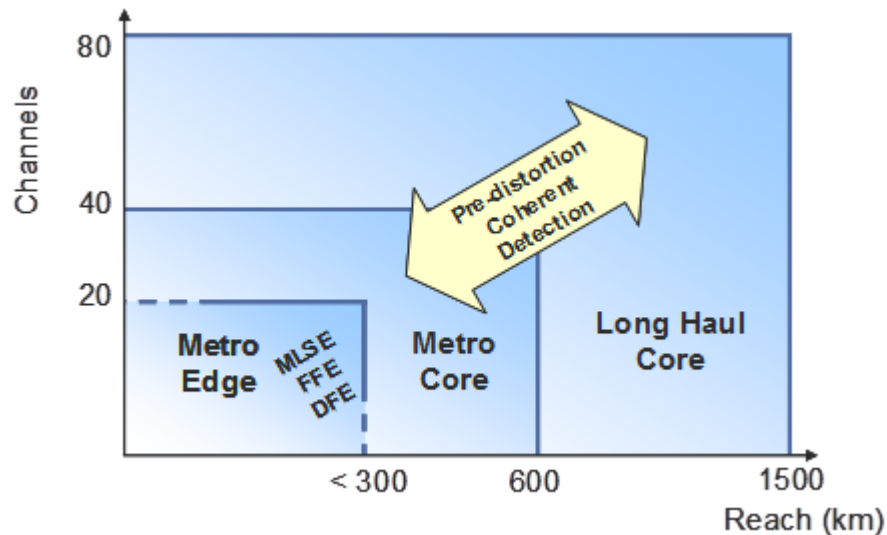


Figure 72 Electronic dispersion compensation techniques for various DWDM applications<sup>45</sup>

DWDM systems employing EDC at only transmitter or receiver with no inline optical dispersion compensation are expected to be more susceptible to fibre nonlinearities due to the optical pulses becoming more highly dispersed during uncompensated fibre transmission.

Simulations are performed to investigate the trade-off in performance when sharing dispersion compensation functionality between the transmitter and receiver to minimise the impact of fibre nonlinearities. Transmission of 10Gb/s over 600km and 1,200km and 40Gb/s over 600km with various modulation formats is investigated: OOK (NRZ and RZ) and phase modulation (RZ-DQPSK).

DCF does have advantages compared with EDC: it is a stable mature technology offering broadband compensation of all DWDM channels simultaneously using one device. DCF also offers the best transmission reach performance due to improved nonlinear tolerance.

At the time of this research there were doubts whether EDC would be future proof for higher bit rates (40Gb/s and 100Gb/s), however this is no longer a unique selling point for DCF following advancements in DSP technology enabling EDC at 100Gb/s. Analogue to digital (A/D) and digital to analogue (D/A) converters with sampling rates of up to 60GSamples/s are now available and together with advanced modulation formats such as DP-QPSK lowering the baud rate required to support 100Gb/s to 28Gbaud.

<sup>45</sup> Source: Ericsson

### 3.10.2 SYSTEM SETUP AND MODELLING PROCEDURE

Figure 73 shows a 600km conventional transmission link with inline dispersion compensation using DCM-150 to compensate for 150km of SMF placed every other span. DSA EDFAs are used to accommodate the DCF in the mid-stage and SSA EDFAs are used where DCF is not required.

Each fibre span is 75km of standard SMF with the following parameters:  $\alpha = 0.22\text{dB/km} + 1\text{dB overhead per span}$  (total span loss 17.5dB), dispersion coefficient  $D = 16.46\text{ ps/nm/km}$ , dispersion slope =  $0.06\text{ ps/nm}^2/\text{km}$ ,  $A_{\text{eff}} = 80\text{ }\mu\text{m}^2$ .

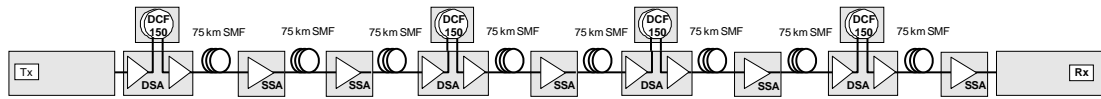


**Figure 73 600km DWDM system with inline DCF (long dispersion map) and DSA / SSA**

Figure 74 illustrates the 600km transmission system with transmitter pre-distortion and receiver equalisation. In order to focus on the impact of nonlinearities noise is kept constant by using an identical amplifier configuration to Figure 73 with a VOA replacing the loss of each DCM in the pre-distorted / receiver equalised system. In practice using pre-distortion and / or receiver equalisation all DSAs can be replaced by cheaper SSAs and DCM removed as shown in Figure 75, resulting in improved OSNR and reduced DWDM infrastructure cost.

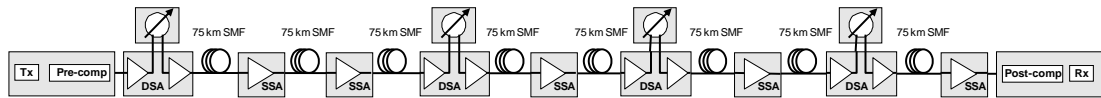


**Figure 74 600km DWDM system with EDC at transmitter and receiver with DSA / SSA**

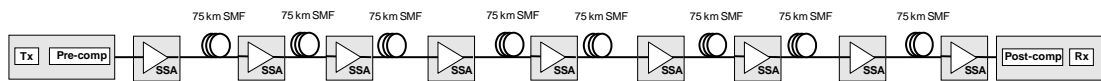


**Figure 75 600km DWDM system with EDC at transmitter and receiver with all SSA**

EDC implementation penalties were ignored allowing the transmitter pre-distortion and receiver equalisation to be modelled in the optical domain as loss-less linear dispersion compensating elements with total dispersion compensation equal to the fibre dispersion:  $9,876\text{ps/nm}$  for 600km and  $19,752\text{ps/nm}$  for 1,200km. Implementation penalties due to  $2 \times$  oversampling at the D/A converters of up to 1.5dB for NRZ-OOK and 0.1dB for RZ-DQPSK have been simulated in [76].

Nonlinear simulations were carried out using the split-step Fourier method with propagation of 5 adjacent channels centred at 1546nm spaced 50GHz apart. Q-values

were obtained as the worst of 6 channels, averaging twenty different simulation runs with different noise seeds, using the same  $2^7-1$  PRBS sequence for each channel, with a random timing offset between each channel in order to de-correlate between each channel and simulation run. The averaging of 20 simulation runs rather than the usual 5 was done to increase the accuracy of the results, due to the increased pulse spreading expected with lumped dispersion compensation at terminals. 10Gb/s transmission over 600km was investigated for NRZ and RZ modulation formats, 10Gb/s over 1,200km was investigated for RZ and RZ-DQPSK and 40Gb/s over 600km was investigated for RZ-DQPSK. In each case to compensate for SPM the residual dispersion of the link was adjusted to slightly under-compensate the transmission fibre by adding a small amount of loss-less linear dispersion to the end of the link until the Q factor was optimised.

### 3.10.3 SIMULATION RESULTS AND ANALYSIS

Figure 76 shows that for 600km 10Gb/s NRZ with EDC the optimum performance is obtained when compensation is divided equally between transmitter and receiver (50% pre-compensation) with a launch power of  $-1\text{dBm}$  per channel. Similar results were obtained with the various modulation formats, distances and bit rates investigated.

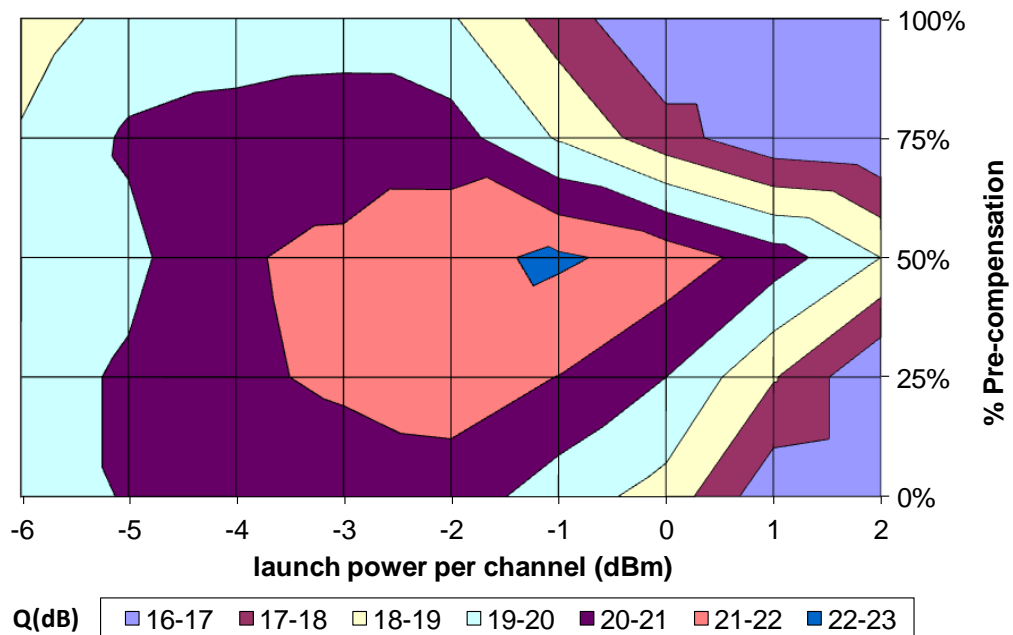


Figure 76 Q-factor contour plot for varying channel launch power and % pre-compensation for 600km 10Gb/s NRZ transmission

Splitting dispersion compensation between transmitter and receiver ends of a transmission link reduces the pulse spread in fibre compared with lumping dispersion compensation either at transmitter or receiver only.

As pulses within a channel spread in time passing through each other, intra channel nonlinear interactions IXPM and IFWM degrade performance as shown schematically in Figure 77 and Figure 78 respectively. With IXPM pulse spreading leads to frequency jitter and then timing jitter. IFWM causes energy transfer between pulses and ghost pulses appear. Both IXPM and IFWM effects degrade the eye with timing and amplitude degradation.

- Intra-channel XPM

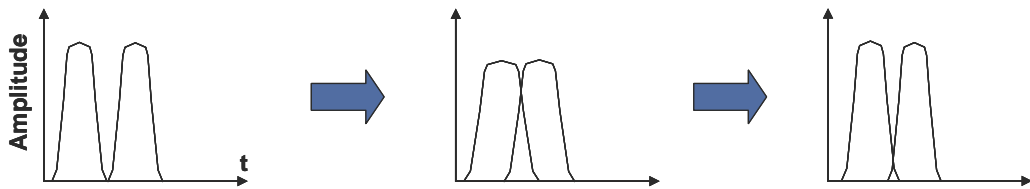


Figure 77 IXPM pulse interactions (after [22])

- Intra-channel FWM

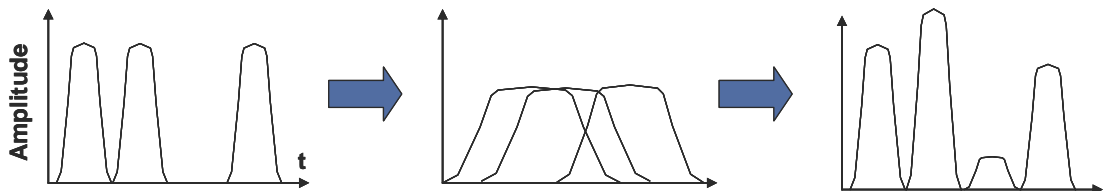


Figure 78 IFWM pulse interactions (after [22])

Figure 79 shows clearly that sharing the compensation between transmitter and receiver (50% pre) gives the best performance with respect to the baseline case of inline optical dispersion compensation, with a Q-penalty of 1dB for 10Gb/s NRZ over 600km. Receiver equalisation (0% pre) slightly outperforms transmitter pre-distortion (100% pre). At low signal powers where nonlinear effects are negligible the performance of each dispersion compensating strategy is similar confirming that nonlinear effects are responsible for the performance degradation seen at high powers using the EDC strategies. Degradation is smallest at 50% pre because the signal is not as highly dispersed and therefore not as susceptible to nonlinear effects as the case of 0% and 100% pre.

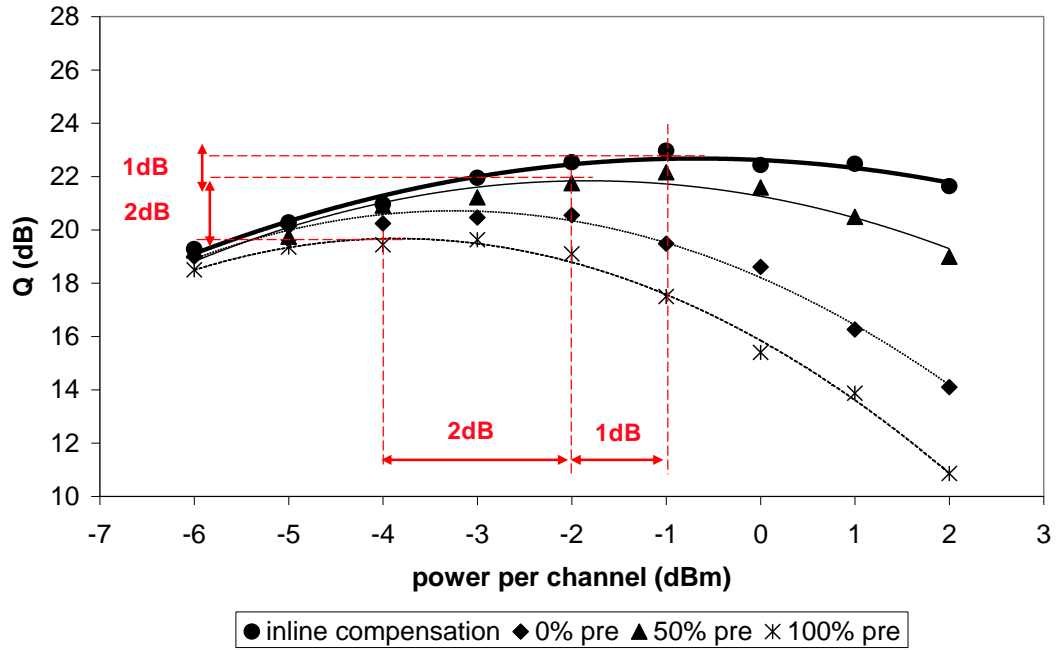


Figure 79 Q-factor for varying channel launch power and CD compensation scheme for 600km 10Gb/s NRZ transmission (after [22])

With RZ modulation, comparing transmission over 600km and 1,200km as shown in Figure 80 and Figure 81 respectively, an increase in nonlinear penalties is seen for the EDC strategy at 1,200km which decreases the optimum launch power by 2dBm per channel. Sharing the compensation between transmitter and receiver (50% pre) gives the best performance with respect to the baseline case of inline optical dispersion compensation, with a Q-penalty of 2dB for 10Gb/s RZ over both 600km and 1,200km. Receiver equalisation (0% pre) slightly outperforms transmitter pre-distortion (100% pre) in both cases.

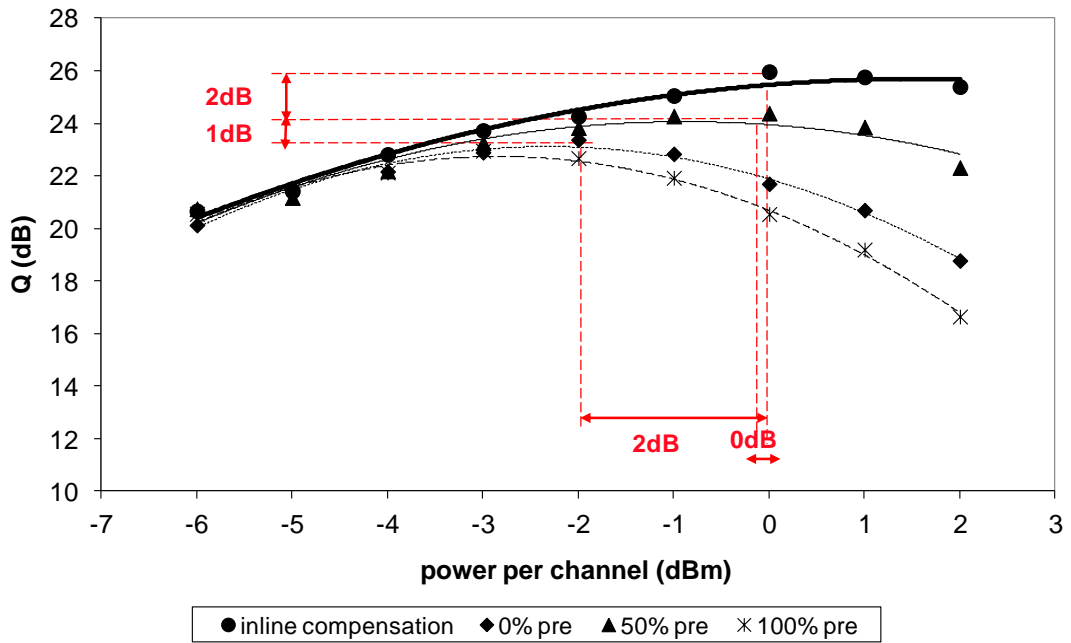


Figure 80 Q-factor for varying channel launch power and CD compensation scheme for 600km 10Gb/s RZ transmission

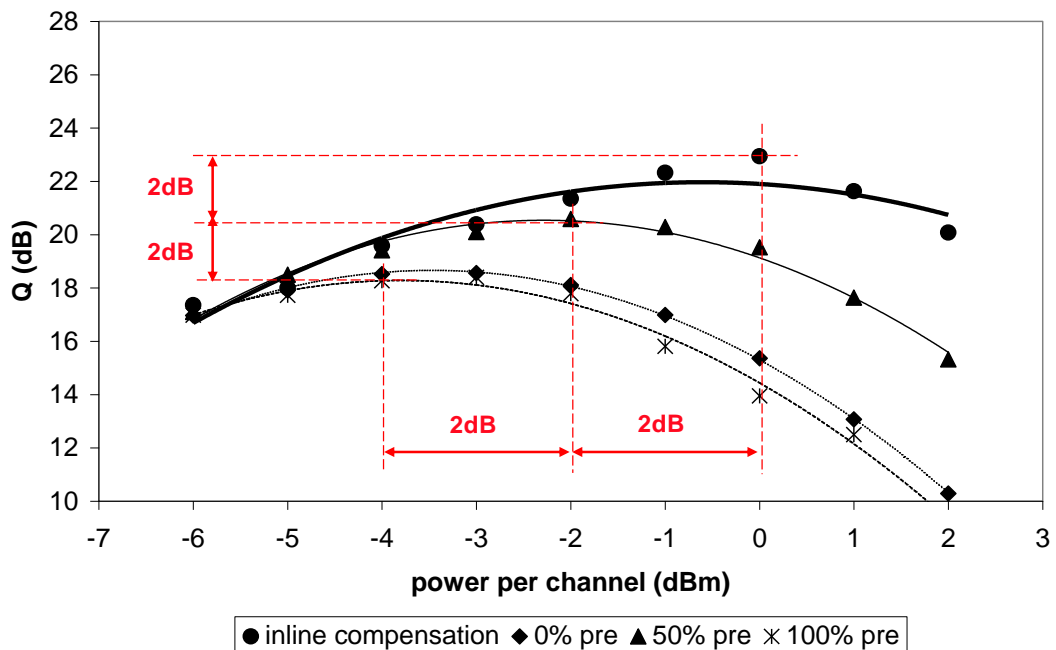


Figure 81 Q-factor for varying channel launch power and CD compensation scheme for 1,200km 10Gb/s RZ transmission (after [22])

Comparing RZ-DQPSK modulation at 10Gb/s and 40 Gb/s shown in Figure 82 and Figure 83, nonlinear penalties are greater at 40Gb/s (2dB vs. 1dB) because of wider pulse broadening meaning that more adjacent bits overlap when the signal is highly dispersed using EDC. Sharing the compensation between transmitter and receiver

(50% pre) gives the best performance with respect to the baseline case of inline optical dispersion compensation, with a Q-penalty of 1dB for 10Gb/s RZ-DQPSK over 1,200km and 2dB for 40Gb/s RZ-DQPSK over 600km. Receiver equalisation (0% pre) slightly outperforms transmitter pre-distortion (100% pre) for 10Gb/s but the opposite is the case at 40Gb/s.

Comparing Figure 81 and Figure 82 there is little Q-factor performance advantage of RZ-DQPSK over on-off keying (OOK) RZ at 10Gb/s over 1,200km using inline compensation, although the penalties with EDC strategies are lower.

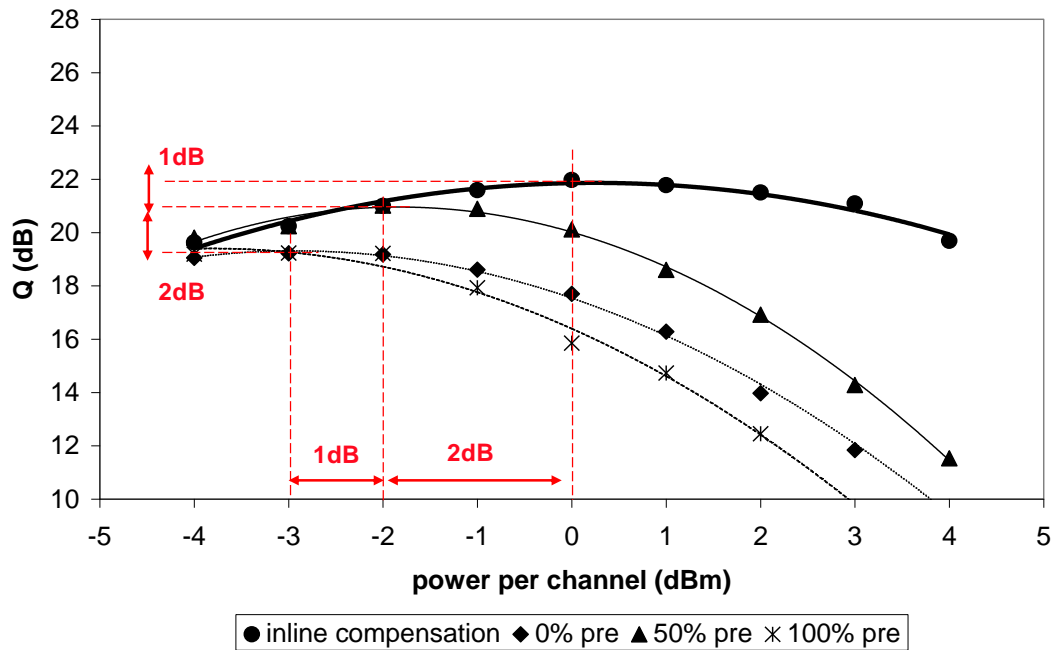


Figure 82 Q-factor for varying channel launch power and CD compensation scheme for 1,200km 10Gb/s RZ DQPSK transmission (after [22])

RZ-DQPSK halves the symbol rate with respect to OOK modulation formats and results in less pulse spread and greater tolerance to nonlinearities. Phase modulated formats have proven to be essential for achieving high spectral efficiency over long-haul transmission distances at 40Gb/s and above line rates [9].

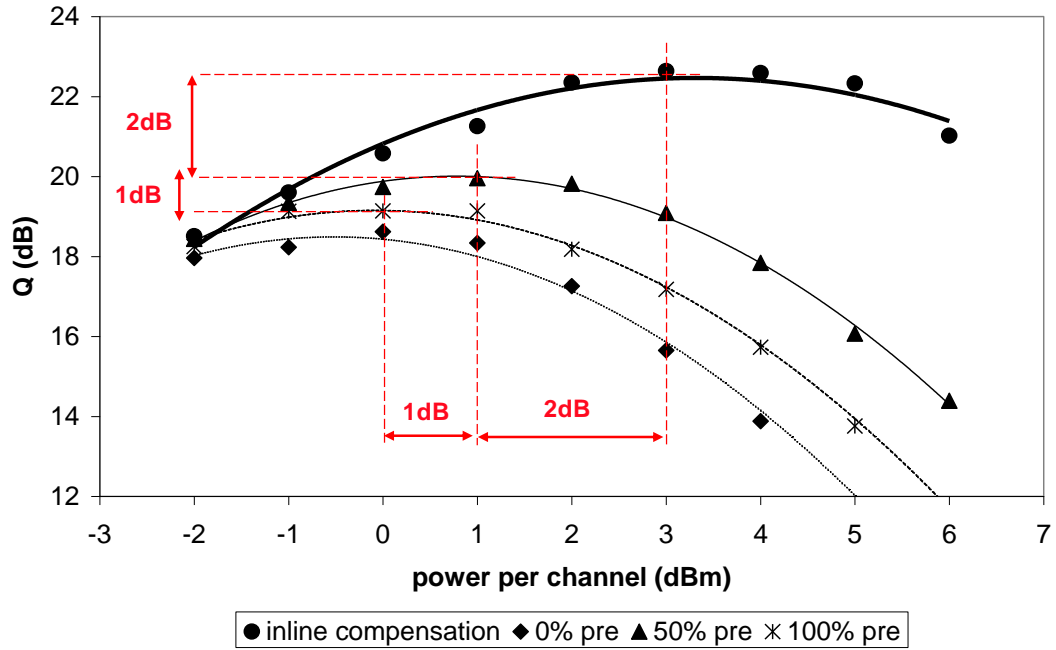


Figure 83 Q-factor for varying channel launch power and CD compensation scheme for 600km 40Gb/s RZ DQPSK transmission (after [22])

#### 3.10.4 CONCLUSIONS OF TECHNICAL COMPARISON OF OPTICAL AND ELECTRONIC DISPERSION COMPENSATION

The impact of fibre nonlinearities on the optimum dispersion compensating strategy for systems employing EDC has been analysed. For varying transmission distances, modulation format, and bit rate the optimum EDC strategy from a nonlinear transmission perspective is to equally share the electronic dispersion compensation between the transmitter and receiver. A small Q-penalty of 1-2dB is seen compared to inline optical dispersion compensation with DCF. With 100% pre-compensation or 100% post-compensation a further penalty of 1-2dB is incurred.

The decreased nonlinear tolerance of the pre-distorted / receiver equalised transmission is consistent with the well-known mechanisms of IXPM and IFWM, resulting from the significant intra-channel pulse overlaps induced by the spreading of the bit energy over many adjacent bit slots. The effects are more significant for the OOK modulation formats compared to the phase-modulated formats since the intensity modulation is not bit pattern dependent in the latter cases. Nevertheless, a greater nonlinear tolerance is achieved by equally sharing the compensation between the transmitter and receiver in all cases because, to first order, the pulse spreading is decreased by a factor of two.

### **3.11 ECONOMICS OF ELECTRONIC DISPERSION COMPENSATION**

Here the economic impact of electronic dispersion compensation on DWDM network design is investigated.

EDC enables a cost reduction in the DWDM infrastructure required to support zero channels on day one up to a maximum of 80 channels over the lifetime of the network. DCF is no longer required if the dispersion can be compensated electronically. DSA EDFAs also become obsolete since they are deployed to accommodate DCF in their mid-stage and can be replaced by much lower cost SSA EDFAs.

EDC techniques operate on a per channel basis i.e. each transponder requires additional electronic functionality to perform electronic dispersion compensation at either transmitter, receiver end or both. This places a price premium on an EDC enabled transponder with respect to a standard transponder.

For EDC to prove cost effective, the saving in DWDM infrastructure cost at zero channels must be high enough to offset the per-channel price premium of an EDC transponder  $\times$  total channel count.

#### **3.11.1 RESULTS AND ANALYSIS**

The cost reduction in a 600km and 1,200km DWDM link is calculated from zero to a maximum 80 channels for varying price premiums for the EDC transponders of 0%, 5%, 10% and 20%. For the 600km link 10Gb/s NRZ transponders are used, and for the 1,200km link 10Gb/s RZ transponders are used. It is assumed that each link is feasible without OEO regeneration for both in-line DCF and EDC configurations; however Q-factor margins will differ as analysed in section 3.10.3.

The cost reduction in DWDM infrastructure before any channels are added to the system with EDC amounts to 29% for a 600km link and 27% for a 1,200km link as shown in Figure 84 and Figure 85 respectively<sup>46</sup>. This is a significant saving in so called “first-in cost” which is a strong deciding factor for operators’ purchasing

---

<sup>46</sup> Due to reasons of commercial sensitivity, the underlying cost assumptions for each network element and transponder card cannot be disclosed in this thesis.

decisions since further expenditure is delayed until service revenue generation occurs [77].

As the number of channels on a link increases the cost saving erodes quickly. For a 600km link at 80 channels the cost saving is 0% with an EDC transponder price premium of 5% per unit. With 40 channels loaded the break-even point is reached for a 10% price premium and a saving of 3% is achieved with a 5% EDC transponder price premium.

For a 1,200km link at 80 channels the cost saving is around 1% with an EDC transponder price premium of 5% per unit. With 40 channels loaded the saving is 5% and 2% with transponder price premiums of 5% and 10% respectively.

Research published by Ciena (formerly Nortel Networks) show much higher network cost savings of around 50% in a 40 hub US core network and 10% in regional / metro sized networks [78]. These more significant cost savings appear to arise from an assumption that EDC offers more system margin than DCF compensated system due to the elimination of DCF and DSA thereby improving transmission reach and hence reducing OEO regeneration. The results presented here do not follow this assumption since inline DCF gives better performance in all simulated links presented in Figure 79 to Figure 83 with no variation in OEO regeneration requirements. Also it is not clear if the DCF was allocated to each span (short dispersion map) or consolidated into every other span (long dispersion map), the former would significantly increase the cost of the baseline optically compensated configuration.

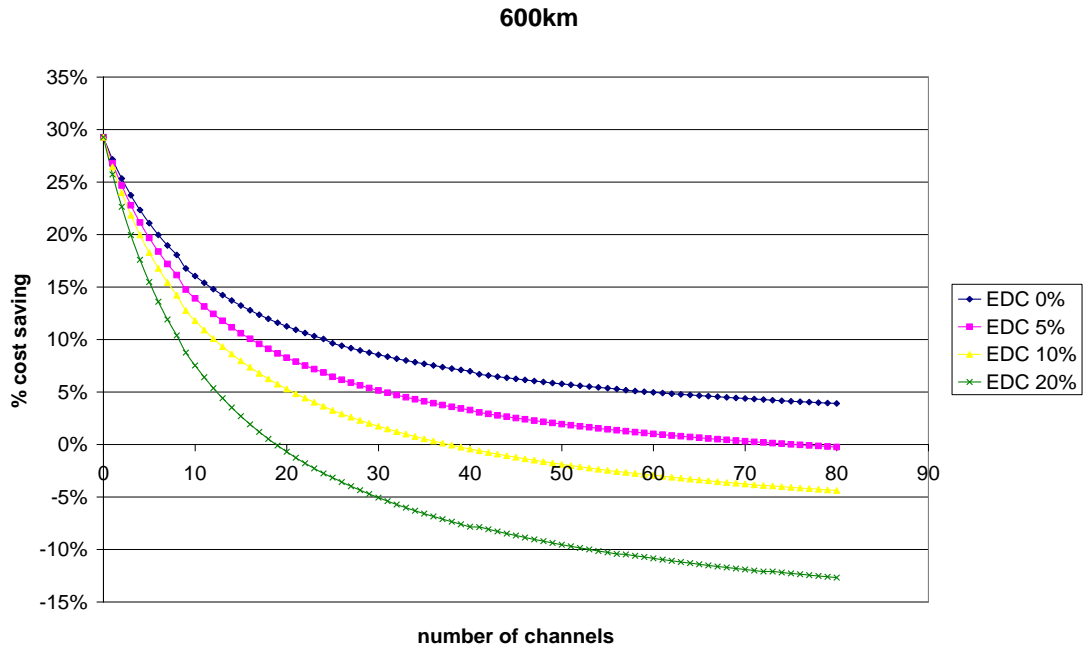


Figure 84 Network cost savings in a 600km link vs. channel count and EDC transponder cost premiums

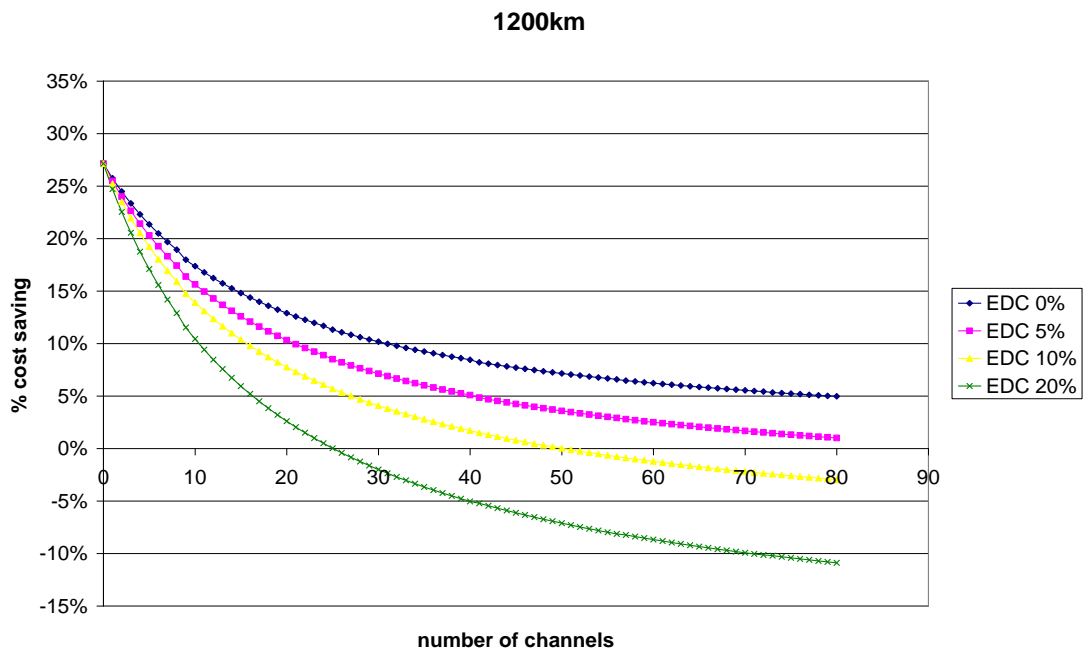


Figure 85 Network cost savings in a 1,200km link vs. channel count and EDC transponder cost premiums

### 3.11.2 CONCLUSIONS OF ECONOMICS OF EDC

In conclusion EDC allows a cost reduction of more than 25% in a zero channel system. A cost advantage is maintained over the lifecycle of the network as it is upgraded from 0 to 80 channels provided the EDC cost premium on each transponder

is below 5%; longer links can tolerate slightly higher transponder cost premiums or offer larger % savings with the same transponder premiums.

### **What is a Reasonable EDC Transponder Price Premium?**

This is an important question which influences the business case for EDC. Development of an EDC enabled transponder DSP requires a significant R&D investment in Application Specific Integrated Circuit (ASIC) design costing 10's \$Millions. An EDC transponder would therefore need to be sold in very high volume to amortise the large R&D investment cost. Once the ASIC is designed, the low cost of silicon fabrication could conceivably result in a profitable product at low EDC transponder price premiums, provided volumes are sufficiently high. A detailed business case would be required to make the investment decision, with assumptions on projected sales volumes, design and production cost, and expected average selling prices, as key input parameters. Industry analyst reports and internal equipment vendor data are suitable sources from which to base these assumptions; confidentiality of both analyst reports and vendor data however prevent the publication of such research. It is clear from industry trends in next generation 100Gb/s systems that DSP enabled EDC is here to stay, and that its benefits are valued by network operators, including the simplicity of link engineering and adaptive compensation of transmission impairments. EDC is not the only driver for using advanced DSP in next generation systems; SD-FEC and software-defined optics are the key drivers towards using DSP.

## **3.12 RECOMMENDATIONS OF FURTHER WORK**

### **Longer Transmission Links**

Transmission over longer transmission links at ULH distances >1,500km are of interest with a target un-regenerated reach of 3,000km at 10Gb/s and 1,500km at 40Gb/s and 100Gb/s. The effects of lumping dispersion compensation at the transmitter / receiver over longer transmission distances should be investigated to determine the maximum possible un-regenerated reach.

Due to the highly dispersed signals the number of overlapping bits become significant: ~50 overlapping bits at 10Gb/s OOK over 600km and ~100 overlapping bits at 40Gb/s RZ-DQPSK over 600km. The PRBS length should be longer than the number of overlapping bits to remove any bit pattern dependence in the nonlinear

penalty, therefore a longer PRBS will be required than the  $2^7-1$  simulated here when increasing transmission distance.

### **Sharing Compensation between Transmitter and Receiver: Implementation**

Sharing dispersion compensation between transmitter and receiver offers the best performance in terms of nonlinear tolerance. This is a very convenient result in terms of implementation: transmitter DSP based EDC could be set to pre-compensate for approximately 50% of the link dispersion based on link engineering tool calculations using only basic data on field deployed fibre e.g. span length, span loss, and fibre type, without the need for detailed CD and PMD measurements. Receiver DSP can be exploited to adaptively compensate for the other 50% of link dispersion  $\pm$  dispersion error due to: the lack of detailed fibre measurement knowledge, optimum compensation of Kerr fibre nonlinearities and differences in connection lengths between DWDM channels in meshed optical networks.

### **3.13 FUTURE TRENDS**

Since carrying out this research significant progress has been made towards implementing electronic compensation of chromatic dispersion and other impairment effects in commercial DWDM systems.

Coherent detection and DSP have emerged as key enabling technologies for 100Gb/s in carrier networks [79]. The OIF have issued an implementation agreement to focus on 100G Dual Polarisation QPSK (DP-QPSK) with Coherent Detection as the main modulation format for 100Gb/s [11].

Compensation of chromatic dispersion and nonlinear impairments have been studied using the principle of digital back propagating the NLS from receiver to transmitter [80], [81] offering greater transmission reach performance.

PMD compensation becomes an issue for 40Gb/s and 100Gb/s transmission over certain older installed fibres with high PMD coefficients; various techniques including electronic methods are detailed in [82].

### **Next Chapter**

Chapter 4 describes the development of a single, flexible multi-reach WDM system, which can address a wide range of network applications from metro to ultra long-

haul on a common platform. The impact of this optimised system architecture on network-level cost and performance is investigated.

## 4 DEVELOPING A FLEXIBLE WDM SYSTEM

Optimising COST and FLEXIBILITY of WDM systems and networks are the primary objectives of the research presented in this chapter, which are achieved by trading off against PERFORMANCE.

The research presented in this chapter contributed to the concept and design phase of the product life cycle of Ericsson's *Marconi MHL 3000* Multi-Reach WDM system. A multi-reach WDM system is defined as a single system capable of addressing the full range of WDM network applications, including Metro, Regional, Long-Haul (LH), Extended Long-Haul (ELH) and Ultra Long-Haul (ULH). WDM can refer to both CWDM and DWDM however this thesis is entirely focused on DWDM.

A techno-economic analysis i.e. an analysis considering a product's technology in terms of its economic costs and benefits [83] was carried out, demonstrating the flexibility and combined low initial and incremental upgrade cost of a single multi-reach WDM system in a typical service provider network compared with the earlier generation separate LH and ULH systems. This work was published in [23] and presented here in section 4.3.

There are only a few examples in the published literature detailing the evolution of WDM systems and networks towards a universal multi-reach system, and all papers were published after the work presented in this thesis was carried out.

Siemens Networks (now Nokia Siemens Networks) published a paper at OFC 2007 reviewing the drivers for, and the enabling technologies for "universal platforms" and their impact on optical network architecture and design [84].

According to [84] DWDM based optical transport equipment has experienced important evolutions in recent years owing to three factors:

Technological advances benefiting from the huge over investment in optical transport research and product development during the late 1990's and early 2000's have improved the performance of optical transport products [84].

Oversupply of bandwidth at the height of the telecoms boom in 2000 and the relatively low demand for new network capacity that followed during the 2001-2004 telecoms industry downturn led to a growing economic pressure on vendors to develop higher performance products with no increase in price [85] and [84]. From

2004 onwards optical transport network deployments entered a new steady growth phase reviving a long suffering industry.

A number of applications are driving demand for more bandwidth and hence deployment of DWDM systems in metro and core Wide Area Networks (WAN). Residential broadband services have been rapidly adopted worldwide including triple-play video distribution, both video on demand (VoD) and Internet Protocol Television (IPTV); consumer video based applications are now the major driver of bandwidth utilisation. Enterprise applications including Storage Area Networking (SAN) for disaster recovery and business continuity, cloud computing [86] and video conferencing are also driving traffic growth. Finally, backhaul of 2G, 3G and emerging 4G mobile services from cellular base stations in Radio Access Network (RAN) hub nodes and mobile switching nodes on the edge of core networks has become an increasingly important source of traffic growth [87] and [88]. Mobile operators are increasingly building their own optical transport networks with DWDM and Ethernet transport rather than their traditional approach of leasing capacity from incumbent fixed-line operators [89].

Movaz Networks (subsequently acquired by ADVA Optical Networking) published a paper in 2006 outlining the concept of an optimised multi-haul DWDM platform [90]. A multi-haul or alternatively named multi-reach DWDM system includes a set of modular network elements that can be combined in an optimal way to satisfy network capacity and performance requirements at the lowest total cost of ownership (TCO). TCO is a measure of the total cost of deploying and running a network taking into account CapEx and OpEx over its full lifecycle.

Reference [90] describes the elements of a Multi-haul DWDM platform and quantifies the cost benefit of different ROADM technologies. System performance is assessed by modelling the power fluctuations in a network containing a sequence of ROADMs, and filtering penalties are investigated experimentally for both AWG and WSS based ROADMs.

In this chapter, section 4.1 describes the evolution of optical transport networks from early LH WDM systems through to ULH and ELH DWDM systems. Section 4.2 describes the Multi-Reach DWDM system components and architecture, and its

advantages compared to earlier generation WDM systems. Finally, an analysis of the economic benefit of a multi-reach DWDM system is presented in section 4.3.

## 4.1 OPTICAL TRANSPORT SYSTEM EVOLUTION

In order to understand the requirements for developing a multi-reach DWDM system for future networks we need to review the historical development of WDM systems and networks.

WDM transmission systems have been commercially available since the mid 1990's. At that time WDM was a disruptive technology capable of economically increasing the usable bandwidth of a single optical fibre pair by an order of magnitude over traditional time division multiplexed (TDM) based SONET<sup>47</sup> / SDH optical networks.

From the mid 1990's first generation point-to-point WDM systems were introduced in the core networks of service providers to provide a rapid expansion in bandwidth and make best use of fibre capacity. WDM augmented the capacity of SDH/SONET and replaced multiple OEO regenerators with optical amplifiers capable of handling multiple wavelengths within a fibre. During the late 1990's, claims that Internet traffic was growing exponentially led many service providers to invest heavily in building-out their long-haul networks.

First generation WDM systems were point-to-point with terminals consisting of multiplexers and de-multiplexers and multi-wavelength WDM transponders at either end of a link with intermediate optical line amplifiers. Early systems could carry a few wavelengths (4, 8 or 16) at line rates of 2.5Gbit/s and later 10Gbit/s over distances up to 600km. Networks consisted of many point-to-point physical links which were static and manually configured.

Second generation WDM systems are capable of establishing dynamic connection-oriented end-to-end light paths in the optical domain with the introduction of the OADM [91]. These new technologies enabled network architectures to evolve from point-to-point to ring and mesh topologies.

---

<sup>47</sup> SONET = Synchronous Optical Networking

### 4.1.1 ULTRA LONG-HAUL DWDM SYSTEMS

Around the year 2000 almost all established equipment vendors and a number of start-up companies were developing ULH DWDM systems capable of transmitting all-optically without costly OEO regeneration over distances up to 3,000km and beyond<sup>48</sup>.

Ericsson developed a ULH DWDM system called *UPLx160* launched in 2001<sup>49</sup>, which formed part of a WDM product portfolio including: an LH DWDM system *PLx80*, a Regional DWDM system *PMA32* and a Metro WDM system *PMM*.

In 2002 Ericsson carried out their first deployment of a ULH DWDM system<sup>50</sup> which at the time was the world's longest un-regenerated terrestrial optical DWDM link [20]. Research presented in chapter 2 of this thesis contributed to this engineering achievement and post-deadline publication at OFC [20].

The key enabling technologies for ULH transmission at 10Gbit/s include:

- RZ modulation with externally modulated lasers
- eFEC
- Optical amplifier technologies including high output power and gain flattened EDFA, hybrid EDFA / Raman and all-Raman amplification.
- Broadband dispersion management
- ROADM
- DGE and power monitoring, enabling “plug and play” network deployment and capacity upgrades.

The benefits of ULH include:

- Reduced CapEx by elimination of transponders for OEO regeneration as illustrated in Figure 86 and Figure 87.
- Reduced OpEx through simpler and quicker installation and provision of bandwidth (fewer physical site visits are required), reduced space and power consumption.

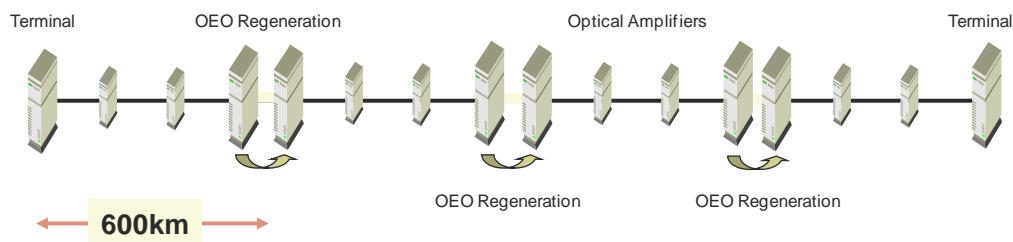
---

<sup>48</sup> Source: [http://www.lightreading.com/document.asp?doc\\_id=2014](http://www.lightreading.com/document.asp?doc_id=2014)

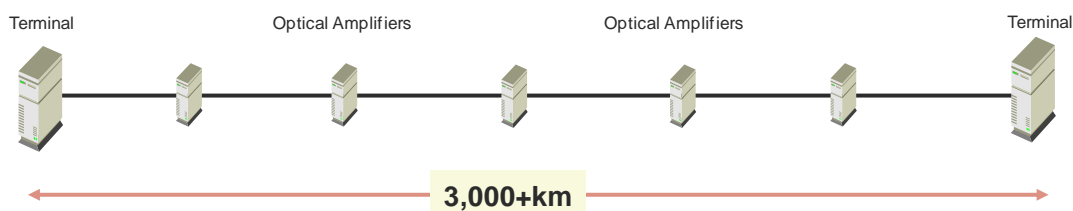
<sup>49</sup> Source: [http://www.lightreading.com/document.asp?doc\\_id=5583&site=supercomm](http://www.lightreading.com/document.asp?doc_id=5583&site=supercomm)

<sup>50</sup> Source: [http://www.lightreading.com/document.asp?doc\\_id=13172](http://www.lightreading.com/document.asp?doc_id=13172)

## Long Haul (LH) DWDM system

Figure 86 Schematic of conventional LH DWDM line system<sup>51</sup>

## Ultra Long Haul (ULH) DWDM system

Figure 87 Schematic of ULH DWDM line system<sup>52</sup>

Because ULH systems require fewer OEO regeneration sites than legacy LH systems the incremental upgrade cost to meet future traffic demands in large scale networks can be significantly reduced.

Figure 88 shows a simplified cost comparison between LH and ULH systems operating at full capacity ( $80 \times 10$ Gbit/s wavelengths) over distances up to 3,000km.

ULH terminal equipment costs are significantly higher than LH as indicated by the intersections to the y-axis at 0km: ULH costs approximately 40% more than LH where the difference arises mainly due to the higher performance (cost) ULH transponders.

Optical amplification costs are slightly higher for ULH systems as indicated by the steeper gradient of the pink line.

OEO regeneration costs in LH systems are indicated by the step increases in the blue line every 600km.

The tradeoffs between higher cost ULH terminal / amplification equipment and reduced OEO regeneration costs result in a marginal cost advantage of LH in the region between 600 and 1,200km and a clear advantage of deploying ULH systems

<sup>51</sup> Source: Ericsson

<sup>52</sup> Source: Ericsson

for links longer than 1,200km: cost benefits of ULH range from approximately 10% to 30% savings for a simple point-to-point link.

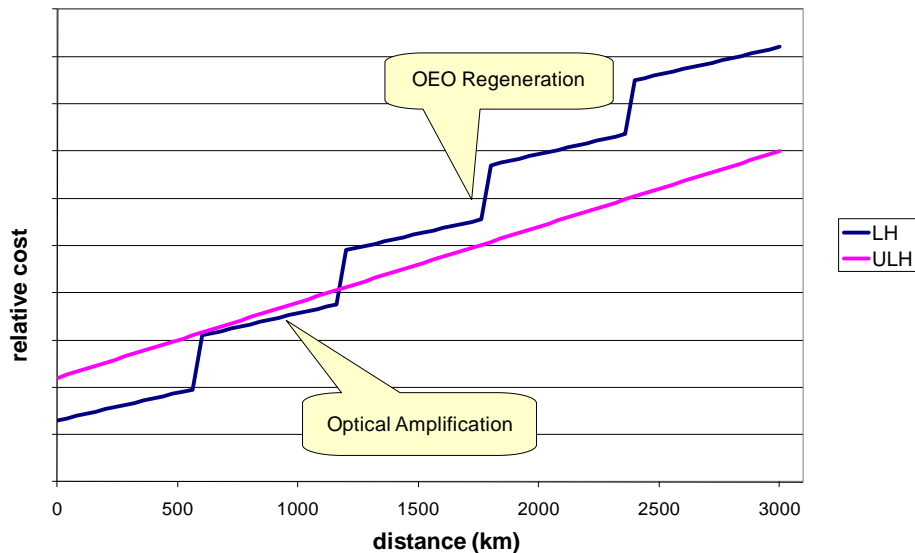


Figure 88 Simplified cost comparison of LH and ULH DWDM line systems<sup>53</sup>

#### 4.1.2 EXTENDED LONG-HAUL DWDM SYSTEMS

By combining ULH technologies of eFEC, high output power EDFA and dynamic per channel levelling with the standard LH modulation format of NRZ, transmission reach performance of up to 1,500km is achievable at moderate cost; such systems are termed extended long-haul (ELH).

The term xLH refers to either ELH or ULH and remained a relative niche within the WDM marketplace as most network connections were sufficiently served by LH system capabilities.

#### 4.1.3 COMBINING LH AND xLH: MULTI-REACH DWDM SYSTEMS

Advanced technologies in xLH systems such as high output power / low-noise amplifiers, dynamic gain equalisation, ROADMs and RZ modulation makes the initial cost high compared to a traditional LH system which uses cheaper amplifiers, no gain equalisation, NRZ modulation and fixed OADM (FOADM).

However LH systems do not scale well at high capacities over long distances due to the frequent OEO regeneration required. Because of the relative small size of the xLH market and intense industry competition it became clear that a separate xLH

<sup>53</sup> For illustrative purpose only, not based on detailed system costs

system could not be economically supported alongside an LH system, so vendors including Ericsson invested in R&D to integrate the functionality of the separate domains into a single flexible multi-reach DWDM system.

## 4.2 MULTI-REACH DWDM SYSTEMS

Service providers favour the low initial cost offered by traditional LH systems in meeting low initial traffic demands and the low per wavelength upgrade cost offered by ULH systems in meeting future requirements for network traffic growth [92]. Operational cost and complexity issues make service providers reluctant to deploy a mixture of DWDM platforms in their networks. These operational issues include separate sparring, training, management and system test requirements. Equipment vendors responded to the market requirements set by service providers and developed multi-reach DWDM systems. By combining the features of LH, ELH and ULH systems in a common modular platform, multi-reach systems are capable of economically addressing a wide range of network applications.

The terminology Multi-Reach was introduced by the industry in 2004. It is defined as “representing next-generation DWDM systems capable of supporting different reaches on different wavelengths within one platform”; it has completely replaced the xLH and LH segments and also incorporates Metro WDM although this particular segment is not investigated in this thesis.

Previous classifications of WDM applications focused on reach as the key differentiating parameter (Metro, LH, ELH and ULH). Today, other parameters including channel count, add/drop functionality and flexibility have become important factors.

Multi-reach systems typically have a reach capability of 100’s of km to > 3,000km before OEO regeneration is needed with capacity scaling up to 80 wavelengths providing up to 0.8Tb/s, 3.2Tb/s and 8Tb/s total capacity at 10Gb/s, 40Gb/s and 100Gb/s per channel respectively.

In 2003 Ericsson pioneered and was first to market with a multi-reach or so called multi-haul DWDM system *Marconi MHL 3000*<sup>54</sup> shown in Figure 89, which has been widely deployed by network operators around the world and continues to

---

<sup>54</sup> [http://www.lightreading.com/document.asp?doc\\_id=40552](http://www.lightreading.com/document.asp?doc_id=40552)

evolve with next generation features such as 40Gb/s, 100Gb/s and MD-ROADM [93].



Figure 89 Ericsson's *Marconi MHL 3000* DWDM system<sup>55</sup>

#### 4.2.1 MULTI-REACH SYSTEM AND NETWORK ARCHITECTURE

The multi-reach DWDM system consists of different types of shelves (or sub-racks) optimised in size for given applications as illustrated in Figure 90.

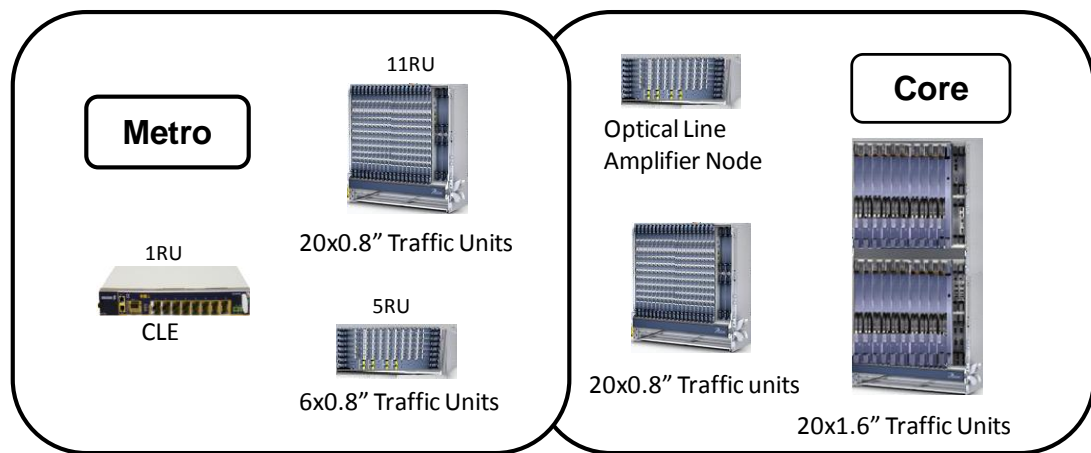


Figure 90 Ericsson *Marconi MHL 3000* WDM system shelves for metro and core applications<sup>56 57</sup>

<sup>55</sup> Source: Ericsson, photograph by Dr Liam Gleeson

<sup>56</sup> Source: Ericsson

<sup>57</sup> RU = rack unit, CLE = customer located equipment

Table 9 briefly summarises the architectural features of each type of DWDM system: LH, ULH and Multi-Reach. The various options are described in detail in the following sub-sections.

<i>System Type</i>	<i>Transponders</i>	<i>Optical Add/Drop</i>	<i>Amplifiers</i>	<i>Application</i>
<i>LH</i>	NRZ	F-OADM (8 channel add/drop)	LH	Short links (<600km) with high proportion of terminating traffic
<i>ULH</i>	RZ	R-OADM (100% add/drop)	ULH (high power, low noise)	Long links (<3,500km) with high proportion of transit traffic
<i>Multi-Reach</i> <i>(MR)</i>	NRZ RZ	F-OADM R-OADM	LH ULH	All core network applications

**Table 9 Summary of LH, ULH and multi-reach DWDM system architectures**

#### 4.2.1.1 Optical Line Amplifiers (OLA)

There are two families of EDFA in the Multi-Reach platform: LH EDFA and ULH EDFA. Each family consists of DSA EDFAs with mid-stage access to accommodate DCF and SSA EDFAs for spans without dispersion compensation and as booster amplifiers placed after high loss OADM and power equalisation devices.

The LH EDFA family has the lowest output power, highest noise figure and lowest unit cost.

The ULH EDFA family has the highest output power and lowest noise figure providing improved link OSNR performance. The ULH EDFA can be combined with dynamic power equalisation at either leveller or ROADM nodes to equalise channel performance across the C-band thus enhancing the link budget.

The ULH EDFA can also be combined with Raman amplification in an EDFA / Raman Hybrid configuration for maximum OSNR and longest reach performance.

#### 4.2.1.2 Transponders

There are two main types of 10Gb/s transponders: 10G NRZ and 10G RZ. 10G XFP (NRZ) detailed in section 2.6 is not considered since it was not available at the time of this analysis.

10G NRZ is for shorter reach applications and has the lowest unit cost using a transmitter with an external MZM laser. Combined with standard G.709 FEC and LH amplifiers 10G NRZ has up to 600km reach performance. Combined with eFEC, ULH amplifiers and DGE, 10G NRZ can achieve up to 1,500km reach performance.

10G RZ is for longer reach applications and has the highest unit cost using a transmitter with an external MZM laser. Combined with eFEC, ULH amplifiers and DGE, 10G RZ can achieve up to 3,000km reach performance. If hybrid Raman/EDFA amplification is deployed up to 4,000km reach performance can be achieved.

### **4.2.1.3 Multiplexer / De-multiplexer**

There are two variants of multiplexer / de-multiplexer: a group multiplexing unit based on AWG and a modular multiplexing unit based on thin-film filters.

The group multiplexing unit multiplexes and de-multiplexes up to 40 channels on a 100GHz spaced grid and two such sets of multiplexing units are interleaved to provide up to 80 channels capacity with 50GHz spacing.

The modular multiplexing unit is a lower cost solution for low initial channel counts and scales in increments of 8 channels up to a maximum of 40 channels. It provides an economical initial system cost where the initial number of wavelengths required is low and high channel count upgrade is not foreseen.

### **4.2.1.4 Optical Add-Drop Multiplexer (OADM)**

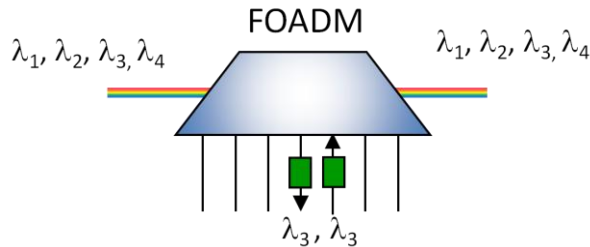
There are two main types of OADMs: fixed OADM (FOADM) and reconfigurable OADM (ROADM).

FOADM is the simplest and lowest cost variant of OADM network elements and is shown schematically in Figure 91. It allows a subset of optical channels passing through a node to be added and dropped by means of fixed add-drop filters based on dielectric thin-film filter technology inserted in the optical path.

Added and dropped channels have to be determined in advance since they are factory configurable thus constraining service providers' flexibility to respond to future changes in traffic requirements.

It is however a low cost solution suitable for networks with predictable demand. FOADM nodes are realised with 4 channel modularity with expansion to

accommodate up to the maximum 8 add and drop channels using  $2 \times 4$  channel filters. Expansion upgrades are traffic affecting i.e. it would lead to disruption of existing network traffic unless the required add / drop filters are equipped on day one or the optical path is protected.

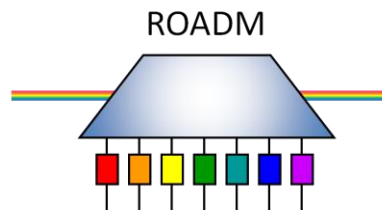


- Limited add/drop: up to 8 channels

**Figure 91 High level schematic of FOADM<sup>58</sup>**

A ROADM is the most flexible and highest performing OADM option and also the most costly; Figure 92 shows a schematic of ROADM. ROADMs have the flexibility to add and drop any number of channels out of the maximum aggregate of 80 channels. ROADMs were based on liquid crystal array wavelength blocker (WB) technology at the time of this research in 2003. Today wavelength selective switch (WSS) based primarily on micro-electro-mechanical systems (MEMS) technology have replaced the liquid crystal array WB as the enabling technology of ROADMs.

ROADMs are also capable of attenuating any of the channels that pass through without being dropped enabling dynamic power equalisation across the DWDM spectrum thereby improving link budgets as studied in detail in chapter 2. Reference [94] provides an overview of the main ROADM switching technologies in DWDM systems and reference [95] provides an overview of WSS technologies in particular.



- Full add/drop: up to 100% of channels

**Figure 92 High level schematic of ROADM<sup>59</sup>**

<sup>58</sup> Source: Ericsson

<sup>59</sup> Source: Ericsson

## 4.2.2 MULTI-REACH NETWORK APPLICATIONS

Figure 93 charts the application of each of the above multi-reach DWDM system options according to the number of channels and reach required. High performance options are highlighted in red and cheaper low performance options are highlighted in blue. It clearly shows that a single multi-reach DWDM platform with modular design and flexible configuration options can address a wider WDM market than LH or ULH systems alone. By tailoring the performance closely to the required application significant economic benefits can be achieved; this is investigated in section 4.3.

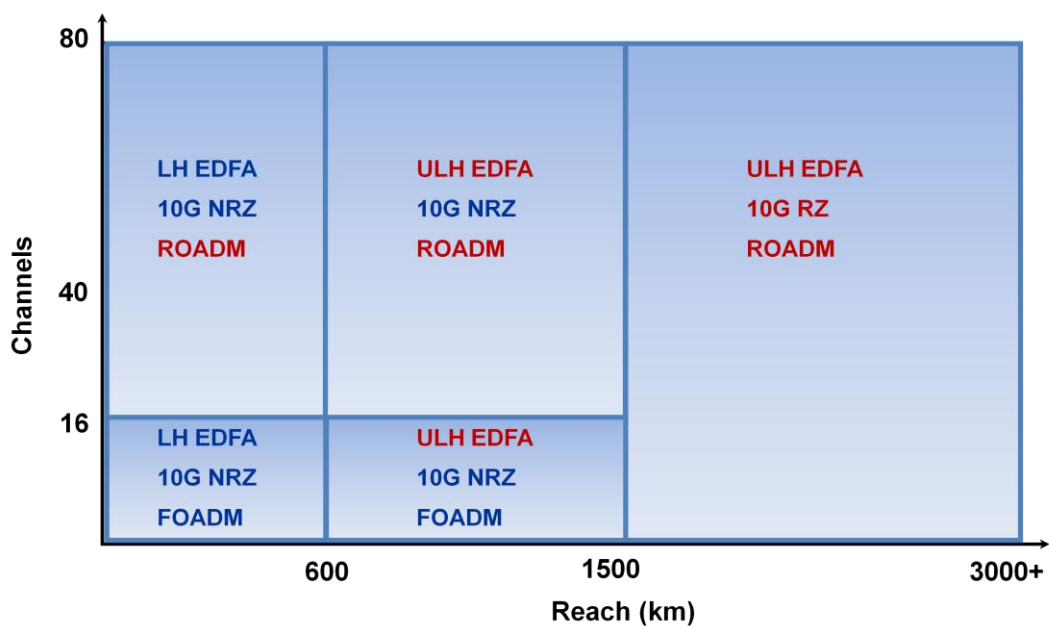


Figure 93 Modular EDFA, transponder and OADM system options for multi-reach DWDM applications

## 4.2.3 ADVANTAGES OF A MULTI-REACH DWDM SYSTEM

There are clear advantages of a common multi-reach DWDM system, including:

- Reduced CapEx for service providers, as will be demonstrated in section 4.3.
- Reduced OpEx for service providers, which is inherently difficult to quantify. A single DWDM system enables a reduced spares inventory, reduced training requirement, simpler network rollout with plug-and-play automated provisioning and a single network management platform.

- Equipment vendors also benefit from focusing their internal development effort on a single product thereby eliminating duplicated R&D expenditure and improving time to market for new features.

### 4.3 MULTI-REACH NETWORK DESIGN CASE STUDY

This section demonstrates the cost savings and flexibility advantage when deploying a multi-reach system in a typical national ring network. This research was published in a peer-reviewed publication [23].

#### 4.3.1 PROCESS AND TOOLS

An economic analysis of one network architecture versus another followed the process outlined in Figure 94. Optical performance evaluation and link design was carried out using *LDT*, described in section 2.11.1 and for critically long connections *LST* described in section 2.11.2 was used to cross-check performance evaluated by the simplified models in *LDT*. The network topology (position of network nodes), fibre physical parameters (span lengths, span losses, CD and DGD) and traffic requirements (number of wavelengths between each node) are the input parameters for the network design.

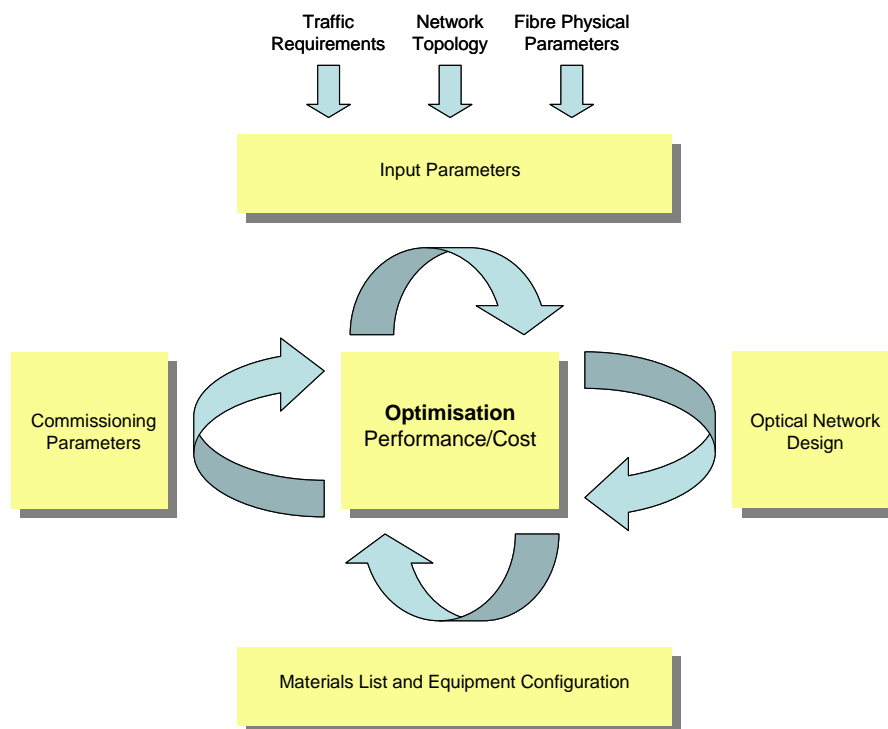


Figure 94 Outline WDM network design process<sup>60</sup>

<sup>60</sup> Source: Ericsson, diagram by Gareth Lloyd Jones

Each link is designed and optimised to give satisfactory BER performance at the lowest possible cost. Once the performance is optimised, an accurate cost is determined by producing a Bill of Materials (BoM) from *LDT* in the form of a spreadsheet listing the individual shelf and line cards required at each node in the network, together with the cost of each item and the total cost of the BoM.

In a complex network it may be necessary to produce multiple network designs comparing the cost of each design, in particular there may be differences in the cost on day one and the scalability of cost with increasing capacity in future years.

Commissioning parameters such as transmitter power settings and amplifier settings are determined by *LDT* to optimise performance of the network design and are automatically transferred to the equipment during field installation via the EMS/NMS.

### 4.3.2 NETWORK TOPOLOGY AND TRAFFIC REQUIREMENTS

The reference network topology is shown in Figure 95 and consists of a ring of 8 nodes with a total circumference of 4,025km, which is representative of a hypothetical national ring network.

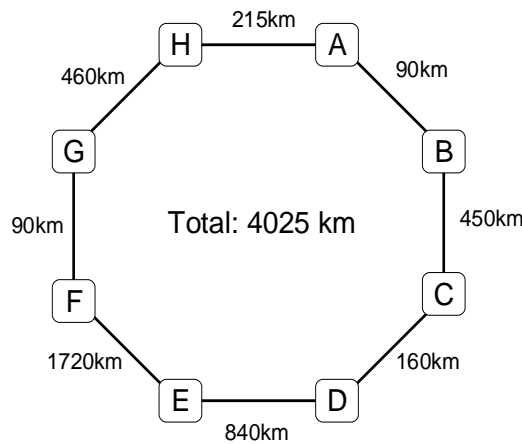


Figure 95 Reference network topology

Figure 96 shows the length in km of connections between each node in the network; the top half of the matrix represents clockwise paths and the bottom half represents anti-clockwise paths.

	A	B	C	D	E	F	G	H
A		90	540	700	1,540	3,260	3,350	3,810
B	3,935		450	610	1,450	3,170	3,260	3,720
C	3,485	3,575		160	1,000	2,720	2,810	3,270
D	3,325	3,415	3,865		840	2,560	2,650	3,110
E	2,485	2,575	3,025	3,185		1,720	1,810	2,270
F	765	855	1,305	1,465	2,305		90	550
G	675	765	1,215	1,375	2,215	3,935		460
H	215	305	755	915	1,755	3,475	3,565	

Figure 96 Length in km of connections between each network node

The traffic demand matrix for the first planning period is shown in Figure 97 with the number of 10Gb/s wavelengths between each node indicated. Each traffic path is protected in a 1+1 configuration therefore the bottom half of the traffic matrix mirrors the top half.

	A	B	C	D	E	F	G	H
A				1		1	1	1
B			1					1
C		1				1	1	1
D	1							1
E							1	1
F	1		1				1	1
G	1		1		1	1		1
H	1	1	1	1	1	1	1	

Figure 97 Traffic demand matrix in period 1

In the second planning period the traffic demand is doubled as shown in Figure 98. The traffic demand matrices are based on a typical demand seen in service provider networks at the time of the research.

	A	B	C	D	E	F	G	H
A				2		2	2	2
B			2					2
C		2				2	2	2
D	2							2
E							2	2
F	2		2				2	2
G	2		2		2	2		2
H	2	2	2	2	2	2	2	

Figure 98 Traffic demand matrix in period 2

LDT is used to optimise the optical performance of each possible connection in the network and indicates whether the link is feasible or not without OEO regeneration. This optimisation process is carried out for the different combinations of transponders and amplifiers. Figure 99 shows the possible un-regenerated connections using 10G NRZ transponders with LH amplifiers. Connections represented by dashed boxes require intermediate OEO regeneration. Figure 100 shows the possible un-regenerated connections using 10G NRZ and 10G RZ transponders with ULH amplifiers.

	A	B	C	D	E	F	G	H
A		NRZ	NRZ	-	-	-	-	-
B	-		NRZ	NRZ	-	-	-	-
C	-	-		NRZ	-	-	-	-
D	-	-	-		NRZ	-	-	-
E	-	-	-	-		-	-	-
F	-	-	-	-	-		NRZ	NRZ
G	NRZ	-	-	-	-	-		NRZ
H	NRZ	NRZ	-	-	-	-	-	

Figure 99 Un-regenerated feasible connections using 10G NRZ transponders with LH amplifiers

	A	B	C	D	E	F	G	H
A		NRZ	NRZ	NRZ	RZ	-	-	-
B	-		NRZ	NRZ	RZ	-	-	-
C	-	-		NRZ	NRZ	-	-	-
D	-	-	-		NRZ	-	-	-
E	RZ	RZ	-	-		RZ	RZ	RZ
F	NRZ	NRZ	RZ	RZ	RZ		NRZ	NRZ
G	NRZ	NRZ	RZ	RZ	RZ	-		NRZ
H	NRZ	NRZ	NRZ	NRZ	RZ	-	-	

Figure 100 Un-regenerated feasible connections using 10G NRZ and 10G RZ transponders with ULH amplifiers<sup>61</sup>

Optimal placement of OEO regeneration and add/drop sites is performed while minimising the overall amount of regeneration in the network i.e. OEO regeneration sites are placed at nodes with the most terminating traffic and where required according to reach performance limits shown in Figure 99 and Figure 100.

<sup>61</sup> Mixing of NRZ and RZ transponders is only possible using the multi-reach system

### 4.3.3 NETWORK DESIGNS

Here each network design is presented and explained, including network designs using a LH system, ULH system and 2 network design options using the multi-reach system.

#### 4.3.3.1 LH Network Design

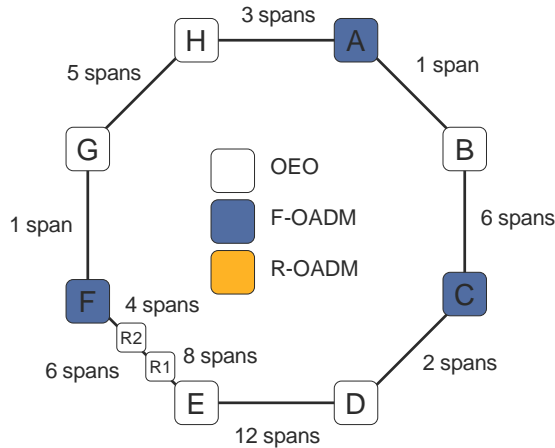


Figure 101 LH network design

Link E to F (clockwise direction) is too long to be feasible using the LH system therefore additional OEO regeneration is required at nodes R1 and R2 as shown in Figure 101. Based on these initial constraints, OEO regeneration sites and low cost FOADMs are placed at the remaining network nodes, taking into account traffic requirements and un-regenerated transmission reach capabilities indicated in Figure 99 with all 10G NRZ transponders.

#### 4.3.3.2 ULH Network Design

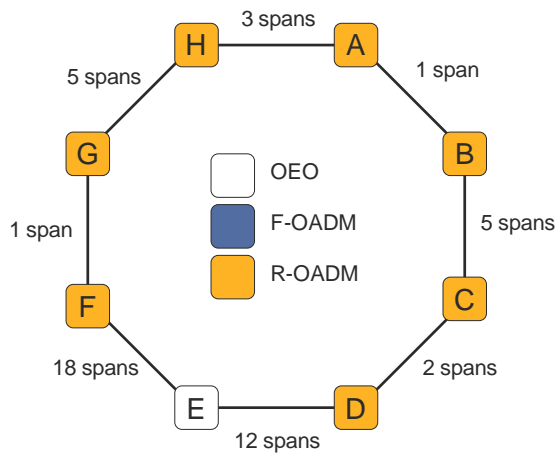


Figure 102 ULH network design

With the enhanced transmission reach capability of the ULH system, link E to F (clockwise) is feasible without OEO regeneration by deploying RZ transponders; two channel equalising network elements are distributed along the link to reduce gain variation.

The next step is to choose which node to perform OEO regeneration. To minimise cost it is preferable to choose the node with the highest terminating traffic requirement; i.e. node H according to the traffic matrices in Figure 97 and Figure 98. However a knock on effect of choosing node H would be to require selective OEO regeneration at node E to reach node F and G in the clockwise direction. Node E is a more suitable choice for complete OEO regeneration as all nodes can be reached except C and D in the clockwise direction however no traffic is expected between these nodes according to the traffic matrices. All other network nodes were chosen as ROADMs since FOADMs are not available in the ULH system. All transponders are longer reach 10G RZ.

Due to the improved noise figure and output power performance of ULH amplifiers one OLA node can be removed from link B to C consolidating 6 fibre spans into 5 spans. This leads to reduced CapEx and significant OpEx savings by removing the real estate required to house the surplus OLA node.

### **4.3.3.3 Multi-Reach Network Designs**

Two alternative network design approaches can be taken with the multi-reach system:

1. Lower initial network cost
2. Lower TCO over the full network lifecycle

The final choice will depend on the priorities of the network operator customer.

#### **Low Initial Cost Multi-Reach Network Design (MR1)**

By mixing LH and ULH amplifier sections, design MR1 shown in Figure 103 requires only 4 OEO regeneration sites compared to the 7 required in the LH only design in section 4.3.3.1. 10G NRZ transponders are deployed on LH amplifier sections and a mixture of 10G NRZ and 10G RZ are deployed on ULH amplifier sections according to the engineering rules defined in Figure 100.

Node G has a traffic requirement in period 2 which exceeds the 8 channel limit of a FOADM therefore an ROADM is required; the traffic requirements of all other nodes can be met using lower cost FOADMs.

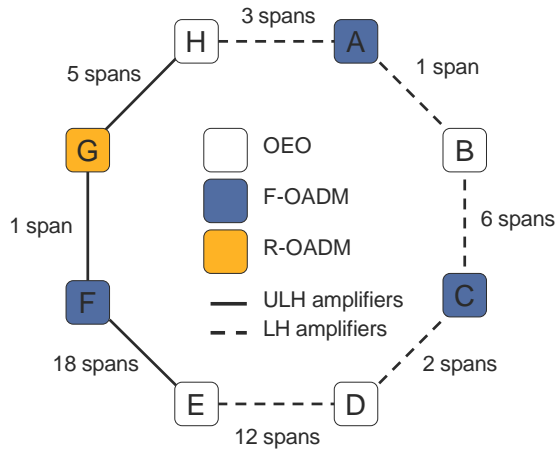


Figure 103 Low initial cost multi-reach network design MR1

**Low Total Cost of Ownership Multi-Reach Network Design (MR2)**

Using ULH amplifiers throughout the network a design based on the ULH design of section 4.3.3.2 with one OEO regeneration node at E is shown in Figure 104. Low cost FOADMs can be deployed at 3 network nodes with ROADMs at all other nodes to support the required traffic demands and to provide channel equalisation capability. Lower cost 10G NRZ transponders can be deployed on shorter connections according to the engineering rules defined in Figure 100 thereby providing further cost savings over the ULH design.

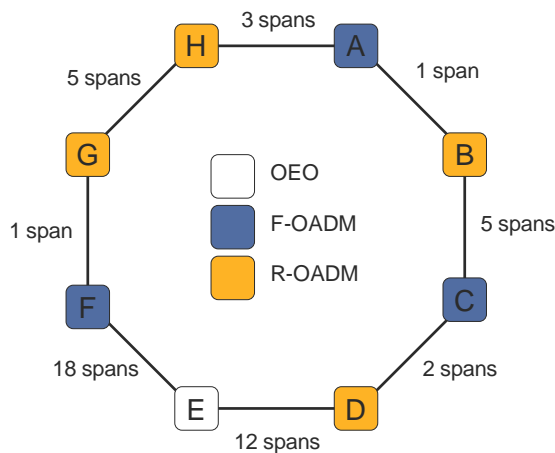


Figure 104 Low per wavelength cost multi-reach network design MR2

#### 4.3.4 NETWORK COST COMPARISON

The total network equipment costs for each design were calculated and re-scaled relative to the cost of the LH design in period 2. These were calculated using Ericsson's internal cost information<sup>62</sup>. A 10% cost reduction was applied to the cost of the equipment required to upgrade from period 1 to period 2 which is a typical annual discount expected by service providers.

##### Period 1

The relative cost of each design in period 1 is shown in Figure 105. In period 1 the multi-reach design MR1 is the cheapest design resulting in a 17% cost saving over the ULH design, 4% saving over the LH design and 2% saving over the multi-reach design MR2. Design MR1 realises significant cost savings over the ULH design due to the cheaper LH OLA and FOADM reducing the OLA and OADM cost, and cheaper mix of NRZ and RZ transponders than the all RZ transponders in the ULH design. The reduced reach of the LH amplifier sections result in an increased cost for the Optical Line Terminals (OLT) and regenerators (Regen) required for the extra OEO regeneration network nodes.

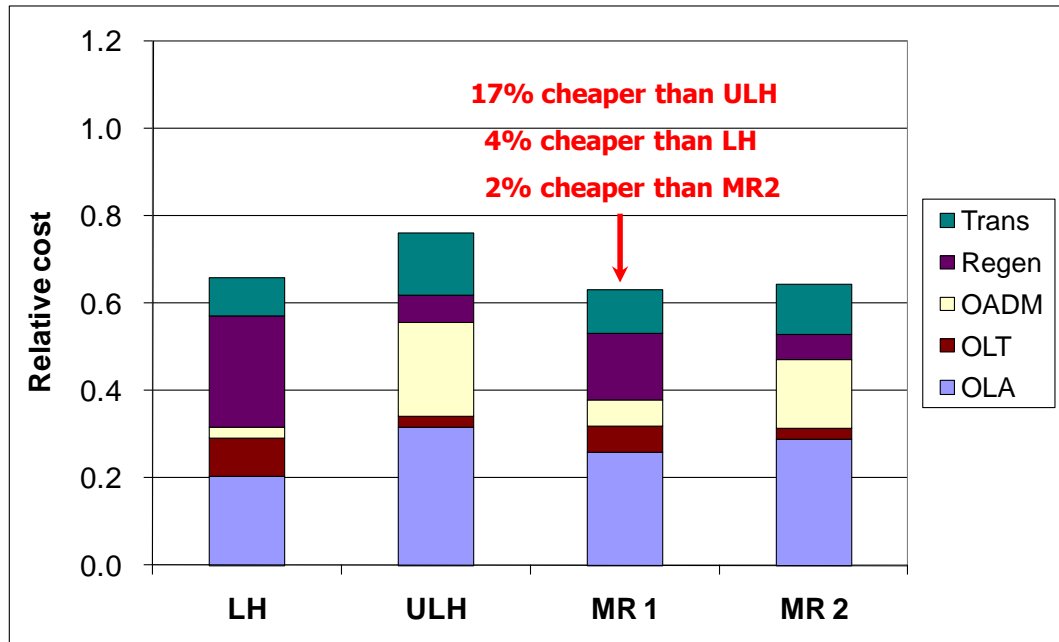


Figure 105 Total network cost for each network design in period 1

<sup>62</sup> Due to reasons of commercial sensitivity, the underlying cost assumptions for each network element and transponder card cannot be disclosed in this thesis.

## Period 2

Looking at the cumulative cost of both planning periods shown in Figure 106, MR2 is the cheapest design saving 19% over the LH design, 14% over the ULH design and 8% over the MR1 design. Design MR2 is successful in saving over the LH design due to the significant reduction in OEO regeneration offsetting the additional cost of ULH OLA and ROADMs. Design MR2 is cheaper than the ULH design due to the deployment of lower cost NRZ transponders for the shorter connections and lower cost FOADM at nodes with low add/drop traffic demands. Since the MR1 design is based on mixed LH and ULH sections it is less economical than the MR2 design at high traffic levels due to the significant increase in OEO regeneration cost.

In conclusion a common multi-reach system has been shown to be cost competitive with LH systems for low traffic demands while also having the flexibility to compete with the low incremental upgrade cost advantage of ULH systems.

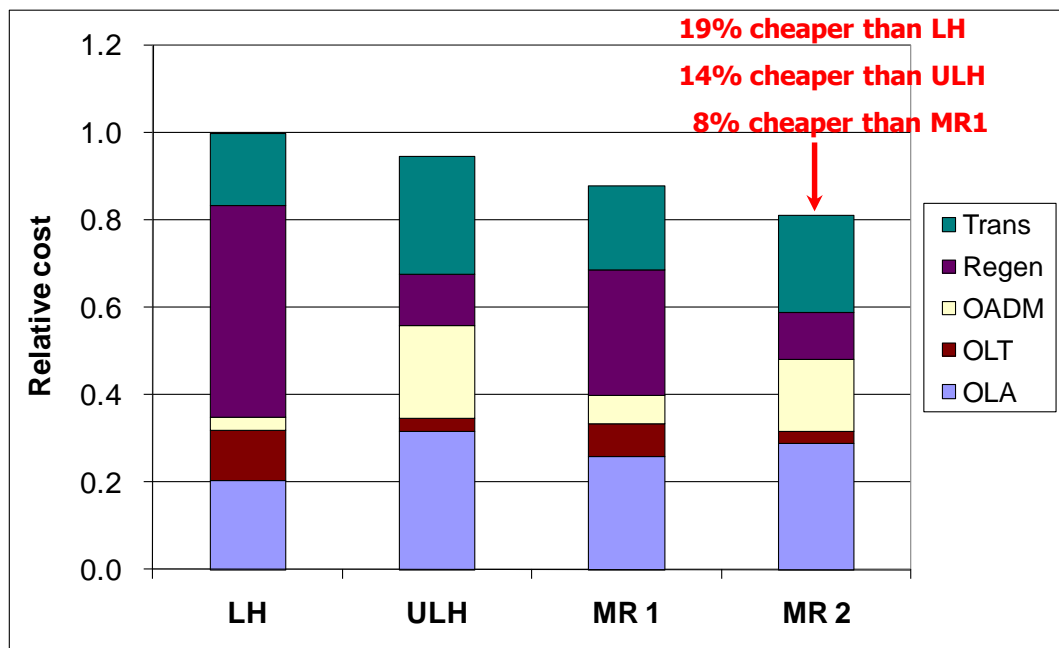


Figure 106 Total cumulative network cost for each network design in period 2

## **4.4 CHAPTER SUMMARY AND CONCLUSIONS**

In this chapter the development of a flexible, multi-reach DWDM system has been detailed including its key system components. An example network design exercise was carried out, comparing designs using the multi-reach system and earlier generation LH and ULH systems, for a typical national scale ring network. A multi-reach system was shown to provide significant cost savings of almost 20% over the LH and ULH systems.

Multi-reach systems are able to offer the low initial infrastructure cost typical of LH systems, combined with the low incremental upgrade cost characteristic of ULH systems, due to the increased optical reach and transparency and availability of both high performance and lower cost network element options. Combining these features on a common, modular platform offers a more cost-effective and scalable solution for core networks.

Finally, chapter 5 builds upon the benefits of multi-reach DWDM systems, by presenting a techno-economic analysis of the increasing level of optical transparency in the evolution from point-to-point OEO regenerated DWDM links to transparent meshed networks with MD-ROADMs.

## 5 TRANSPARENT MESHED NETWORKS

Optimising COST and FLEXIBILITY of WDM networks are the primary objectives of this chapter, which are achieved by trading off against PERFORMANCE.

The research presented here contributed to the development of Multi-Degree ROADM (MD-ROADM) functionality on Ericsson's Multi-Reach WDM system *Marconi MHL 3000*. A MD-ROADM also called Extended OADM (EOADM) or All-Optical Cross Connect (OXC) is an extension of the ROADM architecture described in section 4.2.1.4 to provide all-optical switching functionality at nodes of fibre connectivity (degree) greater than two directions. Hence the MD-ROADM is a key technological building block of transparent meshed optical networks.

A techno-economic analysis was carried out, demonstrating the economic benefit, scalability and flexibility of a MD-ROADM combined with a Multi-Reach WDM system compared with earlier generation OEO based LH systems and Multi-Reach systems with degree-2 ROADMs only. This work was published in a peer-reviewed paper at OFC 2004 [24] (published by OSA) and has been further developed here to include a comparison with state of the art WSS based MD-ROADM technology.

Firstly the evolution of WDM networks is described in section 5.1, followed by descriptions of the OEO network architectures in sections 5.2 and MD-ROADM optical bypass network architectures in section and 5.3. Details of the techno-economic analysis are presented in section 5.4 with conclusions and areas for further development in sections 5.5 and 5.6 respectively.

### 5.1 OPTICAL TRANSPORT NETWORK EVOLUTION

Transparent (i.e. all optical) meshed networks have been talked about in the telecommunications industry for more than a decade [96]. ULH transmission technologies as detailed in section 4.1.1 combined with all-optical MD-ROADM wavelength switching technologies have since made transparent all-optical meshed architectures a reality in operators' networks [97].

Cost reduction is a key driver for evolving WDM networks from point-to-point OEO regenerated links towards transparent meshed networks. Reduction in CapEx over the lifetime of the network is realised whereby the extra cost of long reach interfaces and optical switching equipment is outweighed by the saving in OEO regeneration

equipment no longer required for traffic passing through a node (such traffic is said to optically bypass a node).

OpEx is also reduced by only having to service traffic nodes at the end points of connections when adding capacity to the network. Reduction of OEO equipment also results in lower power consumption and real estate space requirements both of which are significant operating expenses for network operators.

The underlying sub-system architecture of a first generation MD-ROADM node includes a broadcast and select wavelength blocker based on liquid crystal array technology [98].

In 2002 Corning was first to report a network experiment including a 320x320 wavelength port (4 fibre directions with 80 channels per direction), broadcast and select OXC or MD-ROADM [46] and [99].

In 2003 Ericsson integrated a MD-ROADM on its *Marconi MHL 3000* Multi-Reach WDM system, reporting details of its implementation and lab trials of ULH transmission over a meshed network architecture in [31] and [100].

The work presented here builds upon these lab trials to demonstrate the potential scalability and economic benefits of deploying all-optical MD-ROADM together with a Multi-Reach WDM system in an example European national network. This is of particular interest to network operators who are driven to reduce both CapEx and OpEx in their networks.

Deployments of optical meshed networks in service provider networks have subsequently taken place since around 2005; reference [101] reports a deployment by Verizon using Alcatel-Lucent equipment. Reference [102] published by Ericsson in 2009 details the deployment with Chunghwa Telecom in Taiwan of an all optical mesh network including several degree-3 and degree-4 MD-ROADM implemented with WSS technology.

Flexible ROADM technologies were first deployed in core networks where traffic requirements are highest thereby realising the maximum benefit of transparency. Traffic can however be less predictable in metro networks where ROADM and MD-ROADM network elements can provide the flexibility to respond to future changes in traffic growth requirements. Evolution towards lower cost device technologies are more recently driving adoption of ROADMs closer to the edge of the network [85].

## 5.2 OEO NODE ARCHITECTURES

LH DWDM systems perform OEO conversion at every traffic node within a network. A terminal consisting of a multiplexer / de-multiplexer is deployed for each transmission direction within a traffic node. For example a degree 3 node would require 3 terminals as shown in Figure 107.

All traffic is terminated and converted from a coloured DWDM signal on the line side of a transponder to a short reach “grey” 1310nm signal on the client side of a transponder. Traffic can be routed from one terminal to any of the other 2 directions by manually interconnecting short reach 1310nm connections between corresponding grey interfaces using patch cords and a patch panel. Any traffic which is to be added/dropped locally can be connected to a short reach port on a SONET/SDH, OTN or Ethernet switch or an IP router.

OEO regeneration may also be required at intermediate nodes between traffic nodes if the link lengths are beyond the transmission reach limits of the DWDM line system (typically around 600km for LH systems).

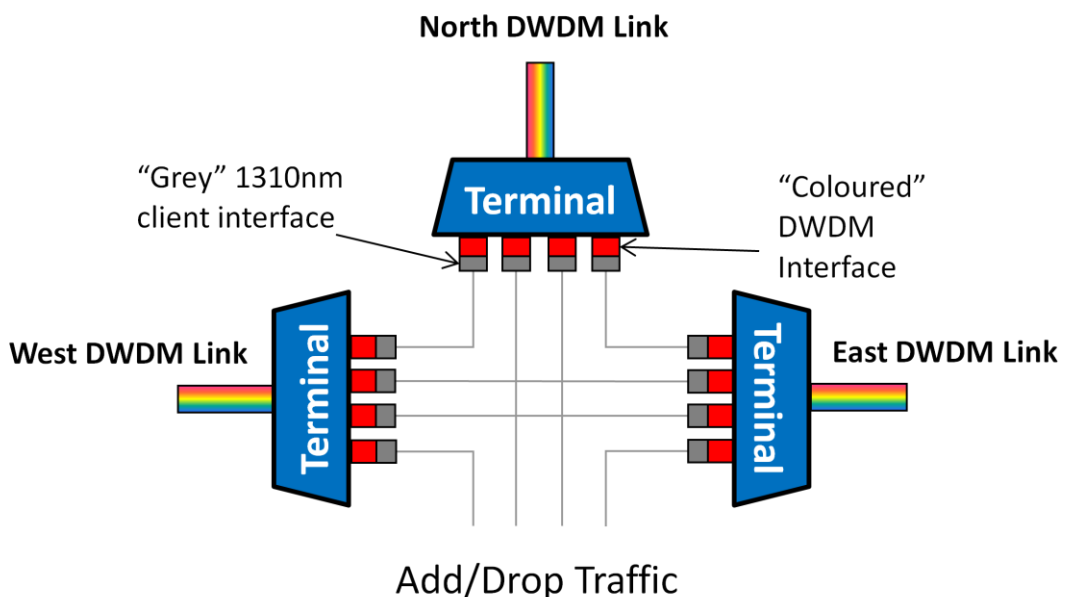


**Figure 107 OEO architecture at degree-3 node with manual reconfiguration**

Node re-configurability in OEO networks can be automated by deploying an optical switch with an electronic switch fabric (i.e. SONET/SDH or OTN) as shown in Figure 108. Each transponder is connected via its short reach client side interface to a switch port. The electronic switch fabric is configured to interconnect with another

switch port linked to the client side interface of a transponder on a different terminal direction, or to a local add/drop port.

Flexibility provided by a reconfigurable switch does however come at a high equipment cost. In the analysis presented here manual reconfiguration is assumed in OEO networks i.e. no optical switch with electronic switch fabric thereby restricting the analysis to comparing the DWDM equipment only.

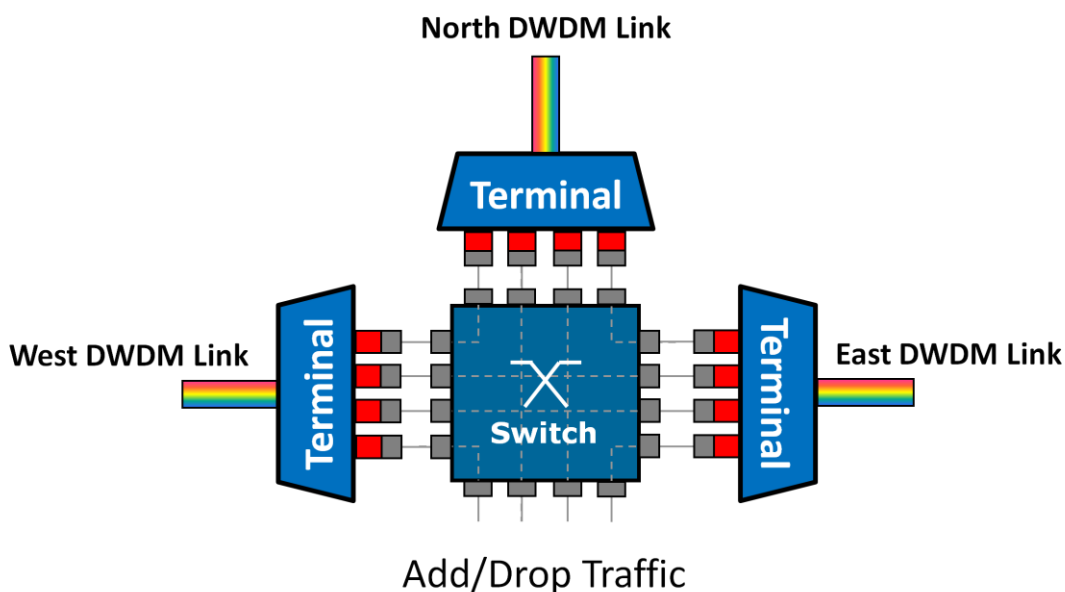


**Figure 108 OEO architecture at degree-3 node with automated reconfiguration**

**Benefits of OEO architecture:** Terminating all traffic entering a node does have advantages. Signals are cleaned up by OEO regeneration, performing re-amplification, re-shaping and retiming (3R regeneration) thus ensuring error free transmission along each link.

Electronic processing can enable performance monitoring of the signal at every node making it simpler to locate faults within a network.

As traffic enters a node via one transponder and exits the node via another it is possible to assign different wavelengths to each WDM link on the ingress and egress of the node. This wavelength conversion functionality is effectively provided for free in OEO networks and can be useful in overcoming wavelength contention issues between highly utilised network links where the wavelength continuity constraint cannot be maintained without wavelength conversion.

The need for complex wavelength planning and careful analogue link engineering is also largely eliminated.

**Disadvantages of OEO architecture:** The main disadvantage of the OEO architecture is the high equipment cost where transponders are required to perform OEO regeneration of every signal regardless of whether it is bypassing or terminating at a node. In addition to the capital expense of the equipment there is an operational cost impact whereby more space is required to house the additional equipment and higher power consumption of electronics and dissipation of heat becomes a problem as networks inexorably scale to higher capacities. Network upgrades also require expensive and time-consuming site-visits to all intermediate terminal nodes whereas more flexible ROADM based architectures only require visits to the end points of each connection.

### 5.3 MD-ROADM NODE ARCHITECTURES

The architectures presented here are aligned with the detailed descriptions and naming conventions given in [103]. First generation MD-ROADM were implemented using liquid crystal array wavelength blocker devices in a broadcast and select architecture [31], [46], [99], and [100].

The most basic degree-2 ROADM architecture is outlined in Figure 109. All links are bi-directional over a pair of fibres however only one direction is shown for simplicity; wavelength blocker modules include two devices, one per direction.

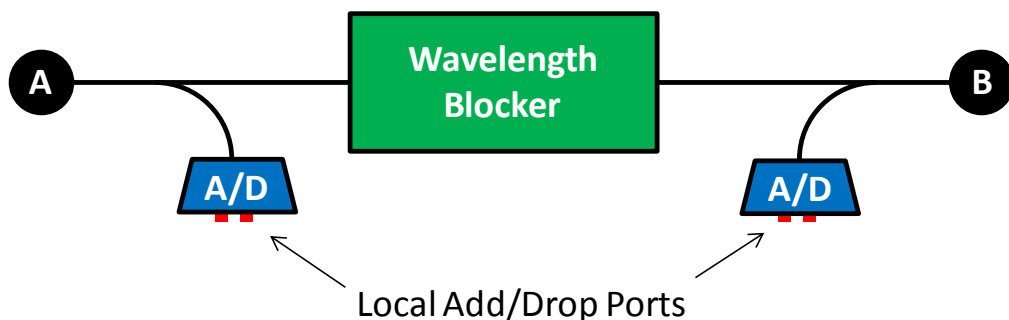


**Figure 109 Degree-2 ROADM node architecture**

An incoming WDM signal from direction A passes through a splitter and is broadcasted through a de-multiplexer (typically an AWG) and received at a local drop port, the signal is also broadcasted towards the wavelength blocker. The wavelength blocker can be set to fully attenuate any of the wavelengths in the passband. A blocked wavelength is dropped at the corresponding drop port of the de-multiplexer and received by a tuneable transponder tuned to the correct wavelength where OEO regeneration takes place. A signal at the dropped wavelength can then

be added after the wavelength blocker via a multiplexer and coupler to join the aggregate WDM signal thereby allowing wavelength re-use.

Channels which are not dropped locally are said to optically bypass the node without any OEO regeneration thereby significantly saving the number of transponders compared with the OEO architecture. A ROADM does cost significantly more than two back-to-back terminals however since typically more than 50% of traffic entering a node is passing through, the reduction in transponder numbers compensates for the increased DWDM infrastructure cost resulting in an overall cost saving at a network level.

Additional components are required at ROADM nodes (and indeed at terminals) and are omitted from the architecture diagrams for simplicity. EDFAs are present on either side of the wavelength blocker to compensate for the loss of the preceding fibre span and the wavelength blocker, splitters and couplers.

DCMs are included at the mid-stage of DSA EDFAs to optimise the dispersion map on a link by link basis so that all possible connections within the network have near optimal dispersion maps regardless of their origin or destination.

Power monitors and an OSC are required to monitor and control the power levels of each channel in the WDM signal.

Signal pre-emphasis and re-emphasis to a desired profile as detailed in section 2.8 is also possible at ROADM and MD-ROADM nodes by controlling the liquid crystal array to attenuate each channel independently. This is particularly important in transparent networks as different channels are likely to have transmitted over varying distances in the network experiencing different gain and loss profiles resulting in an uneven spectrum. Dynamic gain equalisation functionality is effectively provided for free at ROADM nodes. Prior to ROADMs dedicated channel levelling nodes were required approximately after 8 fibre spans as described in section 2.8, adding significant cost to a network. Levelling nodes may still be required in a ROADM network where certain links between ROADMs are longer than about 8 spans.

**Benefits of MD-ROADM:** The primary advantage of ROADM and MD-ROADM is the significant saving of costly OEO regenerators (back to back transponders) that is achieved through optical bypass of transit traffic. A significant saving in CapEx is expected particularly as the network scales to higher capacities.

OpEx is also expected to reduce as the scalability advantage can lead to reduced power consumption and real estate space requirements.

MD-ROADMs can also improve the flexibility of a network to respond to changing traffic demands. Remote re-configurability is possible via the NMS however tuneable transponders and colourless and directionless and contention-less (CDC) MD-ROADMs are required for full flexibility.

**Disadvantages of MD-ROADM:** Increased optical transparency comes at a price. As transmission distances increase, higher specification ULH transmission capabilities are required together with costly ROADM components (WB or WSS) resulting in high upfront costs for DWDM infrastructure. Unless traffic is at a sufficiently high level for the saving in OEO equipment to outweigh the higher DWDM infrastructure cost, the MD-ROADM network may not be economical until late in the network's lifecycle.

Increased transmission distances and optical bypass leads to an analogue network whereby knowledge of fibre span characteristics and careful management of transmission impairments is required to maintain adequate BER for each connection [85]. Complex wavelength planning is also required to avoid / reduce wavelength contention and optimising network cost.

### 5.3.1 NODES OF DEGREE >2 USING ROADM

ULH systems and early Multi-Reach DWDM systems were initially limited to degree-2 ROADM functionality. Network nodes of degree greater than 2 were implemented using a combination of degree-2 ROADM and 1 or more terminals.

Figure 110 shows an example degree-3 node implementation. The ROADM is oriented along the two directions with the most pass-through traffic (i.e. path A-B) in order to maximise the benefit of optical bypass.

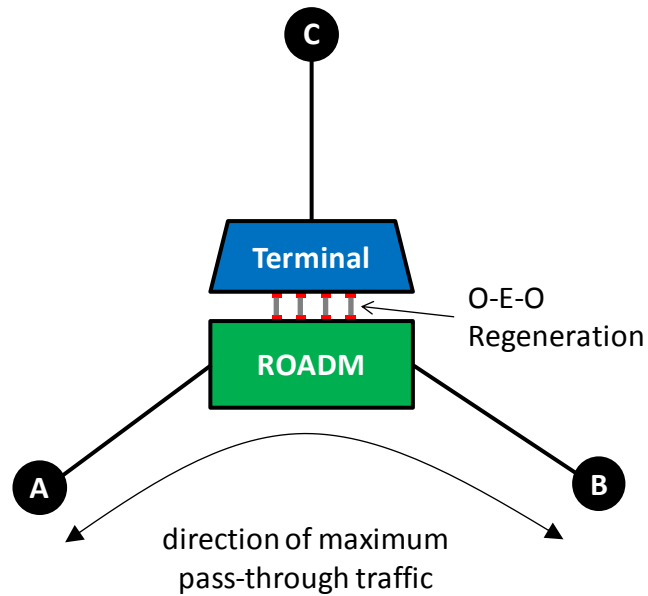


**Figure 110 Degree-3 node using a degree-2 ROADM and a terminal**

Traffic routed between A-C and B-C require OEO regeneration between the terminal and the add/drop ports of the ROADM via back to back transponders interconnected by an optical patch panel.

For the general case of a node of degree  $D$ , OEO regeneration takes place between the add/drop ports of the ROADM and each of the  $D - 2$  terminal branches within the node and also between each of the  $D - 2$  terminal branches themselves. Figure 111 and Figure 112 show a degree 4 and degree 5 node respectively.

A significant disadvantage of this architecture is that the optimal direction of pass-through traffic may deviate from that forecasted at the outset of network planning, thus leading to a potentially sub-optimal network as traffic evolves.

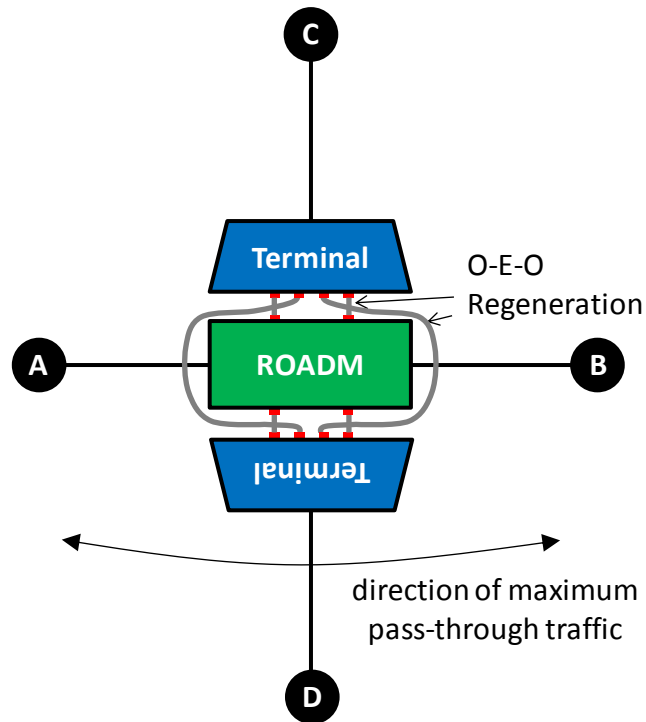


Figure 111 Degree-4 node using a degree-2 ROADM and 2 terminals

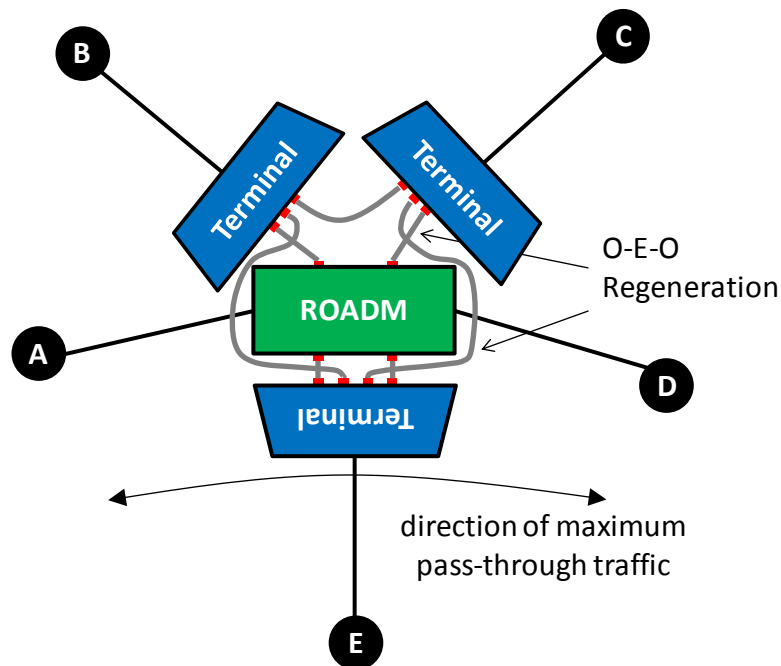


Figure 112 Degree-5 node using a degree-2 ROADM and 3 terminals

A slightly more optimal node architecture given in [103] and shown here in Figure 113 can be achieved for degrees  $> 4$  by orienting 2 ROADMs along 2 routes of maximum through traffic. Unfortunately this was not implemented at the time of the research however the improved economic impact is likely to be relatively small.

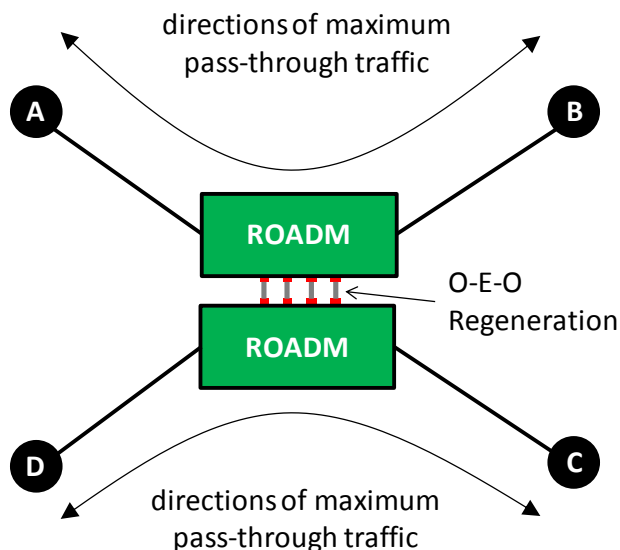


Figure 113 Degree-4 node using 2 degree-2 ROADMs

### 5.3.2 MD-ROADM BASED ON WAVELENGTH BLOCKERS

A MD-ROADM capable of full optical bypass in up to 4 directions with an architecture based on wavelength blockers (WB MD-ROADM) was developed soon after the launch of the Multi-Reach DWDM system. Figure 114 illustrates the architecture of a degree 3 node.

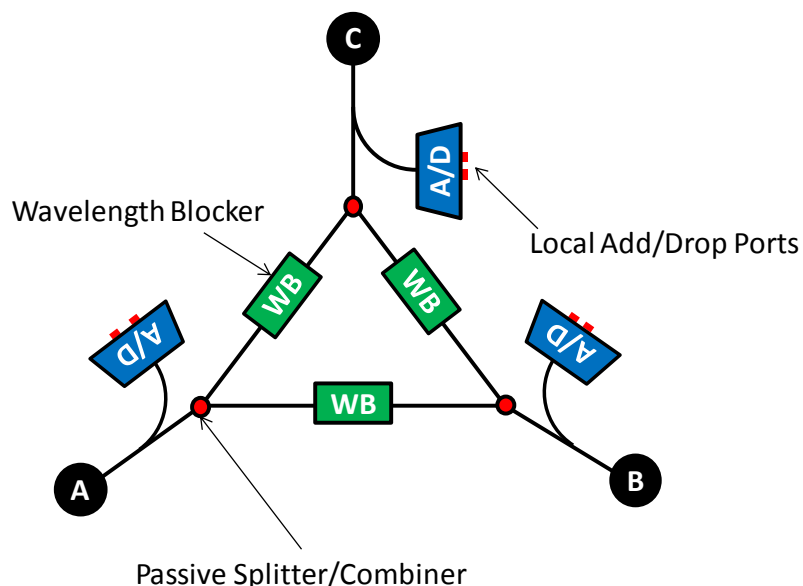


Figure 114 Degree-3 “broadcast and select” WB MD-ROADM node architecture

Incoming signals from each of the three fibre directions A, B and C are broadcasted to the add/drop de-multiplexer and through a passive splitter into two branches with wavelength blockers along each branch. If a particular channel is to be routed all-

optically to path B for example then the wavelength blocker between path A and C would be set to block that particular channel allowing it to only pass through A to B.

For the general case of a degree  $D$  node the through path is split into  $D - 1$  paths with wavelength blockers on each. The number of wavelength blocker devices per node scales with the square of the node degree and since each wavelength blocker module is bi-directional containing one device per direction the number of wavelength blocker modules  $N_{WB}$  scales as

$$N_{WB} = \frac{D(D-1)}{2}$$

Equation 57

A degree-4 node architecture is shown in Figure 115.

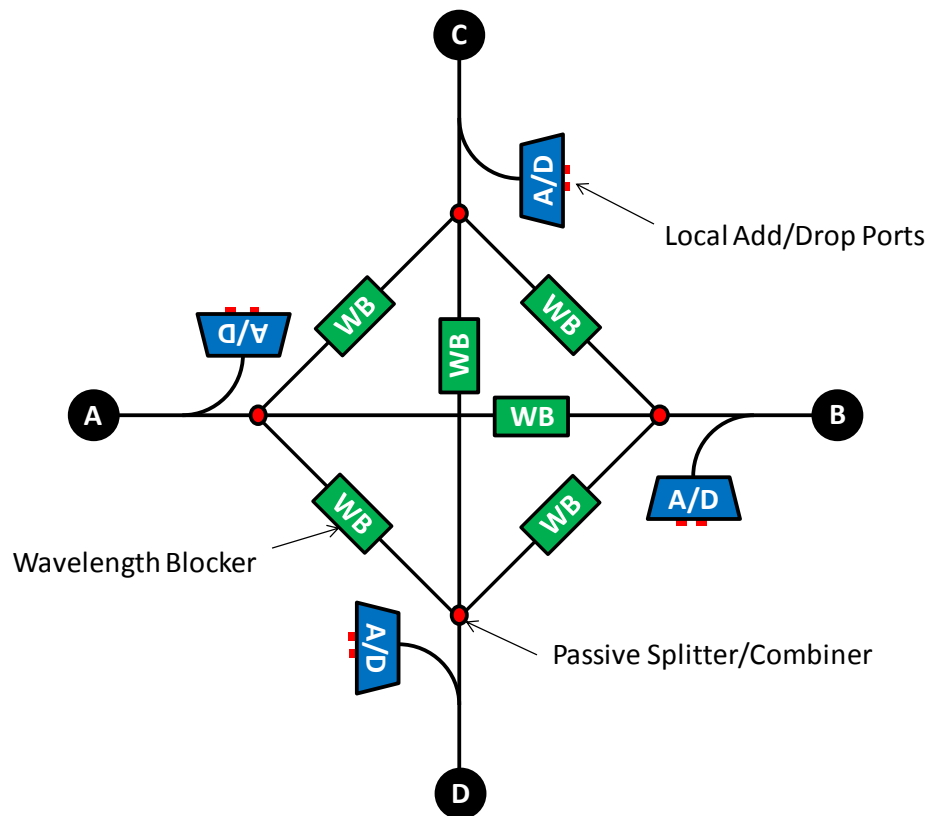


**Figure 115 Degree-4 “broadcast and select” WB MD-ROADM node architecture**

Extending to a degree 5 MD-ROADM node would require 10 wavelength blocker modules as shown in Figure 116, however from an implementation complexity and cost perspective WB MD-ROADM are limited to optically bypass in a maximum of 4 directions.

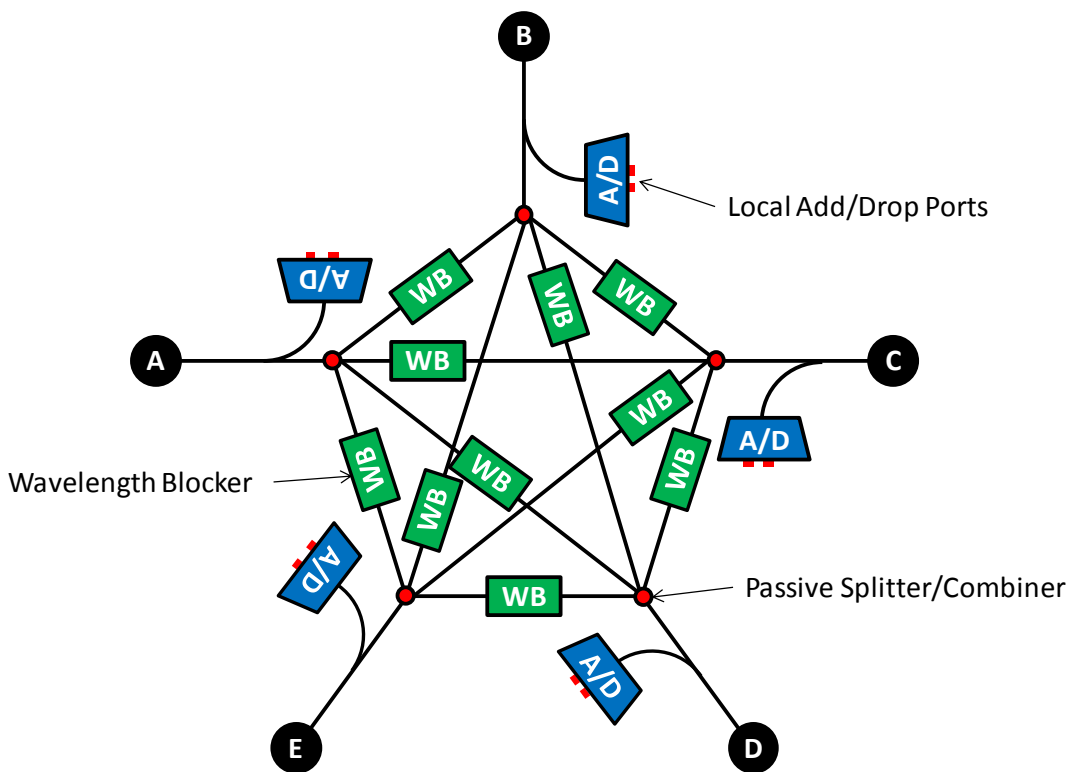


Figure 116 Degree-5 “broadcast and select” WB MD-ROADM node architecture

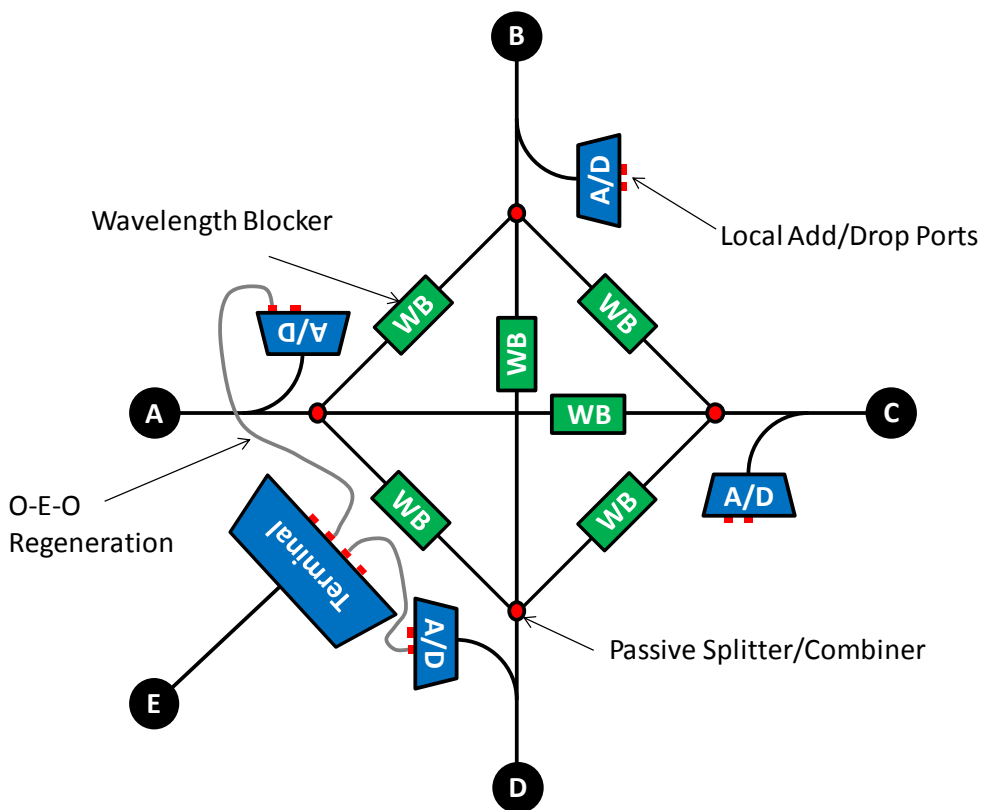


Figure 117 Degree-4 “broadcast and select” MD-ROADM upgraded to degree-5 node architecture with an additional terminal

A degree 5 node is implemented as a degree 4 MD-ROADM with an additional terminal for the 5<sup>th</sup> degree as shown in Figure 117. OEO regeneration occurs between the add/drop ports of each direction on the MD-ROADM and the terminal where a signal passes through the terminal direction and one of the MD-ROADM branches. To minimise regeneration cost the terminal branch is chosen for the route with the lowest pass-through traffic and highest add/drop traffic.

### 5.3.3 MD-ROADM BASED ON WAVELENGTH SELECTIVE SWITCH

Wavelength Selective Switches (WSS) are advanced optical switching modules which today have replaced the WB as the technology of choice for implementing broadcast and select ROADM and MD-ROADM node architectures in meshed optical networks [102].

An  $N \times 1$  WSS is capable of selecting any DWDM wavelength from  $N$  different input fibres and combining these wavelengths on a common output fibre. Conversely a  $1 \times N$  WSS is capable of switching individual wavelengths from a common input port to any of  $N$  output fibres.

A key advantage of WSS versus WB is scalability; the number of WSS modules required in a node scales linearly with degree  $D$  rather than quadratically. WSS result in lower cost and complexity of transparent network nodes and can enable full transparency in more than 4 directions; optical losses are also lower.

In common with WB, WSS are capable of dynamic spectral equalisation of each wavelength to optimise transmission reach performance.

The most common WSS technology is 2D MEMS for high port count WSS ( $9 \times 1$ ) and liquid crystal arrays for low port counts ( $2 \times 1$  &  $4 \times 1$ ) [95]. Liquid crystal on silicon (LCOS) is emerging as a candidate technology for flexible wavelength grid applications i.e. combinations of 50GHz and 100GHz channel spacing and alternatives such as 25GHz closely spaced or 75GHz, 150GHz and higher for high speed rates beyond 100 Gb/s.

Higher port counts modules are appearing on the market with  $1 \times 20$  WSS recently released [104]<sup>63</sup>. Despite network nodes being usually no more than degree-8, such high port count WSS are crucially important for implementing colourless,

---

<sup>63</sup> Source: <http://investor.finisar.com/releaseDetail.cfm?ReleaseID=604799>

directionless nodes [105] and also for interconnecting multiple fibre pairs per direction where parallel DWDM line systems are deployed.

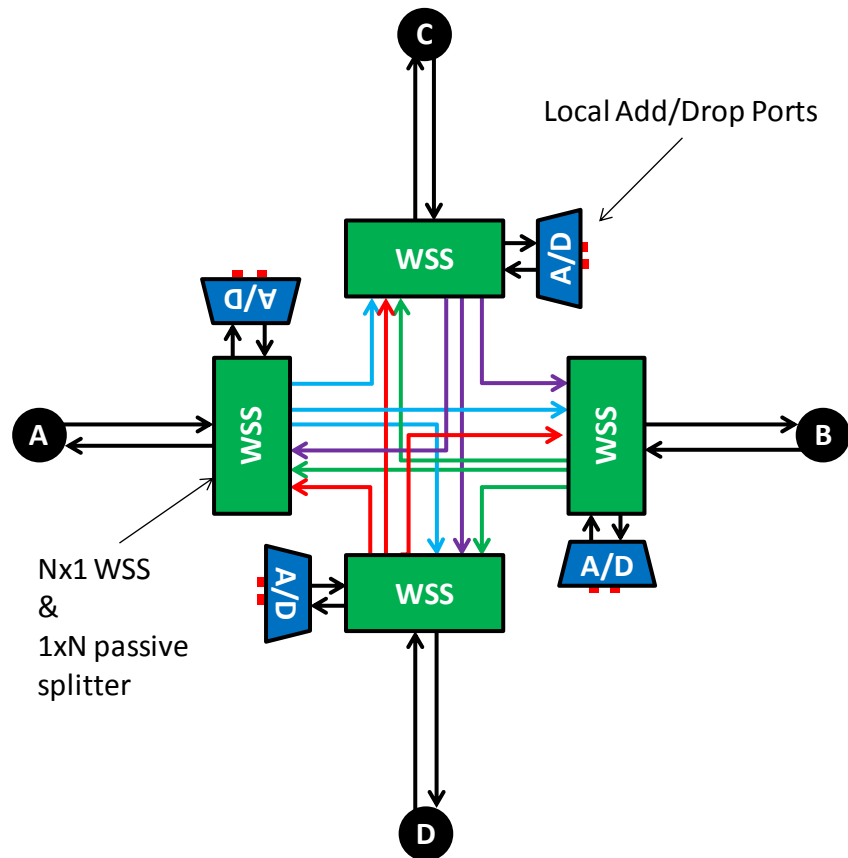


**Figure 118 Degree-4 MD-OADM node architecture with WSS**

An example degree-4 node architecture based on WSS is shown in Figure 118. Each WSS module (shown in green) includes an  $N \times 1$  WSS on the multiplex side and a  $1 \times N$  passive splitter on the de-multiplex side. Fixed multiplexers and de-multiplexers (typically AWG) are used for local add/drop. In this configuration add/drop ports are both coloured (wavelength specific) and tied to one particular direction, therefore the architecture is not fully flexible for automated re-configurability in the event of future changes in traffic demand. For add/drop channels the transponder must be manually connected to the ingress/egress mux/demux port of the correct colour and associated with the correct direction.

The ultimate level of add / drop flexibility can be achieved with all-optical switch based on 3D MEMS technology [106]. Such devices can enable a true  $N:N$  WSS with 100% add / drop capacity, each with colourless, directionless and contention less add / drop access, however due to the high cost these devices have not been widely adopted in commercial networks.

## 5.4 TECHNO-ECONOMICS OF TRANSPARENT MESHED NETWORKS

Here the economic benefits of increasing optical transparency are analysed for a European national core reference network. The network topology and traffic demands are defined, a description of the network design process is given and network designs are performed for 4 different system / network architectures, each with increasing levels of optical transparency as detailed in sections 5.2 and 5.3, and summarised here:

- **LH OEO:** LH DWDM system with OEO at every traffic node
- **ROADM:** Multi-Reach DWDM system with degree 2 ROADM
- **WB MD-ROADM:** Multi-Reach DWDM system with WB MD-ROADM
- **WSS MD-ROADM:** Multi-Reach DWDM system with WSS MD-ROADM

### 5.4.1 REFERENCE NETWORK TOPOLOGY

The reference network is a hypothetical network covering the geography of Germany. The meshed network topology is shown in Figure 119 and consists of 13 traffic nodes interconnected by 19 fibre links of average link length 201km. The fibre links include a total 28 intermediate OLA nodes between traffic nodes and a total 3,825km of fibre in 47 fibre spans of average length 81km.

The network nodes include  $2 \times$  degree-5,  $1 \times$  degree-4,  $4 \times$  degree-3 and  $6 \times$  degree-2 nodes. An important parameter of meshed networks is the average node degree  $D$  given by

$$D = \frac{2L}{N}$$

**Equation 58**

where  $L$  is the number of links and  $N$  is the number of traffic nodes in the network [107]. This reference network has  $D$  of 2.92 which is a typical value for a European national network. For a particular given network a higher average node degree indicates a network which is highly interconnected, US networks typically have lower average node degrees due to lower population density.

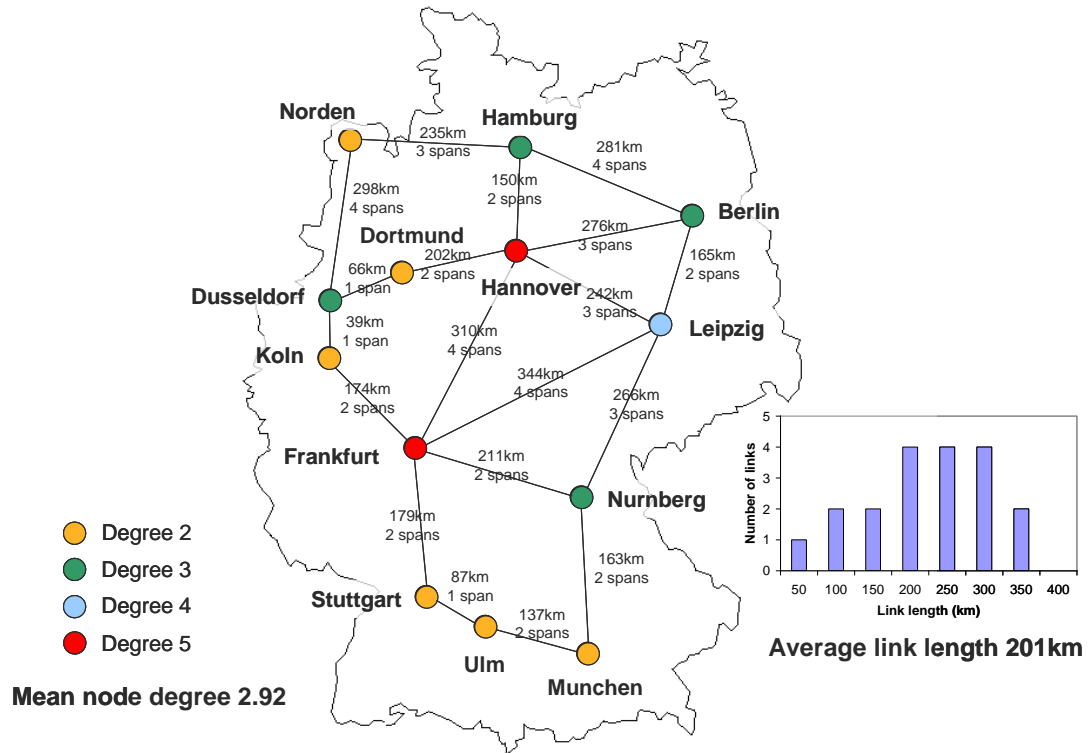


Figure 119 Network topology and parameters (after [24])

## 5.4.2 REFERENCE NETWORK TRAFFIC DEMANDS

A line rate of 10 Gb/s is assumed throughout this study which was typical of commercial networks deployed at the time of this research. The line rate of 40 Gb/s has since achieved mass market adoption after deployment commenced around 2006. 100 Gb/s has now emerged with small scale commercial deployments starting in late 2009 [108].

Here we assume that all traffic demands are at the line rate i.e. there are no sub-rate demands requiring grooming to efficiently fill the DWDM wavelengths. Figure 120 summarises the traffic distribution and growth described here.

Initial traffic requirements are a total working capacity of  $47 \times 10$  Gb/s wavelengths in period 1. Frankfurt and Hannover are the main hub nodes within the network. Traffic is divided in an arbitrary pattern as 40% between adjacent nodes, 30% to/from hub nodes and 30% evenly distributed transit traffic between all other nodes.

In period 2 traffic is increased by 62% to  $76 \times 10$  Gb/s wavelengths with a distribution of 25% between adjacent nodes, 35% from hub nodes and 40% evenly distributed between all other nodes.

In period 3 traffic is increased by 100% to 151×10Gb/s wavelengths with a distribution of 20% between adjacent nodes, 32% from hub nodes and 48% evenly distributed between all other nodes.

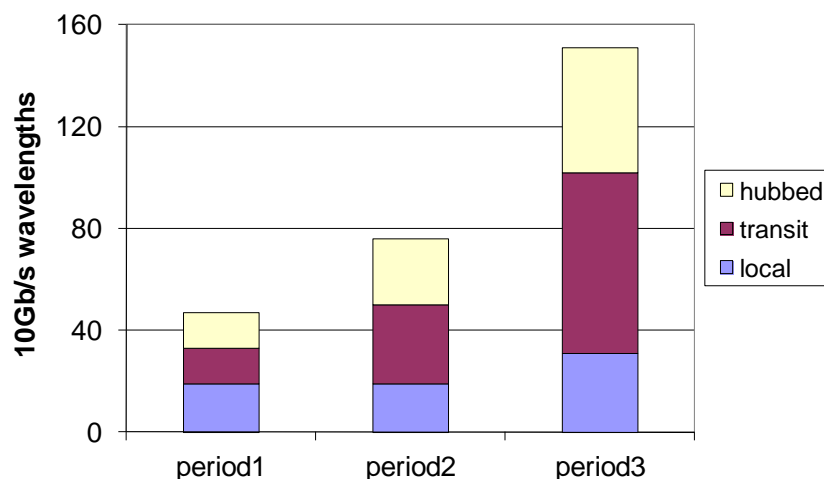


**Figure 120 Traffic distribution and growth forecast**

Traffic churn is assumed to be zero, i.e. traffic demands present in earlier periods are not taken down and removed in later periods.

In total, traffic grows by over 320% from period 1 to period 3. With IP traffic CAGR at around 40%, the 320% growth from period 1 to period 3 should occur within about 3.5 years.

The shift in traffic distribution from adjacent nodes to hub and transit traffic among other nodes is representative of the shift from localised voice traffic to longer distance data centric traffic in later years.

Cumulative traffic matrices for each period are presented in Figure 121 to Figure 123. The bottom half of the matrices represent the working traffic and the upper half represents the protecting traffic assuming 1+1 protection.

	Berlin	Dortmund	Dusseldorf	Frankfurt	Hamburg	Hannover	Koln	Leipzig	Munchen	Norden	Nurnberg	Stuttgart	Ulm
Berlin	0	0	1	1	1	1	0	1	1	0	0	1	0
Dortmund	0	0	1	1	0	1	0	0	1	0	1	1	0
Dusseldorf	1	1	0	1	1	1	1	0	1	1	0	1	0
Frankfurt	1	1	1	0	1	1	1	1	1	1	1	1	1
Hamburg	1	0	1	1	0	1	0	0	1	1	0	1	0
Hannover	1	1	1	1	1	0	1	1	1	1	1	1	1
Koln	0	0	1	1	0	1	0	1	0	0	0	1	0
Leipzig	1	0	0	1	0	1	0	0	0	0	1	0	0
Munchen	1	1	1	1	1	1	1	0	0	0	1	0	1
Norden	0	0	1	1	1	1	0	0	0	0	1	0	0
Nurnberg	0	1	0	1	0	1	0	1	1	1	0	0	0
Stuttgart	1	1	1	1	1	1	1	0	0	0	0	0	1
Ulm	0	0	0	1	0	1	0	0	1	0	0	1	0

Figure 121 Period 1 traffic matrix

	Berlin	Dortmund	Dusseldorf	Frankfurt	Hamburg	Hannover	Koln	Leipzig	Munchen	Norden	Nurnberg	Stuttgart	Ulm
Berlin	1	1	1	3	1	1	0	1	1	1	1	1	0
Dortmund	1	0	1	2	1	1	1	0	1	1	1	1	0
Dusseldorf	1	1	0	1	1	2	1	0	2	1	0	1	0
Frankfurt	3	2	1	0	3	1	1	1	4	1	1	1	1
Hamburg	1	1	1	3	0	1	1	1	2	1	0	2	0
Hannover	1	1	2	1	1	0	2	1	2	1	1	2	1
Koln	0	1	1	1	1	2	0	1	1	0	1	1	0
Leipzig	1	0	0	1	1	1	1	0	1	1	1	1	0
Munchen	1	1	2	4	2	2	1	1	0	0	1	1	1
Norden	1	0	1	1	1	1	0	1	0	0	1	0	0
Nurnberg	1	1	0	1	0	1	1	1	1	1	0	1	0
Stuttgart	1	1	1	1	2	2	1	1	1	0	1	0	1
Ulm	0	0	0	1	0	1	0	0	1	0	0	1	0

Figure 122 Period 2 cumulative traffic matrix

	Berlin	Dortmund	Dusseldorf	Frankfurt	Hamburg	Hannover	Koln	Leipzig	Munchen	Norden	Nurnberg	Stuttgart	Ulm
Berlin	2	2	3	6	2	2	1	1	3	1	2	2	1
Dortmund	2	0	2	4	2	2	2	1	2	1	2	2	1
Dusseldorf	3	2	0	3	2	4	1	1	3	1	1	3	1
Frankfurt	6	4	3	0	4	2	2	2	5	3	2	2	3
Hamburg	2	2	2	4	0	2	1	1	2	1	1	2	1
Hannover	2	2	4	2	2	0	3	2	4	2	2	4	2
Koln	1	2	1	2	1	3	0	2	2	1	2	2	0
Leipzig	1	1	1	2	1	2	2	0	2	1	1	2	1
Munchen	3	2	3	5	2	4	2	2	0	1	2	2	1
Norden	1	1	1	3	1	2	1	1	1	0	2	1	0
Nurnberg	2	2	1	2	1	2	2	1	2	2	0	2	1
Stuttgart	2	2	3	2	2	4	2	2	2	1	2	0	1
Ulm	1	1	1	3	1	2	0	1	1	0	1	1	0

Figure 123 Period 3 cumulative traffic matrix

### 5.4.3 NETWORK DESIGN AND PLANNING: PROCESS AND TOOLS

A commercial network design and planning tool *OPNET SP Guru Transport Planner*<sup>64</sup> (formerly called *WDM Guru*, when this work was initially carried out) was used to solve the wavelength routing and assignment (WRA) problem. The network

<sup>64</sup> [http://www.opnet.com/solutions/network\\_performance/spguru\\_transport\\_planner.html](http://www.opnet.com/solutions/network_performance/spguru_transport_planner.html)

topology shown in Figure 119 was inputted along with the traffic matrices for the three periods.

WRA was done using a shortest path first algorithm to minimise the transmission distance, thereby minimising OEO regeneration requirements and hence cost. Dedicated 1+1 path protection is chosen as the simplest form of protection whereby two connection paths between source and destination nodes are established and a protection switch at the destination selects the path with the better signal. The protection path is chosen as the shortest link disjoint path to the working path. Dedicated 1+1 protection is the most reliable form of protection and is quickest as the receiver instantly switches to the protection path. However its main disadvantage is that a large amount of spare capacity has to be provisioned in the network and is therefore less efficient than alternative shared protection schemes. At the time of this research the network design and planning tool was incapable of performing WRA with shared protection therefore the benefits of shared protection were not analysed.

There are a total of 156 possible connections between all nodes including both working and protection paths. The WRA process resulted in connection lengths varying from 39km to 1,873km with an average length of 581km. By comparison US networks typically have average connection lengths  $> 1,000\text{km}$  [109].

A distribution of the connection lengths is shown in Figure 124 for all paths (both working and protection) and Figure 125 shows the distribution split between working and protection paths.

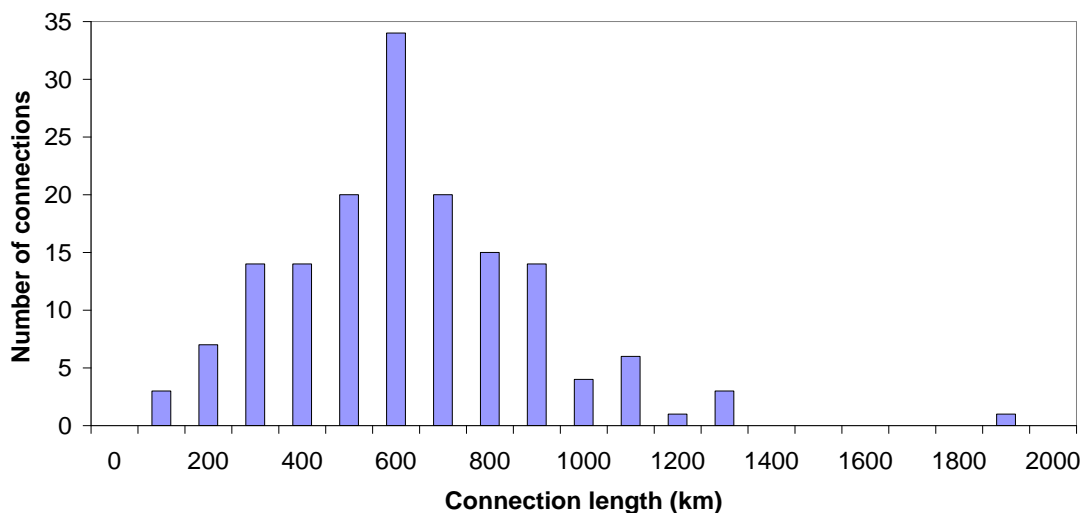
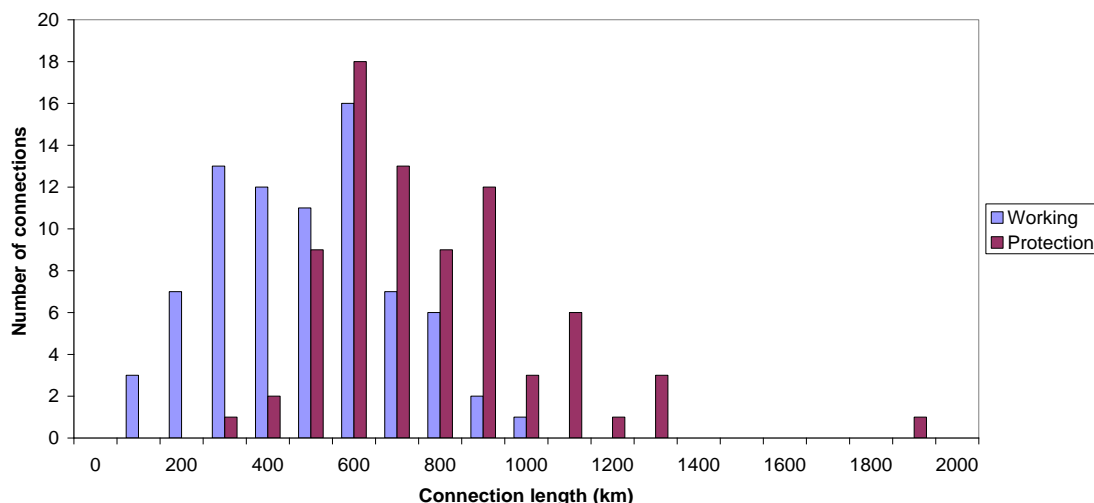
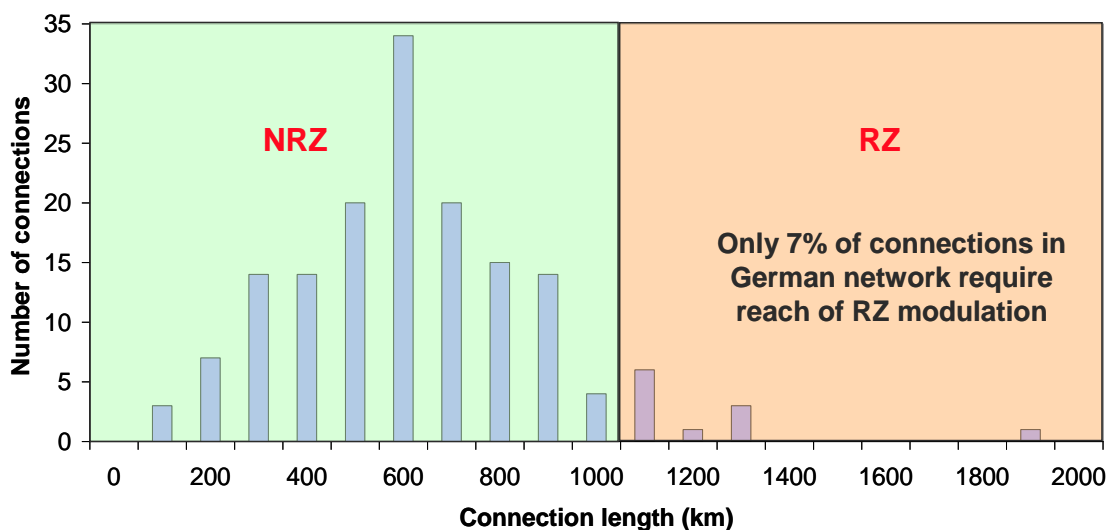


Figure 124 Distribution of all possible working and protection connection lengths (after [24])



**Figure 125 Connection length distribution separating working and protection paths**

In simple point-to-point links 10G NRZ reach is limited to around 1,000km and 10G RZ reach is limited to around 2,500km although individual link characteristics can lead to significantly different performance limits. Figure 126 gives an approximate indication of which part of the connection length distribution can be covered with NRZ transponders and which require the extended reach of RZ transponders. Only 11 (7%) of all connections require the extended reach of RZ transponders and all connections are feasible without any intermediate regeneration. Detailed link engineering is described in section 5.4.4



**Figure 126 Connection length distribution with approximate reach performance of 10G NRZ and 10G RZ transponders**

While RZ looks like a niche application area in a network of this scale, Figure 127 shows a significant number of connections requiring RZ transponders in a typical US

network and a large proportion beyond the reach of RZ transponders requiring selective intermediate OEO regeneration.

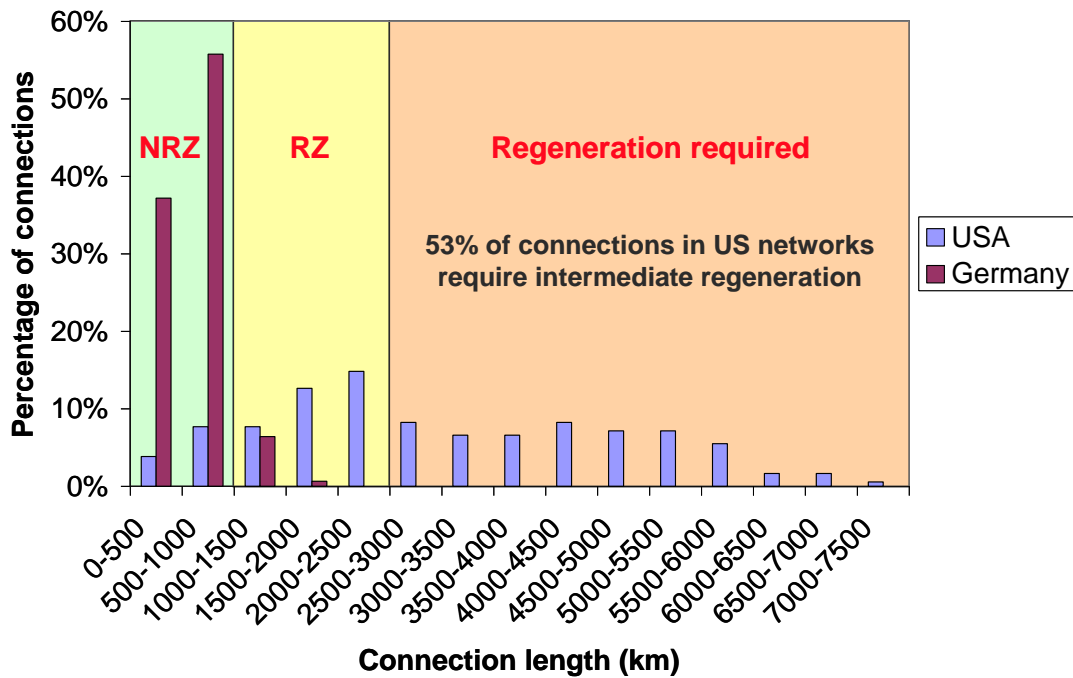


Figure 127 Connection lengths and approximate transponder reach in US and German networks. US network connection lengths from *OPNET SP Guru Transport Planner*.

In an optical bypass enabled network channels approaching the transmission reach limits at ROADM and MD-ROADM nodes would undergo selective regeneration i.e. only those channels entering a node which are approaching the reach limit would be regenerated while shorter reach channels bypass the node all-optically.

#### 5.4.4 LINK ENGINEERING

Based on the WRA results, DWDM systems are allocated to the links and link engineering rules are used to determine which connections can be achieved using NRZ transponders with standard LH amplifiers, and which require the improved reach of higher specification ULH amplifiers with NRZ transponders, or RZ transponders for ultimate reach. Link engineering rules are in the form of span budgets which have been compiled from extensive numerical simulations. Span budgets state the maximum span loss which can be tolerated in a link consisting of a specific number of spans each of the same span loss.

The introduction of ROADMs and MD-ROADMs in DWDM networks can cause penalties which impact transmission performance. An OSNR penalty is incurred as a result of the loss of ROADM components, splitters and couplers as extra amplification is required to overcome these losses resulting in additional amplifier noise. Optical filtering penalties are also incurred at each ROADM node due to the multiplexing and de-multiplexing process as channels pass through the ROADM filters resulting in a narrowed passband; this penalty increases through a cascade of ROADM nodes. Channel cross-talk can also be an issue. A comprehensive description of ROADM penalties is detailed in chapter 8 of [37]; for the purpose of this study a simple design rule is desirable. Extensive simulations carried out by other modelling team colleagues approximate the transmission reach performance impact of each ROADM / MD-ROADM node passed through to reduce the span budget by the equivalent of 1 span.

Each individual connection is cross-checked with a look up table for the span budget performance of each amplifier / transponder combination taking into account a 1 span penalty for each ROADM / MD-ROADM passed through transparently. Figure 128 shows the amplifier and transponder combinations required to support each connection. Out of a 156 possible connections between all traffic nodes, 49 can be achieved using LH amplifiers and NRZ transponders, a further 96 can be achieved using ULH amplifiers and NRZ transponders, while the remaining 11 connections can be achieved using ULH amplifiers and RZ transponders. *LDT* was used to design each link ensuring the correct amplifier and DCMs were chosen for each line amplifier and traffic node.

	Berlin	Dortmund	Dusseldorf	Frankfurt	Hamburg	Hannover	KoIn	Leipzig	Munchen	Norden	Nurnberg	Stuttgart	Ulm
Berlin		880	814	586	426	407	583	518	989	842	797	818	852
Dortmund	478		725	279	599	589	686	623	682	587	490	1097	1010
Dusseldorf	544	66		578	418	523	752	557	939	653	776	1163	1076
Frankfurt	509	512	213		790	586	617	477	403	695	610	598	511
Hamburg	281	352	533	460		557	634	446	863	716	712	1099	1012
Hannover	276	202	268	310	150		307	441	713	566	521	895	808
KoIn	683	105	39	174	572	484		549	978	869	815	1202	1873
Leipzig	165	444	510	344	392	242	518		747	855	555	653	610
Munchen	594	873	616	374	875	671	548	429		1056	614	553	640
Norden	516	364	298	511	235	385	337	627	914		893	1293	1247
Nurnberg	431	710	424	211	671	508	385	266	163	722		387	477
Stuttgart	765	458	392	179	639	489	353	523	224	690	390		690
Ulm	731	545	479	266	726	576	440	566	137	777	300	87	

Key	LH NRZ	ULH NRZ	ULH RZ
Number of Connections	49	96	11
Percentage of connections	31%	62%	7%

Figure 128 Connection lengths in km coded by amplifier and transponder types required to support adequate span budget performance for error free transmission

## 5.4.5 NETWORK DESIGNS

Four different network design solutions were produced as described in sections 5.4.5.1 to 5.4.5.4 each based upon a different generation DWDM system and ROADM with increasing levels of optical transparency and node degree capability.

A BoM was compiled by *LDT* for each network design option and planning period in the form of a spreadsheet listing the individual shelf and line cards required at each network node together with the cost of each item and the total cost of the BoM<sup>65</sup>.

### 5.4.5.1 LH DWDM System with OEO at Every Traffic Node

The network architecture is based on the node architectures described in section 5.2. Shortest reach LH amplifiers and NRZ transponders are deployed throughout the network. OEO regeneration of the entire WDM spectrum is carried out at every traffic node via back-to-back transponders. All links are within the reach limits of the LH NRZ transmission system therefore no intermediate OEO regeneration is required between traffic nodes.

Figure 129 shows a high-level view of the network design: a terminal is placed at each direction (degree) of every node to facilitate multiplexing and de-multiplexing of the aggregate WDM signal. A patch panel is used to manually interconnect the client side of back to back transponders providing OEO regeneration.

---

<sup>65</sup> Due to reasons of commercial sensitivity, the underlying cost assumptions for each network element and transponder card cannot be disclosed in this thesis.

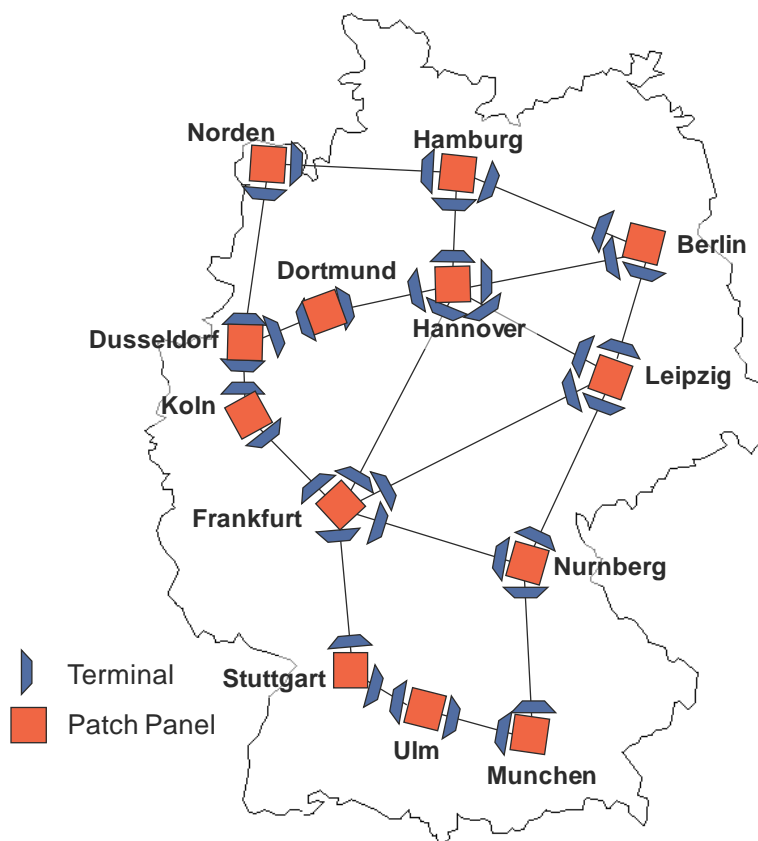


Figure 129 Opaque OEO LH network design

#### 5.4.5.2 Multi-Reach DWDM System with Degree-2 WB ROADM

The network architecture is based on the node architectures described in section 5.3 and 5.3.1; a high level diagram of the network design is shown in Figure 130. ROADMs are deployed at degree 2 nodes enabling the adding and dropping of channels or optical by-pass without regeneration, according to the traffic requirements and transmission reach limits of the DWDM line system. Degree 3, 4 and 5 nodes have ROADMs deployed between the two branches with the most pass through traffic thereby minimising the number of transponders required for OEO regeneration. Terminals are deployed on all other branches with OEO regeneration between each fibre direction via back-to-back transponders interconnected by a patch panel.

All connections can be achieved using shorter reach NRZ transponders due to the terminals breaking down the network architecture into shorter reach islands of transparency.

Further cost optimisation is achievable by using the flexibility of a multi-reach DWDM system and choosing the lower cost LH amplifier option on point-to-point links between adjacent nodes as highlighted by red lines in Figure 130 i.e. Hannover–Berlin, Frankfurt–Leipzig and Frankfurt–Nurnberg.

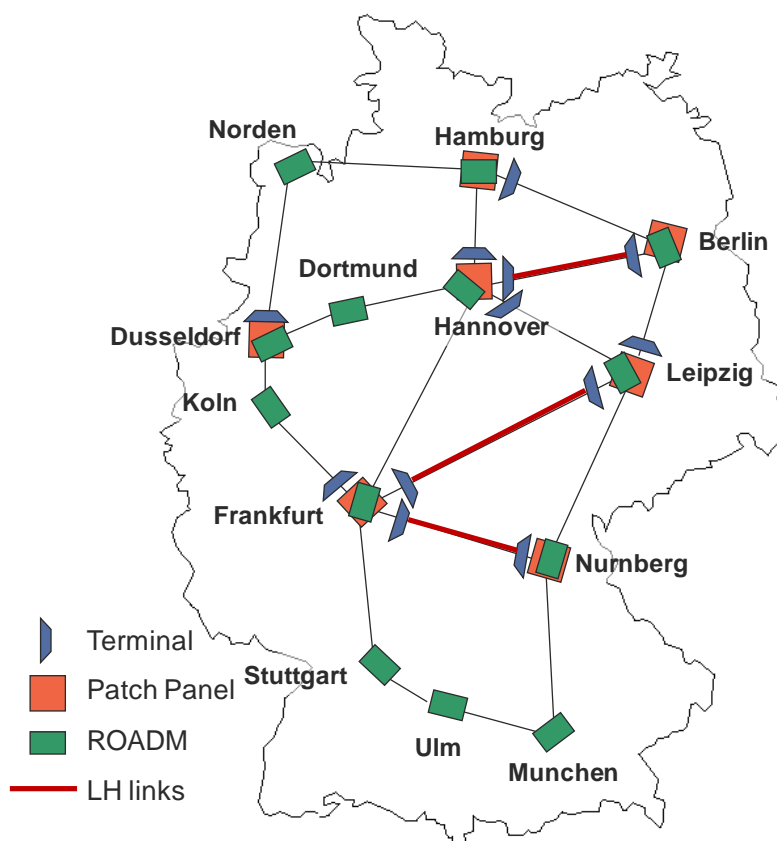


Figure 130 Semi-transparent network design with degree-2 ROADM

### 5.4.5.3 Multi-Reach DWDM System with WB MD-ROADM

MD-ROADM based on wavelength blockers (WB) can enable full optical bypass at nodes up to degree-4 as detailed in section 5.3.2. WB based MD-ROADM does not scale beyond a maximum degree-4, therefore degree-5 nodes Frankfurt and Hannover require an additional terminal for the 5<sup>th</sup> direction; Figure 131 provides a high-level diagram of the network. The terminal is placed on the branch with the most terminating traffic and least amount of pass through traffic, thereby minimising the number of transponders required for OEO regeneration. Transponders of terminated channels are connected back-to-back to transponders on the appropriate add/drop port direction of the MD-ROADM via an optical patch panel.

Longer reach and more expensive ULH amplifiers are required in all line systems within the network since deploying cheaper LH amplifiers would introduce the need for selective OEO regeneration for some connections. This would result in increased CapEx and OpEx as the network scales to higher capacities.

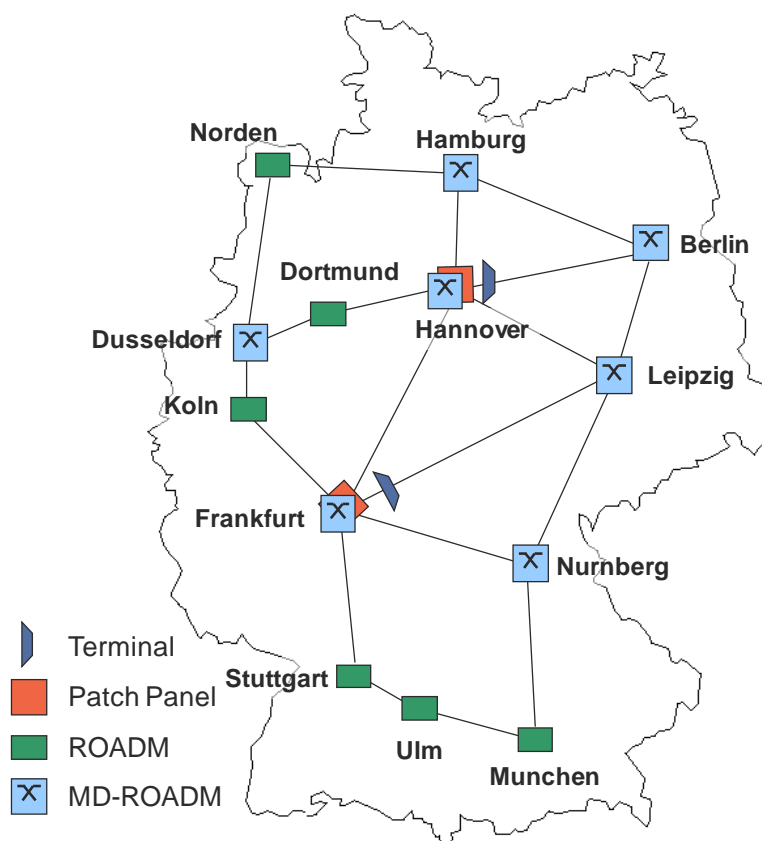


Figure 131 Semi-transparent network design with WB MD-ROADM

#### 5.4.5.4 Multi-Reach DWDM system with WSS MD-ROADM

WSS overcomes the limitation on number of degrees supported by the WB based MD-ROADM, enabling full optical bypass in up to 9 degrees; which is more than adequate for the maximum node degree-5 in the reference network. Figure 132 provides a high-level diagram of the network with WSS at every node and longer reach ULH amplifiers everywhere to avoid selective OEO regeneration.

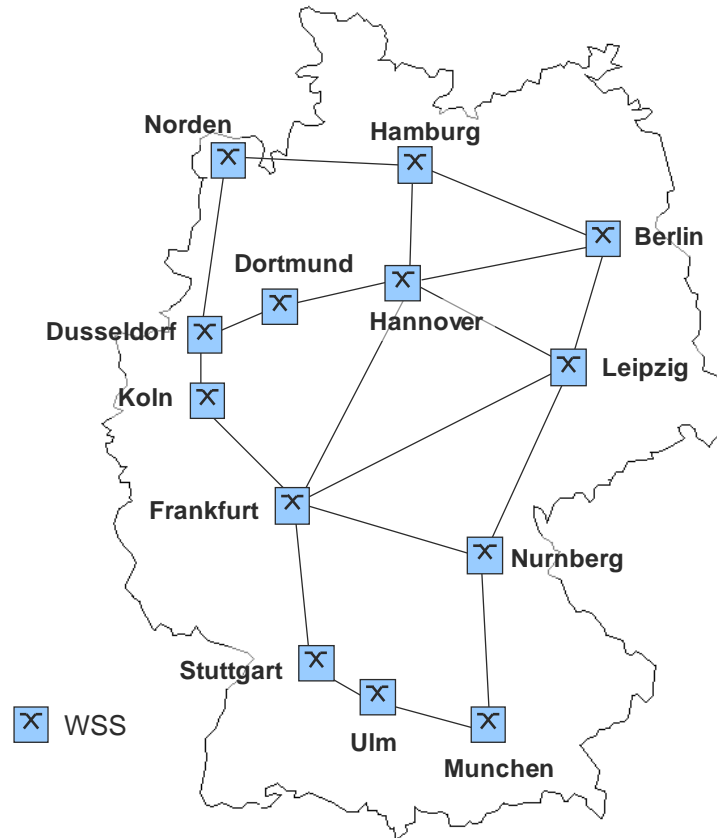


Figure 132 Fully transparent network design with WSS based MD-ROADM

#### 5.4.5.5 Wavelength Contention

Wavelength contention issues are avoided for the traffic demands analysed by upgrading certain routes from 40 channels to 80 channel capacity line systems in period 3, as highlighted in red within Figure 133. This upgrade is non traffic affecting and is achieved by adding multiplexers / de-multiplexers for the second group of 40 channels spaced 100GHz apart which are offset by 50GHz to the first group of 40 channels also spaced 100GHz apart. For the traffic demands investigated this is a lower cost option than performing wavelength conversion using back-to-back transponders.

Average link utilisation figures are: Period 1: 36%, Period 2: 58%, Period 3: 75%

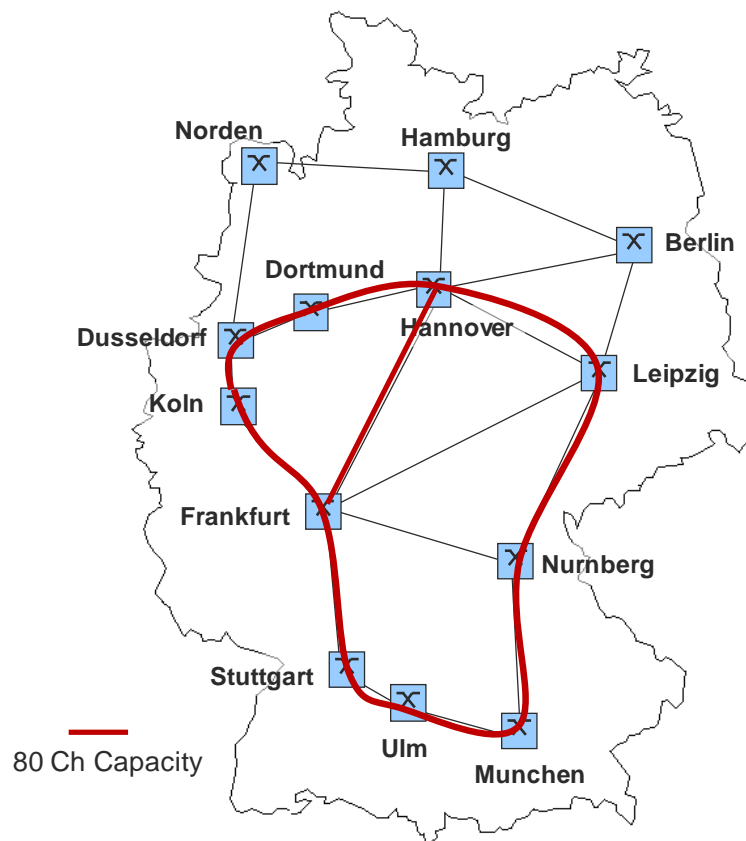


Figure 133 Network routes upgraded from 40 to 80 channels in period 3

#### 5.4.6 TECHNO-ECONOMIC COMPARISON RESULTS AND ANALYSIS

Results of the techno-economic analysis are summarised in Figure 134 and Table 10. Costs of each option are normalised to the cost of the LH OEO solution in period 1.

Even at the low traffic level in period 1, the LH OEO solution is the highest cost option. Costs decrease incrementally as the level of optical bypass capability is increased in subsequent generation solutions with the WSS MD-ROADM solution having the lowest cost, saving a significant 12% versus the LH OEO solution.

As traffic grows beyond period 1, the cost differential between the LH OEO and other solutions increases significantly to the point where the WSS MD-ROADM option is 46% cheaper than LH OEO in period 3.

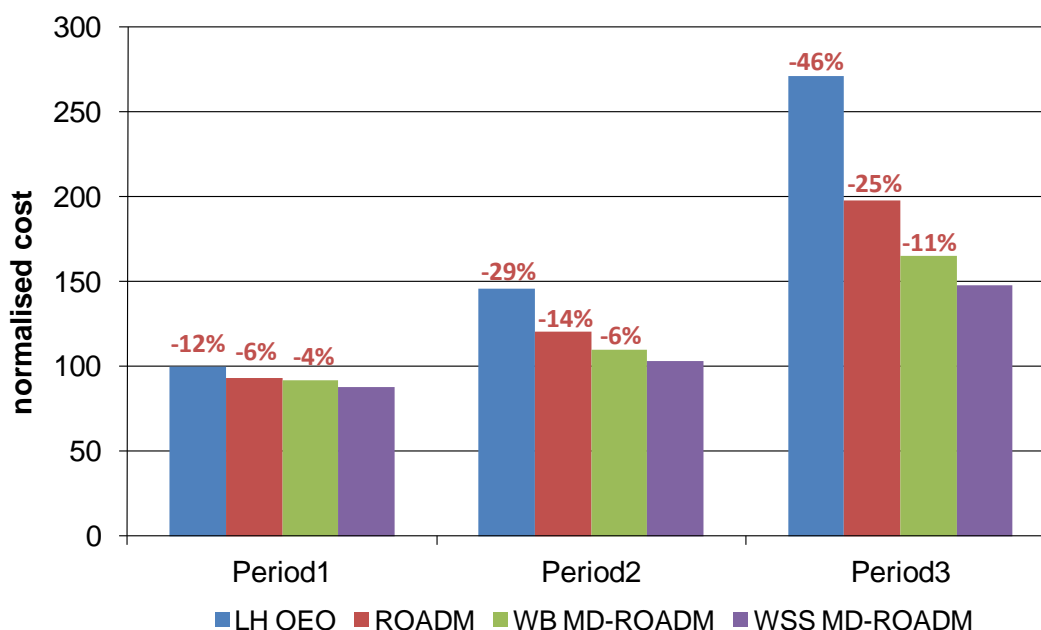


Figure 134 Total network CapEx cost for different solutions at each planning period (% cost savings of the WSS MD-ROADM solution versus each of the other solutions are highlighted in red text) (after [24])

Saving w.r.t.	Solution	Period 1	Period 2	Period 3
LH	ROADM	7 %	18 %	27 %
	WB MD-ROADM	8 %	25 %	39 %
	WSS MD-ROADM	12%	29%	46%
ROADM	WB MD-ROADM	1 %	9 %	17 %
	WSS MD-ROADM	6%	14%	25%
WB MD-ROADM	WSS MD-ROADM	4%	6%	11%

Table 10 Total network % cost savings for each solution and period (after [24])

Figure 135 to Figure 137 show a breakdown of the network cost into 2 main components: *DWDM infrastructure* and *transponders*. DWDM infrastructure includes all system components apart from transponders i.e. line amplifiers, DCM, multiplexers / de-multiplexers, ROADM / MD-ROADM components, power monitors, OSC and shelves to accommodate the cards and provide links to the EMS / NMS.

Investing in higher upfront DWDM infrastructure cost with MD-ROADM pays off in later years as the cost of transponders required for scaling the network to higher capacities increases at a slower rate.

The LH OEO solution has the lowest infrastructure cost of all solutions but requires significantly more transponders. Introducing ULH amplifiers for improved reach, and ROADMs and MD-ROADMs for optical transparency increases the infrastructure cost however the increase is more than offset by a saving in transponder numbers. The net cost saving due to optical transparency is further exaggerated as traffic grows in periods 2 and 3.

Infrastructure cost increases as optical transparency is incrementally increased up to WB MD-ROADM then a further small decrease occurs with the introduction of WSS MD-ROADM due to the improved scalability of WSS multi-degree nodes in terms of the number of ROADM modules required.

Transponder costs decrease as optical transparency is increased as more and more back-to-back transponders are eliminated due to the reduced OEO requirements.

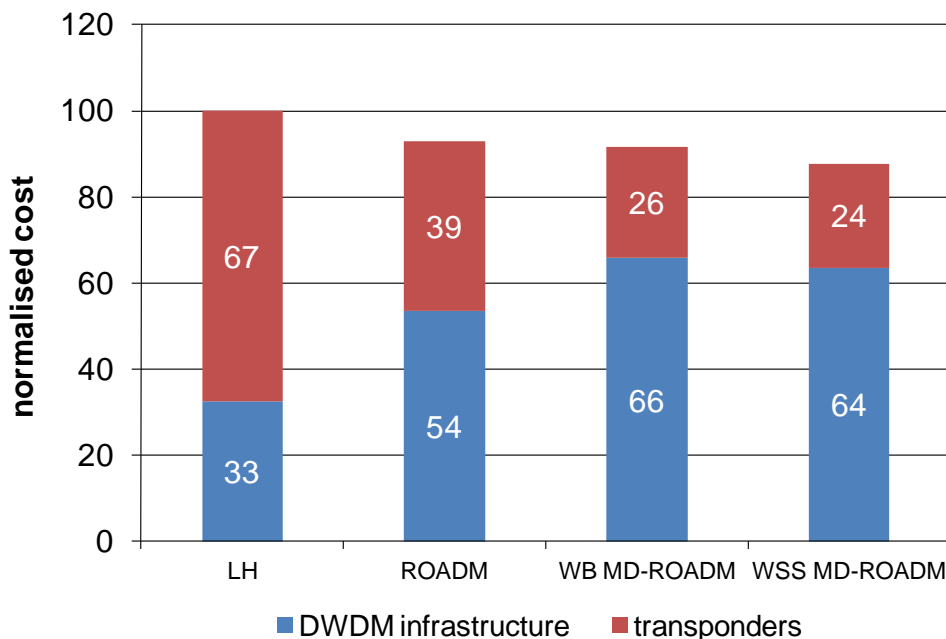


Figure 135 Period 1 total network cost split between DWDM infrastructure and transponders

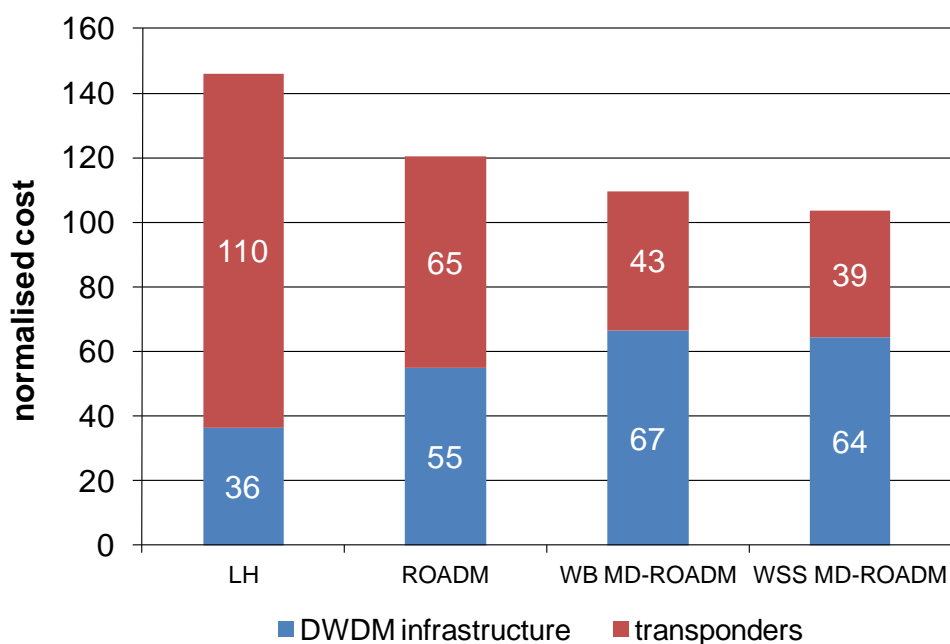


Figure 136 Period 2 total network cost split between DWDM infrastructure and transponders

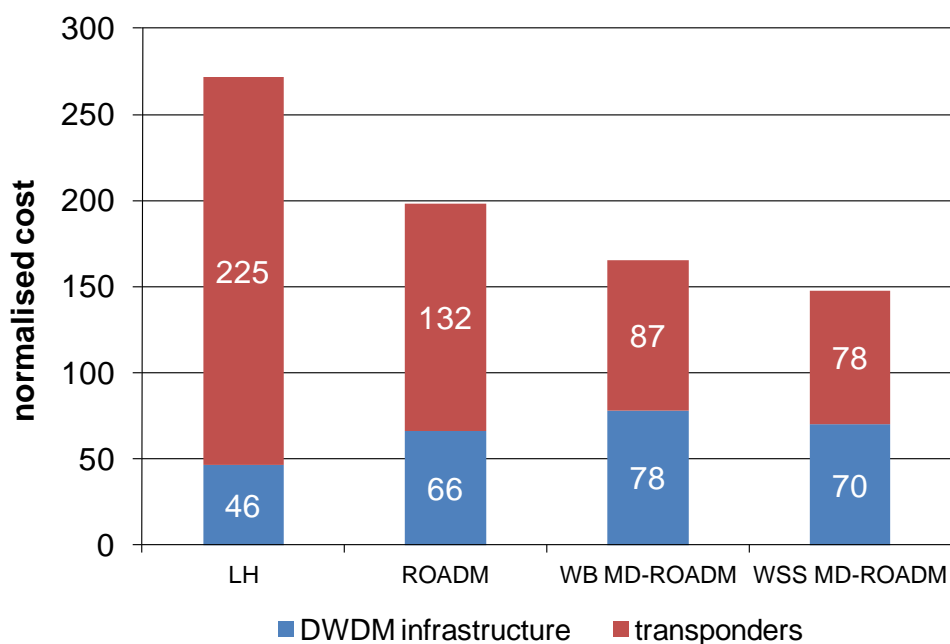


Figure 137 Period 3 total network cost split between DWDM infrastructure and transponders

Transponder numbers for each solution and planning period are detailed in Table 11, the % saving in total transponder numbers moving from one design solution to the next is also presented. The greatest saving is achieved moving from LH OEO to ROADM (around 40%). Moving from ROADM to WB MD-ROADM also brings a

further significant saving of 36% and finally the WSS MD-ROADM brings a further saving of around 10%.

	Period 1				Period 2				Period 3			
	NRZ	RZ	Total	% saving	NRZ	RZ	Total	% saving	NRZ	RZ	Total	% saving
LH OEO	542	0	542		882	0	882		1810	0	1810	
ROADM	316	0	316	42%	526	0	526	40%	1062	0	1062	41%
WB MD-ROADM	192	10	202	36%	318	18	336	36%	640	36	676	36%
WSS MD-ROADM	178	10	188	7%	286	18	304	10%	568	36	604	11%

**Table 11 Total numbers and type of transponders required for each network solution and period with % saving in transponder numbers with respect to previous generation solution**

Table 11 clearly shows 10G RZ transponders are a niche requirement in this reference network. One might question, is it worth developing a long reach transponder as part of a multi-reach DWDM system versus alternatively deploying NRZ throughout and absorbing the relatively small cost of extra OEO regeneration that would be required? In answer to this question, each real network is different and the geographic reach can vary from metro right up to continental size where reaches up to and beyond 3,000km are required. It is therefore desirable to develop a flexible DWDM system which can be customised to each network requirement optimising cost for tendering in a very competitive business environment.

## 5.5 CHAPTER SUMMARY AND CONCLUSIONS

In conclusion, the economic benefits of deploying a transparent meshed network architecture enabled by WSS MD-ROADM in a European national network are significant. Potential CapEx savings with respect to LH OEO are 46%, with respect to ROADM (degree-2) architecture the saving is 25% and with respect to a first generation WB MD-ROADM the saving is 11%.

The savings for this European reference network have proved more significant than in a similar study of US networks [109] which only showed a 5% cost advantage of an all-optical architecture compared to a network architecture using ULH systems with degree-2 ROADM.

Initially it was thought the reason for the improved saving was the shorter connection lengths between European cities, allowing true end-to-end transparency using MD-ROADM. However it is pointed out on page 252 of [103] that the reduced saving found in [109] was due to the use of a MEMS all-optical switch such as that detailed in [106], which is more costly than a MD-ROADM. Also the all-optical switch had a small number of local access ports resulting in a significant amount of wavelength

contention, which required additional transponders to perform wavelength conversion.

An analysis of the economic benefits of MD-ROADM in a US network has subsequently been published in [103]. Results are fairly consistent with the analysis presented in this thesis; an OEO design is 38% more costly than a MD-ROADM. However a degree-2 ROADM design was 14% more costly than a MD-ROADM, which is a significantly smaller difference than the 25% found in this study. The most probable cause of this variation is a slightly more optimal degree-2 ROADM architecture was considered in [103], whereby 2 ROADMs were deployed at nodes of degree-4 and higher, in a similar configuration to that shown in Figure 113. A non-optimal orientation of 2 degree-2 ROADMs results in a 23% more costly design than a MD-ROADM according to [103].

European networks generally have shorter connection lengths than US networks and hence will require less intermediate OEO regeneration making end-to-end transparency a possibility; this factor could still make the economic benefits of MD-ROADM more significant in European networks.

Further optimisation of the network cost structure can be realised by deploying a multi-reach DWDM system combining the features of LH and ULH systems on a single platform, as described in Chapter 4 and [23]. Operators deploying multi-reach systems have the flexibility of choosing LH and/or ULH amplifiers, NRZ and/or RZ transponders to suit the physical layer constraints of the network.

An all-optical meshed network architecture can add additional value to network operators by providing OpEx savings with resulting cost advantages over the whole life cycle of a network as highlighted in [109] and examined in [110]. OpEx savings can result from scalable capacity upgrade enabled by optical bypass, requiring fewer visits to intermediate sites along DWDM links. Faster time to deploy revenue generating services using remotely reconfigurable ROADM is a key competitive advantage for network operators deploying such systems.

## **5.6 FUTURE TRENDS**

Since this work was carried out significant progress has been made towards making transparent meshed networks an operational reality. Here four different features of such networks are outlined.

### 5.6.1 IMPAIRMENT AWARE WRA

Optical bypass enabled networks can result in connection lengths extending from a few km's to 3,000km and above. Simple engineering rules are no longer adequate to model the transmission reach performance of these long connections. Integration of optical link performance calculations into the WRA process is required to accurately optimise network cost and performance: this is termed impairment aware WRA [111].

Underlying fibre link characteristics can result in varying performance between otherwise similar length links. Transmission and fibre impairments need to be estimated using fast analytical calculations, since there is insufficient time to perform the most accurate but computationally intensive nonlinear simulations.

Ericsson have since developed a multilayer optical network design and planning tool *ON Planner* which uses *LDT* as a physical impairment calculation engine within an impairment aware WRA process [112]. Recent developments enable this tool to be linked via the EMS / NMS and Automatically Switched Optical Network (ASON) Control Plane to the actual network equipment, for validating alternative paths through the network when carrying out re-routing and shared mesh restoration following faults.

### 5.6.2 FLEXIBLE ROADM ARCHITECTURES

Despite the re-configurability of ROADM and MD-ROADM and the widespread adoption of tuneable transponders, complete flexibility in remotely reconfiguring optical backbone and metro networks cannot be achieved by the architectures analysed here. The architectures investigated are so called coloured and directional i.e. a transponder of a particular wavelength is tied to a particular add/drop port on an AWG mux/demux which is tied to a particular fibre direction.

WSS can be combined to enable a colourless, directionless and contention-less (CDC) architecture. These configurations require many WSS modules per node, e.g. 16 separate  $1 \times 9$  WSS are required to enable 4 wavelengths of colourless add/drop at an 8 degree node and 24 are required to enable a colourless and directionless capability. Whether a network operator can justify the business case for deploying such a costly and complex architecture on a mass scale remains to be seen.

### 5.6.3 SHARED MESH PROTECTION

Shared mesh protection is an alternative protection scheme to dedicated 1 + 1 protection. In 1:N shared protection a single protection path is shared by N working paths thus requiring significantly less network capacity.

In deciding on the appropriate protection scheme, network architects need to trade-off lower capacity and reduced cost with increased wavelength contention and higher risk of network failures under conditions when more than 1 simultaneous fault occurs.

### 5.6.4 PHOTONIC INTEGRATION: A RETURN TO OEO NETWORKS?

Reducing the cost of OEO is an alternative approach to optical bypass. Advances in photonic integration have enabled significant cost reduction and miniaturisation of transmitter and receiver architectures. Infinera have pioneered large scale photonic integration on Indium Phosphide for their DWDM transmission systems [113] and [114], with low cost OEO regeneration, claiming significant network cost, space and power consumption reductions compared with optical bypass enabled DWDM systems. Despite the traditional wisdom of removing high cost OEO regeneration, OEO does have its advantages, including: performance monitoring at every node, no wavelength continuity constraints and simpler network design and operation algorithms.

A recent acquisition by Huawei of hybrid photonic integration specialist, the Centre for Integrated Photonics (CIP)<sup>66</sup> underlines the increasing importance of photonic integration in realising low cost, power efficient future high capacity optical transport systems.

---

<sup>66</sup> Source: <http://www.gazettabyte.com/home/2012/1/27/huawei-boosts-its-optical-roadmap-with-cip-acquisition.html>

## 6 SUMMARY AND CONCLUSIONS

The work described in this thesis has made significant progress towards its primary objectives of optimising the performance, cost and flexibility of DWDM systems and networks. This objective is driven by intense competition in the telecommunications equipment industry, and the business requirements of network operators to reduce CapEx and OpEx in building, and running their transport networks to meet the exponential growth in Internet traffic.

The link simulation tool developed during this research is capable of accurately assessing the performance of ultra long-haul DWDM systems. By combining two different modelling approaches (wideband spectral power variation and nonlinear simulation), engineering rules which were developed during this research to optimise system architecture by trading-off optimum transmission performance with reduced equipment cost have been adopted in Ericsson's DWDM systems. Optimising the spacing of costly DGE network elements in ultra long-haul systems results in modest cost savings of around 6% with little performance penalty.

Optimum pre-emphasis profile prediction is also made possible by the link simulation tool, enabling simple deployment and optimisation of BER and OSNR performance and power variation across a large bandwidth of DWDM channels.

Optimising dispersion maps by compensating every other span can lead to a modest network infrastructure cost savings of around 6% compared with compensating after each span, with little performance penalty over ELH transmission distance.

EDC can deliver cost savings of as much as 25% in the network infrastructure required to light up a fibre on day one. The percentage cost reduction reduces as transponders are added over the lifetime of the network, but is maintained above zero percent provided the cost premium of an EDC enabled transponder is no more than 5%. Despite modest cost savings in the long term, the ability to reduce first installed cost is a significant competitive advantage when tendering for new network deployments.

Nonlinear tolerance is reduced by 1-2dB using EDC compared to periodic dispersion mapping with DCF; optimum EDC performance is achieved when dispersion compensation is shared equally between transmitter and receiver.

The concept of a flexible, multi-reach DWDM system has been developed, and a techno-economic analysis of the benefits of combining different specification amplifiers, OADMs and transponder modulation formats on a single platform showed network level cost savings of almost 20%.

Economic benefits of multi-reach DWDM systems combined with optical bypass with MD-ROADM in transparent meshed networks result in impressive cost savings of up to 46% compared with earlier generation OEO based long-haul networks.

In summary this thesis has contributed to the theoretical assessment of optical transmission performance showing good alignment between modelling and system measurements. It has also contributed to the practice of designing DWDM networks with the multi-reach platform approach, and network design processes and application of MD-ROADMs to optimising meshed network architectures.

Implications on the industrial sponsor and wider industry include an influential publication highlighting the techno-economic benefits of the multi-reach DWDM platform, promoting Ericsson's technology leadership [24]. Following the conference significant interest was seen in the multi-reach DWDM system from network operators across the world. Ericsson was first to market with a multi-reach DWDM system and over subsequent years grew its revenue and market share significantly. Efficient link simulation and link design tools developed in this research have been critical for quickly performing network design studies when tendering for new business, in addition to the R&D phase of DWDM product development.

## **6.1 CRITICAL EVALUATION OF THE RESEARCH AND RECOMMENDATIONS FOR FURTHER RESEARCH**

### **Limitations of Link Simulation Tool**

Certain operational problems have proven to limit the application of the modelling approach developed in this thesis: typically equipment vendors do not always have sufficient information about network operators' fibre installations and network evolution plans, i.e. exact fibre type, precise fibre loss coefficient, chromatic dispersion, Raman tilt coefficients, number of wavelengths required and wavelength allocation plan. This makes accurate assessment of link performance and pre-emphasis prediction difficult. In addition, detailed EDFA characterisation data is not typically available now that EDFAs have been commoditized as standard modules

purchased from optical component vendors. At the time of this research system vendors such as Ericsson had more detailed exposure to component test results thus enabling fitting the black-box model to actual device measurements.

### **Higher Speed Line Rates: 40Gb/s and 100Gb/s**

The research presented in this thesis was mainly carried out at a time when R&D was focused on 10Gb/s systems. Technology developments in the optical and electronic domains have since led to increased spectral efficiency with higher line rates. 10Gb/s wavelengths are ubiquitous in networks today with 40Gb/s being deployed in many networks worldwide since around 2006. 100Gb/s has been in development since around 2006 with standardisation of the ULH interface ratified in 2009 [11]. Numerous field trials have taken place during 2009-2010 and many commercial deployments have been announced during 2011-2012.

Despite this rapid change, useful lessons learned at 10Gb/s can still be applied at higher line rates. 40Gb/s DWDM systems are multi-reach with different modulation formats optimised for different applications, e.g. DPSK for long reach on low PMD fibre and 100GHz channel spacing, RZ-DQPSK for long reach and improved PMD tolerance and DP-QPSK for maximum reach performance and adaptive compensation of PMD and CD. Different solutions to the standard DP-QPSK modulation format are also emerging at 100Gb/s, particularly for metro network applications. It is therefore important to assess the impact of different modulation formats on the techno-economics of next generation network architectures.

### **Impairment Aware WRA**

Impairment aware wavelength routing and assignment is the next logical step in the evolution of transparent meshed network design. Simplified impairment penalty based link feasibility assessment has been developed within the Link Design Tool and used as a photonic path viability engine within a multi-layer network planning tool. Optimisation studies at the network level should be further developed to include a wider range of topologies and traffic requirements and algorithms developed for optimal cost routing where many design options need to be quickly compared.

### **Electronic Impairment Compensation**

Implementation penalties of electronic dispersion compensation techniques should be accounted for an accurate comparison of performance. Nonlinear effects

compensation is another promising technique which can be implemented in DSP. Applying nonlinear compensation together with EDC can reduce the increased nonlinear penalty that was discovered for the basic EDC configuration, thereby increasing transmission reach.

## APPENDIX 1: EDFA BLACK-BOX MODEL

Here a derivation<sup>67</sup> of the black box model to describe the spectral dependence of EDFA gain and noise figure is described. This work was previously published in [25] and is based upon a model proposed in [44].

### Gain Spectrum

The black-box model [44] provides a simple explanation of the spectral dependence of gain which is suitable from a systems point of view. The model does not require any detailed knowledge of the active medium, or of any other internal amplifier components (e.g., cross section, dopant density, reflection coefficients, or pump wavelengths). The model is based on the effective two-level laser system, meaning that it holds for most commercially available EDFAs.

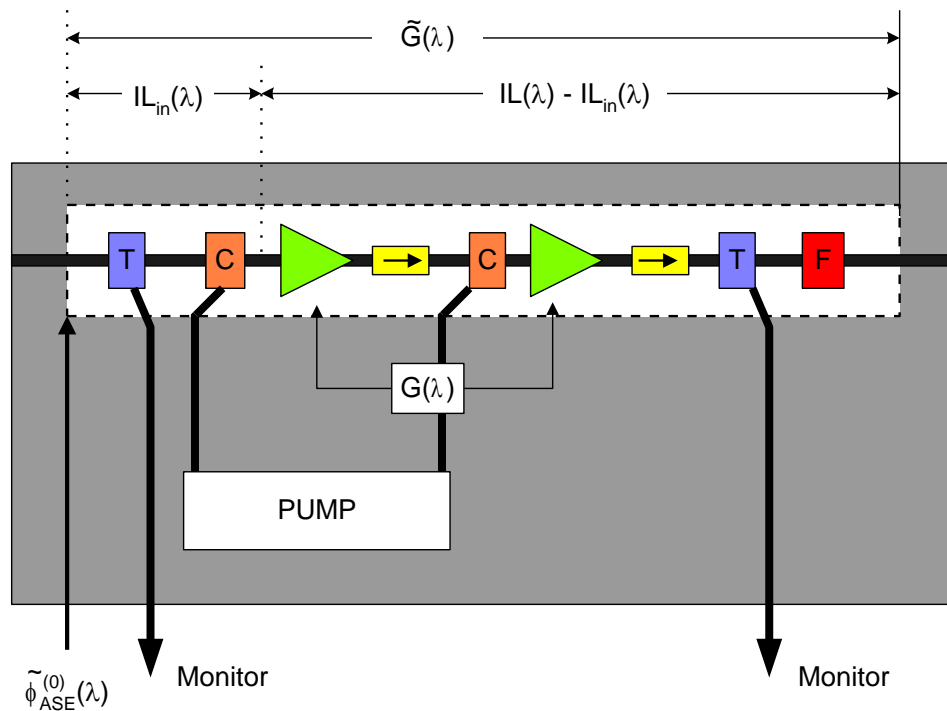


**Figure 138 Schematic of a multi-section EDFA, showing optical isolators ( $\rightarrow$ ), couplers (C) a gain equalising filter (F), and taps (T) for power monitoring (after [44])**

Figure 138 shows a typical compound EDFA which consists of multiple amplifier sections of an overall length  $L$  and a variety of passive optical components, such as optical isolators (to prevent any backward travelling ASE), equalising filters and

<sup>67</sup> Derivation by Dr Jeroen Nijhof

various couplers resulting in a total spectrally dependent insertion loss  $IL(\lambda)$ . The effective gain characteristic  $\hat{G}(\lambda) = G(\lambda)/IL(\lambda)$  of the compound amplifier is shown in [44] as

$$\log\left\{\tilde{G}(\lambda, P_{in})\right\} = \log\left\{\tilde{G}_{ref}(\lambda)\right\} + T_{\lambda_{ref}}(\lambda) \cdot \Delta\tilde{G}$$

Equation 59

where  $\lambda_{ref}$  and  $\hat{G}_{ref}(\lambda_{ref})$  determine a reference operating point of the amplifier and  $\Delta\hat{G}$  is given by Equation 60; a proof of this theorem can be found in [44].

$$\Delta\tilde{G} = \log\left\{\tilde{G}(\lambda_{ref})\right\} - \log\left\{\tilde{G}_{ref}(\lambda_{ref})\right\}$$

Equation 60

The tilt function  $T_{\lambda_{ref}}(\lambda)$  and the reference characteristic  $\hat{G}_{ref}(\lambda)$  can be measured without any knowledge about the EDF and the internal passive optical circuitry of the compound amplifier.

Plotting  $G$  against  $P_{in}$  (the total power of a flat input signal), for  $\lambda_{ref}$ , shown in Figure 139, a linear relationship is seen between the two parameters, meaning that  $\Delta G$  is a constant,  $\Delta G = a_T P_{in}$ , where  $a_T$  is a constant. Similar plots at different  $\lambda_{ref}$ , between 1530 and 1560nm also proved to be linear.

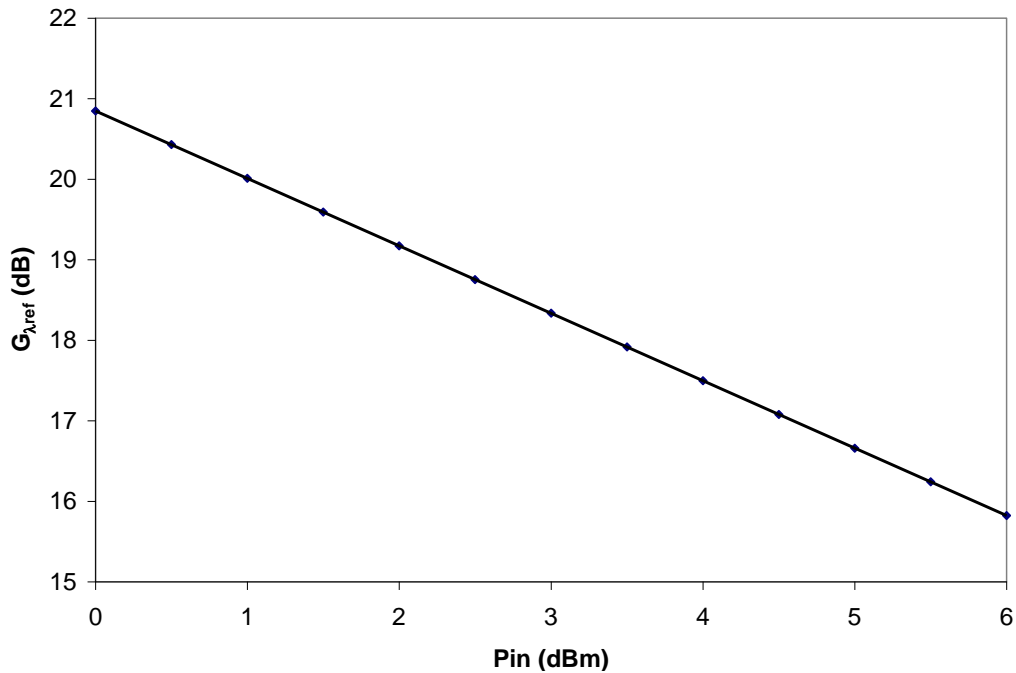


Figure 139 Gain vs. signal power  $P_{in}$  measurements for  $\lambda_{ref}$  (1546nm), the slope is equal to  $a_T$  (after [25])

Equation 59 can be re-written as

$$G(\lambda, P_{in}) = G_{ref}(\lambda) + T_{\lambda_{ref}}(\lambda) \cdot a_T \cdot P_{in}$$

**Equation 61**

By making the reference points  $P_{in\ ref} = 0\text{dBm}$  and  $\lambda_{ref} = 1546\text{nm}$ , third order curves can be fitted to the 3 variables  $P_{in}$ ,  $\lambda$  and  $G$ , so that

$$G(\lambda, P) = a_0 + b_0(\lambda - \lambda_{ref}) + c_0(\lambda - \lambda_{ref})^2 + d_0(\lambda - \lambda_{ref})^3 + P_{in} [a_T + b_T(\lambda - \lambda_{ref}) + c_T(\lambda - \lambda_{ref})^2 + d_T(\lambda - \lambda_{ref})^3]$$

**Equation 62**

where the first 4 terms give the gain at 0dBm, and  $G$  and  $P_{in}$  are indB and dBm respectively.

Experimental measurements of the spectrally varying gain at different input power levels are available for each of the 4 different amplifier gain blocks. Using *GNUplot*, curves were fitted to the 3 parameters.

Figure 140 shows the results for the DSA booster stage amplifier. The green crosses represent results where  $P_{in}$  is greater than 2dBm and the red crosses represent results for all input powers. Each curve shows the 3<sup>rd</sup> order fit to the data at  $P_{in}$  values of 0, 1, 2, 3, 4, and 5dBm and the grey line shows the spectral dependence of the tilt function  $T(\lambda)$ .

The results of the model agree with the experimental data to within  $\pm 0.2\text{dB}$ .

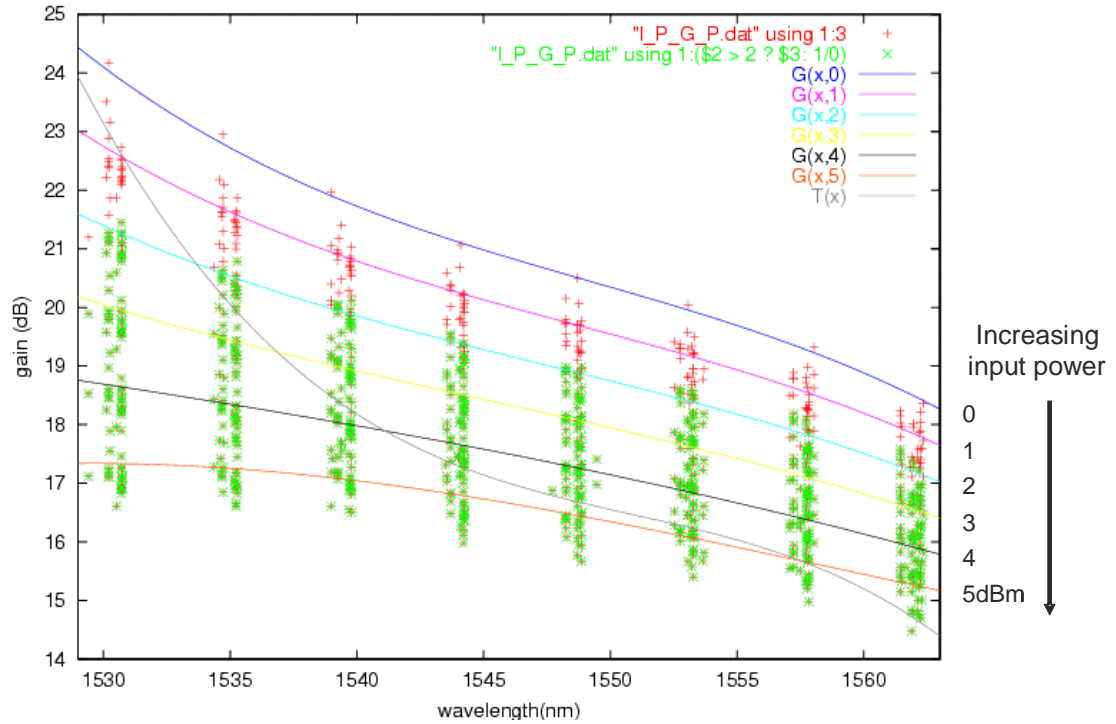


**Figure 140** Measured and modelled spectral gain variation across C-band for DSA booster stage amplifier vs. signal power. Each curve shows the model fit at  $P_{in}$  of 0,1,2,3,4 and 5dBm (after [25])

### Noise Figure Spectrum

The spontaneous emission factor  $n_{sp}$  depends on the inversion of the amplifier as well as the absorption and emission cross-sections  $\sigma_a(\lambda)$  and  $\sigma_e(\lambda)$  at the signal wavelength  $\lambda$ , [115]

$$n_{sp} = \frac{\sigma_e(\lambda)N_2}{\sigma_e(\lambda)N_2 - \sigma_a(\lambda)N_1} = \frac{N_2}{N_2 - \frac{\sigma_a(\lambda)}{\sigma_e(\lambda)}N_1}$$

**Equation 63**

where  $N_2$  is the population density in the upper state and  $N_1$  is the population density in the lower state. As shown by Equation 2, the noise figure,  $F = 2n_{sp}$ . The ratio of the absorption to emission cross-sections will decrease as a function of wavelength; this results in a lower noise figure at longer signal wavelengths for a particular inversion. For complete inversion,  $n_{sp}$  is at best 1, meaning the lowest noise figure attainable is 2 (3dB); this is known as the 3dB quantum limit.

As for the gain model, a black-box model is preferred for the spectrally dependent noise figure, which does not require any detailed knowledge of the active medium or internal amplifier components.

From [44], for optical pre-amplifiers the differential gain at the input is usually high, therefore the equivalent ASE input flux depends mainly on the input inversion  $I(0)$ , i.e.

$$\frac{\phi_{ASE}^{(0)}(\lambda)}{\phi_{ASE,0}} \approx \frac{\gamma(\lambda)I(0)}{(\alpha(\lambda) + \gamma(\lambda))I(0) - \alpha(\lambda)} \approx 1 + \frac{\alpha(\lambda)1 - I(0)}{\gamma(\lambda)I(0)}$$

**Equation 64**

where  $I(0)$  is the input inversion,  $\alpha(\lambda)$  is the absorption coefficient, given by  $\sigma_a(\lambda) \times n_{Er}$  (where  $n_{Er}$  is the effective erbium concentration), and  $\gamma(\lambda)$  is the emission coefficient, given by  $\sigma_e(\lambda) \times n_{Er}$ .

In Equation 64 the first term in the product is a function of  $\lambda$  and the second term is a function of  $P_{in}$ , therefore Equation 64 is re-written as

$$n_{sp} = 1 + f(\lambda) \cdot g(P_{in})$$

**Equation 65**

where  $\frac{\phi_{ASE}^{(0)}(\lambda)}{\phi_{ASE,0}}$  has been replaced by the spontaneous emission factor  $n_{sp}$ . A better fit

can be achieved replacing the 1 in Equation 65 with a constant, thus expressing the spontaneous emission factor as

$$n_{sp} = const + f'(\lambda) \cdot g'(P_{in})$$

**Equation 66**

The spectral dependence of the spontaneous emission factor can be well approximated by a 3<sup>rd</sup> order Taylor series. The  $P_{in}$  dependence is modelled by a 2<sup>nd</sup> order Taylor series, therefore

$$n_{sp}(\lambda, P_{in}) = n_{sp0} + \left[ a_1 + b_1(\lambda - \lambda_{ref}) + c_1(\lambda - \lambda_{ref})^2 + d_1(\lambda - \lambda_{ref})^3 \right] \times (1 + b_p P_{in} + c_p P_{in}^2)$$

**Equation 67**

where  $n_{sp0}$ ,  $a_1$ ,  $b_1$ ,  $c_1$  and  $d_1$  are constants, which give the spontaneous emission factor (in linear units) at  $P_{in}$  of 0dBm,  $b_p$  and  $c_p$  are constants which determine the input

power dependence of the spontaneous emission factor and  $P_{in}$  is given in dBm. Using *GNUplot*, curves were fitted to the 3 different parameters.

Figure 141 shows the results for the DSA booster stage amplifier. Each curve shows the 3<sup>rd</sup> order fit to the data at  $P_{in}$  values of 0, 1, 2, 3, 4, and 5 dBm.

The results of the model agree to within  $\pm 0.3$  dB with the measured noise figures.

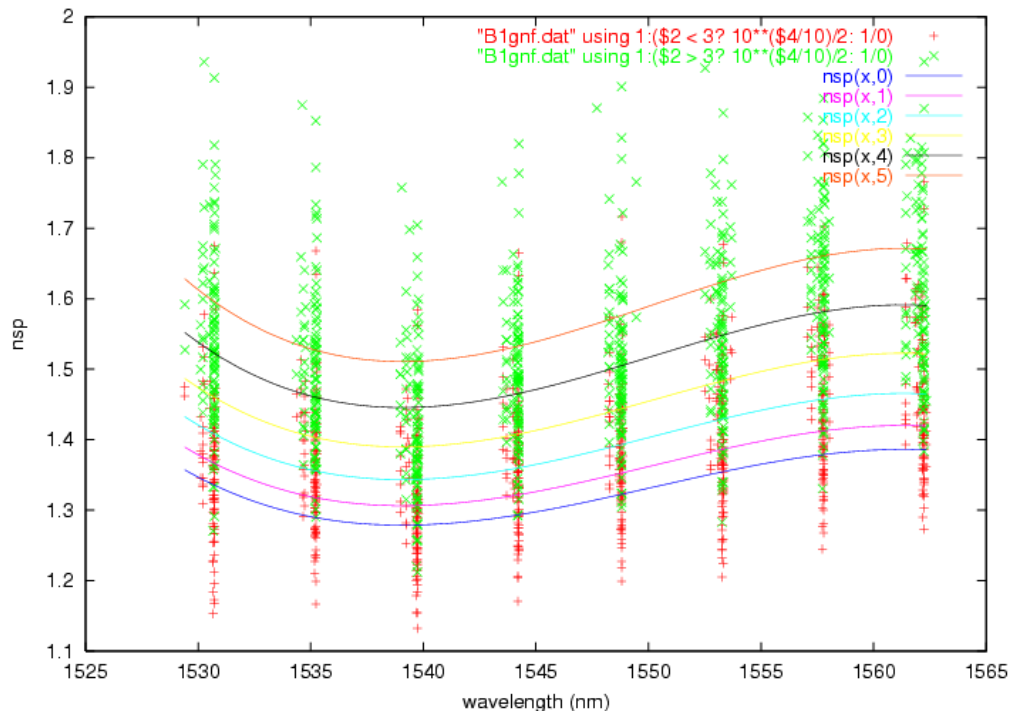


**Figure 141 Measured and modelled spectrally dependent spontaneous emission factor of DSA booster amplifier stage vs. signal power. Each curve shows the fit to the data at  $P_{in}$  values of 0, 1, 2, 3, 4, and 5 dBm (after [25])**

As shown in Figure 142 and Figure 143 for the DSA booster amplifier stage, (other amplifiers show similar behaviour) the fit of the noise figure data, is not as good as that of the gain, with much random variation between amplifiers. The reasons for the great variation in the noise figure are:

- Difficulty in measuring OSNR experimentally
- Greater dependency of noise figure on the cross sections [116]

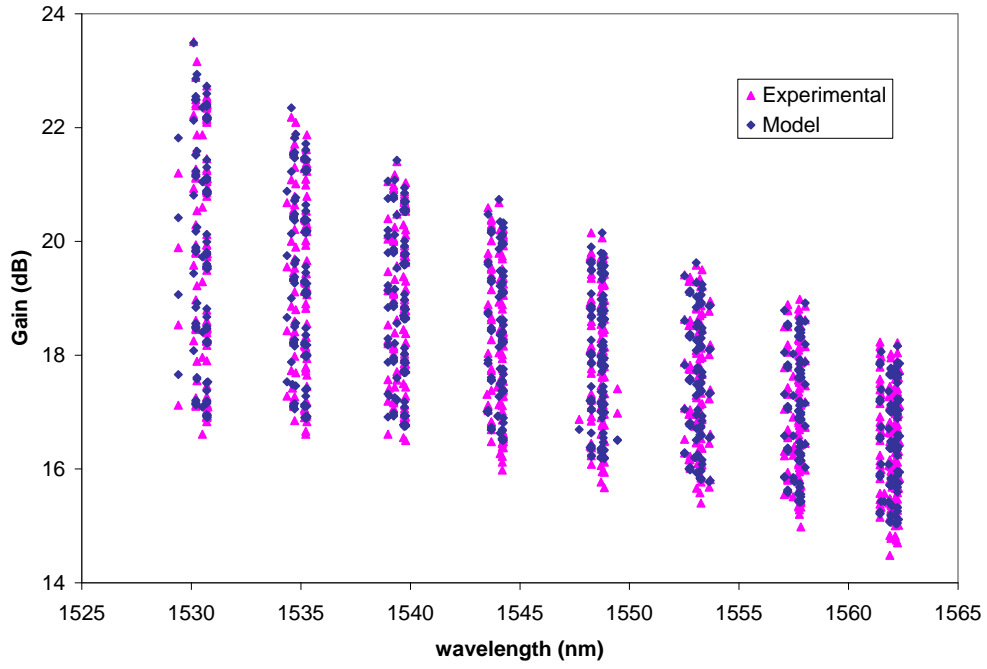


Figure 142 Comparison of measurements and black-box model for DSA booster stage amplifier gain spectrum

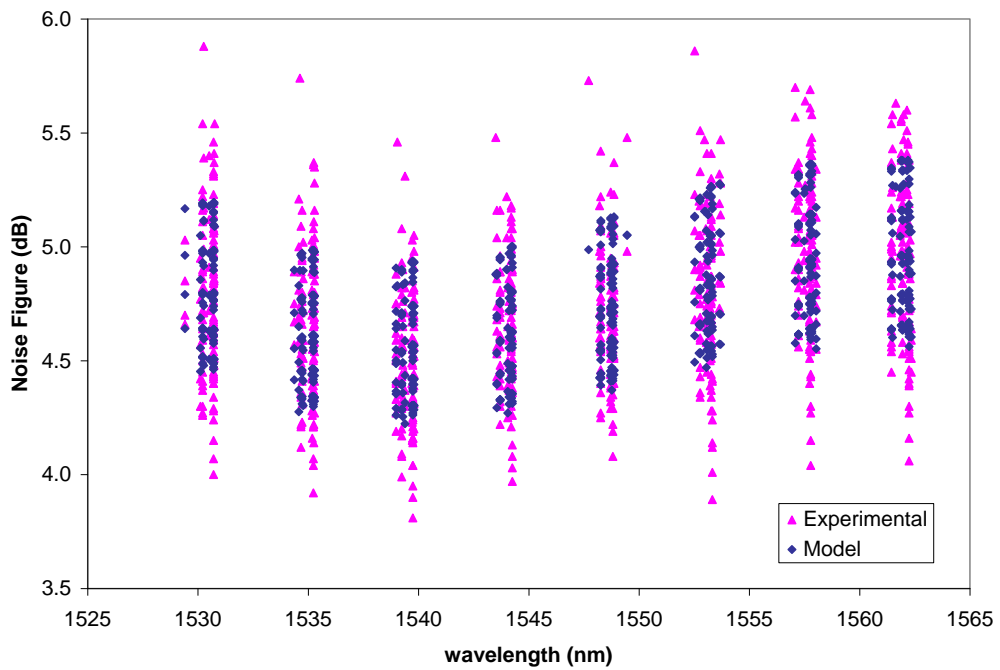


Figure 143 Comparison of measurements and black-box model for DSA booster stage amplifier noise figure

---

**REFERENCES**

- [1] K. C. Kao and G. A. Hockham, 'Dielectric-fibre surface waveguides for optical frequencies', *Electrical Engineers, Proceedings of the Institution of*, vol. 113, no. 7, pp. 1151–1158, 1966.
- [2] A. D. Ellis, Jian Zhao, and D. Cotter, 'Approaching the Non-Linear Shannon Limit', *Journal of Lightwave Technology*, vol. 28, no. 4, pp. 423–433, Feb. 2010.
- [3] P. P. Mitra and J. B. Stark, 'Nonlinear limits to the information capacity of optical fibre communications', *Nature*, vol. 411, no. 6841, pp. 1027–1030, Jun. 2001.
- [4] J. M. Kahn and K.-P. Ho, 'Communications technology: A bottleneck for optical fibres', *Nature*, vol. 411, no. 6841, pp. 1007–1010, Jun. 2001.
- [5] S. Gringeri, E. B. Basch, and T. J. Xia, 'Technical considerations for supporting data rates beyond 100 Gb/s', *IEEE Communications Magazine*, vol. 50, no. 2, p. s21–s30, Feb. 2012.
- [6] M. Camera, B.-E. Olsson, and G. Bruno, 'Beyond 100Gbit/s: System implications towards 400G and 1T', in *2010 36th European Conference and Exhibition on Optical Communication (ECOC)*, 2010.
- [7] "Cisco Visual Networking Index: Forecast and Methodology, 2009-2014 [Visual Networking Index] - Cisco Systems." 02-Jun-2010.
- [8] D. Cooperson, J. Mazur, and M. Walker, 'Increased focus on network power consumption to lower opex, go green', Ovum, Mar. 2009.
- [9] P. J. Winzer and R.-J. Essiambre, 'Advanced Modulation Formats for High-Capacity Optical Transport Networks', *Lightwave Technology, Journal of*, vol. 24, no. 12, pp. 4711–4728, 2006.
- [10] P. J. Winzer and R.-J. Essiambre, 'Advanced Optical Modulation Formats', *Proceedings of the IEEE*, vol. 94, no. 5, pp. 952–985, 2006.
- [11] 'OIF-FD-100G-DWDM-01.0 - 100G Ultra Long Haul DWDM Framework Document'. Jun-2009.
- [12] H. S. Few, M. F. C. Stephens, A. Straw, W. Forysiak, B. K. Nayar, and L. M. Gleeson, 'Experimental Comparison of Fibre and Grating-Based Dispersion Compensation Schemes for 40 channel 10Gb/s DWDM systems', in *Optical*

- 
- Communications, European Conference on, 2006. ECOC 2006.* 2006, paper Th3.2.5.
- [13] J. McNicol, M. O’Sullivan, K. Roberts, A. Comeau, D. McGhan, and L. Strawczynski, ‘Electrical domain compensation of optical dispersion [optical fibre communication applications]’, in *Optical Fiber Communication Conference, 2005. Technical Digest. OFC/NFOEC, 2005*, paper OThJ3.
- [14] D. McGhan, C. Laperle, A. Savchenko, Chuandong Li, G. Mak, and M. O’Sullivan, ‘5120-km RZ-DPSK transmission over G.652 fiber at 10 Gb/s without optical dispersion compensation’, *Photonics Technology Letters, IEEE*, vol. 18, no. 2, pp. 400–402, 2006.
- [15] R.I. Killey, P.M. Watts, V. Mikhailov, M. Glick, and P. Bayvel, ‘Electronic dispersion compensation by signal predistortion using digital Processing and a dual-drive Mach-Zehnder Modulator’, *Photonics Technology Letters, IEEE*, vol. 17, no. 3, pp. 714–716, 2005.
- [16] P. M. Watts, ‘Chromatic dispersion compensation using electronic signal processing in high speed optical communication’, PhD Thesis, UCL, 2008.
- [17] R. Waegemans, ‘Digital Electronic Predistortion for Optical Communications’, PhD Thesis, UCL, 2009.
- [18] S. J. Savory, ‘Digital Coherent Optical Receivers: Algorithms and Subsystems’, *IEEE Journal of Selected Topics in Quantum Electronics*, vol. 16, no. 5, pp. 1164–1179, Oct. 2010.
- [19] G. L. Jones, J. H. B. Nijhof, and W. Forysiak, ‘Optimisation of 80× 10Gbit/s Ultra long-haul DWDM systems’, in *Proceedings of the London Communications Symposium, 2002*.
- [20] A. R. Pratt, P. Harper, S. B. Alleston, P. Bontemps, B. Charbonnier, W. Forysiak, L. Gleeson, D. S. Govan, G. L. Jones, D. Nettet, J. H. B. Nijhof, I. D. Phillips, M. F. C. Stephens, A. P. Walsh, T. Widdowson, and N. J. Doran, ‘5,745 km DWDM transcontinental field trial using 10 Gbit/s dispersion managed solitons and dynamic gain equalization’, in *Optical Fiber Communications Conference, 2003. OFC 2003, 2003*, post-deadline paper PD26.
- [21] G. L. Jones, ‘Dispersion maps for extended long haul DWDM’, in *UCL Postgraduate Poster Session, 2003*.

- 
- [22] G. L. Jones, J. H. B. Nijhof, W. Forysiak, and R. I. Killey, ‘Comparison of optical and electronic dispersion compensation strategies’, *Optical Fibre Communications and Electronic Signal Processing, The IEE Seminar on*, 2005. 2005.
- [23] G. L. Jones, J. H. B. Nijhof, and W. Forysiak, “Cost and flexibility advantage of a multi haul DWDM platform,” *Proceedings of the London Communications Symposium*, 2003.
- [24] G. L. Jones, W. Forysiak, and J. H. B. Nijhof, ‘Economic benefits of all-optical cross connects and multi-haul DWDM systems for European national networks’, in *Optical Fiber Communication Conference, 2004. OFC 2004*, 2004, paper WH2.
- [25] G. L. Jones, ‘Modelling the Spectral Dependence of Noise in Ultra Long Haul Optical Fibre Communication Systems’, MSc Thesis, Aston University, 2002.
- [26] R. Ramaswami and K. Sivarajan, *Optical Networks: A Practical Perspective, Second Edition*, 2nd ed. Morgan Kaufmann, 2001.
- [27] T. L. Koch, and I. P. Kaminow, Eds., *Optical Fiber Telecommunications IIIA*, Academic Press, 1997.
- [28] A. Tychopoulos, O. Koufopavlou, and I. Tomkos, ‘FEC in optical communications - A tutorial overview on the evolution of architectures and the future prospects of outband and inband FEC for optical communications’, *Circuits and Devices Magazine, IEEE*, vol. 22, no. 6, pp. 79–86, Dec. 2006.
- [29] A. R. Chraplyvy, J. A. Nagel, and R. W. Tkach, ‘Equalization in amplified WDM lightwave transmission systems’, *Photonics Technology Letters, IEEE*, vol. 4, no. 8, pp. 920–922, 1992.
- [30] A. R. Chraplyvy, R. W. Tkach, K. C. Reichmann, P. D. Magill, and J. A. Nagel, ‘End-to-end equalization experiments in amplified WDM lightwave systems’, *Photonics Technology Letters, IEEE*, vol. 5, no. 4, pp. 428–429, 1993.
- [31] A. R. Pratt, B. Charbonnier, P. Harper, D. Nettet, B. K. Nayar, and N. J. Doran, ‘40×10.7 Gbit/s DWDM transmission over a meshed ULH network with dynamically re-configurable optical cross connects’, in *Optical Fiber Communications Conference, 2003. OFC 2003*, 2003, post-deadline paper PD9.
- [32] O. K. Tonguz and F. A. Flood, ‘EDFA-based DWDM lightwave transmission systems with end-to-end power and SNR equalization’, *Communications, IEEE Transactions on*, vol. 50, no. 8, pp. 1282–1292, 2002.

- 
- [33] O. K. Tonguz and F. A. Flood, 'Gain equalization of EDFA cascades', *Lightwave Technology, Journal of*, vol. 15, no. 10, pp. 1832–1841, 1997.
- [34] M. Mehendale, M. Vasilyev, and S. Tsuda, 'Optimum pre-emphasis in ultra-long-haul transmission systems', in *Lasers and Electro-Optics, Conference on, 2003. CLEO '03*. 2003, paper CFJ7.
- [35] E. Ciaramella, L. Giorgi, A. D'Errico, F. Cavaliere, G. Gaimari, and G. Prati, 'A highly effective technique for setting the power pre-emphasis in WDM optical systems', *Lightwave Technology, Journal of*, vol. 24, no. 1, pp. 342–356, 2006.
- [36] E. Ciaramella, S. Brugioni, E. Matarazzo, F. Cavaliere, and L. Giorgi, 'Automated Performance Equalization in WDM Networks with inline Optical Add Drop Multiplexers', in *Optical Fiber Communication, Conference on /National Fiber Optic Engineers Conference, 2008. OFC/NFOEC 2008*. 2008, paper NWE3.
- [37] I. P. Kaminow, T. Li, and A. E. Willner, Eds., *Optical Fiber Telecommunications V B: Systems and Networks*. Academic Press, 2008.
- [38] T. Schmidt, C. Malouin, Xing Pan, and Jin Hong, '40G DWDM: A case study in market fragmentation', in *Communications and Photonics Conference and Exhibition (ACP), 2009 Asia*, 2009, vol. 2009-Supplement, pp. 1–7.
- [39] J.-P. Faure, B. Lavigne, C. Bresson, O. Bertran-Pardo, A. C. Colomer, and R. Canto, '40G and 100G deployment on 10G infrastructure: Market overview and trends, coherent versus conventional technology', in *Optical Fiber Communication (OFC), collocated National Fiber Optic Engineers Conference, 2010 Conference on (OFC/NFOEC)*, 2010, paper OThE3.
- [40] A. H. Gnauck, G. Raybon, S. Chandrasekhar, J. Leuthold, C. Doerr, L. Stulz, A. Agarwal, S. Banerjee, D. Grosz, S. Hunsche, A. Kung, A. Marhelyuk, D. Maywar, M. Movassaghi, X. Liu, C. Xu, X. Wei, and D. M. Gill, '2.5 Tb/s (64×42.7 Gb/s) transmission over 40×100 km NZDSF using RZ-DPSK format and all-Raman-amplified spans', in *Optical Fiber Communication Conference and Exhibit, 2002. OFC 2002*, 2002, paper FC2.
- [41] T. Li, 'The impact of optical amplifiers on long-distance lightwave telecommunications', *Proceedings of the IEEE*, vol. 81, no. 11, pp. 1568–1579, 1993.

- 
- [42] E. Desurvire, *Erbium-Doped Fiber Amplifiers: Principles and Applications*. Wiley-Interscience, 1994.
- [43] G. P. Agrawal, *Fiber-optic Communication Systems*, 3rd ed. Wiley-Blackwell, 2002.
- [44] J. Burgemeier, A. Cords, R. Marz, C. Schaffer, and B. Stummer, ‘A black box model of EDFA’s operating in WDM systems’, *Lightwave Technology, Journal of*, vol. 16, no. 7, pp. 1271–1275, 1998.
- [45] T. L. Koch, and I. P. Kaminow, Eds., *Optical Fiber Telecommunications IIIB*. Academic Press, 1997.
- [46] M. Vasilyev, I. Tomkos, M. Mehendale, J.-K. Rhee, A. Kobayakov, M. Ajgaonkar, S. Tsuda, and M. Sharma, ‘Transparent ultra-long-haul DWDM networks with “broadcast-and-select” OADM/OXC architecture’, *Lightwave Technology, Journal of*, vol. 21, no. 11, pp. 2661–2672, 2003.
- [47] G. P. Agrawal, *Nonlinear Fiber Optics*, 2nd ed. Academic Press, 1995.
- [48] J. B. Rosolem, A. A. Juriollo, and M. A. Romero, ‘S-band EDFA using standard erbium-doped fibre’, *Electronics Letters*, vol. 43, no. 22, Oct. 2007.
- [49] M. Shtauf and O. Rosenberg, ‘Polarization-dependent loss as a waveform-distorting mechanism and its effect on fiber-optic systems’, *Journal of Lightwave Technology*, vol. 23, no. 2, pp. 923–930, Feb. 2005.
- [50] I. P. Kaminow and T. Li, Eds., *Optical Fiber Telecommunications IV-B: Systems and Impairments*, Academic Press, 2003.
- [51] G. P. Agrawal, *Applications of Nonlinear Fiber Optics*, 1st ed. Academic Press, 2001.
- [52] F. Forghieri, R. W. Tkach, A. R. Chraplyvy, and D. Marcuse, ‘Reduction of four-wave mixing crosstalk in WDM systems using unequally spaced channels’, *Photonics Technology Letters, IEEE*, vol. 6, no. 6, pp. 754–756, 1994.
- [53] R.-J. Essiambre, B. Mikkelsen, and G. Raybon, ‘Intra-channel cross-phase modulation and four-wave mixing in high-speed TDM systems’, *Electronics Letters*, vol. 35, no. 18, pp. 1576–1578, Sep. 1999.
- [54] M. Zirngibl, ‘Analytical model of Raman gain effects in massive wavelength division multiplexed transmission systems’, *Electronics Letters*, vol. 34, no. 8, pp. 789–790, Apr. 1998.

- 
- [55] C. Scheerer, C. Glingener, A. Farbert, J.-P. Elbers, and G. Fischer, ‘SRS crosstalk in preemphasized WDM systems’, in *Optical Fiber Communication Conference, 2000*, 2000, paper WM28.
- [56] J. Zyskind and A. Srivastava, Eds., *Optically Amplified WDM Networks*. Academic Press, 2010.
- [57] R. H. Hardin and F. D. Tappert, ‘Applications of the Split-Step Fourier Method to the Numerical Solution of Nonlinear and Variable Coefficient Wave Equations’, *SIAM Review*, vol. 15, no. 2, p. 423, Apr. 1973.
- [58] J. W. Cooley and J. W. Tukey, ‘An Algorithm for the Machine Calculation of Complex Fourier Series’, *Mathematics of Computation*, vol. 19, no. 90, pp. 297–301, Apr. 1965.
- [59] K. J. Blow and D. Wood, ‘Theoretical description of transient stimulated Raman scattering in optical fibers’, *IEEE Journal of Quantum Electronics*, vol. 25, no. 12, pp. 2665–2673, Dec. 1989.
- [60] K. J. Blow, ‘System Analysis Using the Split Operator Method’, in *Optical Solitons*, vol. 613, K. Porsezian and V. C. Kuriakose, Eds. Springer Berlin Heidelberg, 2002, pp. 127–140.
- [61] T. Yu, W. M. Reimer, V. S. Grigoryan, and C. R. Menyuk, ‘A mean field approach for simulating wavelength-division multiplexed systems’, *Photonics Technology Letters, IEEE*, vol. 12, no. 4, pp. 443–445, 2000.
- [62] N. S. Bergano, F. W. Kerfoot, and C. R. Davidson, ‘Margin measurements in optical amplifier system’, *Photonics Technology Letters, IEEE*, vol. 5, no. 3, pp. 304–306, 1993.
- [63] Q. Zhang, M. I. Hayee, C. Ma, M. Howieson, A. Rahman, A. Miner, R. Kapadia, C. Tavva, R. Bajracharya, and H.-W. Huang, ‘On the Gaussian approximation and margin measurements in optical amplifier systems’, in *Information Sciences and Systems, 43rd Annual Conference on, 2009. CISS 2009*. 2009, pp. 919–924.
- [64] E. A. Golovchenko, A. N. Pilipetskii, N. S. Bergano, C. R. Davidson, F. I. Khatri, R. M. Kimball, and V. J. Mazurczyk, ‘Modeling of transoceanic fiber-optic WDM communication systems’, *Selected Topics in Quantum Electronics, IEEE Journal of*, vol. 6, no. 2, pp. 337–347, 2000.
- [65] ‘ITU-T Recommendation G.975.1: Forward error correction for high bit-rate DWDM submarine systems’. ITU-T, Feb-2004.

- 
- [66] F. Chang, K. Onohara, and T. Mizuochi, 'Forward error correction for 100 G transport networks', *Communications Magazine, IEEE*, vol. 48, no. 3, p. S48–S55, 2010.
- [67] A. Lowery, O. Lenzmann, I. Koltchanov, R. Moosburger, R. Freund, A. Richter, S. Georgi, D. Breuer, and H. Hamster, 'Multiple signal representation simulation of photonic devices, systems, and networks', *Selected Topics in Quantum Electronics, IEEE Journal of*, vol. 6, no. 2, pp. 282–296, 2000.
- [68] H. Bulow, F. Buchali, and A. Klekamp, 'Electronic Dispersion Compensation', *Journal of Lightwave Technology*, vol. 26, no. 1, pp. 158–167, Jan. 2008.
- [69] F. Forghieri, R.W. Tkach, and A.R. Chraplyvy, 'Dispersion compensating fiber: Is there merit in the figure of merit?', *Photonics Technology Letters, IEEE*, vol. 9, no. 7, pp. 970–972, 1997.
- [70] H. Bissessur, L. Pierre, D. Penninckx, J.-P. Thiery, and J.-P. Hamaide, 'Enhanced phase-shaped binary transmission for dense WDM systems', *Electronics Letters*, vol. 37, no. 1, pp. 45–46, Jan. 2001.
- [71] R. J. Nuyts, Yong Kwan Park, and P. Gallion, 'Dispersion equalization of a 10 Gb/s repeated transmission system using dispersion compensating fibers', *Journal of Lightwave Technology*, vol. 15, no. 1, pp. 31–42, Jan. 1997.
- [72] B. Zhu, L. Leng, L. E. Nelson, S. Stulz, T. N. Nielsen, and D. A. Fishman, 'Experimental investigation of dispersion maps for 40x10 Gb/s transmission over 1600 km of fiber with 100-km spans employing distributed Raman amplification', in *Optical Fiber Communication Conference and Exhibit, 2001. OFC 2001*, 2001, paper TuN3.
- [73] A. Färbert et al., 'Performance of a 10.7 Gb/s receiver with digital equaliser using maximum likelihood sequence estimation', in *Proceedings of ECOC 2004*, Stockholm, Sweden, 2004, post-deadline paper Th4.1.5.
- [74] F. Buchali, H. Bulow, W. Baumert, R. Ballentin, and T. Wehreu, 'Reduction of the chromatic dispersion penalty at 10 Gbit/s by integrated electronic equalisers', in *Optical Fiber Communication Conference, 2000*, 2000, paper ThS1.
- [75] M.G. Taylor, 'Coherent detection method using DSP for demodulation of signal and subsequent equalization of propagation impairments', *Photonics Technology Letters, IEEE*, vol. 16, no. 2, pp. 674–676, 2004.

- [76] P. J. Winzer and R.-J. Essiambre, 'Electronic pre-distortion for advanced modulation formats', in *31st European Conference on Optical Communication, 2005. ECOC 2005*, 2005, paper Tu4.2.2.
- [77] T. Kupfer and S. Aramideh, 'Economics of electronic equalization in metro core DWDM networks', in *The 16th Annual Meeting of the IEEE Lasers and Electro-Optics Society, 2003. LEOS 2003*, 2003, paper WQ3.
- [78] M. P. Belanger and M. Cavallari, 'Network cost impact of solutions for mitigating optical impairments: comparison of methods, techniques, and practical deployments constraints', *Lightwave Technology, Journal of*, vol. 24, no. 1, pp. 150–157, 2006.
- [79] K. Roberts, '100G - Key technology enablers of 100Gbit/s in carrier networks', in *Optical Fiber Communication Conference and Exposition (OFC/NFOEC), 2011 and the National Fiber Optic Engineers Conference, 2011*, paper NWA1.
- [80] E. Ip, A. P. T. Lau, D. J. F. Barros, and J. M. Kahn, 'Compensation of dispersion and nonlinearity in WDM transmission using simplified digital backpropagation', in *IEEE/LEOS Summer Topical Meetings, 2008 Digest of the*, 2008, paper TuC3.4.
- [81] D. S. Millar, S. Makovejs, C. Behrens, S. Hellerbrand, R. I. Killey, P. Bayvel, and S. J. Savory, 'Mitigation of Fiber Nonlinearity Using a Digital Coherent Receiver', *IEEE Journal of Selected Topics in Quantum Electronics*, vol. 16, no. 5, pp. 1217–1226, Oct. 2010.
- [82] H. Bülow, C. Xie, A. Klekamp, X. Liu, and B. Franz, 'PMD Compensation/mitigation techniques for high-speed optical transport', *Bell Labs Technical Journal*, vol. 14, no. 1, pp. 105–124, Mar. 2009.
- [83] P. Mcfedries, 'The Age of Spimes [Technically Speaking]', *Spectrum, IEEE*, vol. 47, no. 10, p. 25, 2010.
- [84] M. W. Chbat and H.-J. Schmidtke, 'Falling Boundaries from Metro to ULH Optical Transport Equipment', in *Optical Fiber Communication, Conference on, and the National Fiber Optic Engineers Conference, 2007. OFC/NFOEC 2007*. 2007, paper NTuA3.
- [85] E. B. Basch, R. Egorov, S. Gringeri, and S. Elby, 'Architectural tradeoffs for reconfigurable dense wavelength-division multiplexing systems', *Selected Topics in Quantum Electronics, IEEE Journal of*, vol. 12, no. 4, pp. 615–626, 2006.

- 
- [86] Shuai Zhang, Shufen Zhang, Xuebin Chen, and Xiuzhen Huo, ‘Cloud Computing Research and Development Trend’, in *Future Networks, 2010. ICFN '10. Second International Conference on*, 2010, pp. 93–97.
- [87] S. Chia, M. Gasparroni, and P. Brick, ‘The next challenge for cellular networks: backhaul’, *Microwave Magazine, IEEE*, vol. 10, no. 5, pp. 54–66, 2009.
- [88] Z. Ghebretensaé, J. Harmatos, and K. Gustafsson, ‘Mobile broadband backhaul network migration from TDM to carrier ethernet’, *Communications Magazine, IEEE*, vol. 48, no. 10, pp. 102–109, 2010.
- [89] ‘Operators get ready for the wireless broadband revolution - fibresystems.org’ . .
- [90] S. Tibuleac, M. Filer, S. Grindstaff, and D. Atlas, ‘Design and optimization of multi-haul DWDM networks’, in *Network Architectures, Management, and Applications IV*, Gwangju, South Korea, 2006, Proceedings of SPIE Vol. 6354.
- [91] B. Mukherjee, *Optical WDM networks*. Birkhäuser, 2006.
- [92] K. Tse, ‘Tradeoffs for performance in long-haul transmission systems: a carrier’s perspective’, *presented in the Optical Fiber Communications Conference, 2003. OFC 2003*, 2003, paper FE1.
- [93] ‘Marconi MHL 3000 Optical DWDM Solution datasheet’  
<http://archive.ericsson.net/service/internet/picov/get?DocNo=28701-FGC1010609&Lang=EN&HighestFree=Y>
- [94] A. Viglienzoni and R. M. Dorward, ‘Evolution of switching technology in DWDM networks’, in *Photonics in Switching, 2009. PS '09. International Conference on*, 2009.
- [95] J. Homa and K. Bala, ‘ROADM Architectures and Their Enabling WSS Technology’, *Communications Magazine, IEEE*, vol. 46, no. 7, pp. 150–154, 2008.
- [96] A. A. M. Saleh, ‘Transparent optical networking in backbone networks’, in *Optical Fiber Communication Conference, 2000*, 2000, paper ThD7.
- [97] H.-J. Schmidtke and M. W. Chbat, ‘Optical Meshed Networks: From Concept to Deployment’, in *Optical Fiber Communication and the National Fiber Optic Engineers Conference, 2007. OFC/NFOEC 2007. Conference on*, 2007, paper NThC1.

- 
- [98] A. Boskovic, M. Sharma, N. Antoniadis, and M. Lee, ‘Broadcast and select OADM nodes application and performance trade-offs’, in *Optical Fiber Communication Conference and Exhibit, 2002. OFC 2002*, 2002, paper TuX2.
- [99] I. Tomkos, M. Vasilyev, J.-K. Rhee, M. Mehendale, B. Hallock, B. Szalabofka, M. Williams, S. Tsuda, and M. Sharma, ‘Ultra-Long-Haul DWDM network with 320x320 wavelength-port “Broadcast & Select” OXCs’, in *Optical Communication, 28th European Conference on, 2002. ECOC 2002*. 2002, Post-deadline paper PD2.1.
- [100] L. M. Gleeson, M. F. C. Stephens, P. Harper, A. R. Pratt, W. Forsyiaik, D. S. Govan, B. K. Nayar, I. D. Phillips, B. Charbonnier, M. D. Baggott, H. S. Sidhu, I. E. Tilford, and P. M. Greig, ‘40 x 10.7 Gb/s Meshed ULH Network with Remotely Managed All-Optical Cross Connects and Add-Drop Multiplexing’, in *Proceedings of ECOC 2003*, 2003, Post-deadline paper Th4.4.7.
- [101] P. Hofmann, E. E. Basch, S. Gringeri, R. Egorov, D. A. Fishman, and W. A. Thompson, ‘DWDM long haul network deployment for the Verizon GNI nationwide network’, in *Optical Fiber Communication Conference, 2005. Technical Digest. OFC/NFOEC*, 2005, paper OTuP5.
- [102] A. R. Pratt and W. Forsyiaik, ‘Commercial Realization of an all Optical Mesh Network: Extending the Photonic Layer to the End-User’, in *Proceedings of OECC2009*, paper ThLP76.
- [103] J. M. Simmons, *Optical Network Design and Planning*, 1st ed. Springer, 2008.
- [104] ‘Finisar Introduces World’s First 1x20 High Port Count Wavelength Selective Switch With Flexgrid(TM) Technology’. Finisar Press Release, 13-Sep-2011.
- [105] S. Gringeri, B. Basch, V. Shukla, R. Egorov, and T. J. Xia, ‘Flexible architectures for optical transport nodes and networks’, *IEEE Communications Magazine*, vol. 48, no. 7, pp. 40–50, Jul. 2010.
- [106] V. Kaman, R. J. Helkey, and J. E. Bowers, ‘Multi-Degree ROADMs with Agile Add-Drop Access’, in *Photonics in Switching, 2007*, 2007, paper TuA2.5.
- [107] N. Geary, ‘Optical network planning: process, analysis and optimisation’, EngD Thesis, University of London, 2003.
- [108] ‘Verizon Deploys Commercial 100G Ultra-Long-Haul Optical System on Portion of Its Core European Network’. Verizon Press Release, 14-Dec-2009.

- 
- [109] A. Chiu and C. Yu, 'Economic benefits of transparent OXC networks as compared to long systems with OADMs', in *Optical Fiber Communications Conference, 2003. OFC 2003*, 2003, paper WQ2.
- [110] N. Geary, A. Antonopoulos, and John O'Reilly, 'Analysis of the potential benefits of OXC-based intelligent optical networks', *Optical Networks Magazine*, vol. 4, no. 2, Apr. 2003.
- [111] M. Gagnaire and S. Zahr, 'Impairment-aware routing and wavelength assignment in translucent networks: State of the art', *Communications Magazine, IEEE*, vol. 47, no. 5, pp. 55–61, 2009.
- [112] "ERICSSON OPTICAL NETWORKS PLANNER Multilayer Network Planning Tool."  
<http://archive.ericsson.net/service/internet/picov/get?DocNo=28701-FGC1010524&Lang=EN&HighestFree=Y>
- [113] D. F. Welch, F. A. Kish, R. Nagarajan, C. H. Joyner, R. P. Schneider, V. G. Dominic, M. L. Mitchell, S. G. Grubb, T.-K. Chiang, D. Perkins, and A. C. Nilsson, 'The Realization of Large-Scale Photonic Integrated Circuits and the Associated Impact on Fiber-Optic Communication Systems', *Journal of Lightwave Technology*, vol. 24, no. 12, pp. 4674–4683, Dec. 2006.
- [114] S. Melle, R. Dodd, C. Liou, M. Sosa, and M. Yin, 'Network planning and economic analysis of an innovative new optical transport architecture: The digital optical network', in *National Fiber Optic Engineers Conference, 2005*, paper NTuA1.
- [115] E. Desurvire, 'Spectral noise figure of Er<sup>3+</sup>-doped fiber amplifiers', *IEEE Photonics Technology Letters*, vol. 2, no. 3, pp. 208–210, Mar. 1990.
- [116] C. R. Giles and D. Di Giovanni, 'Spectral dependence of gain and noise in erbium-doped fiber amplifiers', *IEEE Photonics Technology Letters*, vol. 2, no. 11, pp. 797–800, Nov. 1990.